R-14-14

Flow and transport modelling on the vault scale

Supporting calculations for the safety assessment SR-PSU

Elena Abarca, Orlando Silva, Andrés Idiart,
Albert Nardi, Jordi Font, Jorge Molinero

Amphos[21] Consulting S.L.

March 2014

Svensk Kärnbränslehantering AB
Swedish Nuclear Fuel
and Waste Management Co

Box 250, SE-101 24 Stockholm
Phone +46 8 459 84 00

ISSN 1402-3091
SKB R-14-14
ID 1427449

Flow and transport modelling on the vault scale

Supporting calculations for the safety assessment SR-PSU

Elena Abarca, Orlando Silva, Andrés Idiart,
Albert Nardi, Jordi Font, Jorge Molinero

Amphos[21] Consulting S.L.

March 2014

Summary

Eleven separate vault-scale submodels have been extracted from the geometries of the SFR 1 and SFR 3 repository-scale models. The submodels are implemented in separate COMSOL files and run for the Base case (shoreline positions 1, 2 and 3). As a verification of the correct implementation, the results of the vault-scale submodels are postprocessed and compared with the repository-scale model in terms of the flow rates within the vault. Overall, the differences with the repository-scale models are in the range 0–26%. A mesh sensitivity analysis was carried out using the 1BMA submodel. The results for the different meshes show no significant influence of the mesh refinement on the solution. The relative error, calculated as the difference between the solutions obtained with successive finer meshes, is lower than 2%.

Thereafter, the 1BMA submodel has been utilized to study the effects of concrete degradation on the flow rates in the different vault elements. Due to the uncertainty in the effective hydraulic conductivity of the concrete 1BMA beams/drainage system, we considered two hydraulic scenarios: (i) a case with a low effective conductivity of the beams/drains system equal to the structural concrete conductivity; (ii) a case of high conductivity beams. For both scenarios, two types of concrete degradation of the 1BMA vault have been studied. First, degradation of different elements of the vault (e.g. concrete floor, concrete walls, etc) in all the compartments has been considered. Thereafter, alternative situations where only some of the waste compartments of the vault are degraded due to preferential flow paths from the SFR 1 repository-scale model have been analyzed.

For the case of low conductivity beams, the results of the vault elements degradation indicate that concrete degradation has a moderate impact on the total flow in the 1BMA vault. The highest increments in the total tunnel flow occur in the cases considering the concrete floor degradation. In contrast, significant effects of concrete degradation are predicted on the flow profiles in the waste compartments and the total flow through the waste domain. The largest differences with respect to the Base case are found for shoreline position 2. The results have shown that the degradation of concrete vault elements induces an internal redistribution of the flow. According to the model, the degradation of the concrete of the inner and outer walls of the waste compartments has the highest impact on total flow through the waste domain. Degradation of lids, floor, and outer walls is the second most unfavorable situation. The cases of the degradation of one outer concrete wall and of both outer concrete walls have the lowest impact compared to the other degradation cases.

The degradation of concrete in a given compartment has a moderate impact on the total flow through the 1BMA vault. Shoreline position 1 is the most sensitive to the increase of tunnel flow. The two cases considering the degradation of the compartments affected by fracture areas result in the highest tunnel flows. In general, the effect of the compartment degradation scenarios is a redistribution of the flow within the vault. The waste flow increases locally in the degraded waste compartments. This increase in flow is accompanied by a reduction in the waste flow in the adjacent intact compartments.

For the case of high conductivity beams, the concrete degradation does not affect the total tunnel flow but it has a significant impact on the flow through the waste domain and, consequently, on the flow redistribution within the 1BMA vault. The cases of vault element degradation studied in this work show that the degradation of elements in contact with the backfill plays an important role in the redistribution of flow within the vault. The hydraulic conductivity contrast between degraded elements and backfill is significantly reduced by concrete degradation, which enhances the water exchange between the waste and fractures. The degradation of the floor, inner and outer walls has a major impact on the total flow through the waste domain. In general, flow rates through other vault elements are almost unaffected by concrete degradation, with some few exceptions where waste flow increase is compensated by a reduction of flow through other elements.

The compartment-level concrete degradation also results in a redistribution of the flow within the vault where the waste flow increases locally in the degraded waste compartments whereas the waste flow is reduced in the adjacent compartments. The local waste flow increases up to four orders of magnitude for the complete degradation cases in shoreline positions 2 and 3. The total flow through the gravel area also decreases to compensate the increase in the degraded compartments. The effect of compartment degradation on the tunnel flow is negligible. For all shoreline positions the worst case scenario corresponds to the complete concrete degradation state of compartments affected by fractures.

The Silo submodel has been used to setup a local mass transport model under steady-state conditions in order to calculate mass fluxes for this repository part. For shoreline position 1, solute transport around the Silo is diffusion dominated and the extension of the solute plume is relatively large. Solute transport is dominated by advection for shorelines positions 2 and 3. In these cases, the solute plume is narrower around the Silo compared to shoreline position 1, but extends upwards and downwards, conditioned by the most permeable fracture zones. Solute concentrations resulting from steady-state conditions lack information about residence times and species velocities. Therefore, particle-tracking simulations have been performed to increase the understanding of those additional aspects. These particles are transported exclusively by advection. A simulation time of 1000 years has been considered. For the advective-dominated cases there is a clear correlation between the isosurfaces and the corresponding particle footprints. That means the concentration plume takes less than 1000 years to reach a steady state situation. For shoreline position 1, where diffusion dominates, the particle tracking simulation shows that a particle leaving the Silo will be almost in the same location after 1000 years.

To have an estimate of the mass release rate, two different indicators have been analyzed: the water outflow rate, denoted as Q_{out}, and the equivalent flow rate, denoted as Q_{eq}. Although variables Q_{eq} and Q_{out} are calculated using different types of data and assumptions, both result in values of the same order of magnitude for shoreline position 1. This result is to be expected since the analytical solution to obtain Q_{eq} is based on assumptions that are met for shoreline position 1, that is, a vertical flow direction and a diffusion dominated system. Q_{eq} and Q_{out} differ by up to an order of magnitude for shoreline positions 2 and 3. In these cases, the flow field does not meet the assumptions for which the Q_{eq} concept is defined. Therefore, in these cases Q_{out} seems to be a more accurate variable to estimate a mass flow of solute released from the Silo.

Sammanfattning

Elva delmodeller av enskilda förvarssalar har extraherats från flödesmodeller över SFR 1 och SFR 3. Flödesfält för ett basfall, omfattande tre strandlinjepositioner, har beräknats i COMSOL. Flöden genom förvarssalar beräknade med delmodellerna har jämförts med motsvarande resultat från flödesmodeller över SFR 1 och SFR 3. Skillnaderna i beräknade flöden varierar mellan 0–26%. Känsligheten hos beräknade resultat som funktion av meshstorlek har analyserats för delmodellen över 1BMA. Resultaten var i huvudsak opåverkades av gradvis förfinad meshning. Det relativa felet mellan två stegvis förfinade mesh var mindre än 2%.

Delmodellen över 1BMA har sedan använts för att studera effekten av betongdegradering på flödet genom förvarsdelen. På grund av osäkerhet rörande den effektiva hydrauliska konduktiviteten hos grundläggingsbalkarna in 1BMA har två fall undersökts: (i) ett fall där balkarna har samma låga hydrauliska konduktivitet som övrig konstruktionsbetong i förvaret; (ii) ett fall där balkarna har tillskrivits en hög hydraulisk konduktivitet. För båda fall har två scenarion för degradering studerats. Det ena betraktar degradering av förvarselement, exempelvis betongväggar och golv, vilka påverkar alla förvarsfack samtidigt. Det andra scenariot betraktar fackvis degradering som ett resultat av föredragna flödesvägar genom SFR1.

I fallet med grundläggingsbalkar med låg hydraulisk konduktivitet visar resultaten att elementvis degradering har en måttlig påverkan på det totala flödet genom 1BMA. Störst påverkan på det totala flödet uppstår vi degradering av golvet. Däremot observeras väsentliga skillnader på fördelningen av flödet mellan fack och på det totala flödet genom avfallet. Strandlinjeposition 2 uppvisar störst skillnader i flöden jämfört med basfallet. Modellen visar att degradering av yttre och inre väggar har störst påverkan på det totala flödet genom avfallet. Degradering av golv, tak och ytterväggar har näst störst påverkan. Fallen där en eller båda ytterväggar degraderar har minst påverkan jämfört med andra beräkningsfall.

Fackvis degradering av betong har en måttlig påverkan på det totala flödet genom 1BMA. Strandlinjeposition 1 är mest känsligt i detta avseende. Degradering av fack i närheten av sprickzoner resulterar i största ökningen av flöden genom förvarssalen. Generellt leder fackvis degradering till en omfördelning av flödet. Flöden genom avfallet ökar i degraderade fack, åtföljt av ett minskande flöde genom avfallet i angränsade fack.

I fallet med grundläggingsbalkar med hög hydraulisk konduktivitet påverkar betongdegraderingen ej det totala flödet genom förvarssalen. Däremot har den stor påverkan på storleken av avfallsflödet i BMA och på flödesfördelning mellan fack. För elementvis betongdegradering visar resultat att de element som står i kontakt med förvarets återfyllnad har stor betydelse. Degradering minskar kontrasten mellan element och återfyllnad och ökar därmed utbytet mellan vatten i sprickzoner och avfallet. Degradering av golv, inner- och ytterväggar har stor påverkan på flödet genom avfallet. I allmänhet påverkas flödet i andra förvarselement endast litet av betongdegradering med några få undantag, där flödet genom avfallet omfördelas.

Fackvis betongdegradering leder också till en omfördelning av flödet i förvarssalen. Flöden genom avfallet ökar i degraderade fack samtidigt som det avtar i angränsade fack. Det lokala flödet genom avfallet kan öka med upp till fyra storleksordningar för fullständigt degraderade fack. Det totala flödet genom återfyllnaden avtar samtidigt. Effekten av fackvis degradering på det totala tunnelflödet är försumbart. För alla strandlinjepositioner så är påverkan störst för fullständigt degraderade fack närheten av sprickzoner.

En delmodell över Silon har använts för att simulera lokal masstransport under stationära förhållanden, med målet att beräkna massflux från förvarsdelen. För strandlinjeposition 1 domineras masstransporten runt Silon av diffusion och utbredningen av den plym av lösta ämnen som transporteras från förvarsdelen är relativt stor. För strandlinje position 2 och 3 domineras masstransporten av advektion. Plymen av lösta ämnen är mindre utbredd och påverkas av flödet i permeabla sprickzoner. Koncentrationsfälten från de stationära simuleringarna saknar information om uppehållstid och hastighet hos transporterade ämnen. Partikelspårning har använts för att bättre förstå dessa aspekter. I dessa simuleringar transporteras partiklar enbart av det advektiva flödet, detta under tusen år. För de fall då advektiv transport

dominerar så korrelerar beräknade partikelspår och koncentrationsfält. Det betyder att det tar mindre än tusen år för utvecklingen av masstransporten att nå ett stationärt tillstånd. För strandlinjeposition 1, där diffusion dominerar, så visar simulering av partikelspår att partiklar som lämnat Silon kommer att befinna sig på näst intill samma plats efter 1000 år.

Två olika indikatorer på hastigheten för uttransport av massa från Silon har analyserats: Utflödeshastigheten av vatten, kallad Q_{out}, samt den ekvivalenta flödeshastigheten, Q_{eq}. Även om Q_{eq} och Q_{out} beräknas utifrån olika data och utifrån olika antaganden så är de av samma storleksordning för strandlinjeposition 1. Detta är förväntat då den analytiska lösningen för att beräkna Q_{eq} grundar sig på antaganden som uppfylls för strandlinjeposition 1, nämligen ett vertikalt riktat flöde och att diffusion dominerar masstransporten. Q_{eq} och Q_{out} skiljer sig däremot med upp till en storleksordning för strandlinjepositioner 2 och 3. I dessa fall uppfylls inte de antaganden som förutsätts för beräkning av Q_{eq}. Därför framstår Q_{out} som en mer noggrann variabel för att i dessa fall utvärdera uttransporten av massa från Silon.

Contents

1 Background and motivation

In earlier work, numerical models set up and solved in COMSOL Multiphysics were developed to simulate the hydrological behavior of the near-field of the SFR (Abarca et al. 2013). This was achieved by the implementation of two larger models, one for the SFR 1 and another for the repository extension, SFR 3. The main objectives of the modelling were to increase the understanding of the near-field hydrology and to generate consistent input data to radionuclide transport calculations.

During the modelling work of the SFR repository, some specific questions were raised concerning (1) the effects and extent of concrete degradation of the 1BMA structure and (2) the transport of solutes around the Silo. To answer those questions, more detailed investigations of individual vaults were required. Vault scale models were created to handle the large numbers of simulations required for detailed investigations and to provide useful tools for future modelling activities.

2 Objectives

The main objectives of the present work are:

1. To implement a set of separate submodels of all the vaults of the SFR 1 and the SFR 3.
2. To investigate the degradation of concrete barriers in the 1BMA, treating the degradation of individual vault elements (e.g. the concrete floor, or the outer and inner walls) and comparments separately.
3. To calculate an equivalent mass flux around the Silo based on a local mass transport model of the Silo under steady-state conditions.

3 Methodology

Eleven separate vault-scale submodels have been extracted from the geometry of the SFR 1 and SFR 3 repository-scale models. The boundary conditions for these submodels are extracted from the Base case results of the SFR 1 and SFR 3 repository-scale models for shoreline positions 1, 2, and 3, as defined in Abarca et al. (2013). The Base case refers to a given set of hydraulic properties for the different barriers (Table 3-1 and Table 3-2) and to a given conductivity field for the rock. The rock conductivity field corresponds with the Base_Case1_DFN_R85 in Odén et al. (2014). The hydro-geological model is based on the combined regional and local geological model version 1.0 (Curtis et al. 2011, SKB 2013), containing all the modeled deformation zones Figure 3-1). Three different descriptions of the top boundary in DarcyTools serve as input to produce the boundary conditions for the repository-scale models. These descriptions outline the time-evolution of the groundwater flow and correspond to three different positions of the repository relative to the shoreline of the sea:

- Shoreline position 1 (in the global warming and early periglacial climate cases, this position would correspond to the situation at 2000 AD): corresponds to a submerged repository.
- Shoreline position 2 (in the global warming and early periglacial climate cases, this position would correspond to the situation at 3000 AD): corresponds to an intermediate case in which the shoreline is above the repository.
- Shoreline position 3 (in the global warming and early periglacial climate cases, this position would correspond to the situation at 5000 AD): corresponds to land conditions dominating above the repository.

Table 3-1. Hydraulic conductivity values for the materials in the SFR 1 repository considered in the Base Case.

Repository components	Materials		K (m/s)
Tunnels	Backfill		1.00E–03
Vaults	Construction concrete		8.30E–10
	Concrete Backfill (BTF vaults)		8.30E–09
	1BMA concrete beams		8.30E–10
	Waste 1–2BTF vaults	K_x*	3.79E–09
		K_y*	6.65E–09
		K_z*	6.79E–09
	Waste 1BLA		1.00E–03
	Waste (BMA)		8.30E–07
	Sand layer		1.00E–07
Silo	Top layer (90% sand, 10% bentonite)		1.00E–09
	Bottom layer (90% sand, 10% bentonite)		1.00E–09
	Waste		8.30E–07
	Silo concrete lid with gas evacuation pipes	K_x=K_y	8.30E–10
		K_z	3.00E–07
	Silo Bentonite Walls		1.54E–12·z(m) + 2.11E–10
Plugs	Structural plug		1.00E–06
	Sealed hydraulic bentonite section		1.00E–12

* homogenized values calculated with formulation in Appendix B of Holmén and Stigsson (2001), based on vault dimensions, configuration, and waste and concrete material properties.

Table 3-2. Hydraulic conductivity values for the materials in the SFR 3 repository.

Materials	K (m/s)
Concrete	8.30E–10
Backfill	1.00E–03
BRT grouted waste	8.30E–09
2BMA waste	8.30E–07
Sand layer	1.00E–07
2BMA gravel layer	1.00E–03

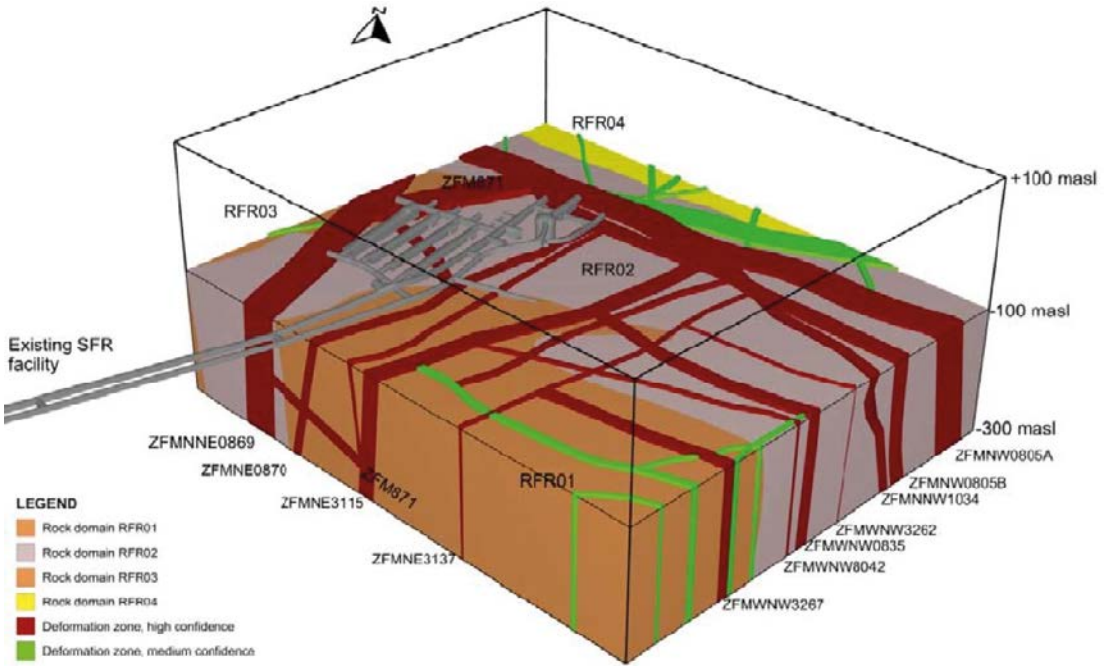

Figure 3-1. *Rock domains and deformation zones included in the SFR local model, version 1.0 Adapted from Curtis et al. (2011).*

The submodels are implemented in separate COMSOL files and run for the Base case (shoreline positions 1, 2 and 3). As a verification of the correct implementation, the results of the vault-scale submodels are postprocessed and compared with the repository-scale model results in terms of the flow rates within the vault. Thereafter, the 1BMA submodel has been employed to study the effect of concrete degradation on the flow rates in the vault. As explained in Abarca et al. (2013), it is difficult to estimate the effective conductivity of the concrete beams/drainage system beneath concrete floor of the 1BMA. The concrete beams can be degraded and the drainage system may be clogged. To account for this uncertainty we have considered two limiting cases: (i) A case with a low effective conductivity of the beams/drains system, equal to the conductivity of structural concrete. (ii) A case with high hydraulic conductivity beams equal to the conductivity of the highly permeable backfill in the vault. For both cases, two types of concrete degradation have been studied. First, we simulate the degradation of the different vault elements (e.g. concrete floor, concrete walls, etc) in all the compartments. Thereafter, we analyze some alternative situations where only the concrete elements of selected waste compartments are degraded. In another modelling excercise, the Silo submodel has been used to setup a local mass transport model under steady-state conditions in order to calculate an equivalent mass flux.

3.1 Vault-scale submodels

The geometry of each vault-scale submodel has been extracted from the repository-scale models according to the following criteria:

- Each submodel contains exclusively one vault.
- A part of the bedrock surrounding each vault is included in the submodel to avoid boundary effects as the hydraulic properties of the vault are modified. The extent of the submodel bedrock domain is set so that the intersection with the access tunnels is minimized. It also minimizes the number of cropping 2D planes to facilitate the extraction of the boundary conditions.
- The vertical planes of the bedrock boundaries are located at mid-distance between two adjacent vaults. This means that two adjacent vault-scale models share the same boundary (Figure 3-2).
- The distances "vault roof – top model boundary" and "vault floor – bottom model boundary" are equal or greater than half the lateral spacing between vaults.
- In the case of the Silo, the rock boundaries have been extended further from the vault to enable the simulation of solutes being transported from the Silo.

The resulting eleven vault-scale submodel domains are illustrated in Figure 3-2. The dimensions of the vaults together with vertex coordinates are presented in Table 3-3. Note that the reference coordinate system (position and orientation) used for the model domains is consistent with the system used in the SDM report (SKB 2013).

The model domains are discretized into meshes of tetrahedral quadratic finite elements (Figure 3-3). The total number of elements per model domain is presented in Table 3-4 together with the number of elements to represent each vault, that is, excluding the rock domain. The geometric representation of the SFR 3 vaults is less complex than for the SFR 1 case, resulting in smaller meshes.

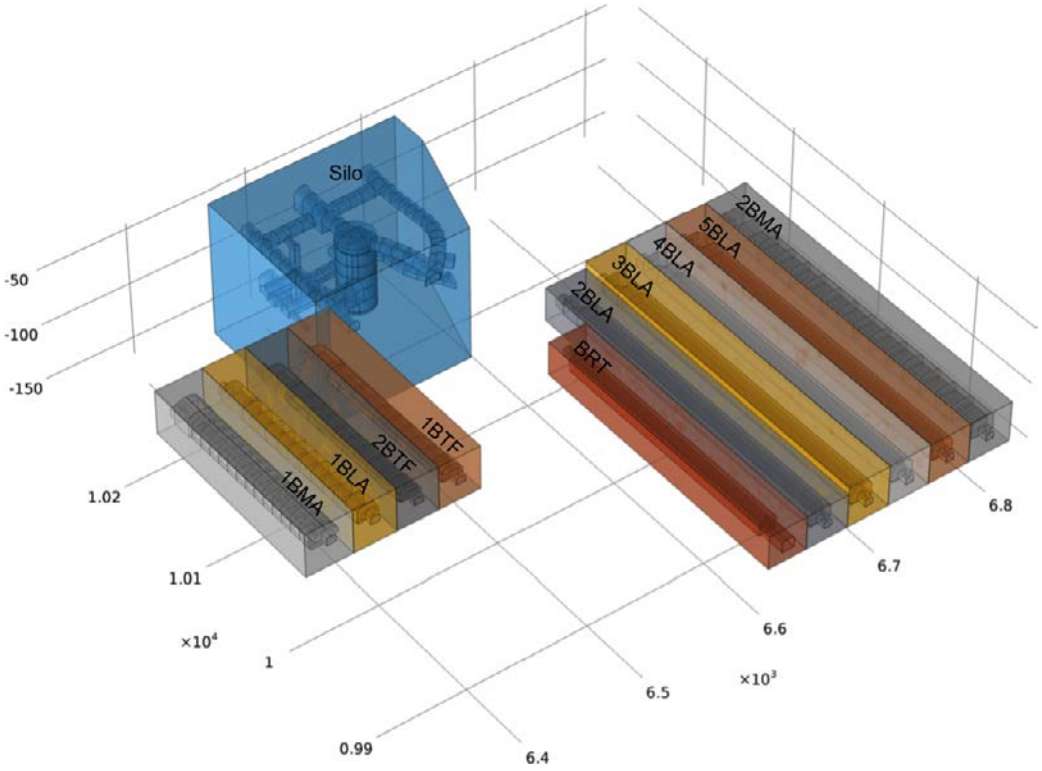

Figure 3-2. *SFR submodel domains considered in the simulations.*

Table 3-3. Dimensions of the SFR vault submodel domains and coordinates of one corner.

	Length	Width	Height	X_{min}	Y_{min}	Z_{min}
1BMA	175	38.56	38.4	6,326.88	9,977	–96
1BLA	175	35.21	38.4	6,365.44	9,977	–96
2BTF	175	34.48	38.4	6,400.66	9,977	–96
1BTF	175	34.4	38.4	6,435.14	9,977	–96
BRT	242	32.83	30	6,606.16	9,839	–144
2BLA	292	35.77	30	6,638.99	9,839	–144
3BLA	292	35.81	36	6,674.76	9,839	–144
4BLA	292	35.79	36	6,710.56	9,839	–144
5BLA	292	35.73	36	6,746.36	9,839	–144
2BMA	292	36.94	36	6,782.08	9,839	–144

Table 3-4. Total number of quadratic elements in the submodel domains and vaults.

	Total number of elements	Elements in vault	Degrees of freedom	Elements in vault (repository-scale model)
1BMA*	7,646,290	6,100,709	10,216,409	2,605,733
1BLA	5,337,585	3,698,085	7,127,663	584,019
2BTF	6,161,047	4,321,898	8,227,246	618,385
1BTF	5,936,364	4,172,849	7,929,726	618,579
Silo	1,779,468	833,156	2,583,155	785,572
BRT	1,850,169	795,321	2,475,976	851,717
2BLA	531,919	204,254	714,589	70,652
3BLA	583,251	238,245	783,673	70,413
4BLA	569,452	224,577	765,270	70,283
5BLA	585,912	237,849	787,245	70,658
2BMA	4,422,490	2,771,176	5,912,478	3,311,767

*Comparison is made with mesh B (see Table 4-1).

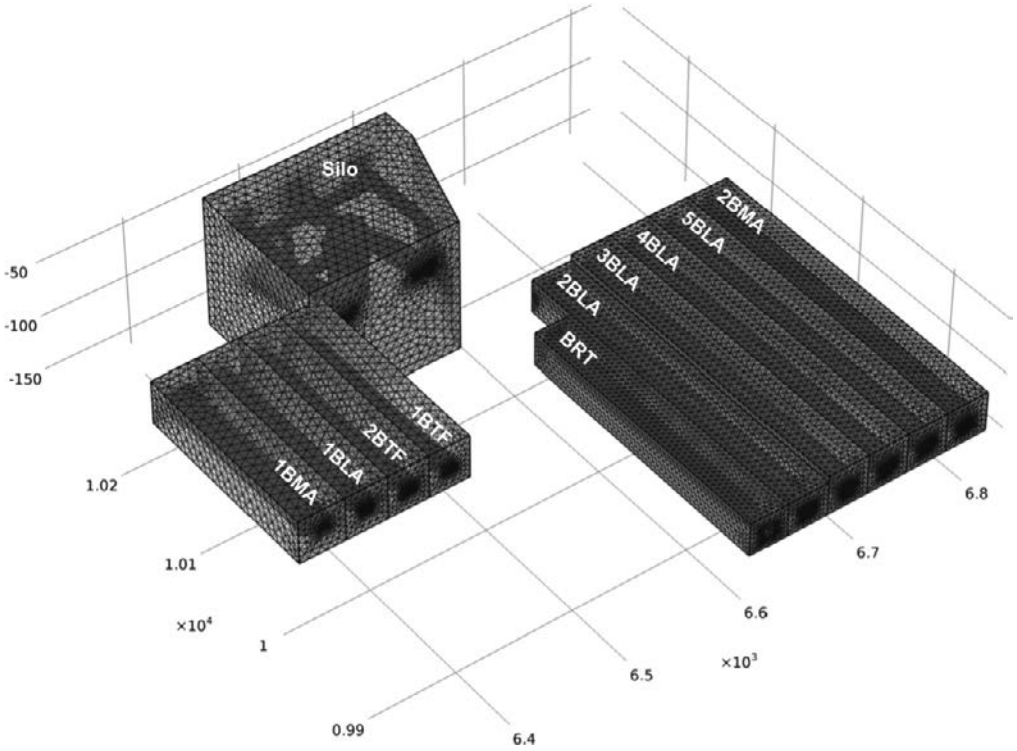

Figure 3-3. Composition of the vault-scale model meshes.

3.2 Boundary conditions and rock properties

The boundary conditions for each submodel are extracted from the results of the Base case of the repository-scale models, as defined in Abarca et al. (2013). A set of planes, shown in Figure 3-4 for SFR 3, containing all the submodel boundaries are defined to extract the calculated driving pressure from the Base case for shoreline positions 1, 2, and 3.

The rock hydraulic conductivity field is imported into the COMSOL submodels using the same methodology than for the repository-scale models (see Abarca et al. 2013). A subset of the rock conductivity field is extracted directly from the DarcyTools model by means of the iDC interface, and is then interpolated with a linear interpolation method onto the COMSOL finite element mesh. The hydrogeological model is based on the local geological model 1.0 presented in Curtis et al. (2011) and SKB (2013). The rock conductivity field corresponds to the Case 1 (Base_Case1_DFN_R85) of the regional-scale model in DarcyTools, which is presented in more detail in Odén et al. (2014).

3.3 Validation: flow rate comparison with the repository-scale model results

A set of simulations with all the vault-scale models considering the parameterization of the Base case have been performed to compare the results with the SFR 1 and SFR 3 repository-scale models. The results of the vault-scale models are then post-processed to verify that the pressure boundary conditions reproduce similar flow rates as with the repository-scale models.

The results of the comparison are presented in Table 3-5 and Table 3-6 for the SFR 1 and SFR 3 vaults, respectively. Overall, the differences with the repository-scale models are in the range 0–26%. In more detail, the differences are larger in the SFR 1 submodels as compared with the SFR 3 submodels. In the latter case, the range reduces to 0–3%, except for the 2BMA normalized flow in the waste, for which differences of up to 24% are observed for shoreline position 3. The reasons why the differences are smaller in the SFR 3 case are related to the simplicity of the geometry of the different vaults and the simpler division of the vault domain for computing flow rates as compared with the SFR 1 model.

In the case of the SFR 1 submodels, the differences are smaller than 10% for all the vaults and shoreline positions, except for the Silo. In this case, the differences increase from 8% for shoreline position 1, to more than 20% for shoreline position 3. The higher values with respect to the rest of the vaults may be due to the curved geometries where flow rates are computed. To confirm this, flow rates in the waste have been computed in planar surfaces of an inner part of the waste volume, as defined in Abarca et al. (2013, Figure 3-15), and compared with similar flow rates from the SFR 1 model. The results indicate a difference of around 10% in this case, consistent with the differences in the rest of the vaults.

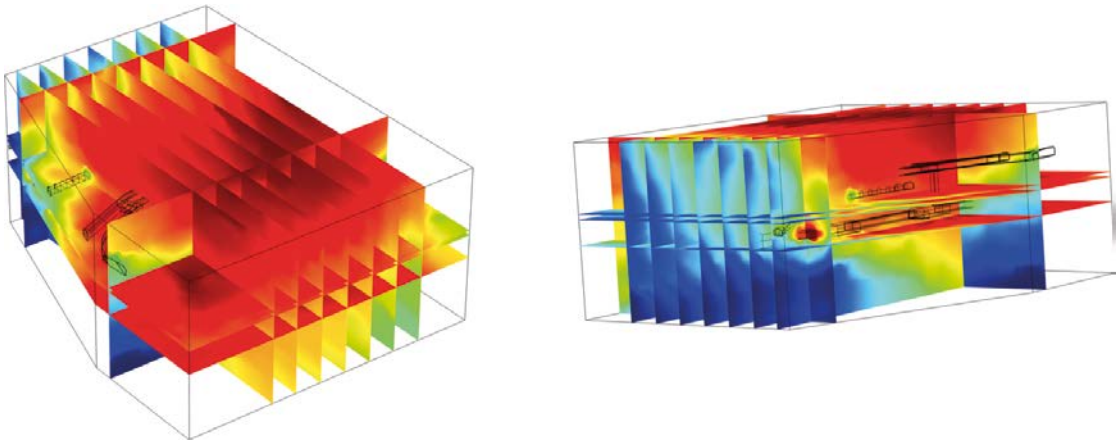

Figure 3-4. *Set of planes used to extract the results of the SFR 3 repository-scale model to impose as boundary conditions in the SFR 3 vault submodels.*

Table 3-5. Flow rates through tunnels and waste domains for the different SFR 1 vaults and comparison with the flow rates computed with the repository-scale model (negative values indicate lower flow rates in the submodel compared to the SFR 1 model).

		Shoreline position 1		Shoreline position 2		Shoreline position 3	
		Total flow ($m^3 \cdot year^{-1}$)	Difference	Total flow ($m^3 \cdot year^{-1}$)	Difference	Total flow ($m^3 \cdot year^{-1}$)	Difference
Vault	1BMA	0.041	–9.7%	28.846	–5.1%	62.348	–6.3%
	1BLA	0.126	–5.2%	63.259	–3.0%	143.319	–2.4%
	1BTF	0.027	–2.8%	7.265	–6.9%	16.428	–8.5%
	2BTF	0.048	1.8%	19.447	–2.2%	40.293	–7.3%
	Silo	0.004	–8.4%	0.621	–16.3%	1.164	–26.3%
Waste	1BMA	0.007	–10.9%	1.180	–7.4%	3.148	–8.2%
	1BLA	0.117	–4.6%	59.314	–3.3%	135.548	–2.5%
	1BTF	0.008	–9.6%	1.570	–8.5%	3.156	–9.8%
	2BTF	0.008	–9.4%	2.204	–9.0%	4.095	–10.4%
	Silo	0.004	–8.7%	0.572	–16.1%	1.077	–20.6%

Table 3-6. Flow rates through tunnels, waste domains, and loading areas for the different SFR 3 vaults and comparison with the flow rates computed with the repository-scale model (negative values indicate lower flow rates in the submodel compared to the SFR 3 model).

		Shoreline position 1		Shoreline position 2		Shoreline position 3	
		Total flow ($m^3 \cdot year^{-1}$)	Difference	Total flow ($m^3 \cdot year^{-1}$)	Difference	Total flow ($m^3 \cdot year^{-1}$)	Difference
Vault	2BLA	0.12	–0.8%	16.27	0.1%	27.12	0.1%
	3BLA	0.08	–3.0%	19.67	0.4%	30.36	0.8%
	4BLA	0.09	–1.4%	14.00	1.0%	23.79	0.2%
	5BLA	0.10	–0.3%	12.85	–1.3%	20.25	–1.4%
	BRT	0.07	0.5%	11.32	0.1%	19.97	0.1%
	2BMA	0.30	–0.5%	24.64	0.8%	31.37	1.0%
Waste	2BLA	0.09	–0.04%	12.31	–0.2%	20.30	–0.3%
	3BLA	0.06	–1.1%	13.42	–0.3%	20.03	–0.3%
	4BLA	0.07	–0.8%	8.64	–0.6%	15.37	–0.6%
	5BLA	0.07	–0.01%	9.26	–1.2%	14.76	–1.2%
	BRT	0.01	1.2%	1.59	0.6%	2.84	0.5%
	2BMA*	0.000002	–3.7%	0.00018	–16.2%	0.0002	–24.2%
Loading area	2BLA	0.06	1.6%	7.91	1.4%	14.99	1.2%
	3BLA	0.02	0.3%	9.98	0.2%	16.97	0.05%
	4BLA	0.03	–0.8%	10.94	0.4%	17.26	0.5%
	5BLA	0.03	0.1%	5.76	0.01%	8.43	0.1%
	2BMA	0.02	–0.3%	3.99	–0.9%	5.22	–1.0%

The waste flow for the 2BMA* corresponds to the normalized flow per waste compartment.

4 1BMA concrete degradation with low conductivity beams

Two sets of degradation cases for the 1BMA vault have been studied for the scenario of low conductivity beams. In a first set the degradation of different vault elements (e.g. concrete floor, concrete walls, etc) has been considered. In a second set, only some of the waste compartments of the vault are assumed to degrade due to preferential flow paths from the SFR 1 repository-scale model. As a preliminary step, a mesh sensitivity analysis has been carried out. This is also motivated by the fact that degradation of different parts of the 1BMA vault could lead to more complex flow conditions at a detailed submodel scale, requiring a finer discretization. This sensitivity analysis also allowed evaluating the consistency of the boundary conditions and the radius of influence that result from the submodels set up, as presented in Section 3.

4.1 Mesh sensitivity analysis

The objective of the mesh sensitivity analysis is to ensure that the results of the numerical model are not mesh dependent to any significant extent. Starting from the finite element mesh of the 1BMA in the repository-scale SFR 1 model (which has been imported into the submodel), the mesh has been refined to increase the number of elements in the concrete domain. The convergence of the solution is analyzed with the ratio Q_{waste}/Q_{vault}, where Q_{waste} and Q_{vault} are the total flow rates through the waste and vault, respectively. The criterion that has been followed is to refine the mesh until Q_{waste}/Q_{vault} converges to a constant value or until the mesh becomes too large. Figure 4-1 shows the domain considered for the 1BMA vault submodel. The simulation case corresponds to the Base case defined in (Abarca et al. 2013) and has been calculated with the three shoreline positions under study.

In addition to the repository-scale 1BMA mesh, a total of five finite element meshes have been generated, labeled as meshes A, B, C, D, and E, respectively. Basic information on the mesh refinement in each of these is summarized in Table 4-1. Mesh A is the coarsest mesh, similar to the 1BMA mesh of the SFR 1 repository-scale model. Mesh B doubles the number of elements with respect to mesh A, within the vault and also the total number of elements. Mesh C is even finer than the mesh B, with a 20% increase in total number of elements and within the vault. It also includes at least 2 finite elements along the thickness of all the concrete walls of the 1BMA vault (see Figure 4-2). Mesh D is finer than mesh C (10% increase in total number of elements) but the concrete walls of the 1BMA vault are discretized with only one finite element across their thickness. Finally, mesh E is the most refined mesh, at least 2 finite elements along the thickness of all the concrete walls and a 60% increase in the total number of elements compared to mesh D, although with practically the same number of elements in the vault. The meshes were generated as a sequence of submeshes over different subdomains of the model. The finite element size was controlled by adjusting the default parameters with additional custom options available in COMSOL. For instance, mesh C is composed of 6 submeshes: one for the rock domain; one for the waste domain; one for the lids, floor, inner, and outer concrete walls of the waste compartments; one for the east and west backfill gravel; one for the top and bottom backfill gravel; and one for the plugs.

In the Base case, the hydraulic conductivity of the concrete of the different barriers of the vault is set to $8.3 \cdot 10^{-10}$ m·s^{-1}, while the hydraulic conductivity of the backfill is set to 10^{-3} m·s^{-1}. The convergence of the solution is assessed by comparing (1) the flow rates through the different materials of the 1BMA compartments, and (2) the Q_{waste}/Q_{vault} ratio obtained with each mesh for shoreline positions 1, 2 and 3. In addition, the solutions have been compared with the results of the SFR 1 repository-scale model.

Table 4-1. Total number of quadratic elements of the meshes considered in the mesh sensitivity analysis of the 1BMA submodel.

FE mesh	Total number of elements	Elements in vault	At least two elements along wall thickness
SFR 1 model	–	2,611,715	No
A	3,786,364	2,987,841	No
B	7,646,290	6,100,709	No
C	9,162,206	7,523,272	Yes
D	10,037,882	8,587,197	No
E	15,910,442	8,587,097	Yes

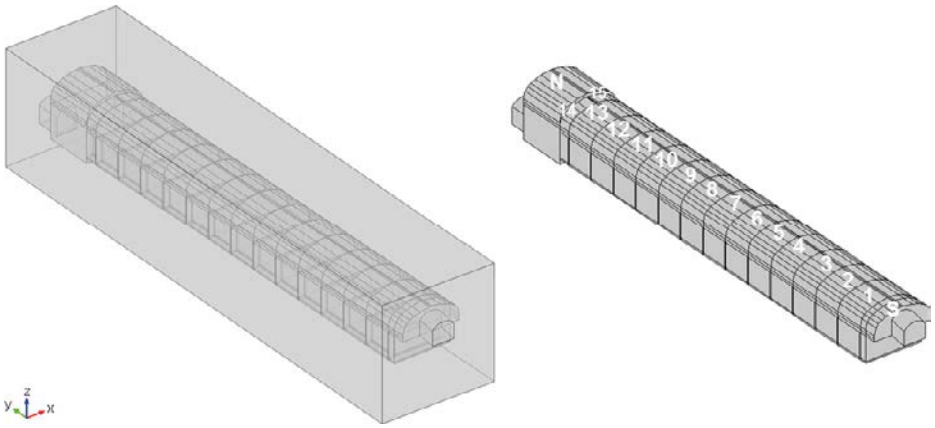

Figure 4-1. *Domain used in the flow simulations of the 1BMA submodel (left) and numbering of compartments, where S and N refer to the south and north loading areas (right).*

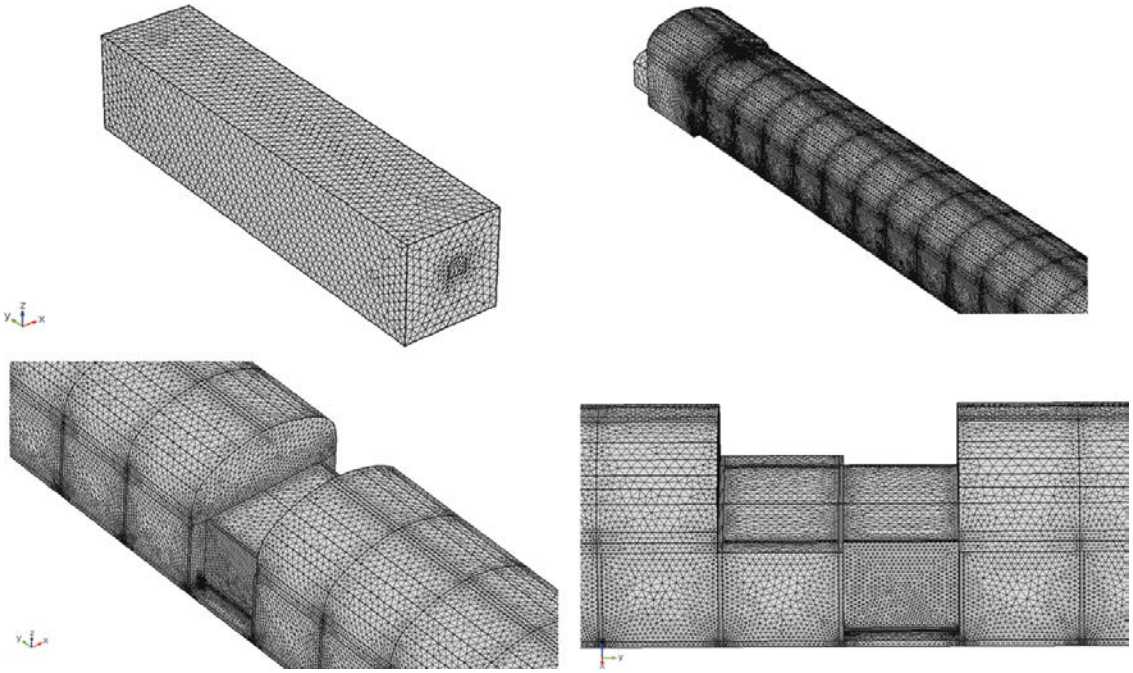

Figure 4-2. *Different views of mesh C, which has been selected from the mesh sensitivity analysis as the most appropriate for the concrete degradation simulations.*

The results of the flow rates through the different parts of the 1BMA vault are presented in Figure 4-3 to Figure 4-7. As a general trend, the flow rates calculated with the different meshes of the 1BMA submodel present a slight departure from the SFR 1 repository-scale model results. In particular, flow rates through the waste and bottom gravel compartments show almost no influence by the mesh (see Figure 4-3 and Figure 4-5). Still, a deviation from the repository-scale model is observed in the flow rate through compartments 1 to 9 in the top gravel for shoreline position 1 (see Figure 4-4). Notably, the difference between solutions obtained with different meshes is very small, except in the flow rates through compartments 1 to 7 of the west and east gravels for shoreline position 1 (see Figure 4-6 and Figure 4-7). In that case, an oscillation of the flow within these compartments is displayed by the solution obtained with the finer meshes.

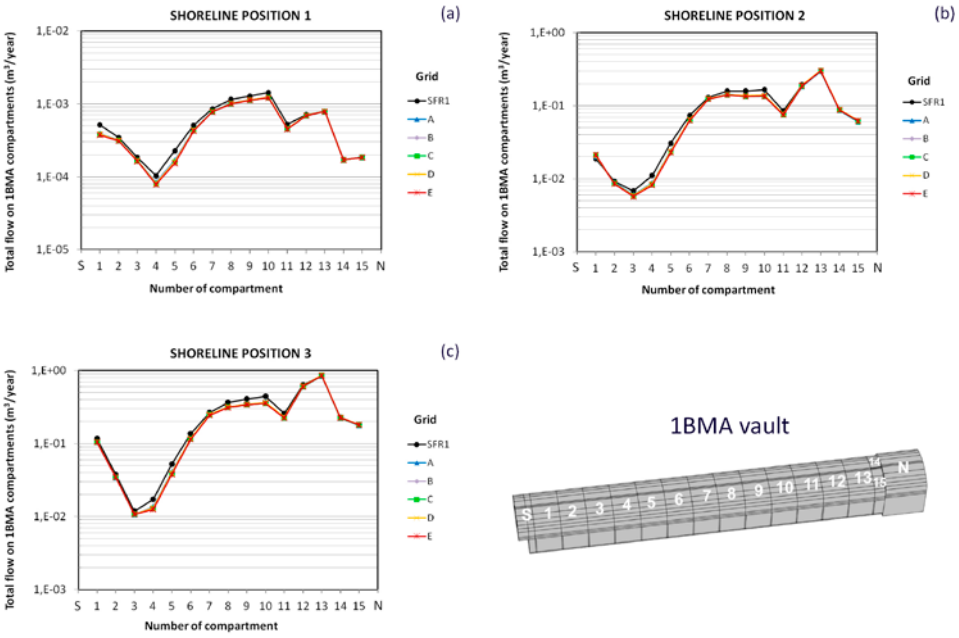

Figure 4-3. *Flow rates through the waste compartments simulated with different meshes and compared with the SFR 1 repository-scale model solution.*

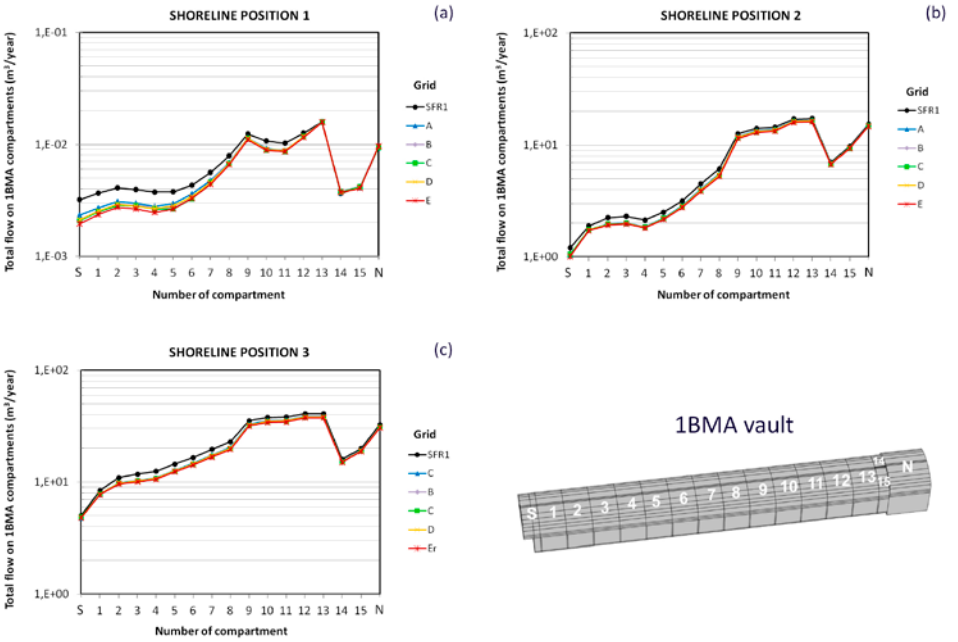

Figure 4-4. *Flow rates through the top gravel simulated with different meshes and compared with the SFR 1 repository-scale model solution.*

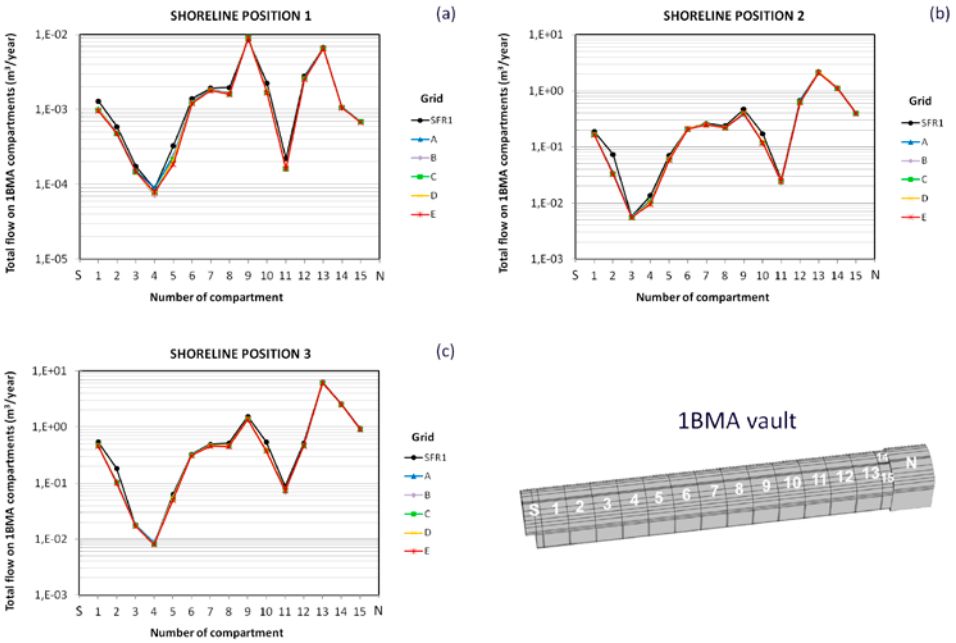

Figure 4-5. *Flow rates through the bottom gravel simulated with different meshes and compared with the SFR 1 repository-scale model solution.*

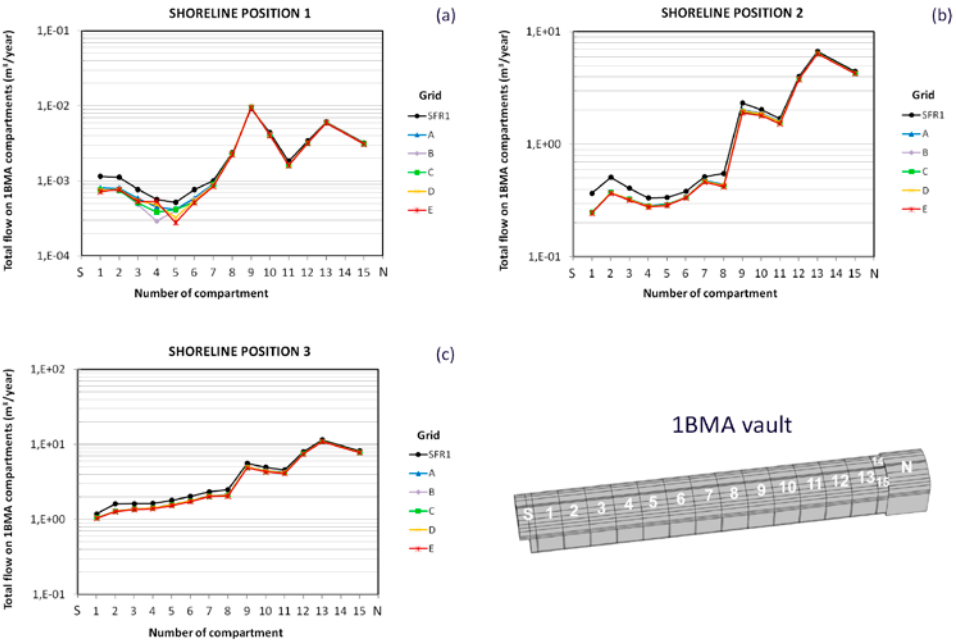

Figure 4-6. *Flow rates through the east gravel simulated with different meshes and compared with the SFR 1 repository-scale model solution.*

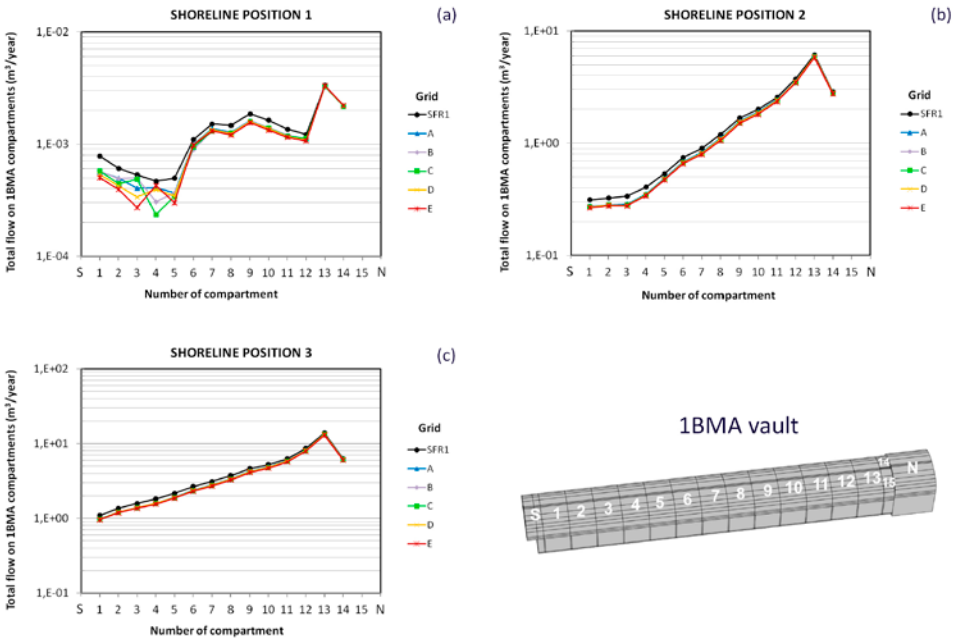

Figure 4-7. *Flow rates through the west gravel simulated with different meshes and compared with the SFR 1 repository-scale model solution.*

The total flow rates through the vault and through the waste obtained with each mesh are summarized in Table 4-2 and also illustrated in Figure 4-8. The relative difference with respect to the flow rate values obtained in the SFR 1 repository-scale model is also included. On average, the total flow rates through the vault and waste are between 7.2 and 8.9% lower than the SFR 1 repository-scale model, respectively. In general, the total flow rates decrease as the mesh is refined. Convergence of the solution seems to be reached with most of the meshes. Relatively higher differences are found for shoreline position 1, in part due to the small magnitude of the flow.

The results of the ratio Q_{waste}/Q_{vault} for the different meshes are shown in Figure 4-9. It may be observed that there is almost no influence of the mesh refinement on this ratio. The relative error, calculated as the difference between the solutions obtained with successive finer meshes, is lower than 2%.

Table 4-2. Total flow rates through the tunnel and waste obtained with different meshes.

		Shoreline position 1		Shoreline position 2		Shoreline position 3	
	Mesh	Total flow ($m^3 \cdot year^{-1}$)	Difference	Total flow ($m^3 \cdot year^{-1}$)	Difference	Total flow ($m^3 \cdot year^{-1}$)	Difference
Vault	SFR 1	0.046	–	30.38	–	66.55	–
	A	0.042	–7.8%	29.26	–3.7%	63.20	–5.0%
	B	0.041	–9.7%	28.85	–5.1%	62.35	–6.3%
	C	0.041	–10.1%	28.64	–5.7%	61.90	–7.0%
	D	0.041	–9.5%	28.77	–5.3%	62.19	–6.5%
	E	0.040	–11.2%	28.33	–6.8%	61.13	–8.1%
Waste	SFR 1	0.008	–	1.27	–	3.43	–
	A	0.007	–10.6%	1.18	–7.5%	3.15	–8.2%
	B	0.007	–10.9%	1.18	–7.4%	3.15	–8.2%
	C	0.007	–11.7%	1.17	–7.9%	3.13	–8.7%
	D	0.007	–11.0%	1.20	–5.8%	3.19	–7.1%
	E*	0.007	–12.3%	1.18	–7.7%	3.13	–8.7%

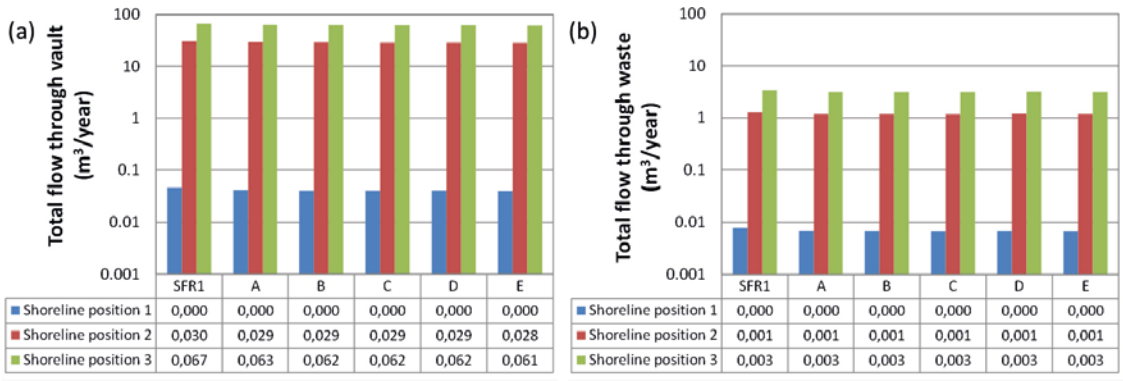

	SFR1	A	B	C	D	E
Shoreline position 1	0,000	0,000	0,000	0,000	0,000	0,000
Shoreline position 2	0,030	0,029	0,029	0,029	0,029	0,028
Shoreline position 3	0,067	0,063	0,062	0,062	0,062	0,061

	SFR1	A	B	C	D	E
Shoreline position 1	0,000	0,000	0,000	0,000	0,000	0,000
Shoreline position 2	0,001	0,001	0,001	0,001	0,001	0,001
Shoreline position 3	0,003	0,003	0,003	0,003	0,003	0,003

Figure 4-8. *Total flow rates ($m^3 \cdot year^{-1}$) through the vault (a) and waste compartments (b) of the 1BMA submodel obtained with different meshes and compared with the flow rates of the SFR 1 repository-scale model.*

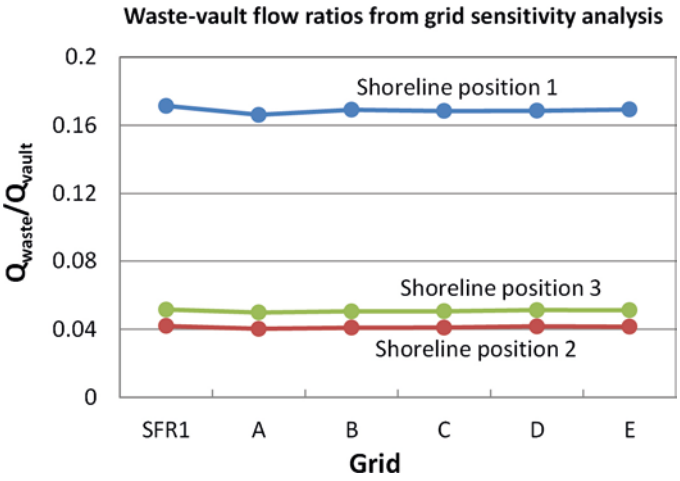

Figure 4-9. *Ratio of flow rates through the waste and through the vault of the 1BMA submodel for different meshes and for the three shoreline positions.*

In light of the above results, which indicate that there are no significant differences between the different meshes studied, it was decided to adopt the mesh C to perform the hydraulic assessment of the concrete degradation of the 1BMA submodel. The reasons are that (1) in mesh C the concrete walls have more than 2 finite elements across the thickness, which is considered key to achieve a proper numerical description of the concrete degradation, (2) the refinement of the rest of the elements in the model is considered sufficient, and (3) at the same time the model can be solved in a reasonable amount of time.

Possible sources of error between the repository-scale model and the 1BMA submodel are the mesh effect on the boundary conditions and the radius of influence assumed in the construction of the submodels. To simulate concrete degradation of different vault elements the same boundary conditions of the Base case (i.e. corresponding to intact concrete) have been assumed in all cases. Accordingly, two types of checks were performed. First, two interpolation methods to calculate the pressure distribution at the boundary of the domain were compared: nearest-neighbor interpolation, and linear interpolation, which is the method considered in the SFR 1 repository-scale model simulations. This simple comparison gives an indirect measure of the mesh effect on the boundary conditions.

As shown in Figure 4-10, the flow rates through the waste compartments are not dependent on the interpolation method. The same is observed in the rest of the 1BMA elements, except for the flow rates through the bottom gravel for shoreline position 1, for which linear interpolation deviates appreciably from the SFR 1 repository-scale model around compartment number 3 (Figure 4-11).

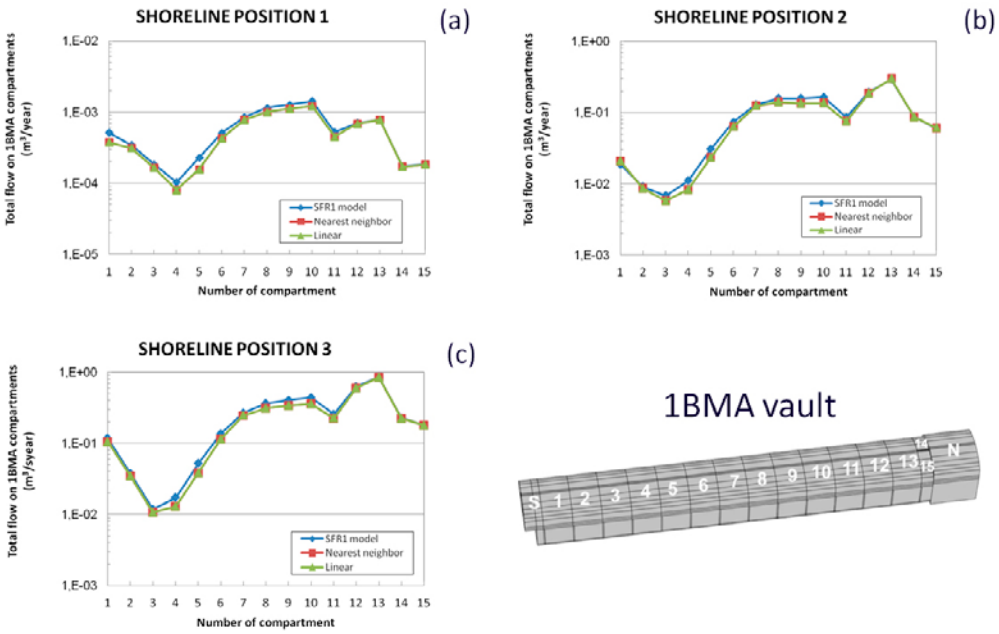

Figure 4-10. *Comparison of nearest-neighbor and linear interpolation methods to calculate the pressure boundary conditions of the 1BMA submodel in terms of the flow rates through the waste compartments.*

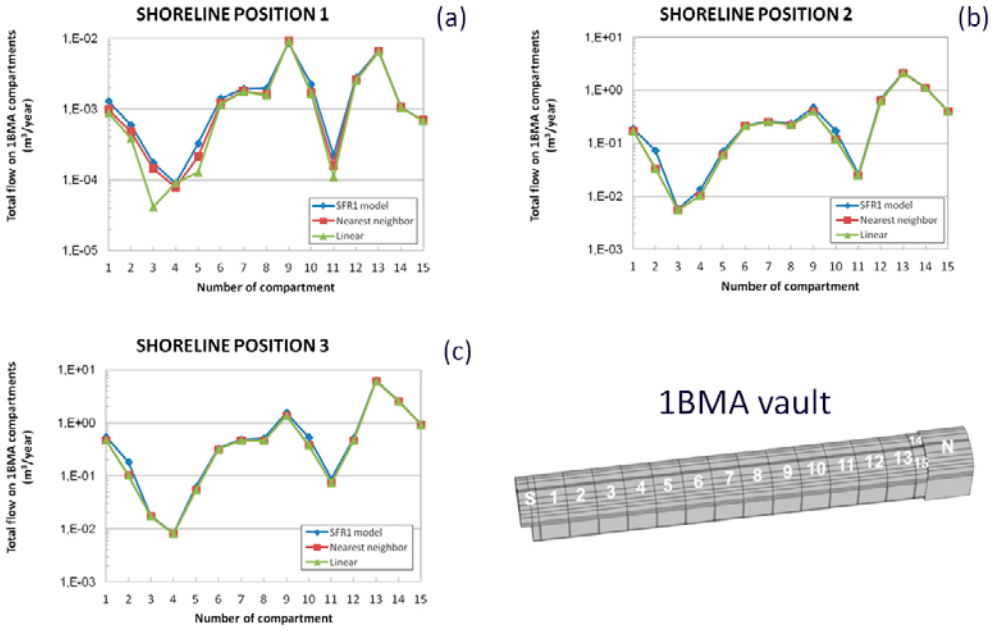

Figure 4-11. *Comparison of nearest-neighbor and linear interpolation methods to calculate the pressure boundary conditions of the 1BMA submodel in terms of the flow rates through the bottom gravel.*

It may be concluded that, overall, the interpolation method used to calculate the boundary conditions has no significant impact on the solution. It was decided to adopt the nearest-neighbor interpolation in the 1BMA submodel, to be consistent with the method applied to define the boundary conditions in the SFR 1 repository-scale model. This assumption also leads to a slightly better fit of the flow rates between the submodel and the repository-scale model (see Figure 4-10 and Figure 4-11).

A second check of the boundary conditions is related to the assessment of the radius of influence. To this end, the complete degradation case of the 1BMA at the submodel scale has been simulated, assuming as boundary conditions the same pressure distribution resulting from the Base case that considers an intact concrete state. The results have been compared with a simulation of the repository-scale model that also considers complete degradation of the concrete barriers. Thus, since the same parameterization is used in both models, a good match between the results would indicate that the pressure boundary conditions are imposed away from the radius of influence. Figure 4-12 displays the flow rates calculated for shoreline position 3. The figure shows that the flow rates resulting from the repository-scale model is well reproduced by the simulation of the 1BMA submodel. The relative difference is less than 8%. It may thus be concluded that the size of the rock domain adopted to construct the submodels is appropriate, i.e. that the radius of influence is smaller than the rock domain size.

4.2 Vault element degradation

Different states of concrete degradation are assumed for specific concrete elements common for all the compartments of 1BMA vault (e.g. floor, lid, and inner and/or outer walls). For each degradation case, the effect of the concrete degradation has been studied with a set of three simulations of increasing concrete hydraulic conductivity (K=10^{-7}, 10^{-5}, 10^{-3} m·s^{-1}, respectively). Each degradation state is simulated for shorelines positions 1, 2, and 3 (as defined in Abarca et al. 2013).

Six different vault element degradation cases were studied, as shown in Figure 4-13:

- Case 1: Concrete floor degradation.
- Case 2: Simultaneous concrete floor and inner walls degradation.
- Case 3: Degradation of an outer (east or west) concrete wall.
- Case 4: Degradation of the two outer walls (east and west).
- Case 5: Degradation of outer and inner concrete walls.
- Case 6: Simultaneous degradation of floor, outer walls and concrete lid.

Thus, the concrete degradation study involves a total of 54 simulations, in addition to the Base case results. For the Base case scenario, the hydraulic conductivity of concrete and backfill material was set to 8.3·10^{-10} m·s^{-1} and 10^{-3} m·s^{-1}, respectively.

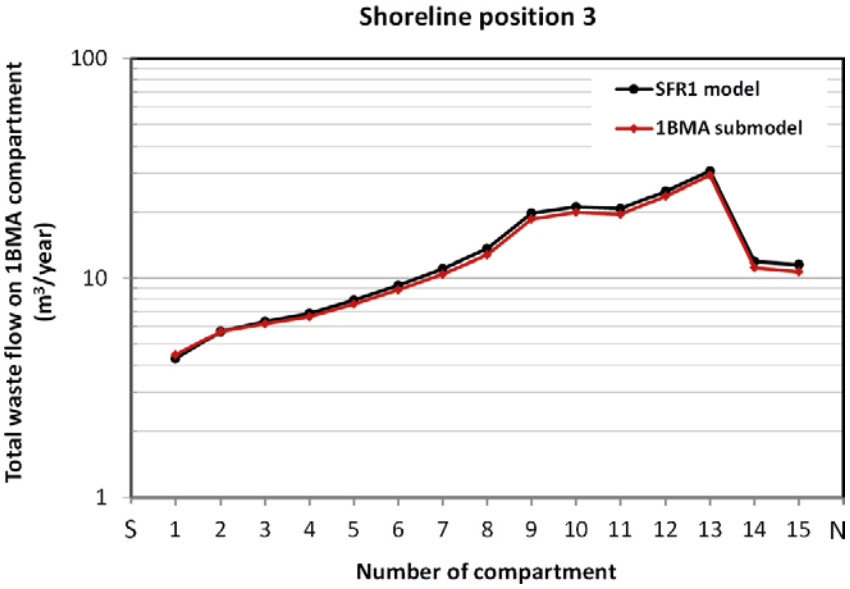

Figure 4-12. *Assessment of radius of influence by comparing flow rates through the waste resulted from the complete degradation at SFR 1 and 1BMA scales (shoreline position 3).*

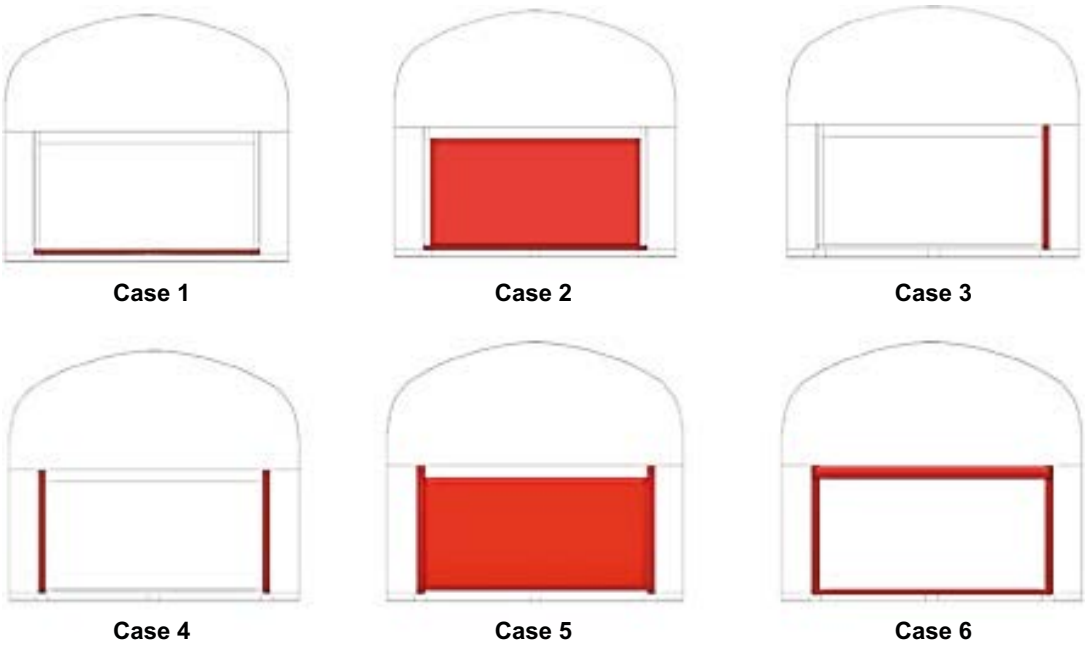

Figure 4-13. *Vault elements (in red) to be degraded homogeneously for all the waste compartments in each case.*

In order to specify the degradation of different parts of the vault domain the 1BMA submodel was separated in COMSOL into the following elements (as geometric entities): rock, concrete floor, concrete lids, inner concrete walls, outer concrete walls, waste, backfill, bottom gavel, concrete beams, and short plugs. The hydraulic conductivity of different vault elements considered in each simulation is presented in Table 4-3. The parameters of the Base case are included for comparison. This set of simulations was run for shoreline positions 1, 2, and 3.

Table 4-3. Hydraulic conductivity ($m \cdot s^{-1}$) of 1BMA elements assumed in the simulations of vault element degradation.

			1BMA vault element hydraulic conductivity ($m \cdot s^{-1}$)						
Case		**ID**	**Floor**	**Inner Walls**	**W outer wall**	**E outer wall**	**Lids**	**Backfill**	**Beams**
Base case		–	8.30E–10	8.30E–10	8.30E–10	8.30E–10	8.30E–10	1.00E–03	8.30E–10
Case 1	Moderate	1	1.00E–07	8.30E–10	8.30E–10	8.30E–10	8.30E–10	1.00E–03	8.30E–10
	Severe	2	1.00E–05	8.30E–10	8.30E–10	8.30E–10	8.30E–10	1.00E–03	8.30E–10
	Complete	3	1.00E–03	8.30E–10	8.30E–10	8.30E–10	8.30E–10	1.00E–03	8.30E–10
Case 2	Moderate	4	1.00E–07	1.00E–07	8.30E–10	8.30E–10	8.30E–10	1.00E–03	8.30E–10
	Severe	5	1.00E–05	1.00E–05	8.30E–10	8.30E–10	8.30E–10	1.00E–03	8.30E–10
	Complete	6	1.00E–03	1.00E–03	8.30E–10	8.30E–10	8.30E–10	1.00E–03	8.30E–10
Case 3	Moderate	7	8.30E–10	8.30E–10	8.30E–10	1.00E–07	8.30E–10	1.00E–03	8.30E–10
	Severe	8	8.30E–10	8.30E–10	8.30E–10	1.00E–05	8.30E–10	1.00E–03	8.30E–10
	Complete	9	8.30E–10	8.30E–10	8.30E–10	1.00E–03	8.30E–10	1.00E–03	8.30E–10
Case 4	Moderate	10	8.30E–10	8.30E–10	1.00E–07	1.00E–07	8.30E–10	1.00E–03	8.30E–10
	Severe	11	8.30E–10	8.30E–10	1.00E–05	1.00E–05	8.30E–10	1.00E–03	8.30E–10
	Complete	12	8.30E–10	8.30E–10	1.00E–03	1.00E–03	8.30E–10	1.00E–03	8.30E–10
Case 5	Moderate	13	8.30E–10	1.00E–07	1.00E–07	1.00E–07	8.30E–10	1.00E–03	8.30E–10
	Severe	14	8.30E–10	1.00E–05	1.00E–05	1.00E–05	8.30E–10	1.00E–03	8.30E–10
	Complete	15	8.30E–10	1.00E–03	1.00E–03	1.00E–03	8.30E–10	1.00E–03	8.30E–10
Case 6	Moderate	16	1.00E–07	8.30E–10	1.00E–07	1.00E–07	1.00E–07	1.00E–03	8.30E–10
	Severe	17	1.00E–05	8.30E–10	1.00E–05	1.00E–05	1.00E–05	1.00E–03	8.30E–10
	Complete	18	1.00E–03	8.30E–10	1.00E–03	1.00E–03	1.00E–03	1.00E–03	8.30E–10

The degradation of the concrete beams that serve as a support for the concrete floor has not been considered in this section. Thus, all the simulations presented here consider that beams are intact or have a low conductivity (Table 4-3). This is important given their role on the groundwater flow in the 1BMA (see Abarca et al. 2013 for more details). This assumption is conservative in the sense that an intact concrete state of the beams leads to higher flows through the waste than a case of an hydraulic design of the vault with high conductivity beams or they are completely degraded.

Next, the simulation results of the vault element degradation cases are presented in detail. For the sake of brevity, we only show flow rates through the waste compartments of 1BMA vault. Flow rates within other vault elements have been included in Appendix A.

4.2.1 Case 1: Floor degradation

This section explores the effect of degradation of the concrete floor on the local flow rates in the waste and on the total vault flow.

Figure 4-14 shows that as the floor degrades the flow rate through the waste compartments increases. Degradation effects are relatively small for compartments 3, 4, and 5, where flow rates are low, especially for shoreline position 1. As expected, zones of higher flow present an appreciable deviation from the Base case situation. In particular, for shoreline positions 2 and 3, the complete degradation of the concrete floor produces a more homogeneous flow profile compared to the other degradation states.

The total flow through the 1BMA vault and waste domain for all the degradation states and the three shoreline positions are presented in Table 4-4. A systematic increase of the total flow through the waste may be observed, while the total flow through the vault increases only slightly (a maximum increase of 14% with respect to the Base case is observed). This leads to a significant increase of the ratio between the flow through the waste and the flow through the vault in all cases.

Overall, flow rates through other vault elements are not significantly affected (see Appendix A, Figure A-1 to Figure A-4, for more details). A minor effect of concrete degradation is found on the flow rates through the top and lateral backfill of compartments 1–7 for shoreline position 1, where degradation induces a reduction of the flow compared to the Base case. This seems to be consistent with the vertical flow pattern that was calculated in the SFR 1 repository-scale model for that shoreline position. An increase of the flow rates within compartments 9 to 12 of the west gravel with respect to the Base case is also observed for shoreline position 1.

Table 4-4. Summary of total flow ($m^3 \cdot year^{-1}$) through the 1BMA vault and waste domain for the concrete floor degradation case (Case 1) and the three shoreline positions.

Case 1 Degradation state	Vault total flow ($m^3 \cdot year^{-1}$)	Waste total flow ($m^3 \cdot year^{-1}$)	Waste normalized	Waste/Vault ratio
	Shoreline position 1			
Base case	4.09E–02	6.90E–03	100%	16.84%
Moderate	4.38E–02	1.59E–02	230%	36.21%
Severe	4.65E–02	2.21E–02	321%	47.56%
Complete	4.66E–02	2.27E–02	329%	48.65%
	Shoreline position 2			
Base case	28.6	1.17	100%	4.10%
Moderate	29.2	3.00	255%	10.26%
Severe	29.8	4.67	398%	15.66%
Complete	29.9	7.33	625%	24.55%
	Shoreline position 3			
Base case	61.9	3.13	100%	5.06%
Moderate	63.5	8.24	263%	12.98%
Severe	64.9	12.9	411%	19.83%
Complete	65.0	16.3	520%	25.03%

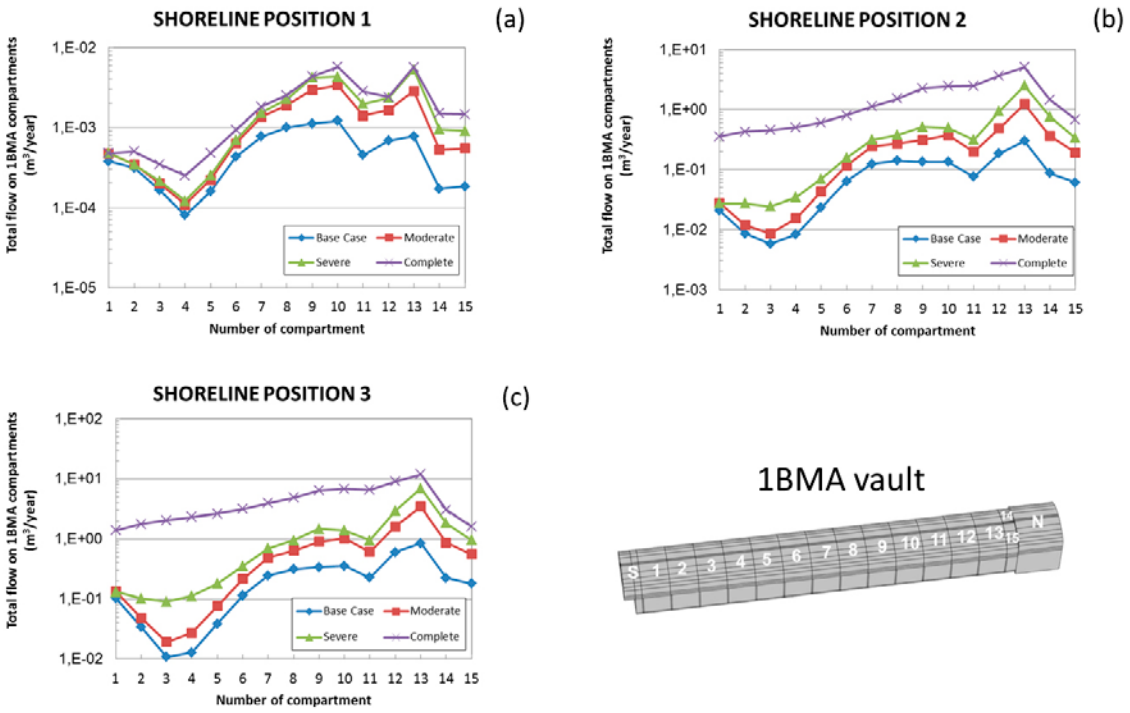

Figure 4-14. *Flow rates ($m^3 \cdot year^{-1}$) through the waste compartments of 1BMA submodel for floor degradation.*

Conclusions: The flow rates through the waste increase significantly as concrete floor degradation proceeds, while the total flow through the vault shows only a minor increase. This leads to an increase in the fraction of the total flow through the vault that enters the waste, from 5% in the Base case to 25% in the complete degradation state (for shoreline positions 2 and 3). A flow rate profile similar to the Base case is displayed for the moderate and severe degradation states. The complete degradation state leads to significant differences with respect to the Base case, showing appreciably higher flow rates (more than five times than the Base case) and a more homogeneous profile. In general, flow rates through other vault elements are not significantly affected by concrete floor degradation.

4.2.2 Case 2: Degradation of floor and inner walls

Degradation of the concrete floor and inner walls should increase the connectivity between waste compartments, and thus also increase the flow rates with respect to the Base case and the case of floor degradation only (Case 1). The increase in connectivity is reflected in Figure 4-15, which shows flow profiles of more homogeneous shape compared to the concrete floor degradation case (Case 1) for all shoreline positions. The increase in the total flow through the waste with respect to the Base case is shown in Table 4-5, being of more than one order of magnitude for the complete degradation state for shoreline positions 2 and 3. However, for shoreline position 1 lower flow rates resulted from complete degradation within compartments 1 to 8 with respect to the moderate and severe degradation states. This could be due to the fact that concrete floor degradation enhances the dominant vertical flow for shoreline position 1. However, this effect on the total flow could be compensated by the degradation of inner concrete walls, which would enhance horizontal flow between waste compartments, especially for complete degradation.

The total flow through the waste is similar for Case 1 and Case 2. An increase of 20–30% is found for the moderate degradation state with respect to Case 1, while the severe degradation state leads to almost the same flow through the waste (2–4% difference). In turn, the complete degradation state is the only case leading to a significant increase with respect to Case 1, especially for shoreline positions 2 and 3 for which the total flow through the waste is doubled.

Table 4-5. Summary of total flow ($m^3 \cdot year^{-1}$) through the 1BMA vault and waste domain for the concrete floor and inner walls degradation case (Case 2) and the three shoreline positions.

Case 2 Degradation state	Vault total flow ($m^3 \cdot year^{-1}$)	Waste total flow ($m^3 \cdot year^{-1}$)	Waste normalized	Waste/Vault ratio	Case2/Case1 waste total flow ratio
	Shoreline position 1				
Base case	4.09E–02	6.90E–03	100%	16.84%	1.00
Moderate	4.52E–02	1.96E–02	284%	43.25%	1.23
Severe	4.61E–02	2.16E–02	314%	46.86%	0.98
Complete	4.62E–02	2.51E–02	364%	54.37%	1.11
	Shoreline position 2				
Base case	28.6	1.17	100%	4.10%	1.00
Moderate	29.7	3.90	336%	13.25%	1.32
Severe	30.0	4.54	387%	15.15%	0.97
Complete	30.0	1.49	1,266%	49.53%	2.03
	Shoreline position 3				
Base case	61.9	3.13	100%	5.06%	1.00
Moderate	64.7	10.8	346%	16.74%	1.31
Severe	65.3	12.4	396%	18.98%	0.96
Complete	65.4	32.5	1,038%	49.69%	2.00

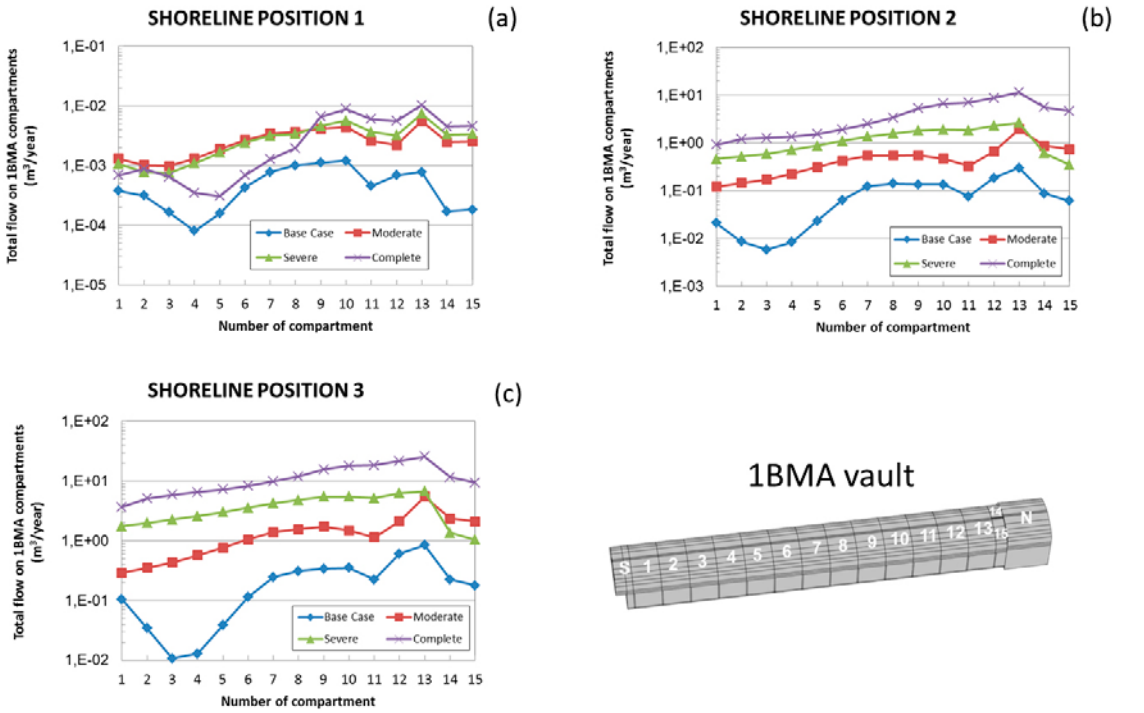

Figure 4-15. Flow rates ($m^3 \cdot year^{-1}$) through the waste compartments of 1BMA submodel for degradation of floor and inner walls.

The total flow through the vault shows only a small increase, especially for shoreline position 1 (a maximum of 12% increase is observed). The total flow through the waste increases up to about half of the total flow through the vault for the complete degradation state and the three shoreline positions.

Figure 4-17 to Figure 4-19 and Figure 4-20 to Figure 4-22 show the Darcy velocity field and the distribution of its magnitude for three different vertical cross-sections (xz planes) of the 1BMA vault (Figure 4-16) and for shoreline positions 1 and 3, respectively. Velocities are normalized with respect to the maximum magnitude of the Darcy velocity obtained for each shoreline position.

For shoreline position 1, the Darcy velocity field is quite vertical and follows the distribution of rock conductivity (see e.g. Figure 4-17 to Figure 4-19 for y = 10,106 m). Floor degradation promotes an upward vertical flow of water into the vault and waste. Within the first half of the vault, flow through the backfill is higher for moderate and severe than for complete degradation (see Figure 4-17 to Figure 4-19 for y = 10,056 m). This is consistent with the flow rate profiles depicted in Figure 4-15. The vertical flow through the waste is connected with high rock conductivity zones, e.g. at y = 10,056 m. That is, concrete floor degradation promotes preferential flow paths connecting the vault with the rock. A different pattern is observed for shoreline position 3 (Figure 4-20 to Figure 4-22). The flow through the waste increases as the degradation of inner walls and floor proceeds. The same occurs with the flow through the backfill. Also, the direction of the flow within the waste changes to vertically downward for moderate and severe degradation (see Figure 4-20 and Figure 4-21 for y = 10,106 m). However, preferential flow paths connecting vertical flow through the vault with the flow through the rock are found again. In addition, as degradation increases the flow through the lids and outer walls decreases.

Regarding the flow through other barriers, degradation also partially reduces the flow rates through top and lateral gravels (see Appendix A, Figure A-5, Figure A-7, and Figure A-8).

Conclusions: Degradation of floor and inner walls increases the flow rates with respect to the Base case and the case of concrete floor degradation only (Case 1). This increase is particularly important in the complete degradation state for shoreline positions 2 and 3 (more than one order of magnitude increase with respect to the Base case and two times the flow of the complete degradation state of Case 1). In general, complete degradation causes higher flow rates than moderate and severe degradation. Floor degradation enhances the dominant vertical flow for shoreline position 1, which is compensated by degradation of inner walls that enhance horizontal flow between waste compartments. This could be the cause of lower flow rates for complete degradation for shoreline position 1. In addition, floor degradation promotes preferential flow paths connecting the vault with the rock.

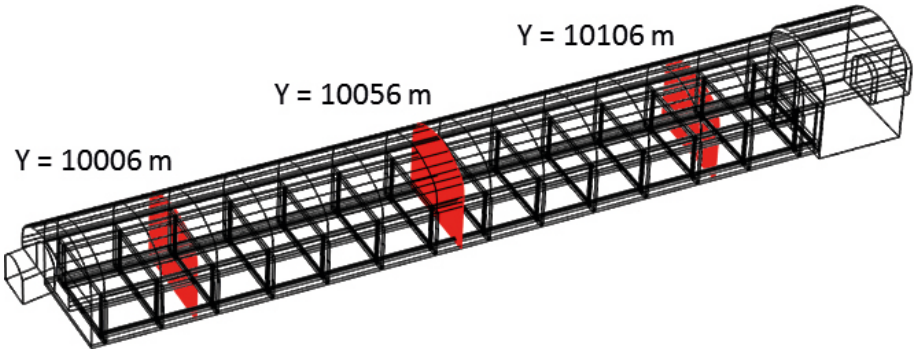

Figure 4-16. *Observation vertical cross-sections (xz planes) of the 1BMA submodel for which results are presented: Y = 10,006 m, Y = 10,056 m, and Y = 10,106 m.*

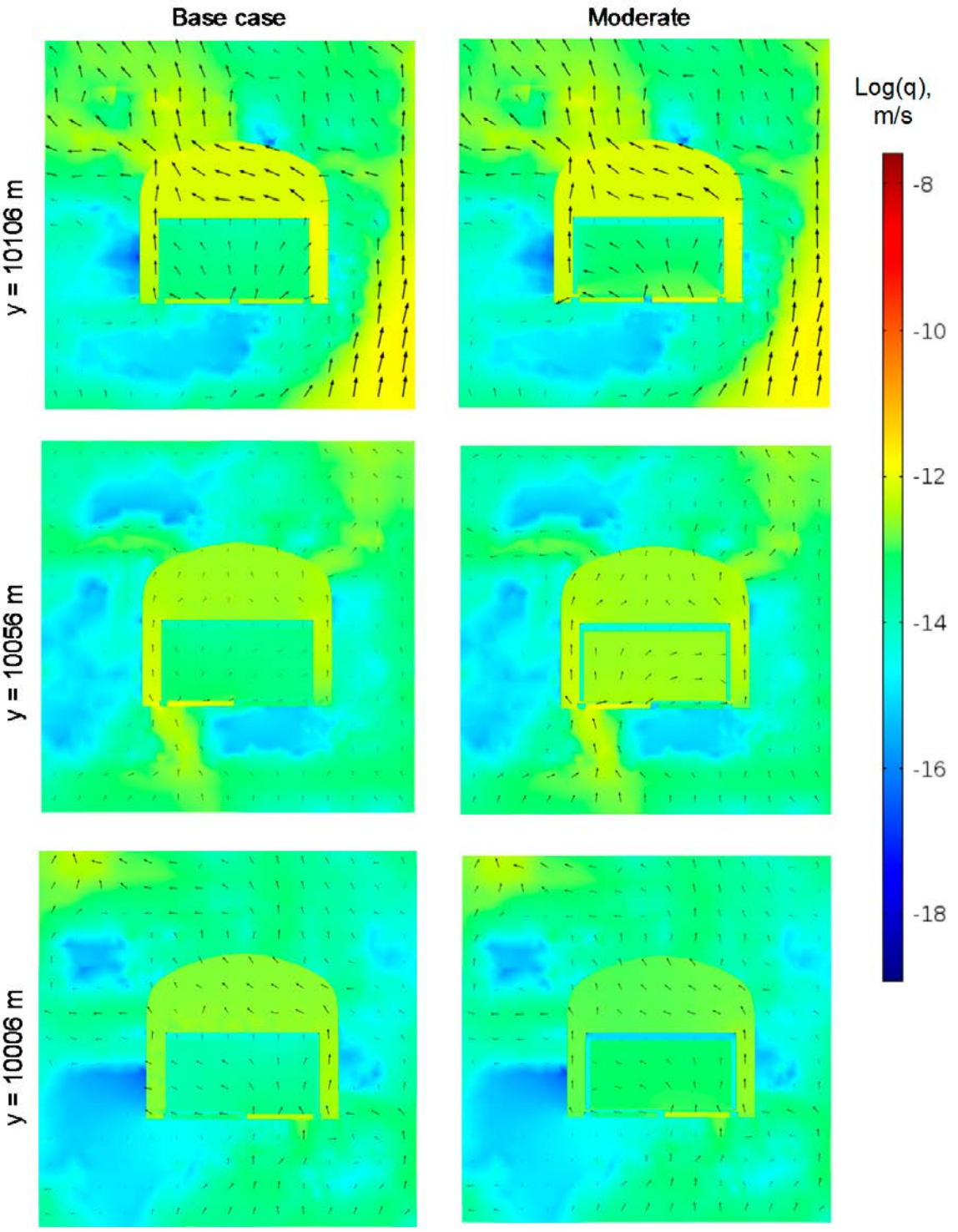

Figure 4-17. *Impact of moderate floor and inner walls degradation on water Darcy fluxes and its magnitude at three vertical cross-sections (xz planes) of the 1BMA submodel for shoreline position 1.*

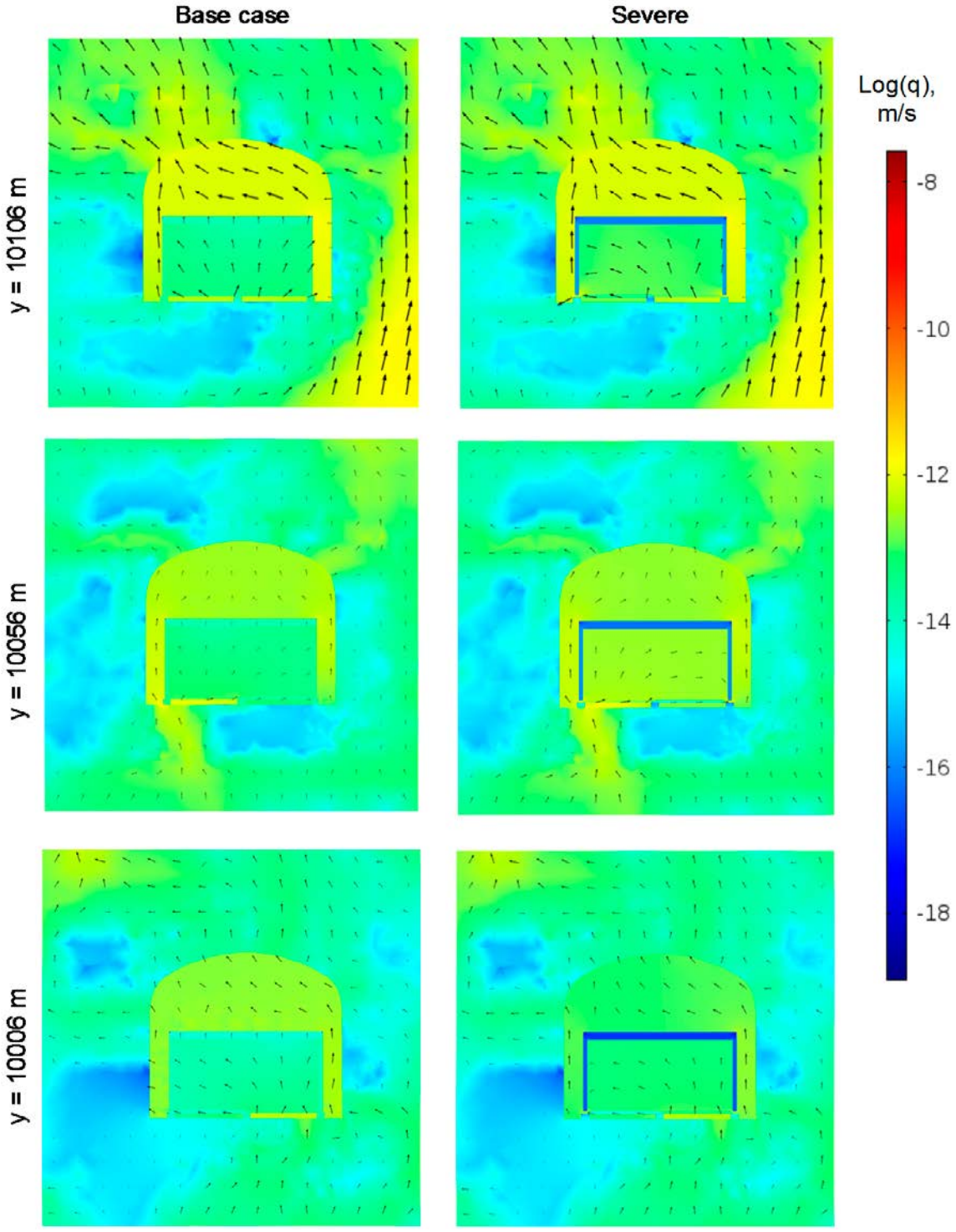

Figure 4-18. *Impact of severe floor and inner walls degradation on water Darcy fluxes and its magnitude at three vertical cross-sections (xz planes) of the 1BMA submodel for shoreline position 1.*

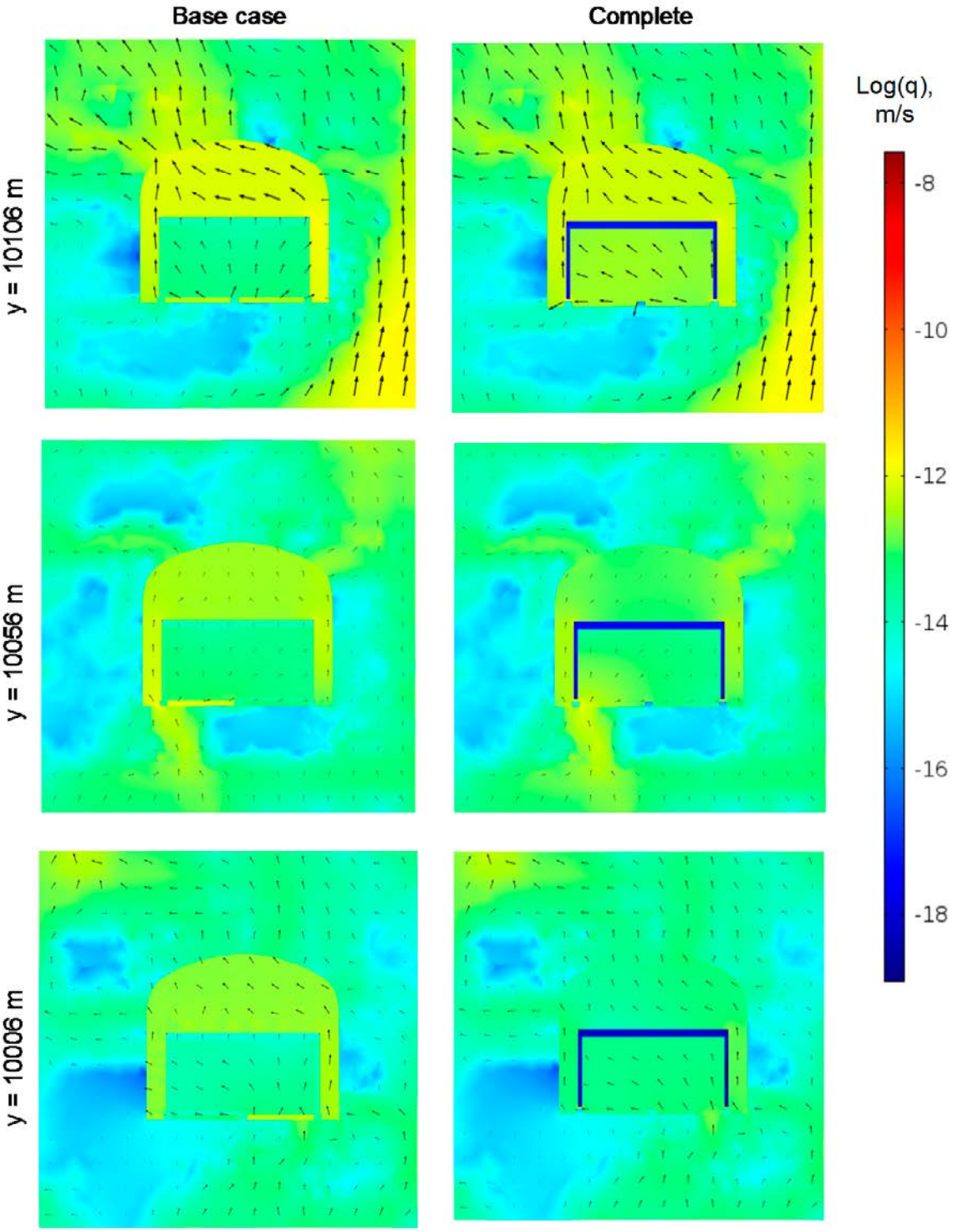

Figure 4-19. *Impact of complete floor and inner walls degradation on water Darcy fluxes and its magnitude at three vertical cross-sections (xz planes) of the 1BMA submodel for shoreline position 1.*

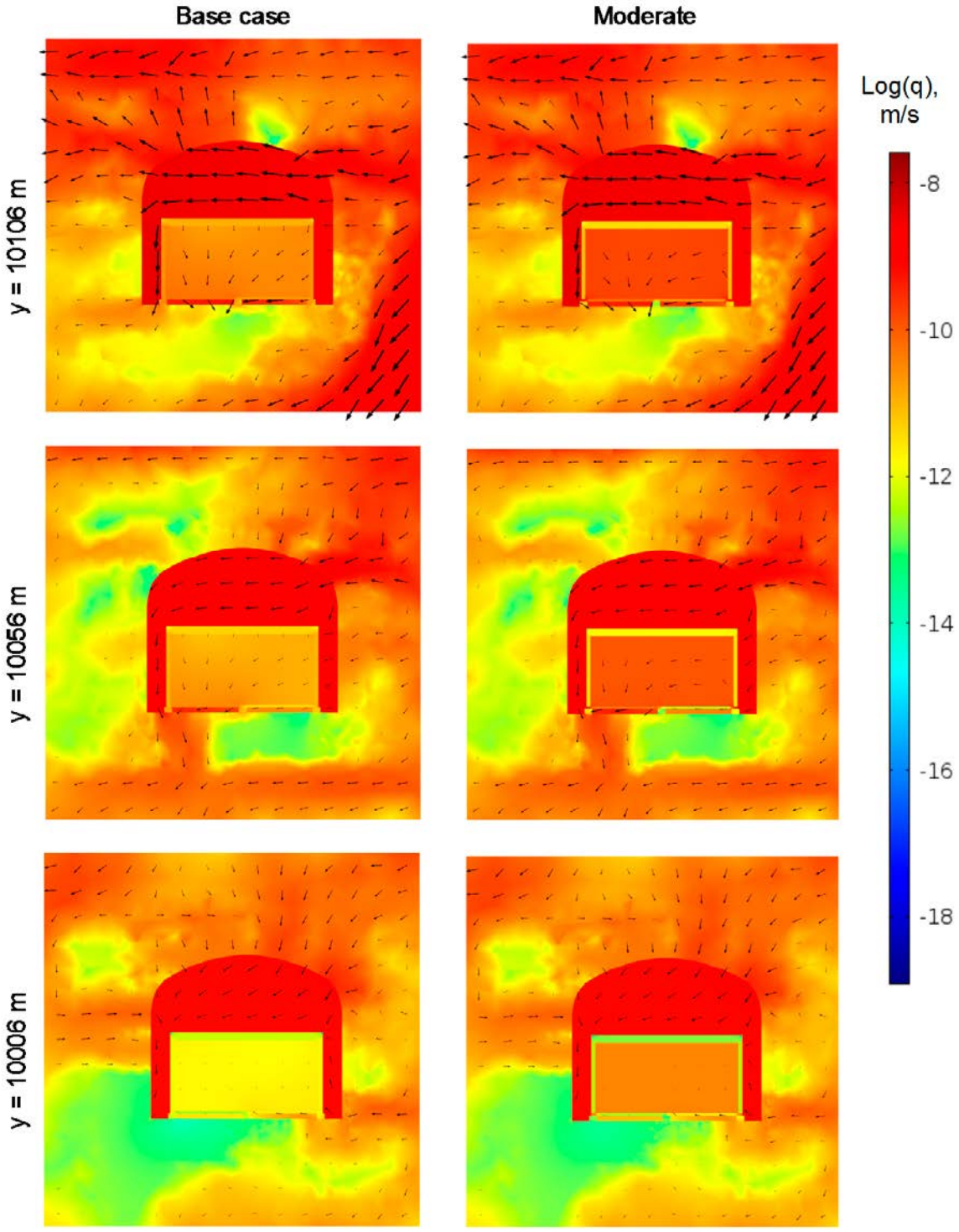

Figure 4-20. *Impact of moderate floor and inner walls degradation on water Darcy fluxes and its magnitude at three vertical cross-sections (xz planes) of the 1BMA submodel for shoreline position 3.*

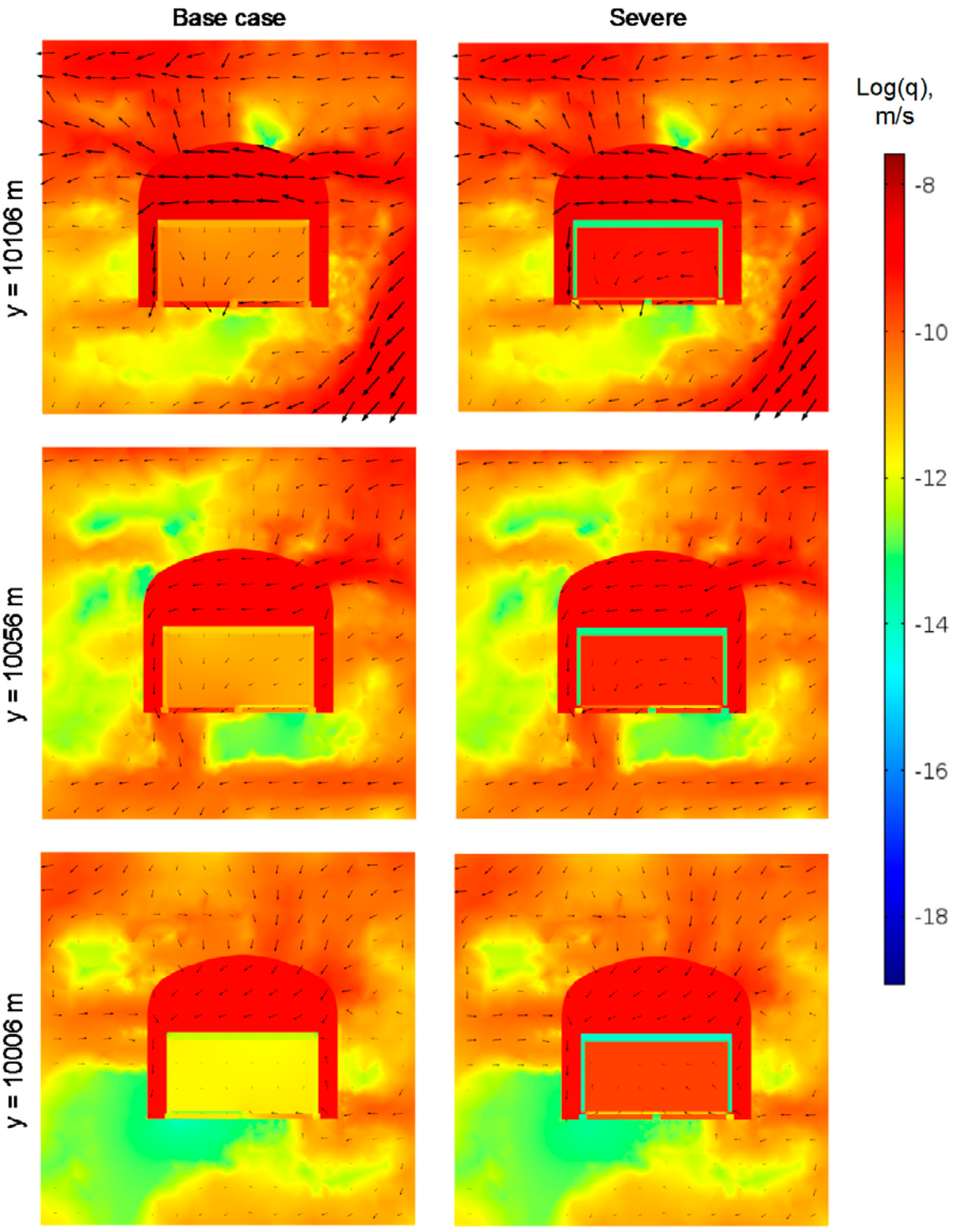

Figure 4-21. *Impact of severe floor and inner walls degradation on water Darcy fluxes and its magnitude at three vertical cross-sections (xz planes) of the 1BMA submodel for shoreline position 3.*

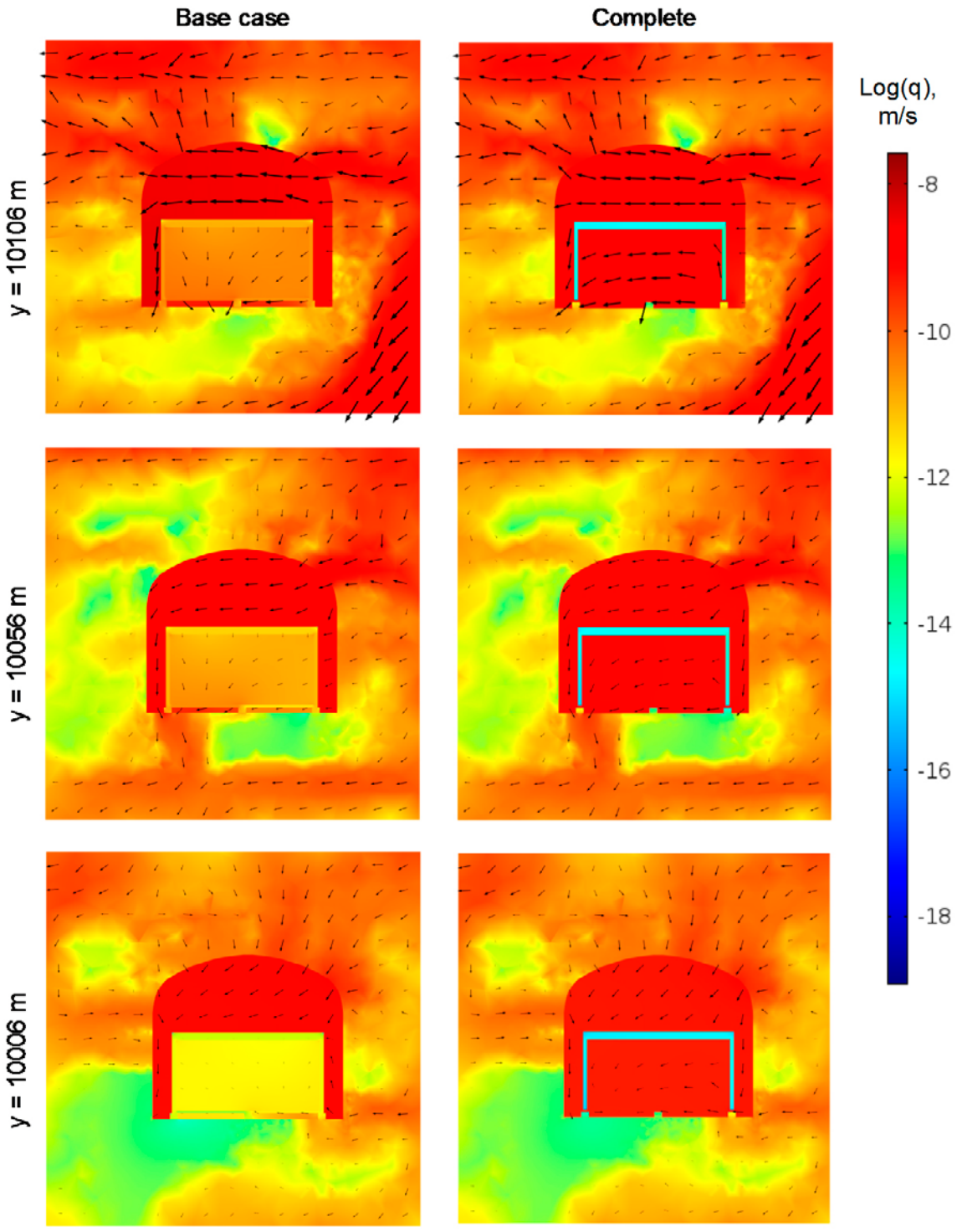

Figure 4-22. *Impact of complete floor and inner walls degradation on water Darcy fluxes and its magnitude at three vertical cross-sections (xz planes) of the 1BMA submodel for shoreline position 3.*

4.2.3 Case 3: Degradation of one outer wall

The next case analyzes the degradation of the eastern wall of the concrete structure. Given that the main direction of the flow for shoreline positions 2 and 3 is SE-NW, the eastern wall should see preferential degradation.

The flow rates through the waste compartments calculated for this case are shown in Figure 4-23. A first inspection reveals that degradation has a minor effect on flow rates in the different compartments, except around the compartments with the lowest (3–5) and the highest (10–13) flow rates. Here, flow rates are generally lower than those calculated in the Base case. The effect on the total flow through the waste, shown in Table 4-6, is an increase of between 34 to 47% with respect to the Base case for the moderate and severe degradation states. However, the complete degradation state leads to a more significant increase, especially for shoreline positions 2 and 3 (3.3 and 2.4 times the total flow in the Base case, respectively).

A redistribution of the flow with respect to the Base case scenario occurs around compartment number 11 (located upstream of zone ZFMNNW1209, see Figure 4-43) for the moderate and severe degradation states. This shadow-like effect, characterized by a decrease in the flow in compartment 11 and an increase in the adjacent compartments (10 and 12), does not occur in the case of complete concrete degradation of the outer east wall. In the latter case, a horizontal groundwater flow enhances the flow within the waste domain. The flow is also reduced with respect to the Base case in the cases of moderate and severe concrete degradation within compartments 1 to 6.

The flow rates through other vault elements (see Appendix A, Figure A-9, Figure A-10, and Figure A-12) are almost unaffected by the degradation of the east wall, except the flow through the east gravel for a complete degradation state, which could be expected given the connectivity between the east gravel and the east concrete wall (see Appendix A, Figure A-11).

Conclusions: Overall, the flow rates through the waste are not significantly affected by concrete degradation of the east outer wall, except in the complete degradation state for shoreline positions 2 and 3 (3.3 and 2.4 times the total flow in the Base case, respectively). A shadow-like effect on flow rates is found around deformation zone ZFMNNW1209.

Table 4-6. Summary of total flow ($m^3 \cdot year^{-1}$) through the 1BMA vault and waste domain for the concrete degradation of the east outer walls (Case 3) and the three shoreline positions.

Case 3 Degradation state	Vault total flow ($m^3 \cdot year^{-1}$)	Waste total flow ($m^3 \cdot year^{-1}$)	Waste normalized	Waste/Vault ratio
	Shoreline position 1			
Base case	4.09E–02	6.90E–03	100%	16.84%
Moderate	4.16E–02	9.24E–03	134%	22.22%
Severe	4.16E–02	9.33E–03	135%	22.42%
Complete	4.16E–02	1.01E–02	147%	24.29%
	Shoreline position 2			
Base case	28.6	1.17	100%	4.10%
Moderate	28.7	1.65	141%	5.75%
Severe	28.7	1.73	147%	6.01%
Complete	28.8	3.93	335%	13.67%
	Shoreline position 3			
Base case	61.9	3.13	100%	5.06%
Moderate	62.3	4.44	142%	7.13%
Severe	62.3	4.56	146%	7.31%
Complete	62.3	7.62	243%	12.23%

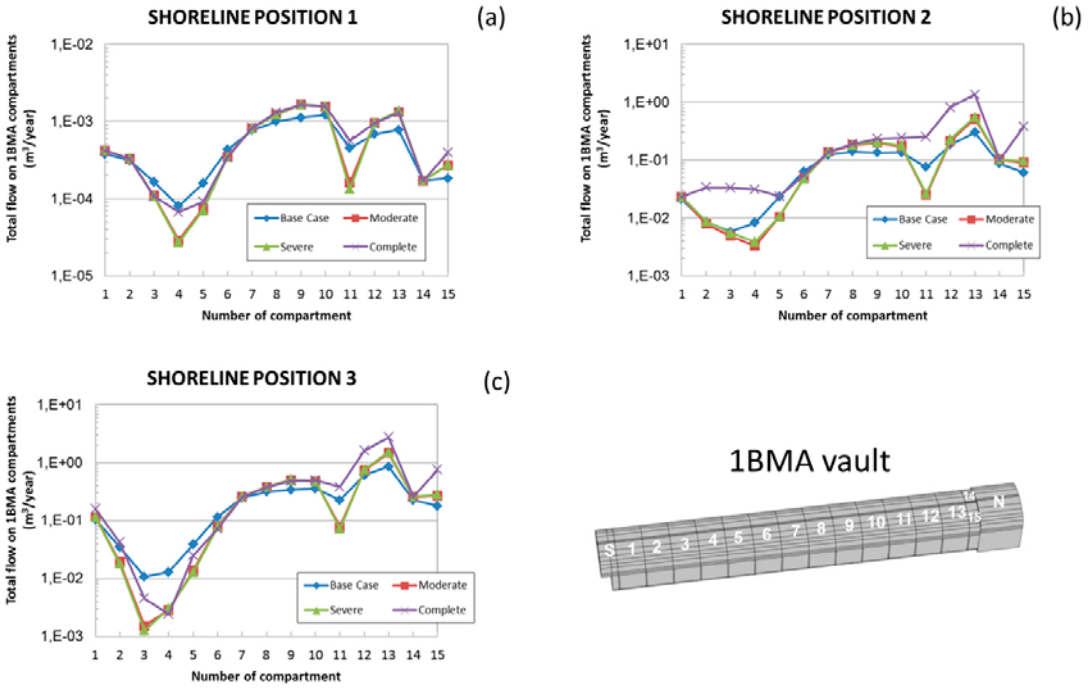

Figure 4-23. *Flow rates ($m^3 \cdot year^{-1}$) through the waste compartments of 1BMA submodel for degradation of east outer wall.*

4.2.4 Case 4: Degradation of outer walls

As a complement to Case 3, an additional scenario has been considered where the degradation is imposed on both outer walls. This situation should modify the flow through the waste domain, especially for shorelines positions 2 and 3 where the groundwater flow is predominantly horizontal. This is confirmed with the results of the total flow through the waste compartments, which is shown in Figure 4-24b and Figure 4-24c for the severe and complete degradation states. Profiles of flow rates within the waste deviate notably from the Base case. A different behavior is displayed for moderate degradation, for which the shadow-like effect around compartment number 11 and flow redistribution described in the previous case are again developed. The flow redistribution observed in this case is not accompanied by an increase in the total flow in the waste domain, which is nearly constant for the three shoreline positions, as shown in Table 4-7 (only a 1–2% difference with the Base case).

A comparison of the total flow in the waste domain between Case 4 and the previous Case 3 for the severe and complete degradation states (see Table 4-7) indicates an increase of 2 to 3 times the total flow in the Base case for shoreline positions 2 and 3. For shoreline position 1, the total flow is much less sensitive to the degradation of the second outer wall, with an increase of 57% only for the complete degradation state.

The flow through the east and west gravels are also modified under complete degradation of both concrete outer walls for shoreline positions 2 and 3 (see Appendix A, Figure A-15 and Figure A-16), which is expected given the connectivity with the concrete outer walls. Unlike the degradation of only one outer wall, for which the flow through the west gravel is slightly reduced with respect to the Base case, the degradation of both outer walls leads to an increase on the flow rates around the fracture zones (ZFMNNW1209 and minor fractures, see Appendix A, Figure A-16a). This is because degradation of west outer wall establishes a connection between the fracture zone and vault compartments within this zone, which promotes higher water flow to the west gravel.

Conclusions: Degradation of both concrete outer walls leads to a significant increase in flow rates within the waste with respect to the Base case. Compared with Case 3, the increase is only observed for the severe and complete degradation states, especially for shoreline positions 2 and 3. Similarly to the degradation of only the east outer wall, the flow distribution within the waste domain responds to the local distribution of the rock conductivity field. Since the inner concrete walls are not degraded in these simulations, a discrete distribution of the groundwater flow between individual waste compartments is observed. A redistribution of flow rates with respect to the Base case is again observed near deformation zone ZFMNNW1209.

Table 4-7. Summary of total flow ($m^3 \cdot year^{-1}$) through the 1BMA vault and waste domain for the concrete outer walls degradation case (Case 4) and the three shoreline positions.

Case 4 Degradation state	Vault total flow ($m^3 \cdot year^{-1}$)	Waste total flow ($m^3 \cdot year^{-1}$)	Waste normalized	Waste/Vault ratio	Case4/Case3 waste total flow ratio
	Shoreline position 1				
Base case	4.09E–02	6.90E–03	100%	16.84%	1.00
Moderate	4.52E–02	1.96E–02	284%	43.25%	1.01
Severe	4.61E–02	2.16E–02	314%	46.86%	1.02
Complete	4.62E–02	2.51E–02	364%	54.37%	1.57
	Shoreline position 2				
Base case	28.6	1.17	100%	4.10%	1.00
Moderate	29.7	3.94	336%	13.25%	1.02
Severe	30.0	4.54	387%	15.15%	2.96
Complete	30.0	1.49	1,266%	49.53%	2.98
	Shoreline position 3				
Base case	61.9	3.13	100%	5.06%	1.00
Moderate	64.7	10.8	346%	16.74%	1.02
Severe	65.3	12.4	396%	18.98%	2.07
Complete	65.4	32.5	1,038%	49.69%	2.74

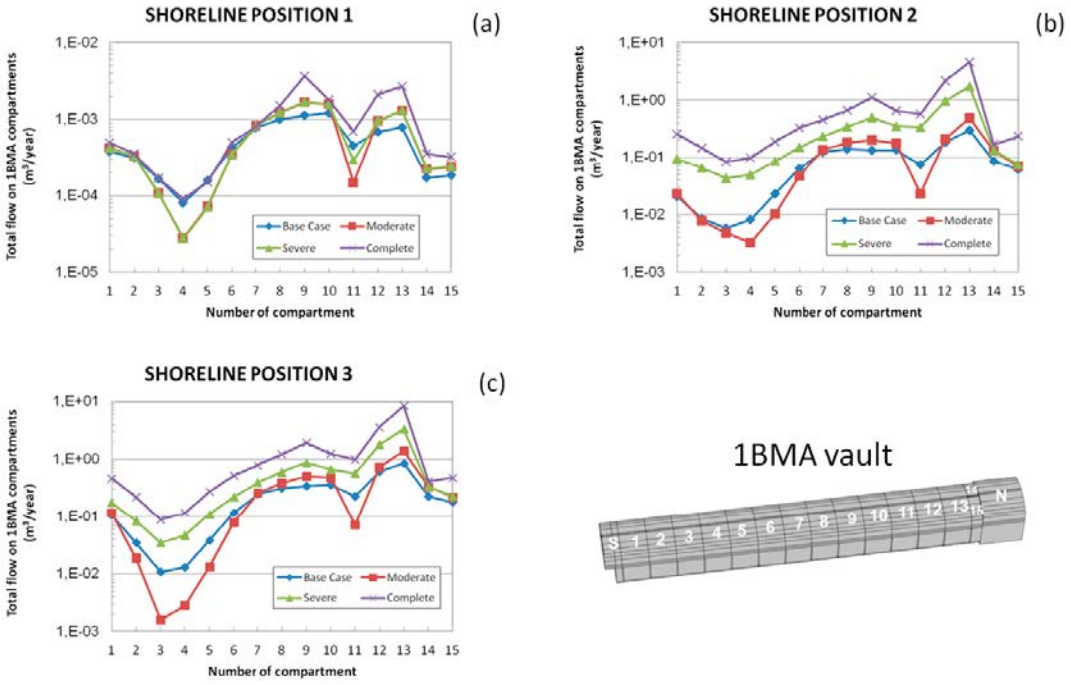

Figure 4-24. Flow rates ($m^3 \cdot year^{-1}$) through the waste compartments of 1BMA submodel for degradation of outer walls.

4.2.5 Case 5: Degradation of inner and outer walls

The following case studies the degradation of all the inner and outer concrete walls of the 1BMA vault. Since the present case enhances the hydraulic connectivity between waste compartments and between rock and vault around high conductivity zones, the flow through the waste should increase when compared to previous cases (especially the horizontal flow component). Calculated flow rates within the waste, shown in Figure 4-25, confirm this. A significant effect of concrete degradation on flow is observed for shoreline position 1 (see Figure 4-25a), even though the total flow through the waste domain is not significantly affected when compared to Case 4 (see Table 4-8). Severe and complete concrete degradation states modifies the flow behavior of the Base case for shoreline positions 2 and 3 (see Figure 4-25b and Figure 4-25c). When compared to degradation of outer walls only (Case 4), the correlation between the flow rates and local rock conductivity distribution is lost due to the hydraulic connection between the compartments.

The total flow in the waste domain obtained for Case 5 is compared to Case 4 results in Table 4-8. The results indicate that only the complete degradation state leads to a significant increase (~45 to 60%) of the total flow compared to Case 4 for shoreline positions 2 and 3. In the rest of the cases, the differences are much smaller.

At the vault level, the increase in flow through the waste domain is partially compensated by a decrease in flow through the top and west gravel, especially for the complete concrete degradation state (see Appendix A, Figure A-17 and Figure A-20). As a result, the total flow through the vault is not affected by concrete degradation in this case, showing a negligible increase of 1–2%.

Figure 4-26 to Figure 4-28 and Figure 4-29 to Figure 4-31 show the Darcy velocity field and the distribution of its magnitude at three different vertical cross-sections (xz planes) of the 1BMA vault (see Figure 4-16) for shoreline positions 1 and 3, respectively. Velocities are normalized with respect to the maximum magnitude of the Darcy velocity obtained for each shoreline position.

Table 4-8. Summary of total flow ($m^3 \cdot year^{-1}$) through the 1BMA vault and waste domain for the concrete inner and outer walls degradation case (Case 5) and the three shoreline positions.

Case 5 Degradation state	Vault total flow ($m^3 \cdot year^{-1}$)	Waste total flow ($m^3 \cdot year^{-1}$)	Waste normalized	Waste/Vault ratio	Case5/Case4 waste total flow ratio
	Shoreline position 1				
Base case	4.09E–02	6.90E–03	100%	16.84%	1.00
Moderate	4.52E–02	1.96E–02	284%	43.25%	0.97
Severe	4.61E–02	2.16E–02	314%	46.86%	0.97
Complete	4.62E–02	2.51E–02	364%	54.37%	1.28
	Shoreline position 2				
Base case	28.6	1.17	100%	4.10%	1.00
Moderate	29.7	3.94	336%	13.25%	0.93
Severe	30.0	4.54	387%	15.15%	1.17
Complete	30.0	14.9	1,266%	49.53%	1.46
	Shoreline position 3				
Base case	61.9	3.13	100%	5.06%	1.00
Moderate	64.7	1.08	346%	16.74%	0.93
Severe	65.3	1.24	396%	18.98%	1.23
Complete	65.4	3.25	1,038%	49.69%	1.61

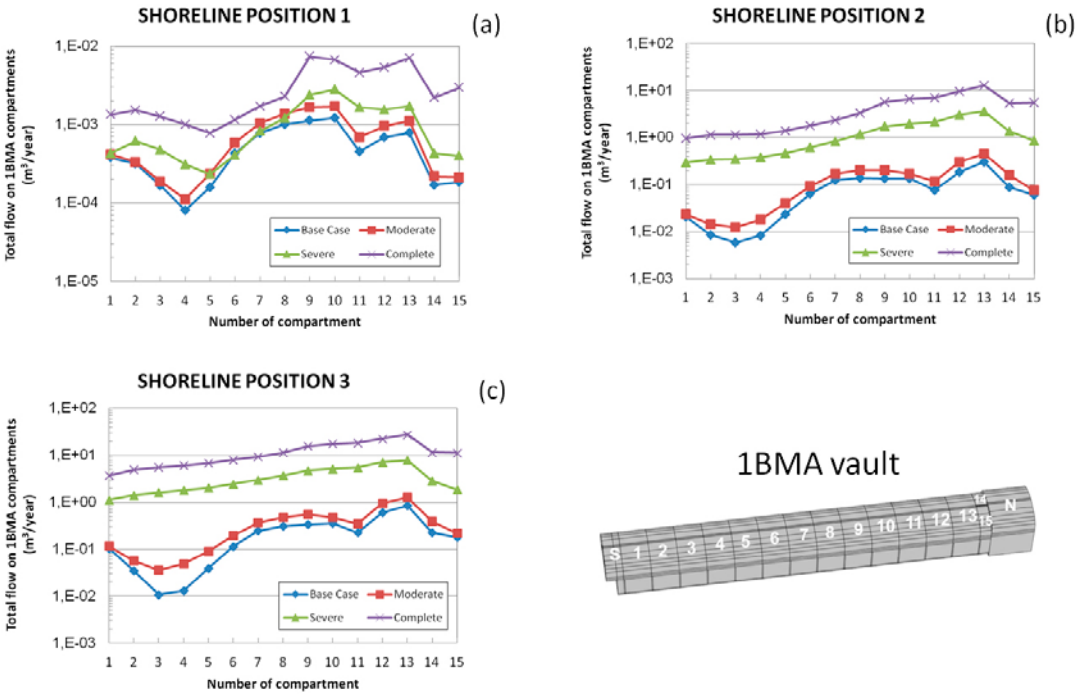

Figure 4-25. *Flow rates ($m^3 \cdot year^{-1}$) through the waste compartments of the 1BMA submodel for degradation of inner and outer concrete walls.*

As in most of the cases, the Darcy velocity field is mainly vertical for shoreline position 1 and follows the distribution of the rock conductivity field (see e.g. Figure 4-26 to Figure 4-28 for y = 10,056, 10,106 m). Comparing Figure 4-17 to Figure 4-19 with Figure 4-26 to Figure 4-28 (y = 10,056 m) it is observed that vertical flow within that particular waste compartment is lower than the one calculated for the case of concrete floor and inner walls degradation (Case 2). This is consistent with the fact that in the present case the floor is not degraded and acts as an efficient flow barrier in the vertical direction. Because of this, the connectivity between waste and high conductivity zones of the rock is notably lower. The total flow through the waste compartments, top gravel, and backfill increases as the degradation of inner and outer walls proceeds. A comparison of Figure 4-20 to Figure 4-22 with Figure 4-29 to Figure 4-31 (y = 10,106 m) for severe and complete degradation also reveals that horizontal flow is higher in the present case (an intact floor acts as a barrier for vertical flow, which favors the horizontal flow within the waste compartments). Complete degradation of the outer concrete walls drives the flow horizontally near the west wall and north of the 1BMA vault (Figure 4-31, y = 10,106 m); while in Case 4 the flow is vertically downward in that zone for the same degradation state (Figure 4-22, y = 10,106 m). In addition, as degradation increases the flow through the (intact) concrete lids decreases.

Conclusions: Compared to the Base case, flow rate profiles through the waste compartments are significantly affected by the severe and complete concrete degradation states of the outer and inner walls of the 1BMA vault. For shoreline positions 2 and 3 in particular, these degradation states lead to a more homogeneous flow rate profile along the waste compartments. The increase in total flow through the waste domain is at least 300% in all cases, showing a maximum increase of more than one order of magnitude for the complete degradation state (for shoreline positions 2 and 3). The total flow through the waste compartments, top gravel and backfill increases as the degradation of inner and outer walls proceeds. The hydraulic connectivity between the waste domain and the high conductivity zones of the rock is considerably lower in the present case, with an intact concrete floor, than when floor degradation is considered (e.g. Case 2). Concrete degradation drives the flow towards the degraded walls. As a consequence, the flow through those waste compartment elements that remain intact is reduced.

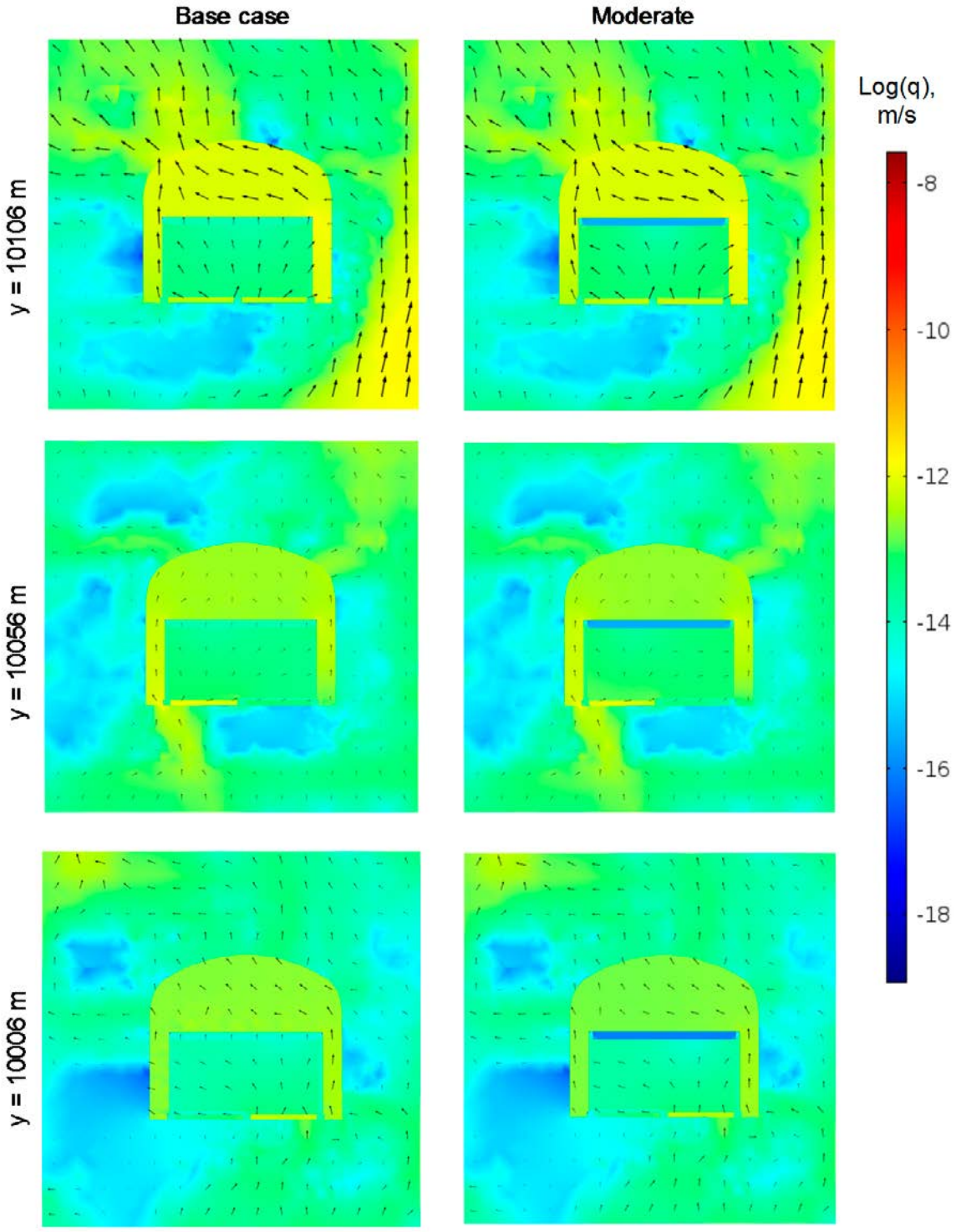

Figure 4-26. *Impact of moderate degradation of the outer and inner walls on the water Darcy fluxes and its magnitude at three cross-sections (xz planes) of the 1BMA submodel for shoreline position 1.*

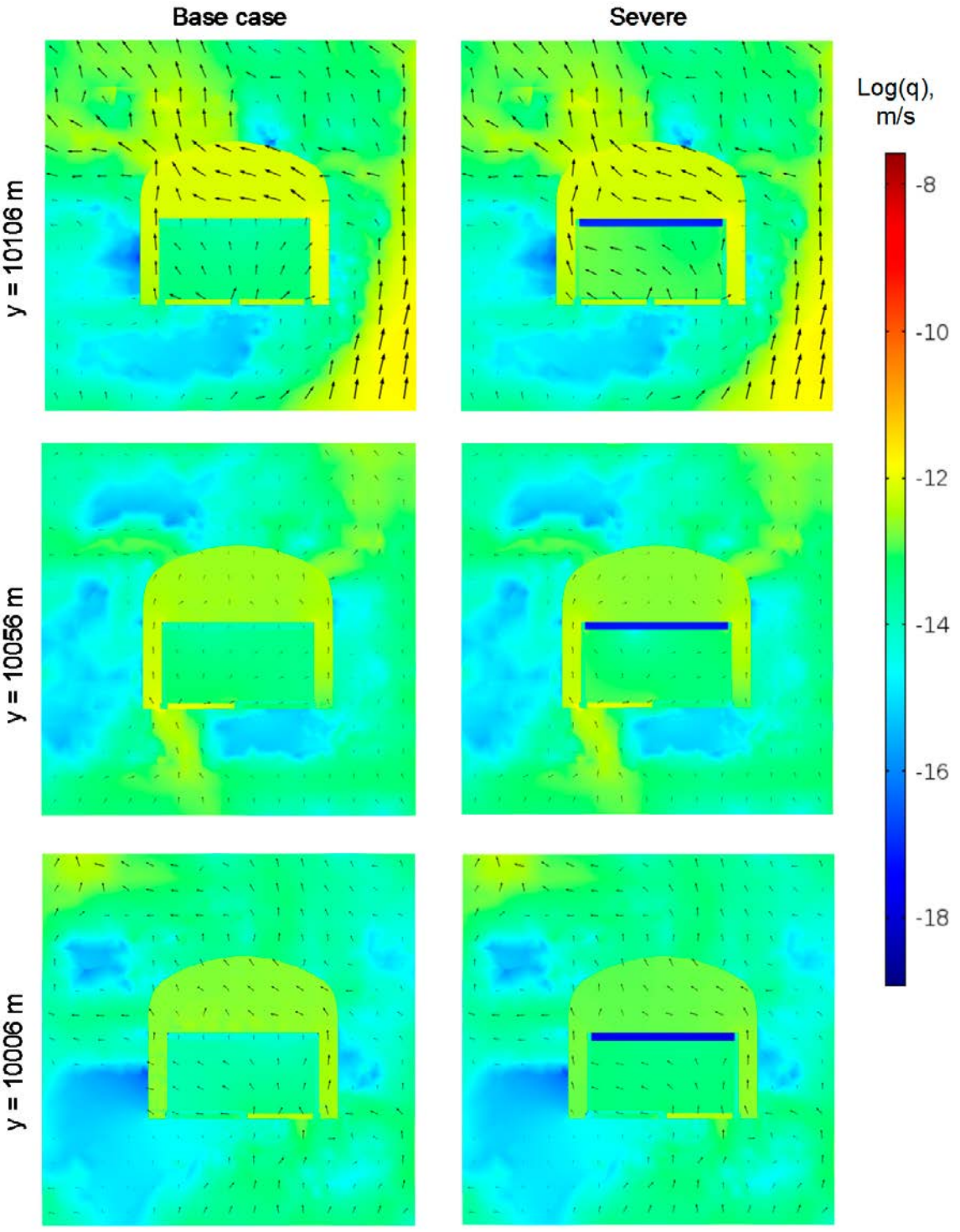

Figure 4-27. *Impact of severe degradation of the outer and inner walls on the water Darcy fluxes and its magnitude at three cross-sections (xz planes) of the 1BMA submodel for shoreline position 1.*

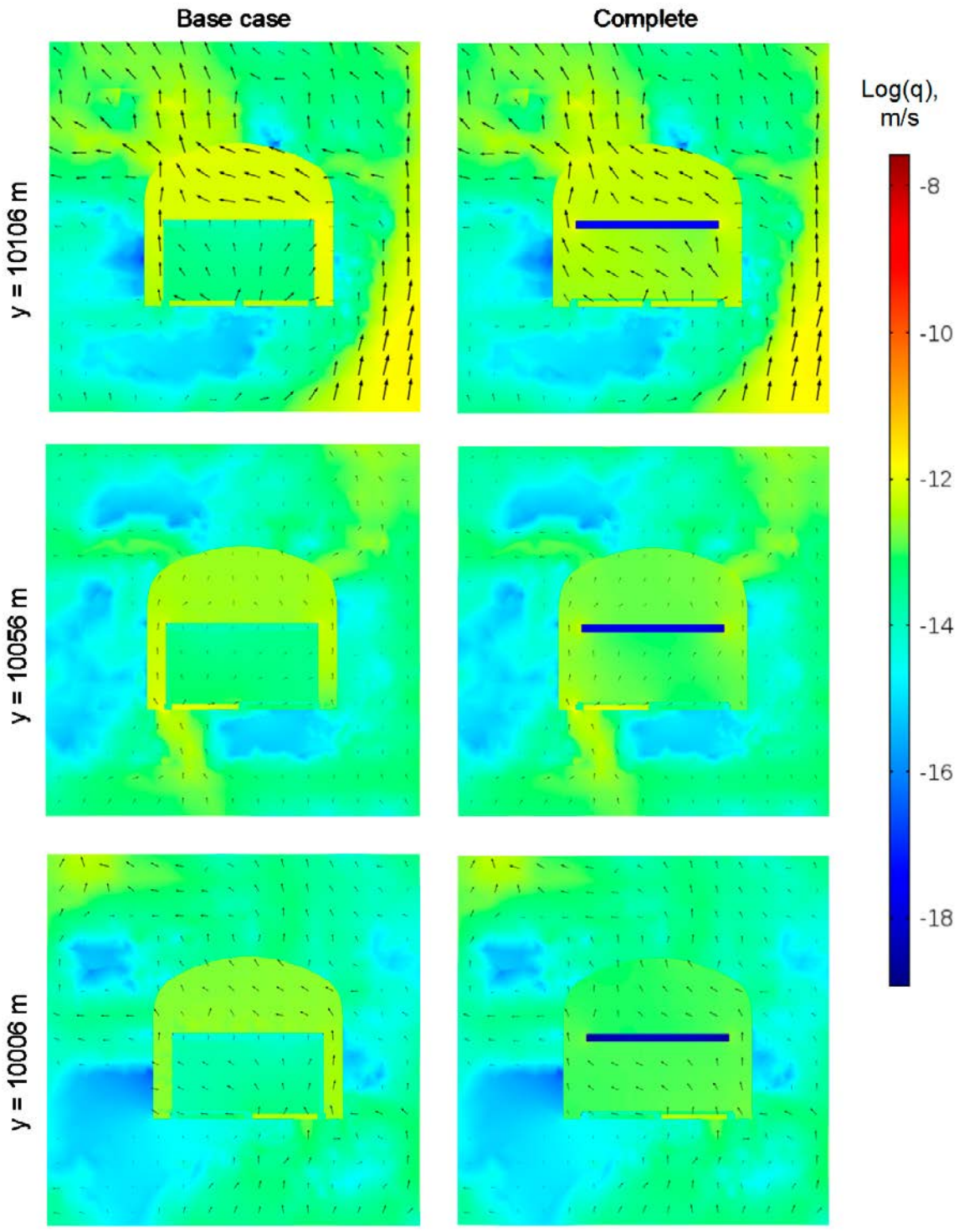

Figure 4-28. *Impact of complete degradation of the outer and inner walls on the water Darcy fluxes and its magnitude at three cross-sections (xz planes) of the 1BMA submodel for shoreline position 1.*

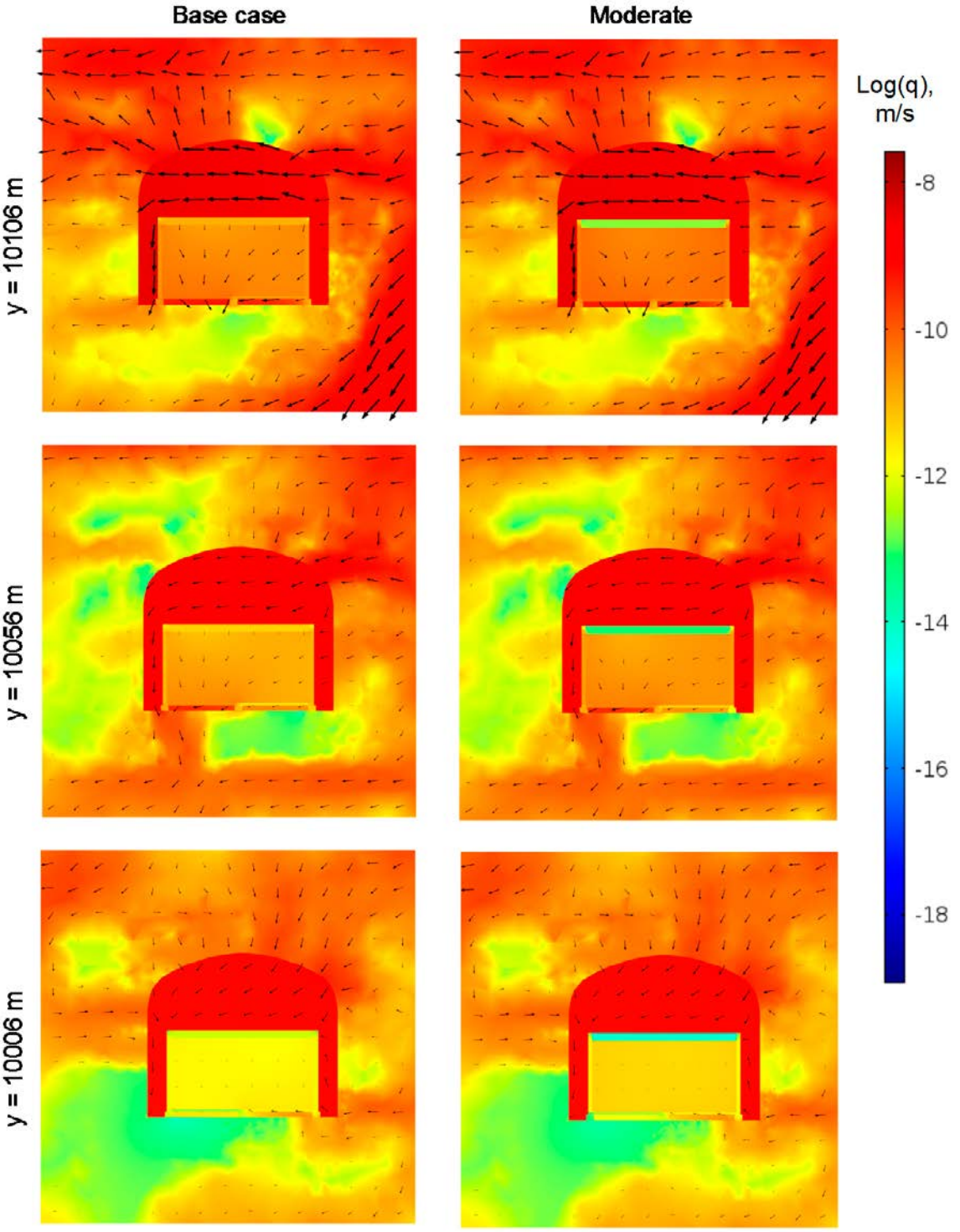

Figure 4-29. *Impact of moderate degradation of the outer and inner walls on the water Darcy fluxes and its magnitude at three cross-sections (xz planes) of the 1BMA submodel 1BMA at for shoreline position 3.*

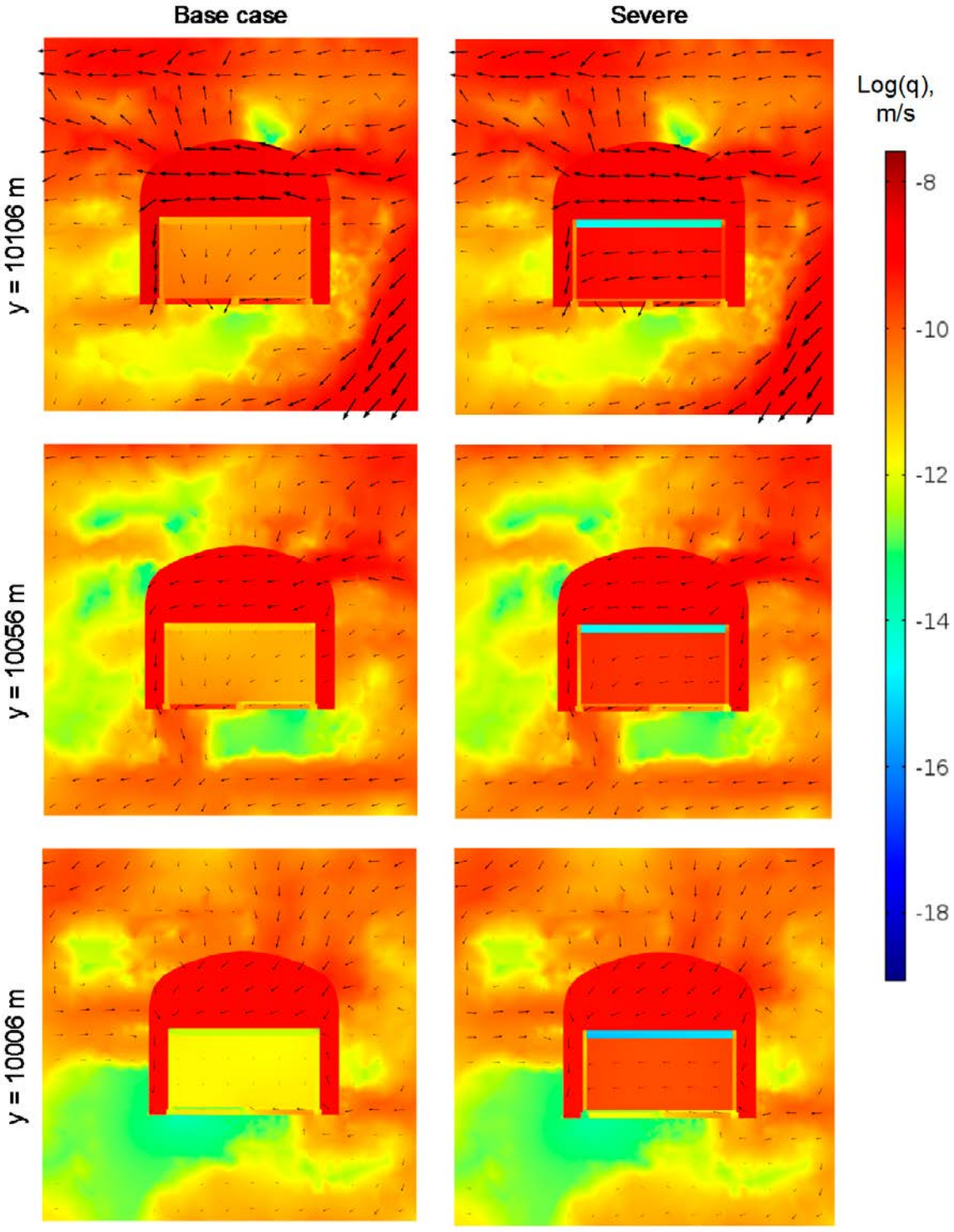

Figure 4-30. *Impact of severe degradation of the outer and inner walls on the water Darcy fluxes and its magnitude at three cross-sections (xz planes) of the 1BMA submodel 1BMA at for shoreline position 3.*

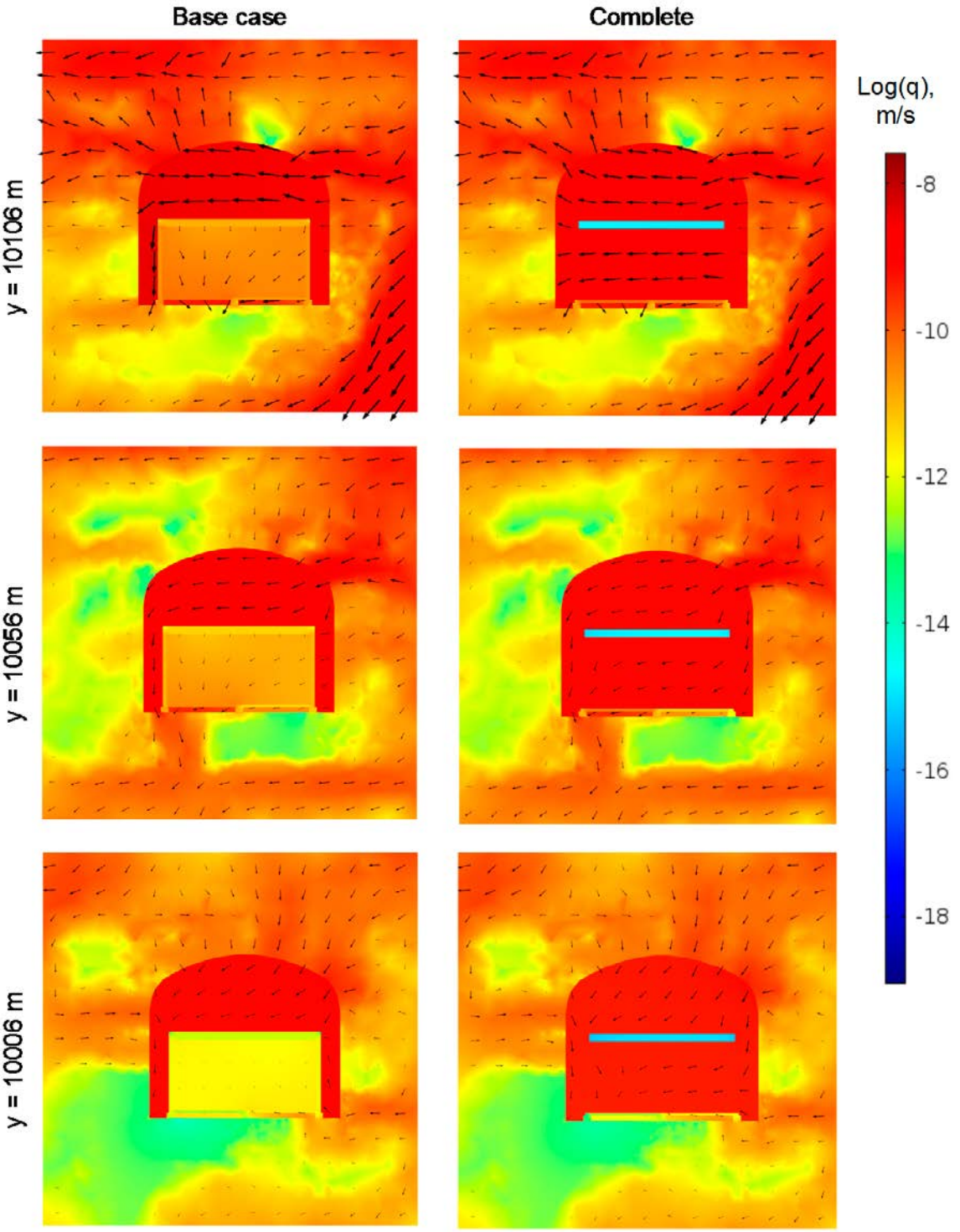

Figure 4-31. *Impact of complete degradation of the outer and inner walls on the water Darcy fluxes and its magnitude at three cross-sections (xz planes) of the 1BMA submodel 1BMA at for shoreline position 3.*

4.2.6 Case 6: Degradation of outer walls, lids, and floor

The next case combines concrete floor, lids, and outer walls degradation. As can be inferred from degradation Cases 1 and 4, the flow pattern of the present case should display similar characteristics. This is confirmed when comparing Figure 4-14, Figure 4-24 and Figure 4-32. However, considering concrete lids degradation in combination with concrete floor and outer walls degradation leads to higher flow rates in all cases when compared to Cases 1 and 4 (Table 4-9).

Table 4-9. Summary of total flow ($m^3 \cdot year^{-1}$) through the 1BMA vault and waste domain for the concrete floor, lids, and outer walls degradation case (Case 6) and the three shoreline positions.

Case 6 Degradation state	Vault total flow ($m^3 \cdot year^{-1}$)	Waste total flow ($m^3 \cdot year^{-1}$)	Waste normalized	Waste/Vault ratio	Case 6/Case 4 waste total flow ratio
	Shoreline position 1				
Base case	4.09E–02	6.90E–03	100%	16.84%	1.00
Moderate	4.52E–02	1.96E–02	284%	43.25%	2.37
Severe	4.61E–02	2.16E–02	314%	46.86%	2.44
Complete	4.62E–02	2.51E–02	364%	54.37%	2.08
	Shoreline position 2				
Base case	28.6	1.17	100%	4.10%	1.00
Moderate	29.7	3.94	336%	13.25%	2.77
Severe	30.0	4.54	387%	15.15%	1.52
Complete	30.0	14.9	1,266%	49.53%	1.34
	Shoreline position 3				
Base case	61.9	3.13	100%	5.06%	1.00
Moderate	64.7	10.8	346%	16.74%	2.86
Severe	65.3	12.4	396%	18.98%	1.79
Complete	65.4	32.5	1,038%	49.69%	1.53

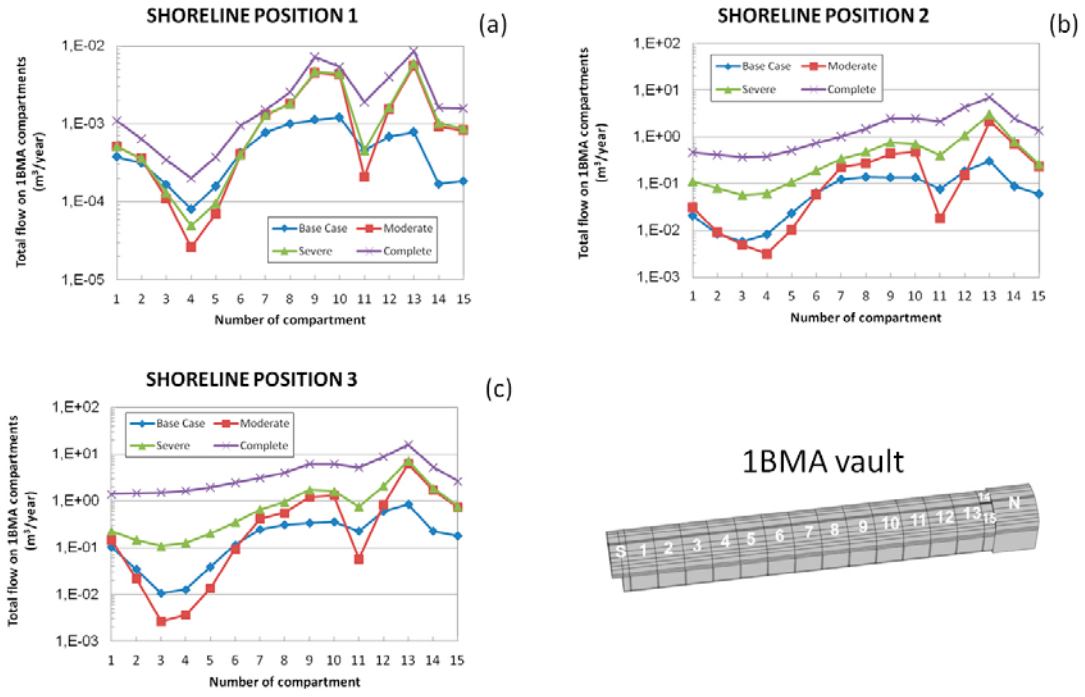

Figure 4-32. Flow rates ($m^3 \cdot year^{-1}$) through the waste compartments of the 1BMA submodel for degradation of outer walls, lids, and floor.

For the moderate degradation state, the total flow within the waste displays a close correlation with the local distribution of rock conductivity. This is due to the fact that the inner walls are not degraded, as in previous cases. A redistribution of flow rates with respect to the Base case is again observed near deformation zone ZFMNNW1209.

On the other hand, the increase in total flow through the waste domain is compensated with a decrease through the top gravel for shoreline position 1 (see Appendix A, Figure A-21). A redistribution of flow rates through the bottom gravel with respect to the Base case is also observed around deformation zone ZFMNNW1209 (see Appendix A, Figure A-21).

Figure 4-33 to Figure 4-35 and Figure 4-36 to Figure 4-38 show the Darcy velocity field and the distribution of its magnitude at three different vertical cross-sections (xz planes) of the 1BMA vault (see Figure 4-16) for shoreline positions 1 and 3, respectively. Velocities are normalized with respect to the maximum magnitude of the Darcy velocity obtained for each shoreline position.

As with other degradation cases, the Darcy velocity field is mainly vertical and follows the distribution of rock conductivity for shoreline position 1 (see e.g. Figure 4-36 to Figure 4-38 for y = 10,056, 10,106 m). Analogously to cases 1 and 2, concrete floor degradation causes water to flow vertically upwards into the vault and waste domain. Flow velocities through the backfill are higher for moderate and severe degradation compared to a complete degradation state (see Figure 4-36 to Figure 4-38 for y = 10,056 m). Similarly to Case 2, concrete floor degradation induces a vertical flow through the waste connected with high rock conductivity zones, e.g. at y = 10,056 m. In contrast, a complete degradation of the concrete lids enhances the hydraulic connectivity between the waste domain and backfill, as compared to moderate and severe degradation states (see Figure 4-36 to Figure 4-38 for y = 10,106 m). Therefore, simultaneous floor and lid concrete degradation promotes preferential flow paths connecting the vault with the rock.

On the other hand, for shoreline position 3 the total flow through the waste compartments increases as the degradation of outer walls, lids, and floor proceeds, as shown in Figure 4-36 to Figure 4-38. The same occurs with the flow through the backfill. Preferential flow paths connecting vertical flow through the vault with the flow through the rock are found again. As opposed to Cases 2 and 5, in this case higher degradation states are related with higher total flow through the degraded elements (lids, floor, or outer walls).

Conclusions: Flow rates through the waste compartments are significantly affected by degradation of lids, floor, and outer walls, generally having a higher impact when compared to other degradation cases (at least for the moderate and severe degradation cases). This is probably related to the fact that in this case all the external concrete barriers of the waste compartments are degraded simultaneously, thus controlling the connectivity between flow through the vault and through the waste domain. For a moderate degradation state the total flow in the waste domain displays a close relation with the local distribution of rock conductivity, which is due to the intact state of the inner concrete walls. A redistribution of flow rates with respect to the Base case is again observed near deformation zone ZFMNNW1209.

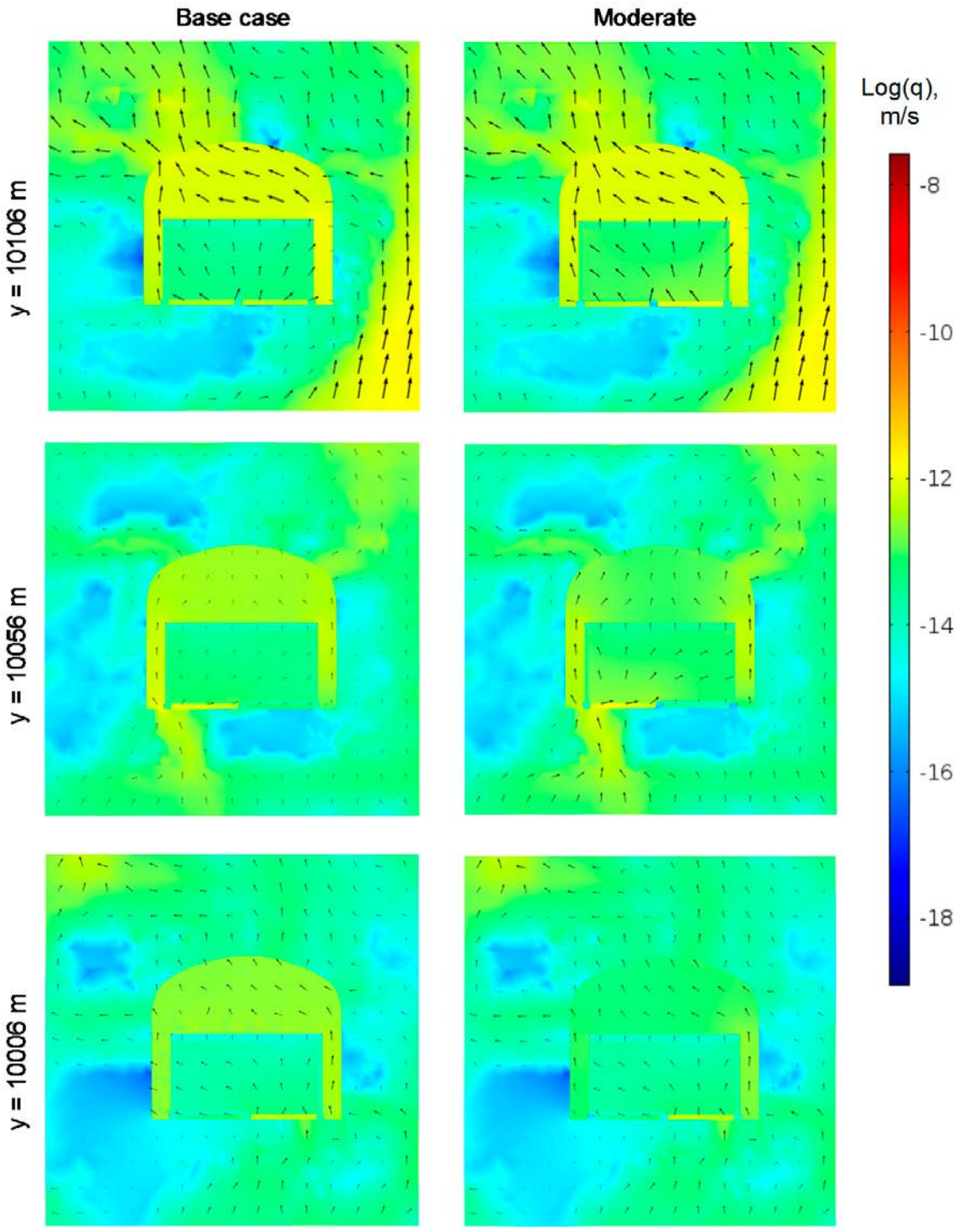

Figure 4-33. *Impact of moderate degradation of outer walls, lids, and floor on water Darcy fluxes ($m \cdot s^{-1}$) and its magnitude at three vertical cross-sections (xz planes) of the 1BMA submodel 1BMA at for shoreline position 1.*

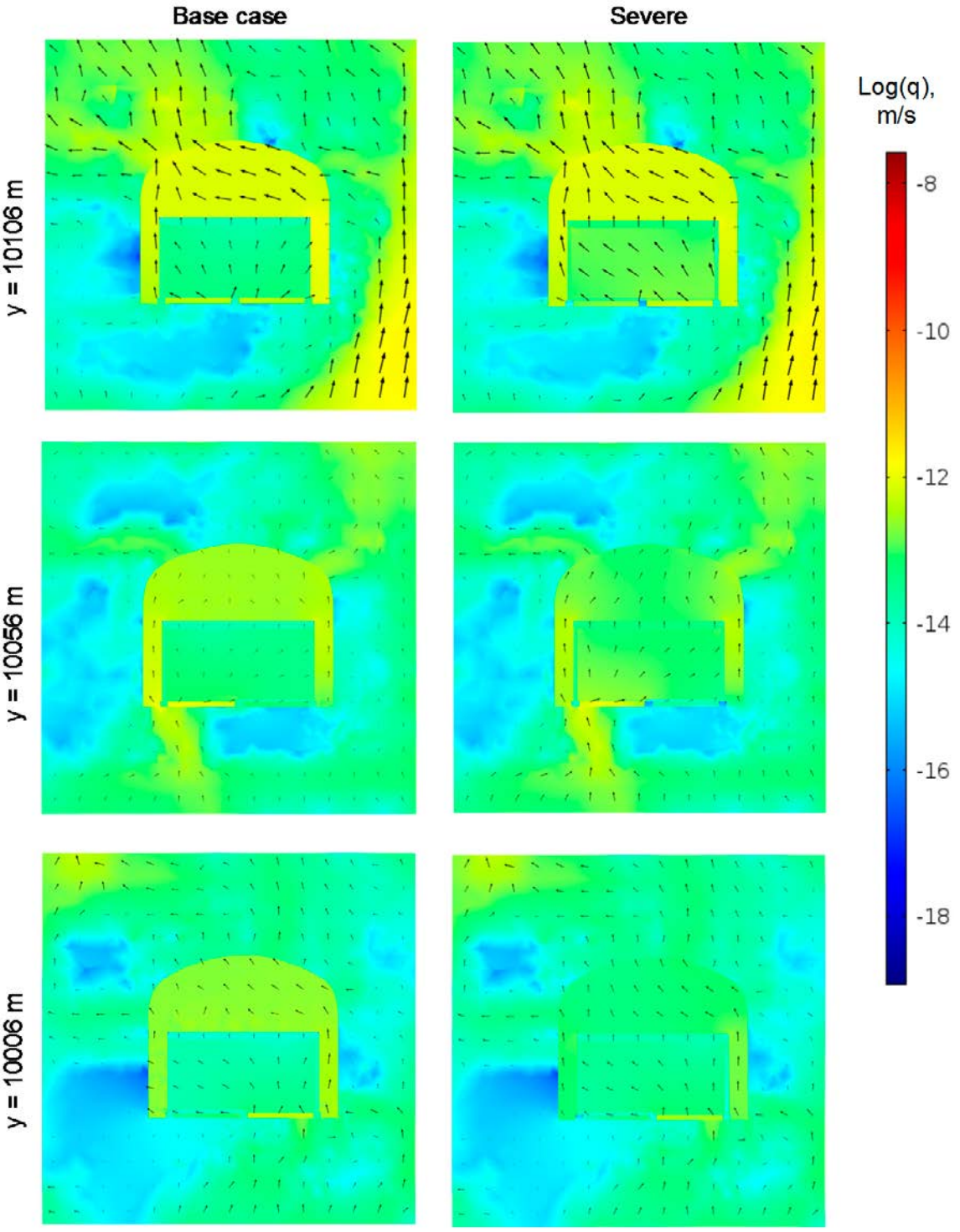

Figure 4-34. *Impact of severe degradation of outer walls, lids, and floor on water Darcy fluxes ($m \cdot s^{-1}$) and its magnitude at three vertical cross-sections (xz planes) of the 1BMA submodel 1BMA at for shoreline position 1.*

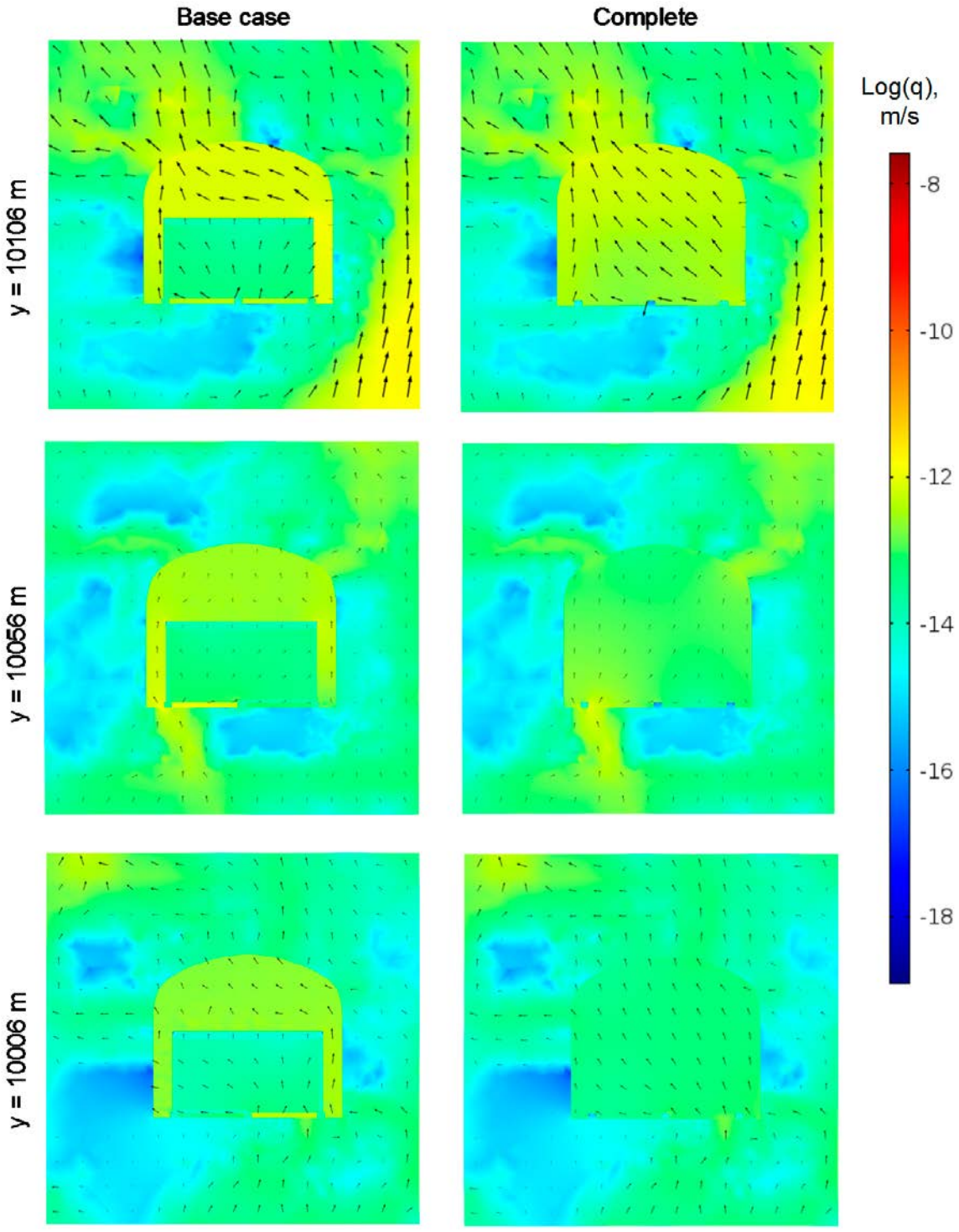

Figure 4-35. *Impact of complete degradation of outer walls, lids, and floor on water Darcy fluxes ($m \cdot s^{-1}$) and its magnitude at three vertical cross-sections (xz planes) of the 1BMA submodel 1BMA at for shoreline position 1.*

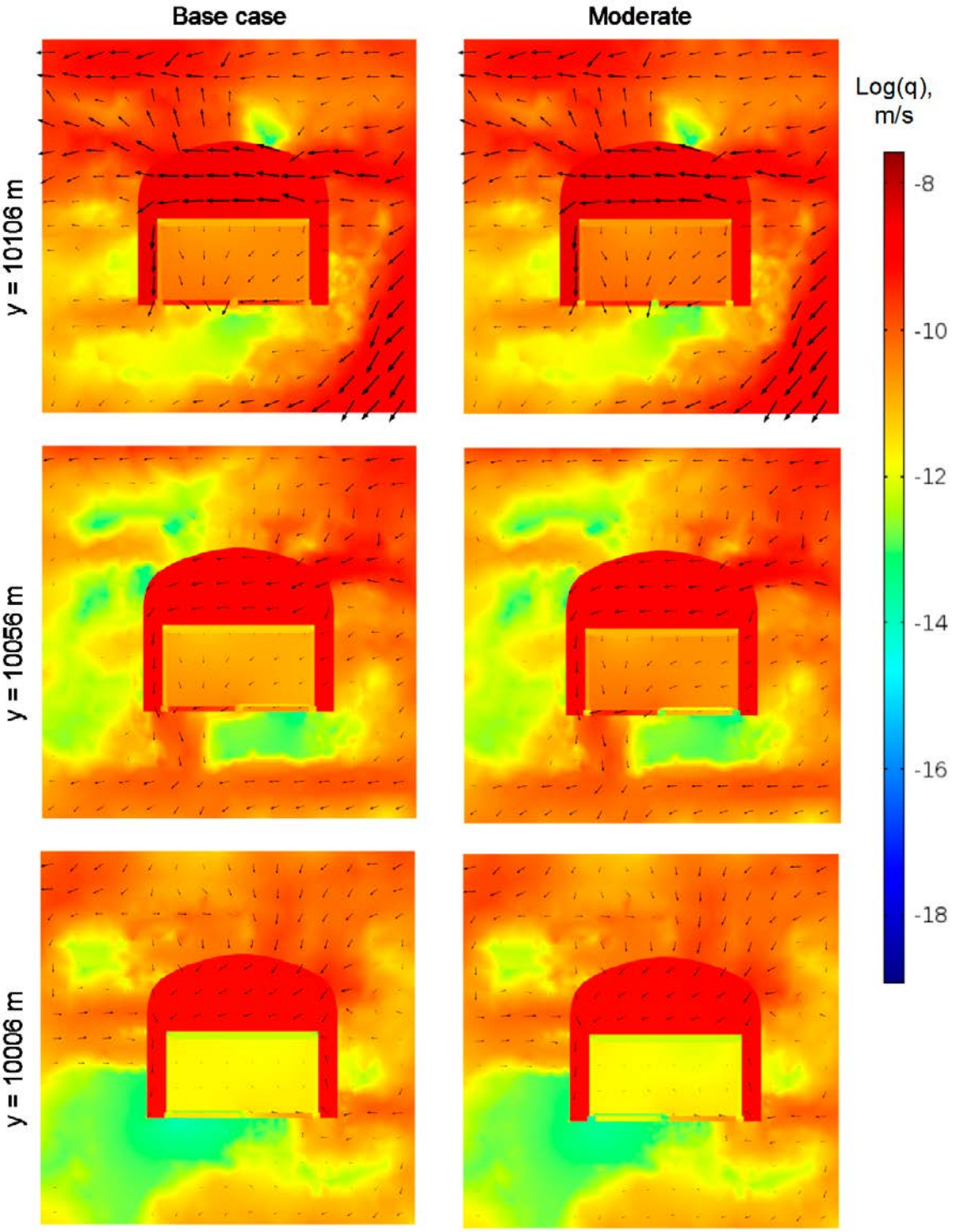

Figure 4-36. *Impact of moderate degradation of outer walls, lids, and floor on Darcy fluxes ($m \cdot s^{-1}$) and its magnitude at three vertical cross-sections (xz planes) of the 1BMA submodel for shoreline position 3.*

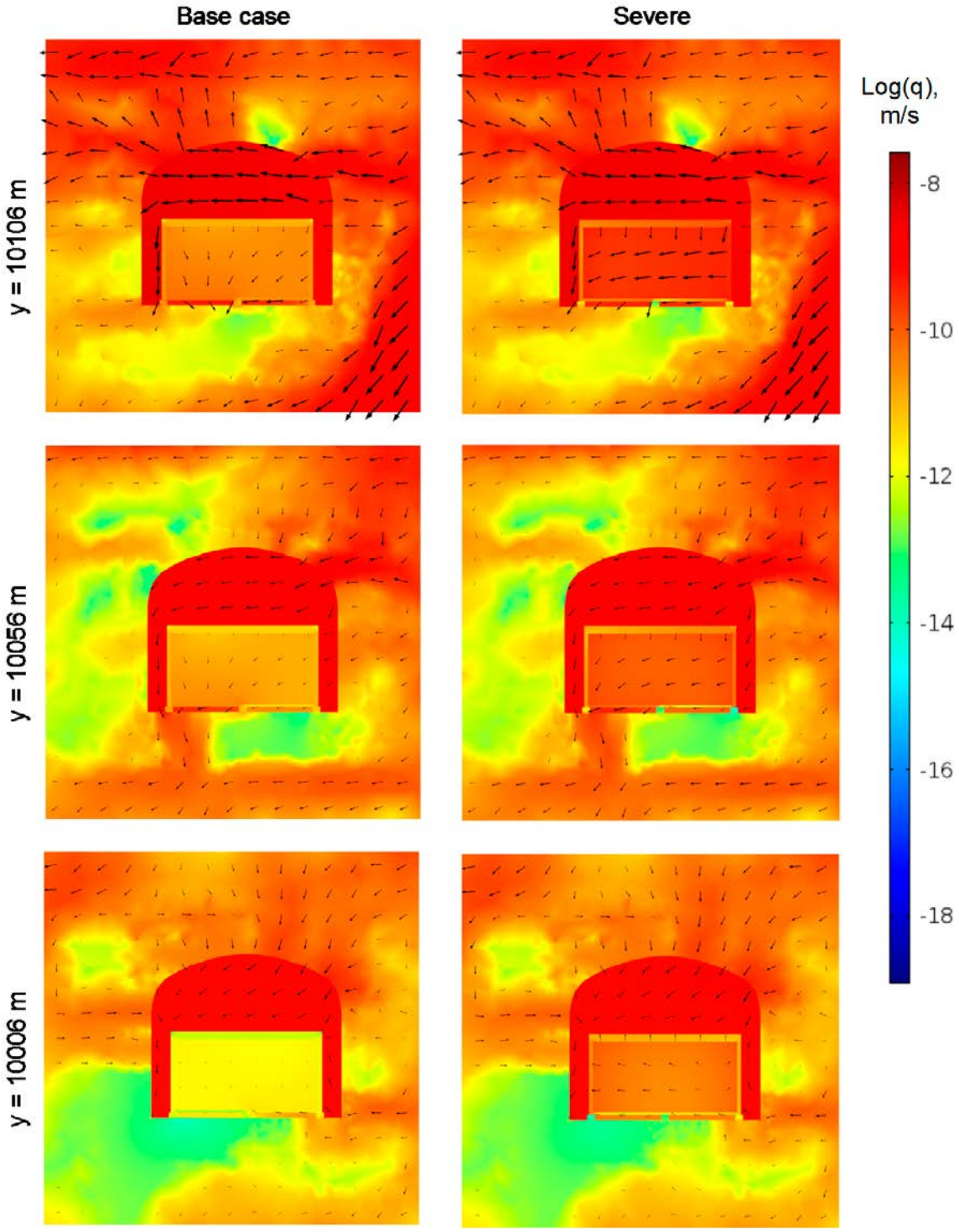

Figure 4-37. *Impact of severe degradation of outer walls, lids, and floor on Darcy fluxes ($m \cdot s^{-1}$) and its magnitude at three vertical cross-sections (xz planes) of the 1BMA submodel for shoreline position 3.*

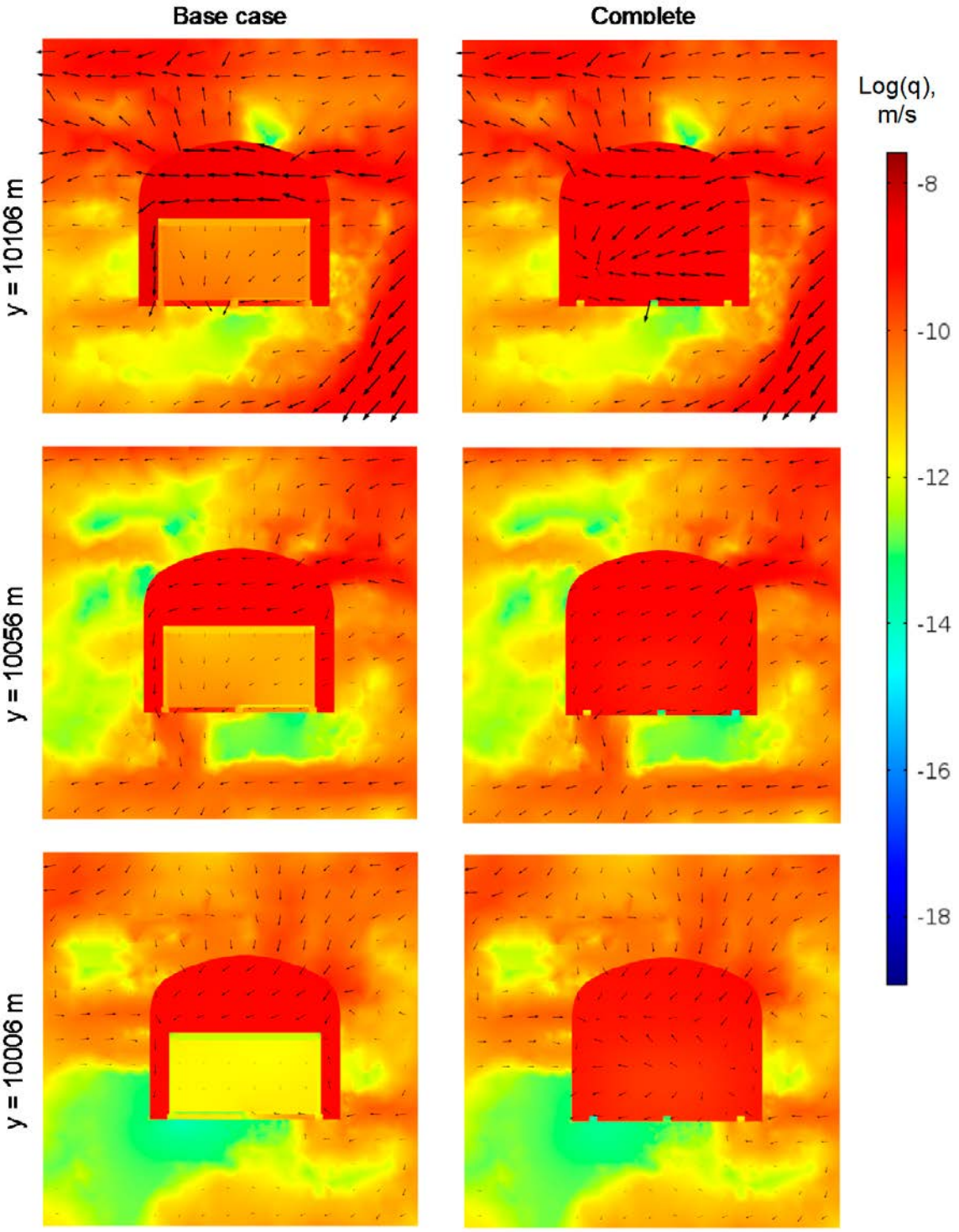

Figure 4-38. *Impact of complete degradation of outer walls, lids, and floor on Darcy fluxes ($m \cdot s^{-1}$) and its magnitude at three vertical cross-sections (xz planes) of the 1BMA submodel for shoreline position 3.*

4.2.7 Summary of vault element degradation scenarios

The results presented for the vault element degradation cases and the three shoreline positions are summarized in Table 4-10 and Table 4-11, Figure 4-39 to Figure 4-41, and Figure A-25 to Figure A-27 of Appendix A. Differences included in Table 4-11 and Table 4-11 correspond to the relative difference between the total flow for a given degradation state with respect to the total flow of the Base case. The results indicate that concrete degradation has a moderate impact in the total flow in the 1BMA vault (less than 15% increase for shoreline position 1 and less than 6% for shoreline positions 2 and 3). The highest increments in the total tunnel flow occur in the cases considering the concrete floor degradation (1, 2 and 6).

Table 4-10. Summary of total flow rates ($m^3 \cdot year^{-1}$) through the 1BMA vault for different vault element degradation cases. Differences with respect to the Base case (positive values indicate higher flow with respect to the Base case).

Case	ID	Shoreline position 1		Shoreline position 2		Shoreline position 3	
		Total flow rate ($m^3 \cdot year^{-1}$)	Difference	Total flow rate ($m^3 \cdot year^{-1}$)	Difference	Total flow rate ($m^3 \cdot year^{-1}$)	Difference
Case 1	1	4.38E–02	6.9%	29.22	2.0%	63.47	2.5%
	2	4.65E–02	13.6%	29.84	4.2%	64.95	4.9%
	3	4.66E–02	13.8%	29.87	4.3%	65.03	5.1%
Case 2	4	4.52E–02	10.4%	29.74	3.8%	64.66	4.5%
	5	4.61E–02	12.7%	29.98	4.7%	65.31	5.5%
	6	4.62E–02	12.9%	30.01	4.8%	65.37	5.6%
Case 3	7	4.16E–02	1.6%	28.74	0.3%	62.30	0.7%
	8	4.16E–02	1.6%	28.75	0.4%	62.32	0.7%
	9	4.16E–02	1.7%	28.76	0.4%	62.35	0.7%
Case 4	10	4.16E–02	1.6%	28.75	0.4%	62.32	0.7%
	11	4.16E–02	1.7%	28.76	0.4%	62.34	0.7%
	12	4.16E–02	1.7%	28.79	0.5%	62.41	0.8%
Case 5	13	4.15E–02	1.3%	29.02	1.3%	62.94	1.7%
	14	4.17E–02	1.9%	29.20	2.0%	63.37	2.4%
	15	4.18E–02	2.0%	29.25	2.1%	63.50	2.6%
Case 6	16	4.63E–02	13.0%	29.77	3.9%	64.79	4.7%
	17	4.66E–02	13.8%	29.86	4.2%	65.01	5.0%
	18	4.66E–02	13.8%	29.92	4.4%	65.14	5.2%

In contrast, significant effects of concrete degradation on the flow profiles in the waste compartments and the total flow through the waste domain are predicted, especially for the Cases 2, 5, and 6. The highest differences with respect to the Base case are found for shoreline position 2 (see Table 4-11). The results have shown that the degradation of concrete vault elements induces an internal redistribution of the flow. According to the model, the degradation of the concrete of the inner and outer walls of the waste compartments has the highest impact on total flow through the waste domain.

Degradation of one outer concrete wall (Case 3) and both outer concrete walls (Case 4), although inducing a significant increase in flow rates through the waste domain, have a smaller impact compared to the other degradation cases. For Cases 3 and 4 the flow distribution within the waste reflects the local distribution of rock conductivity. This is since the concrete walls remain intact, which promote a discrete distribution of the horizontal groundwater flow into individual waste compartments. A redistribution of flow rates with respect to the Base case is observed near deformation zone ZFMNNW1209 for these cases.

In terms of the total flow differences with respect to the Base case (Table 4-11), degradation of outer and inner walls (Case 5) is the most unfavorable case considered. Flow rates through the waste compartments are significantly affected by severe and complete degradation of outer and inner walls, increasing with degradation (the same applies to the backfill). Connectivity between waste compartments and high rock conductivity zones is considerably lower when an intact floor is considered as compared to concrete floor degradation cases (Cases 1 and 2). For Cases 2 and 5 the concrete degradation drives the flow towards the degraded walls and floor. This causes a reduction on the flow through intact waste compartment elements.

The degradation of lids, floor, and outer walls (Case 6) is the second most unfavorable situation, especially for the complete degradation state. Flow rates through the waste are significantly affected by this, having a higher impact on flow compared to other degradation cases. A redistribution of flow rates with respect to the Base case is again observed near deformation zone ZFMNNW1209.

It is noted that the degradation of the concrete beams that serve as a support for the concrete floor has not been considered for the present calculation cases. All the results discussed here consider an intact state of these beams.

Table 4-11. Summary of total flow rates ($m^3 \cdot year^{-1}$) through waste domain of the 1BMA vault for different vault element degradation cases. Differences with respect to the Base case (positive values indicate higher flow with respect to the Base case).

	ID	Shoreline position 1		Shoreline position 2		Shoreline position 3	
		Total flow rate ($m^3 \cdot year^{-1}$)	Difference	Total flow rate ($m^3 \cdot year^{-1}$)	Difference	Total flow rate ($m^3 \cdot year^{-1}$)	Difference
Case 1	1	1.58E–02	130%	3.00	155%	8.24	163%
	2	2.21E–02	221%	4.67	298%	12.88	311%
	3	2.27E–02	229%	7.33	525%	16.28	420%
Case 2	4	1.95E–02	184%	3.94	236%	10.82	246%
	5	2.16E–02	214%	4.54	287%	12.40	296%
	6	2.51E–02	264%	14.86	1,166%	32.49	938%
Case 3	7	9.24E–03	34%	1.65	41%	4.44	42%
	8	9.33E–03	35%	1.73	47%	4.56	46%
	9	1.01E–02	47%	3.93	235%	7.62	143%
Case 4	10	9.33E–03	35%	1.69	44%	4.53	45%
	11	9.53E–03	38%	5.11	336%	9.44	202%
	12	1.59E–02	130%	11.71	897%	20.90	568%
Case 5	13	9.04E–03	31%	1.57	34%	4.20	34%
	14	9.25E–03	34%	5.98	409%	11.63	271%
	15	2.03E–02	195%	17.11	1,357%	33.59	973%
Case 6	16	2.21E–02	220%	4.68	299%	12.94	314%
	17	2.33E–02	238%	7.78	562%	16.92	440%
	18	3.31E–02	380%	15.71	1,238%	32.07	924%

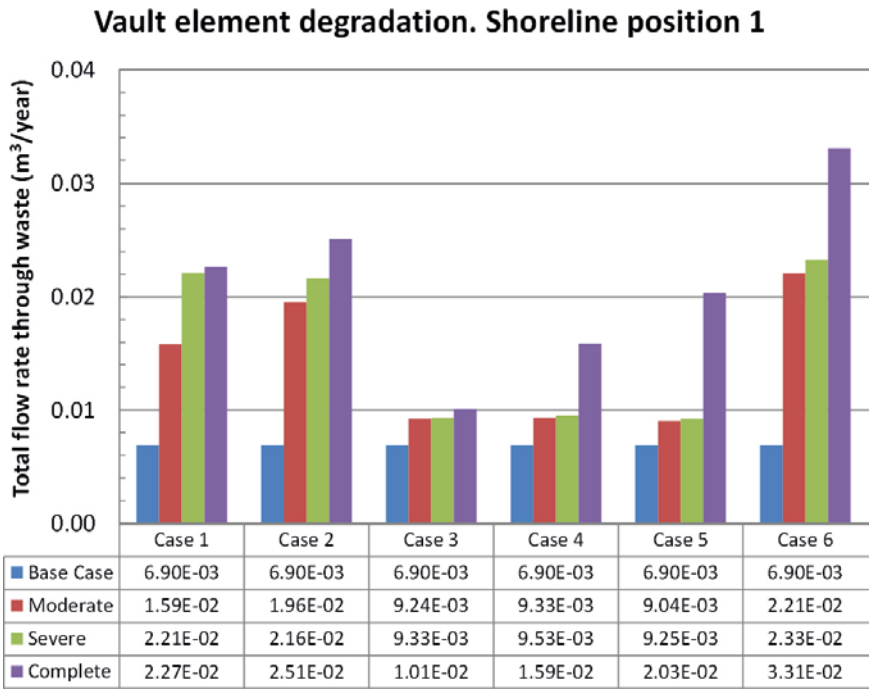

Figure 4-39. *Total flow rates through the waste zone of 1BMA submodel for different scenarios of vault element degradation and comparison with the Base case at shoreline position 1.*

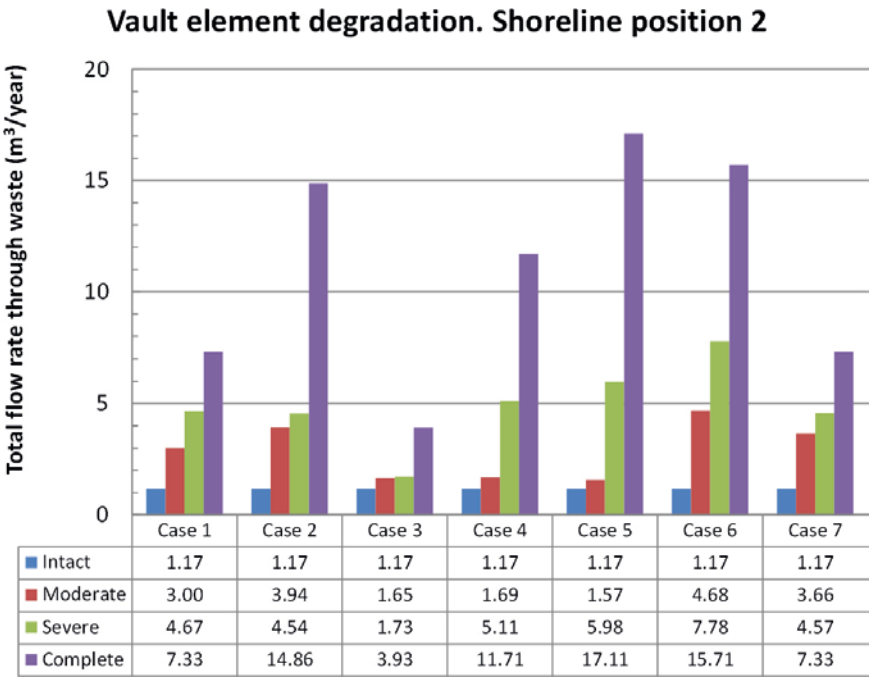

	Case 1	Case 2	Case 3	Case 4	Case 5	Case 6	Case 7
Intact	1.17	1.17	1.17	1.17	1.17	1.17	1.17
Moderate	3.00	3.94	1.65	1.69	1.57	4.68	3.66
Severe	4.67	4.54	1.73	5.11	5.98	7.78	4.57
Complete	7.33	14.86	3.93	11.71	17.11	15.71	7.33

Figure 4-40. *Total flow rates through the waste zone of 1BMA submodel for different scenarios of vault element degradation and comparison with the Base case at shoreline position 3.*

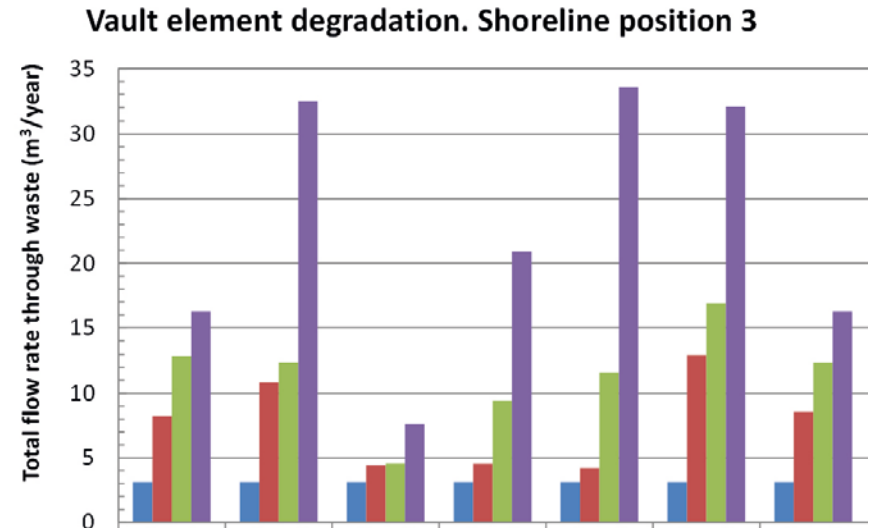

	Case 1	Case 2	Case 3	Case 4	Case 5	Case 6	Case 7
Intact	3.13	3.13	3.13	3.13	3.13	3.13	3.13
Moderate	8.24	10.82	4.44	4.53	4.20	12.94	8.56
Severe	12.88	12.40	4.56	9.44	11.63	16.92	12.37
Complete	16.28	32.49	7.62	20.90	33.59	32.07	16.28

Figure 4-41. *Total flow rates through the waste zone of 1BMA submodel for different scenarios of vault element degradation and comparison with the Base case at shoreline position 3.*

4.3 Compartments degradation

The results for the 1BMA in the repository-scale model have highlighted an important spatial variability in the total flow through the 1BMA waste compartments (Figure 4-42). In this section, the effects of such variability on the hydraulic conductivity of the concrete in the different waste compartments and ultimately on the flow rates are analyzed in detail. To this end, the hydraulic properties of each compartment are defined individually.

Two areas of preferential inflow towards the waste can be identified based on the rock conductivity at the surroundings of the 1BMA vault (Figure 4-43), and on the calculated total flow per waste compartment (Figure 4-42). The main preferential inflow zone is associated with the vertical deformation zone ZFMNNW1209 (former zone 6), which affects the waste compartments 12 to 15. The second inflow zone is the result of two minor fractures affecting waste compartments 9 and 10. The inflow in these compartments is especially significant in the case of vertical upward flow (i.e. shoreline position 1).

Four cases have been considered to evaluate the interaction between preferential flow and concrete degradation. In these scenarios, a different concrete degradation state is assumed for the different waste compartments.

- Case 1: Degradation of the concrete in compartments 12–15 associated with the deformation zone ZFMNNW1209.
- Case 2: Degradation of the concrete in compartments: 3 and 4, which are associated with the lowest flow rates.
- Case 3: Simultaneous concrete degradation of all the compartments affected by fracture zones: 9, 10, 12, 13, 14, and 15.
- Case 4: Compartment degradation proportional to the fluxes calculated for the Base case (intact state of concrete).

For each of these scenarios, the effect of the waste encapsulation (floor, lid, and inner and outer concrete walls) degradation is studied with a set of three simulations of increasing concrete conductivity in addition to the Base case. Similarly to the vault element degradation study (Section 4.2), these simulations correspond to the case of a moderate, a severe and a complete concrete degradation state, gradually increasing the conductivity. The hydraulic conductivity of concrete in each waste compartment is defined in Table 4-12 for simulation Cases 1, 2 and 3 and in Table 4-13 for Case 4. The hydraulic conductivity of the waste domain was increased accordingly, maintaining a contrast of three orders of magnitude between the hydraulic conductivity of the waste and the concrete. However, an upper threshold of the hydraulic conductivity of the waste was set to $1 \cdot 10^{-3}$ m·s^{-1}, which corresponds to the value assigned to the permeable backfill in the vault. The properties of remaining materials were unaltered. Each of these cases is analyzed for shorelines positions 1, 2, and 3 (as defined in Abarca et al. 2013). A total of 36 simulations (three degradation states times three shoreline positions times four cases) have been performed, in addition to the Base case simulations. Table 4-12 and Table 4-13 summarize the parameters considered in each simulation. Colors are used to emphasize the compartments that are degraded in each case as well as the degradation state.

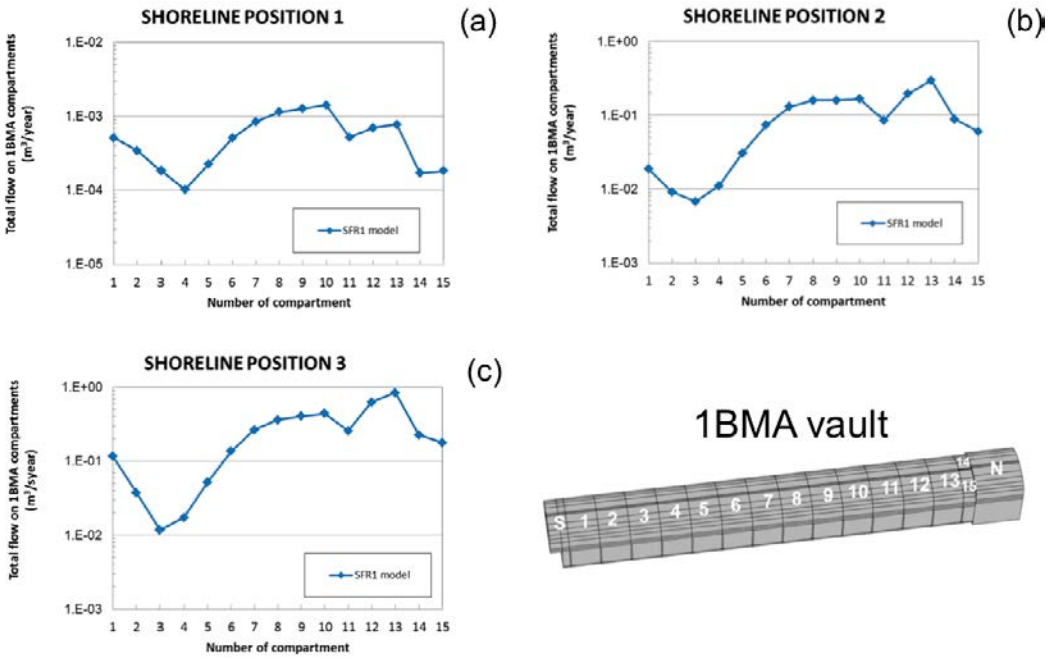

Figure 4-42. *Total flow rates ($m^3 \cdot year^{-1}$) through the waste compartments calculated with the SFR 1 repository-scale model for the Base case.*

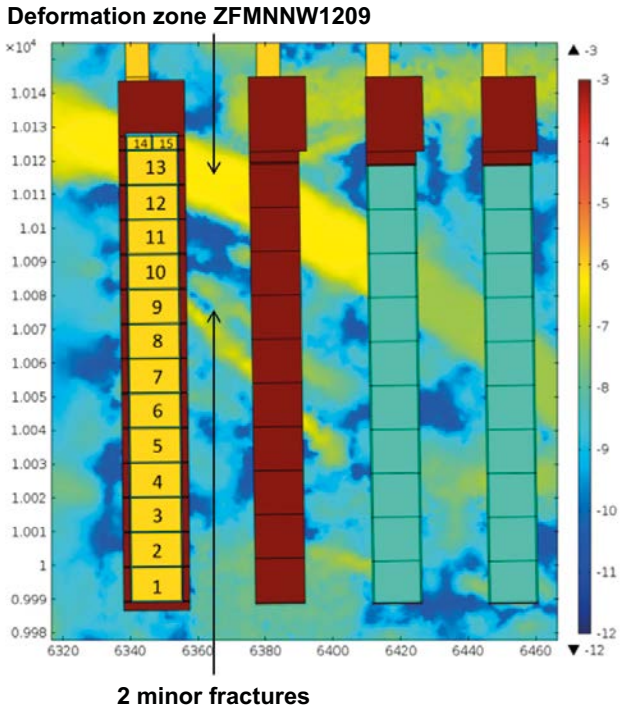

Figure 4-43. *Hydraulic conductivity field, log_{10}(K [m/s]), of the rock and vaults in a horizontal cross-section at z = 82.5 m.*

Table 4-12. Hydraulic conductivity ($m \cdot s^{-1}$) of concrete in each waste compartment assumed in the simulations of compartments degradation.

Hydraulic conductivity ($m \cdot s^{-1}$) of Waste Compartment (WC)																
Case		ID	WC1	WC2	WC3	WC4	WC5	WC6	WC7	WC8	WC9	WC10	WC11	WC12	WC13	WC14	WC15
Case 1	Moderate	1	8.3E–10	8.3E–10	8.3E–10	8.3E–10	8.3E–10	8.3E–10	8.3E–10	8.3E–10	8.3E–10	8.3E–10	8.3E–10	1.0E–7	1.0E–7	1.0E–7	1.0E–7
	Severe	2	8.3E–10	8.3E–10	8.3E–10	8.3E–10	8.3E–10	8.3E–10	8.3E–10	8.3E–10	8.3E–10	8.3E–10	8.3E–10	1.0E–5	1.0E–5	1.0E–5	1.0E–5
	Complete	3	8.3E–10	8.3E–10	8.3E–10	8.3E–10	8.3E–10	8.3E–10	8.3E–10	8.3E–10	8.3E–10	8.3E–10	8.3E–10	1.0E–3	1.0E–3	1.0E–3	1.0E–3
Case 2	Moderate	4	8.3E–10	8.3E–10	1.0E–7	1.0E–7	8.3E–10	8.3E–10	8.3E–10	8.3E–10	8.3E–10	8.3E–10	8.3E–10	8.3E–10	8.3E–10	8.3E–10	8.3E–10
	Severe	5	8.3E–10	8.3E–10	1.0E–5	1.0E–5	8.3E–10	8.3E–10	8.3E–10	8.3E–10	8.3E–10	8.3E–10	8.3E–10	8.3E–10	8.3E–10	8.3E–10	8.3E–10
	Complete	6	8.3E–10	8.3E–10	1.0E–3	1.0E–3	8.3E–10	8.3E–10	8.3E–10	8.3E–10	8.3E–10	8.3E–10	8.3E–10	8.3E–10	8.3E–10	8.3E–10	8.3E–10
Case 3	Moderate	7	8.3E–10	8.3E–10	8.3E–10	8.3E–10	8.3E–10	8.3E–10	8.3E–10	8.3E–10	1.0E–7	1.0E–7	8.3E–10	1.0E–7	1.0E–7	1.0E–7	1.0E–7
	Severe	8	8.3E–10	8.3E–10	8.3E–10	8.3E–10	8.3E–10	8.3E–10	8.3E–10	8.3E–10	1.0E–5	1.0E–5	8.3E–10	1.0E–5	1.0E–5	1.0E–5	1.0E–5
	Complete	9	8.3E–10	8.3E–10	8.3E–10	8.3E–10	8.3E–10	8.3E–10	8.3E–10	8.3E–10	1.0E–3	1.0E–3	8.3E–10	1.0E–3	1.0E–3	1.0E–3	1.0E–3

Table 4-13. Hydraulic conductivity ($m\ s^{-1}$) in concrete of waste compartments assumed in compartment degradation proportional to the flow rate (Case 4).

Case 4	Shoreline position 1			Shoreline position 3			Shoreline position 3		
Compartment	Moderate	Severe	Complete	Moderate	Severe	Complete	Moderate	Severe	Complete
WC1	8.32E–10	1.07E–09	2.50E–08	8.30E–10	3.97E–09	3.18E–07	1.21E–08	1.14E–06	1.14E–04
WC2	8.32E–10	1.08E–09	2.59E–08	8.30E–10	4.42E–09	3.63E–07	1.49E–08	1.42E–06	1.42E–04
WC3	8.32E–10	9.82E–10	1.61E–08	8.30E–10	4.47E–09	3.68E–07	1.66E–08	1.59E–06	1.59E–04
WC4	8.31E–10	9.21E–10	9.91E–09	8.30E–10	4.80E–09	4.01E–07	1.83E–08	1.77E–06	1.76E–04
WC5	8.30E–10	8.30E–10	8.30E–10	8.30E–10	5.80E–09	5.02E–07	2.13E–08	2.06E–06	2.06E–04
WC6	8.40E–10	1.87E–09	1.04E–07	8.30E–10	7.51E–09	6.74E–07	2.56E–08	2.50E–06	2.50E–04
WC7	8.45E–10	2.29E–09	1.47E–07	8.30E–10	9.94E–09	9.19E–07	3.16E–08	3.10E–06	3.10E–04
WC8	8.56E–10	3.44E–09	2.62E–07	8.30E–10	1.36E–08	1.29E–06	4.00E–08	3.95E–06	3.95E–04
WC9	8.74E–10	5.28E–09	4.46E–07	1.00E–03	1.96E–08	1.89E–06	5.24E–08	5.20E–06	5.20E–04
WC10	8.78E–10	5.65E–09	4.83E–07	1.00E–03	2.16E–08	2.09E–06	5.58E–08	5.55E–06	5.55E–04
WC11	8.55E–10	3.37E–09	2.55E–07	8.30E–10	2.26E–08	2.20E–06	5.76E–08	5.72E–06	5.72E–04
WC12	8.56E–10	3.49E–09	2.67E–07	1.00E–03	3.23E–08	3.17E–06	7.91E–08	7.89E–06	7.89E–04
WC13	8.79E–10	5.79E–09	4.97E–07	1.00E–03	4.27E–08	4.22E–06	1.00E–07	1.00E–05	1.00E–03
WC14	8.42E–10	2.09E–09	1.27E–07	1.00E–03	1.46E–08	1.39E–06	3.01E–08	2.96E–06	2.96E–04
WC15	8.42E–10	2.09E–09	1.27E–07	1.00E–03	8.26E–09	7.50E–07	1.88E–08	1.81E–06	1.81E–04

4.3.1 Case 1: Degradation in deformation zone ZFMNNW1209

This section explores the effect of concrete degradation in the compartments 12 to 15, which is associated with the vertical deformation zone ZFMNNW1209. Figure 4-44 shows the results of the total flow rate through the 1BMA waste compartments for the different concrete degradation states and the three shoreline positions. As can be observed, the total flow through the waste compartments 12 to 15 increases as the concrete degrades for all shoreline positions. This increase is mainly due to a redistribution of water within the vault itself, since the tunnel flow increases only by around 4% with respect to the Base case for all cases (Table 4-14). For shoreline positions 2 and 3, the redistribution of flow results in a reduction of the flow through the top and west gravel sections corresponding to the degraded waste compartments (see Figure B-1 and Figure B-4 in Appendix B). The flow increase in compartments 12, 13, 14, and 15 is accompanied by a flow decrease in compartment 11. This result evidences a redistribution of the flow within the 1BMA vault resulting in a shadow effect. The degradation of the concrete structures facilitates the lateral horizontal flow through compartments in the deformation zone. Groundwater flow is redirected towards the degraded compartments, protecting the upstream compartment 11. This effect is not observed for shoreline position 1, where the main flow component is vertical. In this case, the increase of flow in the degraded compartments derives solely from the redistribution of water from the southern top and sides (east and west) gravel compartments (see Figure B-1, Figure B-3 and Figure B-4 in Appendix B).

Conclusions: The concrete degradation of the compartments associated with the deformation zone ZFMNNW1209 significantly increases the flow rate in the degraded waste compartments. The degradation results in a minor increase in the tunnel flow (of around 4%). Therefore, most of the waste flow increase is the result of the flow redistribution within the vault. For shorelines positions 2 and 3, there is a shadow effect that reduces the flow in the adjacent upstream waste compartment.

Table 4-14. Total flow ($m^3 \cdot year^{-1}$) through the 1BMA vault and waste domain for the degradation of compartments 12–15 (Case 1) and the three shoreline positions.

Case 1 Degradation state	Vault total flow ($m^3 \cdot year^{-1}$)	Waste total flow ($m^3 \cdot year^{-1}$)	Waste normalized	Waste/Vault ratio
	Shoreline position 1			
Base case	4.09E–02	6.90E–03	100%	16.84%
Moderate	4.26E–02	1.37E–02	199%	32.24%
Severe	4.26E–02	1.40E–02	203%	32.80%
Complete	4.26E–02	2.01E–02	292%	47.22%
	Shoreline position 2			
Base case	28.6	1.17	100%	4.10%
Moderate	29.5	3.56	303%	12.06%
Severe	29.6	5.64	481%	19.03%
Complete	29.7	1.60	1,360%	53.79%
	Shoreline position 3			
Base case	61.9	3.13	100%	5.06%
Moderate	64.1	10.1	322%	15.73%
Severe	64.4	13.6	435%	21.12%
Complete	64.5	35.2	1,126%	54.64%

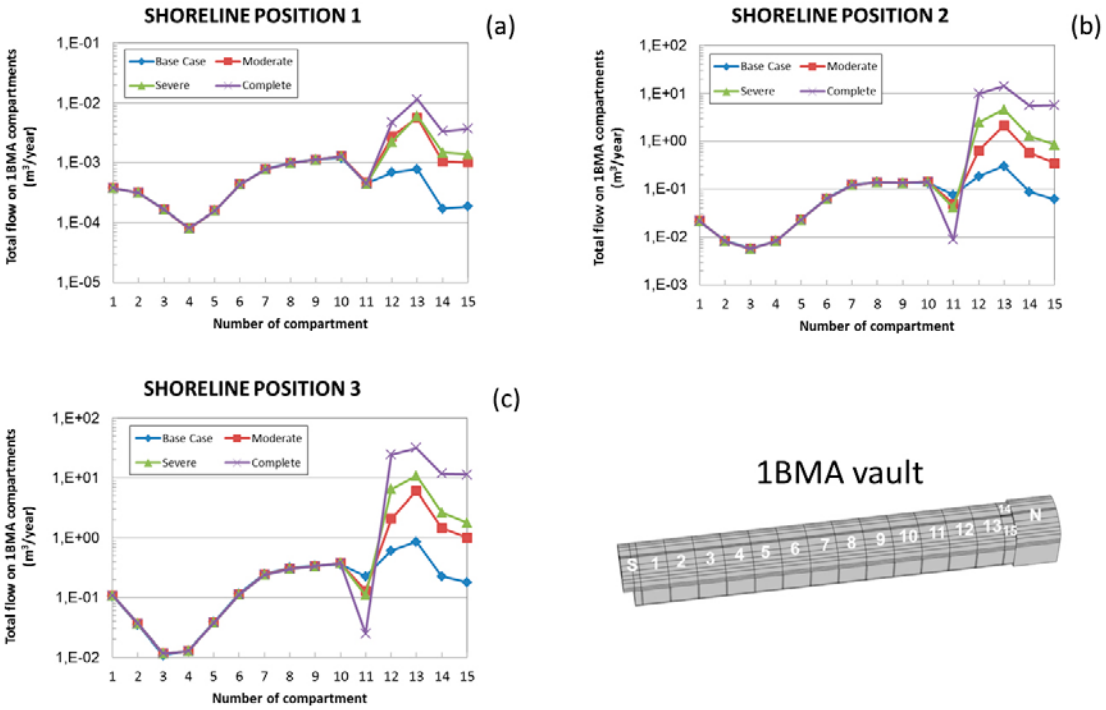

Figure 4-44. *Flow rates ($m^3 \cdot year^{-1}$) through the 1BMA waste compartments for Case 1 of compartments degradation.*

4.3.2 Case 2: Degradation of low flow compartments

The next case analyzes the concrete degradation of waste compartments 3 and 4, associated with the lowest flow rates. The total waste and tunnel flow rates calculated for this case are summarized in Table 4-15. It is worth noting that the tunnel flow remains unaltered for all the degradation states. In turn, the increase of total waste flow is modest for shoreline position 1 (11% for the complete degradation state) and it is almost doubled for the complete degradation state for shoreline position 2. The worst case scenario is the complete concrete degradation at shoreline position 3, which almost triples the waste flow compared to the Base case. The spatial distribution of the waste flow is shown in Figure 4-45. For all shoreline positions, the waste flow rates increase in the degraded compartments 3 and 4. However, for the moderate degradation state, compartments 3 and 4 still display relatively low flow rates (especially for shoreline positions 2 and 3). On the other hand, the waste flow in these compartments is two orders of magnitude larger for the complete degraded concrete case compared to the Base case (for shoreline positions 2 and 3).

As in Case 1, a redistribution of the waste flow accompanied by a shadow effect is observed, especially for shoreline position 1. The waste flow in compartment 2 decreases as the flow is channeled towards the degraded compartments 3 and 4. The flow increase in the degraded compartments is also compensated by changes in the surrounding backfill zones (top, east and west gravel areas, Appendix B).

Conclusions: The concrete degradation of the low flow waste compartments 3 and 4 does not impact the total tunnel flow. Again, the effect is basically restricted to the degraded waste compartments. The moderate concrete degradation state causes a minor (11%) waste total flow increase, whereas the severe and complete degradation doubles and triples the waste total flow, respectively. Again, this flow increase induces a flow redistribution affecting compartment 2 (shadow effect) and the gravel areas associated to these compartments.

Table 4-15. Total flow ($m^3 \cdot year^{-1}$) through the 1BMA vault and waste domain for the degradation of compartments 3 and 4 (Case 2) and the three shoreline positions.

Case 2 Degradation state	Vault total flow ($m^3 \cdot year^{-1}$)	Waste total flow ($m^3 \cdot year^{-1}$)	Waste normalized	Waste/Vault ratio
	Shoreline position 1			
Base case	4.09E–02	6.90E–03	100%	16.84%
Moderate	4.09E–02	6.99E–03	101%	17.08%
Severe	4.09E–02	7.01E–03	102%	17.12%
Complete	4.09E–02	7.67E–03	111%	18.73%
	Shoreline position 2			
Base case	28.6	1.17	100%	4.10%
Moderate	28.6	1.18	101%	4.13%
Severe	28.6	1.35	115%	4.73%
Complete	28.6	2.12	181%	7.41%
	Shoreline position 3			
Base case	61.9	3.13	100%	5.06%
Moderate	61.9	3.14	100%	5.08%
Severe	61.9	4.03	129%	6.51%
Complete	61.9	8.30	265%	13.41%

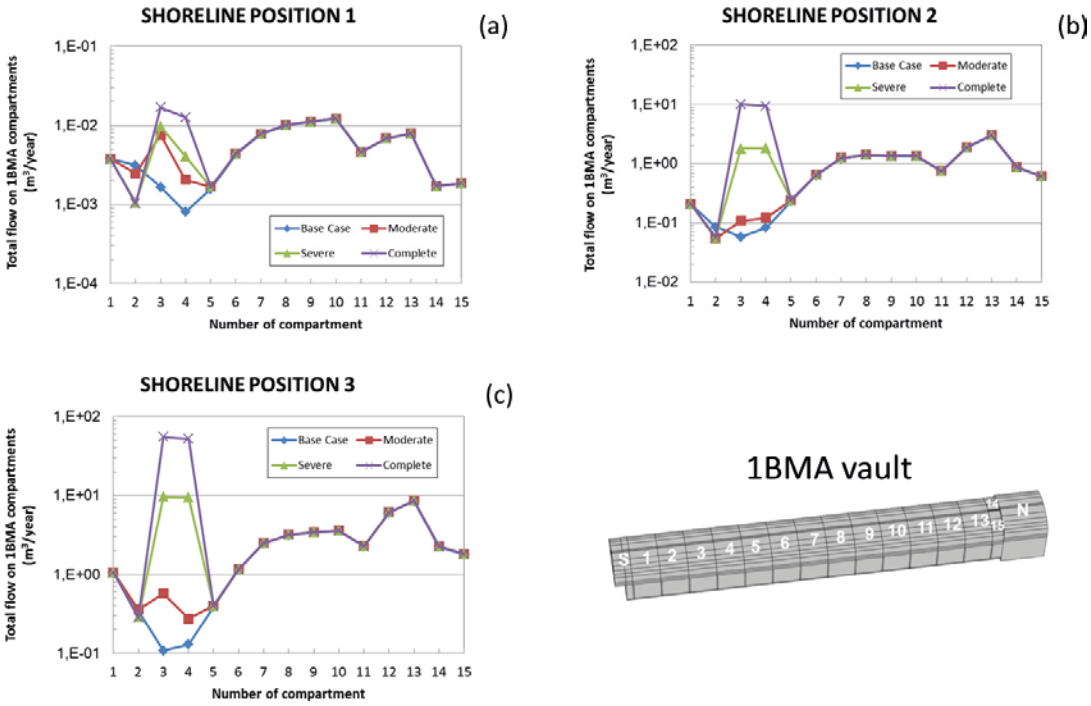

Figure 4-45. Flow rates ($m^3 \cdot year^{-1}$) through the waste compartments of the 1BMA vault for degradation of the low flow compartments 3 and 4.

4.3.3 Case 3: Simultaneous degradation of all compartments affected by fracture zones

This scenario analyzes the concrete degradation of compartments 12, 13, 14 and 15, associated with deformation zone ZFMNNW1209, together with compartments 9 and 10, affected by two minor fractures. Therefore, it addresses the degradation of all the compartments affected by fracture zones, complementing the analysis of Case 1. The effects described in Case 1 (degradation of deformation zone ZFMNNW1209) are also observed in this case. In the case of a complete concrete degradation state the tunnel flow increases by 12% for shoreline position 1 and by 4 to 5% for shoreline positions 2 and 3. This increase is much larger than in Case 1 for shoreline position 1 (Table 4-16). More important is the redistribution of groundwater within the vault. In the completely degraded case, the ratio of total flow through the waste with respect to the total tunnel flow increases from 17% to 68% for shoreline position 1; from 4% to 73% for shoreline position 2, and from 5% to 50% for shoreline position 3.

The distribution of flow along the waste compartments (Figure 4-46) shows an increase in flow in compartments 12 to 15, which is similar to the calculated for Case 1. The compartments 9 and 10, in turn, respond to the concrete degradation with a flow increase of the same order of magnitude as the compartments located in deformation zone ZFMNNW1209. The flow redistribution described in Case 1, where the intact compartment closest to the degraded areas experiences a decrease of flow is also observed in this case. The waste flow is reduced in the two compartments located upstream of the degraded compartments (shadow effect) for the severe and complete degradation of the concrete barriers. Notice that the flow decrease in compartment 11, located in between the two degraded areas, is much larger in this case than in Case 1.

The flow redistribution also affects the backfill domains (Appendix B). Flow across these zones decreases in the intact compartments for shoreline position 1 for all concrete degradation stages, and around the degraded compartments for shoreline positions 2 and 3. Flow across the top gravel in compartment 11 (between the two fractures) also decreases. The redistribution also affects the bottom, east and west gravel and it is more significant for shoreline position 1.

Conclusions: The complete degradation of the concrete around the fracture areas results in an increase of the tunnel flow of 12%, 5%, and 6% for shoreline positions 1, 2, and 3, respectively. More important is the redistribution of the water within the vault. The waste/tunnel total flow ratio increases up to 73% for the completely degraded concrete case (for shoreline position 2). The concrete degradation of all the compartments associated with fracture zones yields a flow increase in the degraded waste compartments accompanied by a reduction of flow in the adjacent intact waste compartments. Compartment 11, located between the two fracture areas presents the lowest flow with a two orders of magnitude flow reduction with respect to the Base case.

Table 4-16. Total flow ($m^3 \cdot year^{-1}$) through the 1BMA vault and waste domain for the degradation of compartments 9, 10, 12–15 (Case 3) and the three shoreline positions.

Case 3 Degradation state	Vault total flow ($m^3 \cdot year^{-1}$)	Waste total flow ($m^3 \cdot year^{-1}$)	Waste normalized	Waste/Vault ratio	Waste flow Case 3/ Case 1
	Shoreline position 1				
Base case	4.09E–02	6.90E–03	100%	16.84%	1.00
Moderate	4.56E–02	2.05E–02	298%	45.08%	1.50
Severe	4.60E–02	2.15E–02	312%	46.86%	1.54
Complete	4.60E–02	3.14E–02	456%	68.40%	1.56
	Shoreline position 2				
Base case	28.6	1.17	100%	4.10%	1.00
Moderate	29.8	4.28	365%	14.38%	1.20
Severe	30.0	7.08	603%	23.63%	1.25
Complete	30.0	22.0	1,874%	73.37%	1.38
	Shoreline position 3				
Base case	61.9	3.13	100%	5.06%	1.00
Moderate	64.8	12.0	384%	18.55%	1.19
Severe	65.3	17.1	547%	26.25%	1.26
Complete	65.3	51.8	1,654%	79.24%	1.47

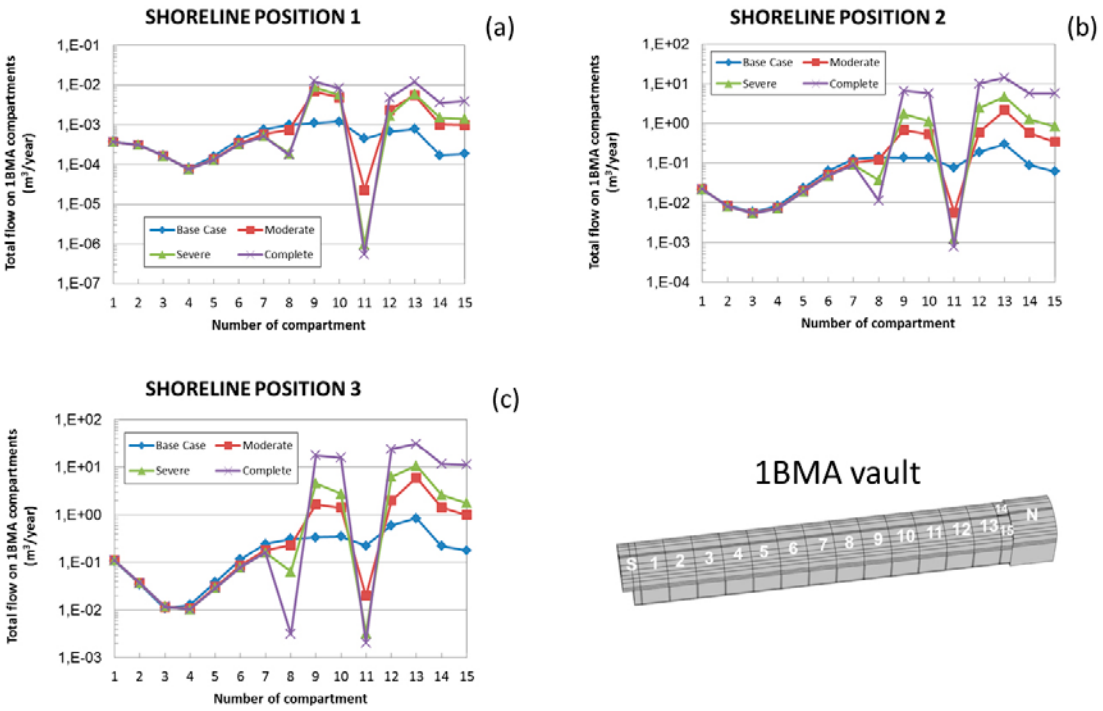

Figure 4-46. *Flow rates ($m^3 \cdot year^{-1}$) through the waste compartments of 1BMA submodel for the three shoreline positions for the simultaneous degradation of all the compartments affected by fracture zones: 9, 10, 12, 13, 14, and 15.*

4.3.4 Case 4: Compartment degradation proportional to the flow rate

Case 4 analyzes concrete degradation proportional to the total flow per waste compartment. Thus, the conductivity of the concrete encapsulation of each waste compartment is set proportional to the waste flow calculated for the intact case (Base case) shown in Figure 4-42. For the three degradation cases (moderate, severe and complete degradation states) the compartment with the lowest total flow conserves the original hydraulic conductivity of $8.3 \cdot 10^{-10}$ m·s^{-1}, while the compartment with maximum flow has the conductivity of the corresponding degradation state ($1.0 \cdot 10^{-7}$ m·s^{-1} in the moderate case; $1.0 \cdot 10^{-5}$ m·s^{-1} in the severe case; $1.0 \cdot 10^{-3}$ m·s^{-1} in the complete degradation case). The linear relationships between the concrete hydraulic conductivity and the waste flow for the three cases is summarized in Table 4-17 and shown graphically in Figure 4-47 (plotted in log-log scale). All cases start with a hydraulic conductivity of $8.3 \cdot 10^{-10}$ m·s^{-1} for the lowest hydraulic conductivity compartment. The three degradation cases result in very different slopes (Table 4-17). The resulting hydraulic conductivity for each compartment is presented in Figure 4-48 for the three different degradation states and the three shoreline positions. The maximum hydraulic conductivity values for complete, severe, and moderate degradation states are found for compartment 13, while the minimum hydraulic conductivity values are found for compartment 3 for shoreline positions 2 and 3, and compartment 4 for shoreline position 1.

Table 4-17. Slope (m) and the y-intercept (A) that define the linear relationship between the concrete hydraulic conductivity per compartment (in m·s^{-1}) and the waste flux (in $m^3 \cdot m^{-2} \cdot s^{-1}$).

	m	A
Moderate	9.62E–12	8.20E–10
Severe	9.70E–10	–1.40E–10
Complete	9.71E–08	–9.62E–08

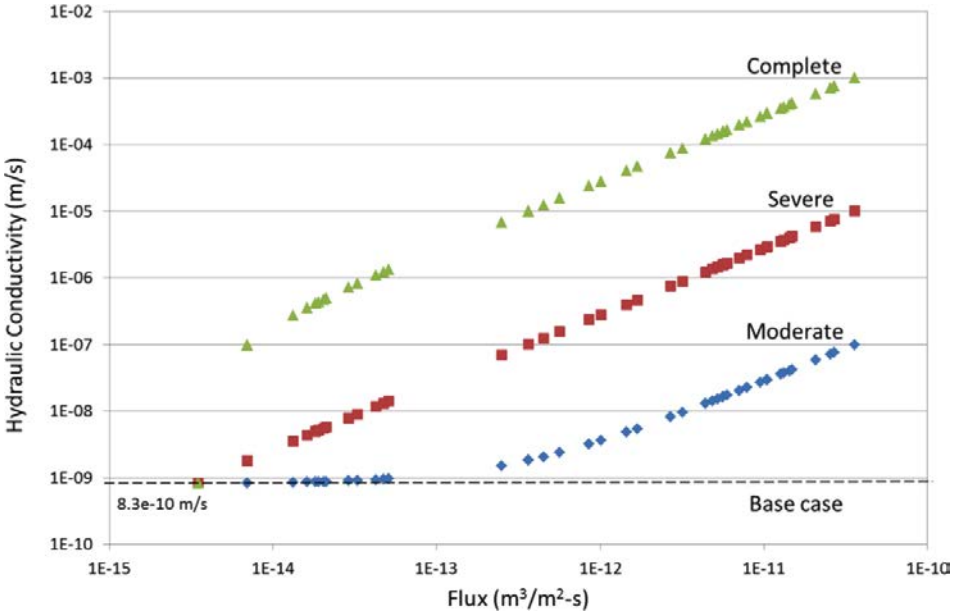

Figure 4-47. *Relationship between concrete hydraulic conductivity ($m \cdot s^{-1}$) and waste fluxes ($m^3 \cdot m^{-2} \cdot s^{-1}$).*

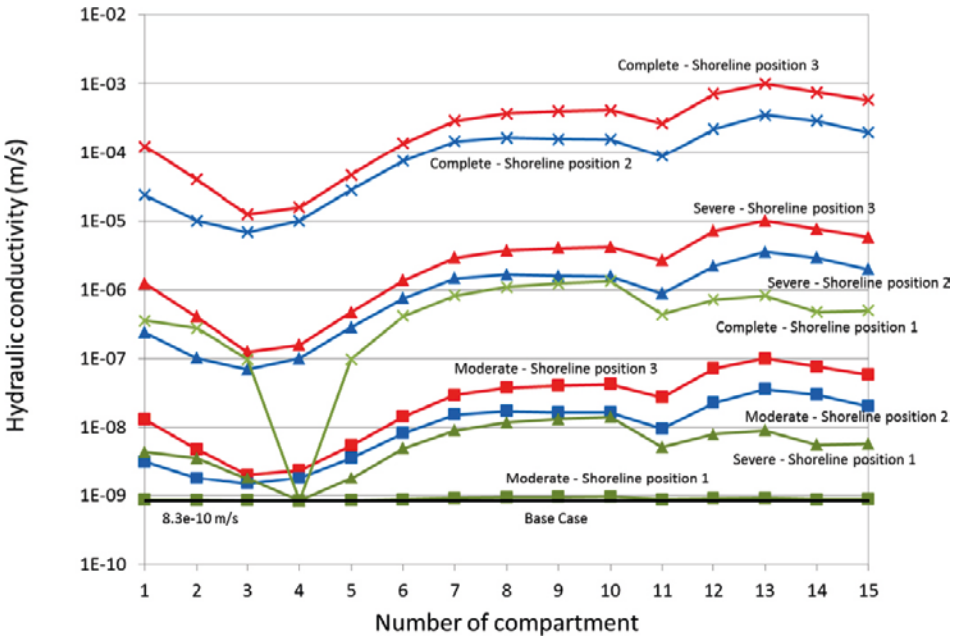

Figure 4-48. *Hydraulic conductivity ($m \cdot s^{-1}$) for each waste compartment for the three concrete degradation states and the three shoreline positions: the variation in the different compartments depends on the concrete degradation state.*

The results show that the tunnel flow increases up to 12% for shoreline position 1 and 5% for shorelines positions 2 and 3, similar to the results for Case 3. There is an important increase in the waste flow with respect to the intact case for all degradation states, especially for shoreline positions 2 and 3 (Table 4-18). The worst case scenarios occur for the completely degraded case and the shoreline positions 2 and 3 where the waste flow increases more than an order of magnitude, accounting for approximately 60% of the tunnel total flow.

Figure 4-49 shows the total flow through the waste compartments. The behavior for shoreline position 1 is very different from shoreline positions 2 and 3. For shoreline position 1, the flow in the moderate and severe degradation cases is very similar to the Base case waste flow. However, the severe degradation case shows a decrease of flow in the low hydraulic conductivity compartments (3, 4, and 5) and an increase of flow in the high conductivity compartments. The results for shoreline positions 2 and

3 present a common pattern: the total flow increases with the degradation state (in the severe case the increase is highest). The moderate case presents flows slightly lower than the Base case in the lowest hydraulic conductivity compartments (2, 3, and 4). This behavior, also observed for shoreline position 1, evidences the positive feedback between flow and concrete degradation. This creates a more heterogeneous flow distribution, with a redirection of the flow towards the most degraded structures and a flow reduction in the less degraded compartments. However, when the degradation reaches a threshold state (here represented by the severe and complete degradation cases), there is a homogenization of the flow along the different compartments. This leads to a consistent increase of flow in all compartments that results in a flatter flow profile, similar to the vault element degradation cases.

The flow redistribution also affects the gravel compartments (Appendix B). In general, the flow through the top, east, and west gravel areas is reduced in the severe concrete degradation cases.

Table 4-18. Total flow ($m^3 \cdot year^{-1}$) through the 1BMA vault and waste domain for the degradation of compartments proportional to the total waste flow (Case 4) and the three shoreline positions.

Case 4 Degradation state	Vault total flow ($m^3 \cdot year^{-1}$)	Waste total flow ($m^3 \cdot year^{-1}$)	Waste normalized	Waste/Vault ratio
	Shoreline position 1			
Base case	4.09E–02	6.90E–03	100%	16.84%
Moderate	4.11E–02	7.35E–03	107%	17.91%
Severe	4.44E–02	1.77E–02	256%	39.78%
Complete	4.62E–02	2.22E–02	322%	48.05%
	Shoreline position 2			
Base case	28.6	11.7	100%	4.10%
Moderate	29.7	41.3	352%	13.91%
Severe	30.0	47.9	408%	15.98%
Complete	30.0	17.2	1,463%	57.20%
	Shoreline position 3			
Base case	61.9	3.13	100%	5.06%
Moderate	64.8	12.3	392%	18.91%
Severe	65.3	15.7	502%	24.07%
Complete	65.4	39.7	1,269%	60.74%

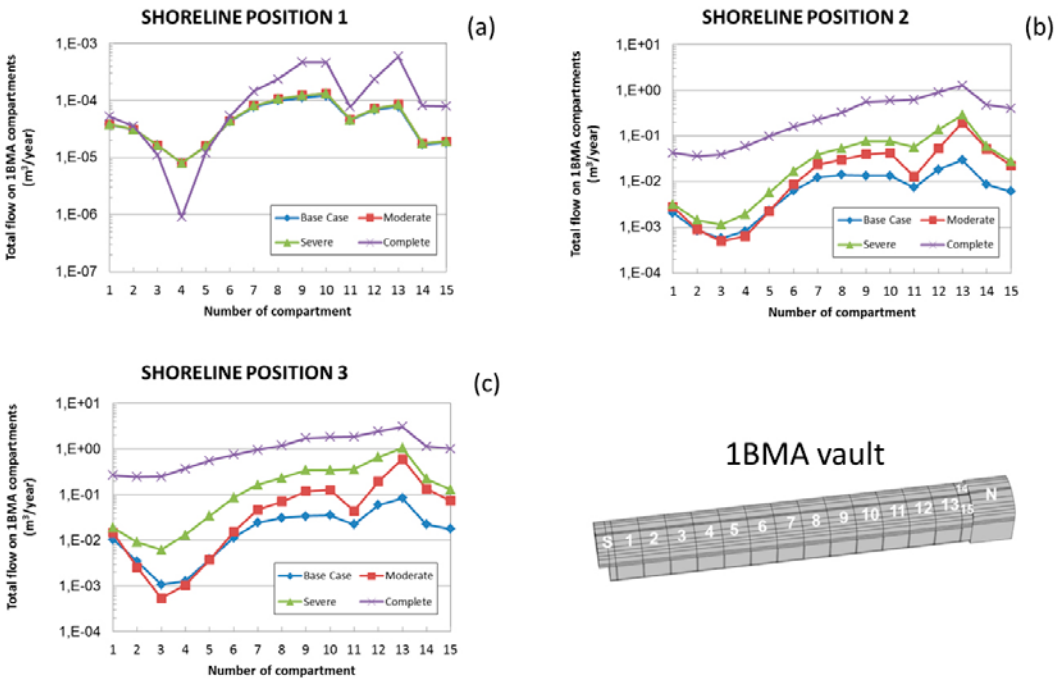

Figure 4-49. Flow rates ($m^3 \cdot year^{-1}$) through the waste compartments of 1BMA submodel for degradation proportional to the Base case waste flow (Case 4) and the three shoreline positions.

Conclusions: A degradation proportional to the waste flow results in an increase in tunnel flow of up to 12% for shoreline position 1. The worst case scenario occurs for the completely degraded case and shoreline position 2 (57% of the tunnel flow). The redistribution of flow shows two distinct patterns for the moderate, severe, and complete concrete degradation states. For a moderate degradation state, there is a feedback between higher flow and higher degradation that results in a redirection of flow towards the most degraded structures and a "protection" of the less degraded compartments. However, for highly degraded cases there is a homogenization of the flow, with a consistent increase of flow in all compartments, similar to the vault element degradation cases.

4.3.5 Summary of compartments degradation scenarios

The results presented for the compartments degradation cases and the three shoreline positions are summarized in Table 4-19 and Table 4-20, and graphically in Figure 4-50, Figure 4-51. , Figure 4-52, and Figure B-17 to Figure B-19 of Appendix B. Differences included in Table 4-19 and Table 4-20 correspond to the relative difference between the total flow for a given degradation state with respect to the total flow of the Base case. The results indicate that concrete degradation has a moderate impact in the total flow through the 1BMA vault. Shoreline position 1 is the most sensitive to the increase of tunnel flow with a maximum increase of 12%. Case 3 and Case 4 result in the highest tunnel flows. Even though not all the compartments are degraded, these values are comparable to highest values obtained in the vault element degradation cases.

Table 4-19. Total tunnel flow rates ($m^3 \cdot year^{-1}$) calculated for different compartments degradation cases and the three shoreline positions.

		Shoreline position 1		Shoreline position 2		Shoreline position 3	
	ID	Total flow rate ($m^3 \cdot year^{-1}$)	Difference	Total flow rate ($m^3 \cdot year^{-1}$)	Difference	Total flow rate ($m^3 \cdot year^{-1}$)	Difference
Case 1	1	4.26E–02	4.1%	29.50	3.0%	64.08	3.5%
	2	4.26E–02	4.1%	29.64	3.5%	64.43	4.1%
	3	4.26E–02	4.1%	29.67	3.6%	64.50	4.2%
Case 2	4	4.09E–02	0.01%	28.65	0.01%	61.90	0.01%
	5	4.09E–02	0.02%	28.65	0.01%	61.91	0.01%
	6	4.09E–02	0.02%	28.65	0.01%	61.91	0.02%
Case 3	7	4.56E–02	11.3%	29.78	4.0%	64.82	4.7%
	8	4.59E–02	12.3%	29.96	4.6%	65.26	5.4%
	9	4.60E–02	12.3%	29.99	4.7%	65.34	5.6%
Case 4	10	4.11E–02	0.3%	29.66	3.5%	64.85	4.8%
	11	4.44E–02	8.5%	29.97	4.6%	65.31	5.5%
	12	4.62E–02	12.9%	30.02	4.8%	65.41	5.7%

Table 4-20. Total waste flow rates ($m^3 \cdot year^{-1}$) calculated for different compartments degradation cases and the three shoreline positions.

		Shoreline position 1		Shoreline position 2		Shoreline position 3	
	ID	Total flow rate ($m^3 \cdot year^{-1}$)	Difference	Total flow rate ($m^3 \cdot year^{-1}$)	Difference	Total flow rate ($m^3 \cdot year^{-1}$)	Difference
Case 1	1	1.37E–02	99%	3.56	203%	10.08	222%
	2	1.40E–02	103%	5.64	381%	13.61	335%
	3	2.01E–02	192%	15.96	1,260%	35.24	1,026%
Case 2	4	6.99E–03	1%	1.18	1%	3.14	0%
	5	7.01E–03	2%	1.35	15%	4.03	29%
	6	7.67E–03	11%	2.12	81%	8.30	165%
Case 3	7	2.05E–02	198%	4.28	265%	12.02	284%
	8	2.15E–02	212%	7.08	503%	17.13	447%
	9	3.14E–02	356%	22.00	1,774%	51.78	1,554%
Case 4	10	7.35E–03	7%	4.13	252%	12.26	292%
	11	1.77E–02	156%	4.79	308%	15.72	402%
	12	2.22E–02	222%	17.17	1,363%	39.73	1,169%

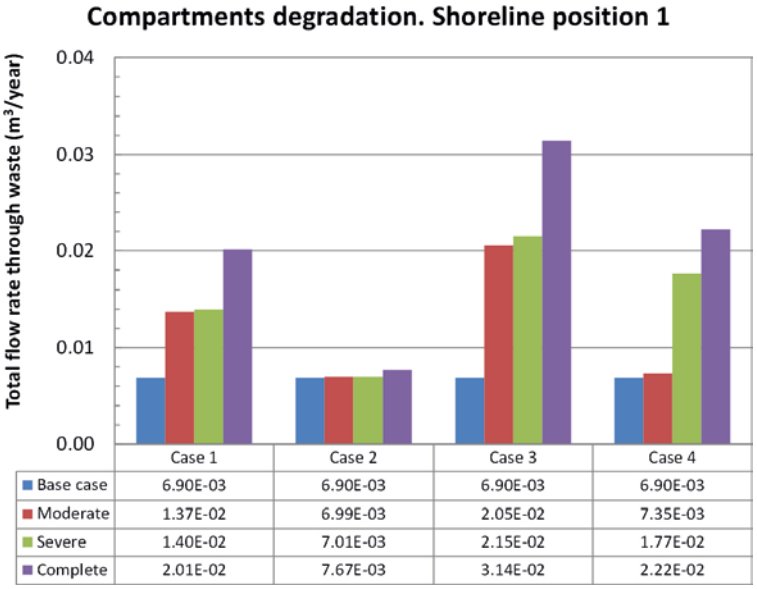

	Case 1	Case 2	Case 3	Case 4
Base case	6.90E-03	6.90E-03	6.90E-03	6.90E-03
Moderate	1.37E-02	6.99E-03	2.05E-02	7.35E-03
Severe	1.40E-02	7.01E-03	2.15E-02	1.77E-02
Complete	2.01E-02	7.67E-03	3.14E-02	2.22E-02

Figure 4-50. *Total flow rates ($m^3 \cdot year^{-1}$) through the waste domain of 1BMA submodel for different cases of compartments degradation and comparison with the Base case for shoreline position 1.*

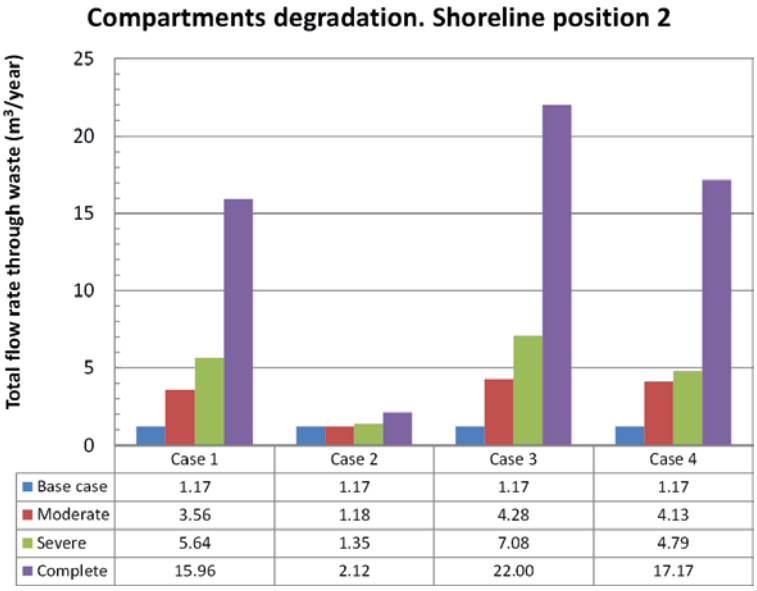

	Case 1	Case 2	Case 3	Case 4
Base case	1.17	1.17	1.17	1.17
Moderate	3.56	1.18	4.28	4.13
Severe	5.64	1.35	7.08	4.79
Complete	15.96	2.12	22.00	17.17

Figure 4-51. *Total flow rates ($m^3 \cdot year^{-1}$) through the waste domain of 1BMA submodel for different cases of compartments degradation and comparison with the Base case for shoreline position 2.*

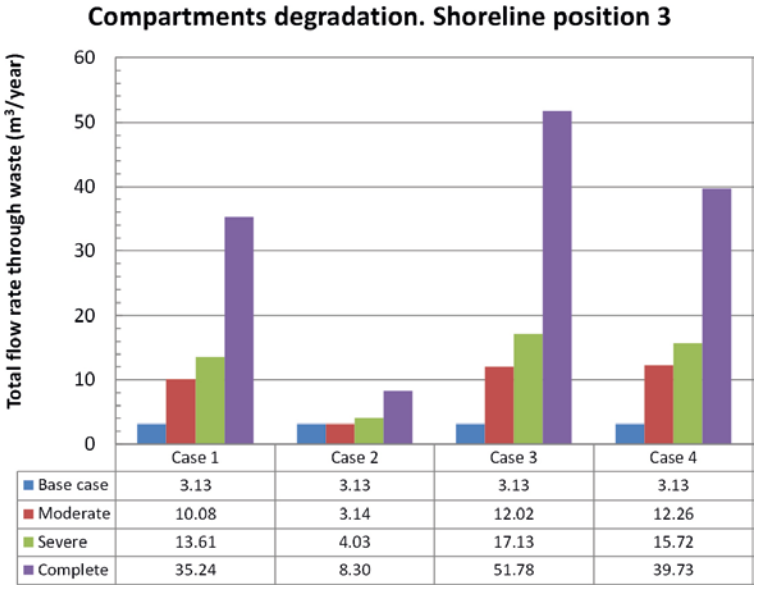

Figure 4-52. *Total flow rates ($m^3 \cdot year^{-1}$) through the waste domain of 1BMA submodel for different cases of compartments degradation and comparison with the Base case for shoreline position 3.*

In general, the effect of the compartment degradation scenarios is a redistribution of the flow within the vault. The waste flow increases locally in the degraded waste compartments. This increase in flow is compensated by a reduction in the waste flow in the adjacent intact compartments. The effect of this decrease reaches a maximum in the case of the concrete degradation in zones associated with all the fracture zones, for the compartment located between degraded zones. The total flow through the gravel area also decreases to compensate the increase in the degraded compartments.

The total flow through the waste domain is shown in Figure 4-50, Figure 4-51, and Figure 4-52 for shoreline positions 1, 2, and 3, respectively. For all shoreline positions the worst case scenario corresponds to the complete concrete degradation state of all compartments affected by fractures (Case 3). On the other hand, the degradation of low flow compartments (Case 2) is the less sensitive case. This effect can be explained by the low conductivity of the rock around these compartments that control the local flow towards the vault.

For shoreline position 1, the effect of moderate and severe concrete degradation is similar in the cases with degradation of fracture zones (Case 1 and 3). However, the complete degradation of the concrete increases substantially the total waste flow.

For shoreline positions 2 and 3, Cases 1, 2, and 4 present a similar pattern: flow increases with the concrete degradation state in a more proportional fashion than for shoreline position 1.

5 1BMA concrete degradation with high conductivity beams

In this chapter the 1BMA concrete degradation under the assumption of high conductivity beams is analyzed. Similarly to chapter 4, the cases of concrete degradation of the different vault elements and the degradation of the different compartment sets are considered. In this case, it is assumed that the hydraulic conductivity of beams is equal to the backfill conductivity (10^{-3} m/s). This represents a situation where beams do not constitute a flow barrier.

Figure 5-1 shows the total flow rates through the waste compartments of a 1BMA vault with high conductivity beams for the Base case. The waste flow displays a spatial variability, but the profiles are different from the results obtained for the model with low conductivity beams. First, the waste flows are three orders of magnitude lower for the case with high conductivity beams. Second, except for shoreline position 1, the flow increases monotonically from south to north. Thus, the minimum waste flow observed around compartments 3 and 4 in a 1BMA vault with low conductivity beams and the peaks in the compartments associated with fracture zones disappear in the case of high conductivity beams.

5.1 Vault elements degradation

To study the concrete degradation of the vaults the same methodology as described in Section 4.2 was followed.

The results of the simulations of the different cases of vault elements degradation are presented below. Only the flow rates through the waste compartments of 1BMA vault are shown in the text. The flow rates within other vault elements have been included in the Appendix C.

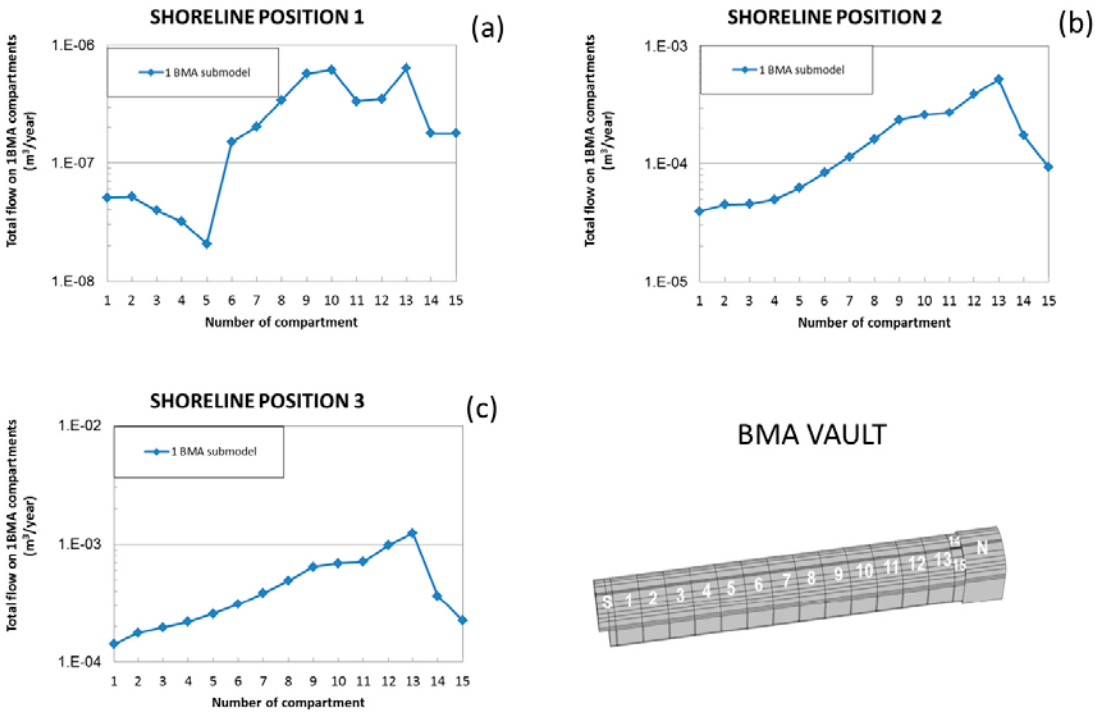

Figure 5-1. *Total flow rates ($m^3 \cdot year^{-1}$) through the waste compartments calculated with the 1BMA vault submodel for the Base case.*

5.1.1 Case 1: Floor degradation

This section explores the effect of the degradation of the concrete floor on the local flow rates in the waste domain and on the total flow entering the 1BMA vault.

Figure 5-2 shows that as the floor degrades the flow rate through the waste compartments increases, with a flow profile similar to that of the Base case. For all shorelines, the total flow rates increase 2 orders of magnitude from moderate to severe degradation and one and half order of magnitude from severe to complete degradation, as expected from the hydraulic conductivity values assumed for each degradation state. That is, the flow rates variations are proportional to the hydraulic conductivity changes caused by the degradation.

The total flow through the 1BMA vault and waste domains for all the degradation states and the three shoreline positions are presented in Table 5-1. A systematic increase of the total flow through the waste is observed, while the total flow through the vault is almost unaffected (less than 1% with respect to the Base case). A significant increase of the ratio between the flow through the waste and the flow through the vault is obtained for complete degradation at all shoreline positions. For this degradation state no flow barriers protect the waste from the water entering the vault from below.

The flow rates through other vault elements (see Appendix C, Figure C-1, Figure C-3 and Figure C-4) are almost unaffected by floor degradation, with the exception of bottom gravel (Figure C-2). The severe and complete degradation yield a flow increase through the bottom gravel at shoreline positions 2 and 3. This is expected given the proximity of the bottom gravel to the floor.

Conclusions: The flow rates through the waste increase significantly as concrete floor degradation proceeds, while the total flow through the vault is nearly unaffected by degradation. The flow rate profile along the different compartments, for all degradation states and shoreline positions, is similar to the Base case profile. The fraction of the total flow through the vault that enters the waste increases to 23% for complete degradation at shoreline position 1 and to 12% for complete degradation at shorelines positions 2 and 3, respectively. This is because for complete degradation, the permeabilities of floor, backfill and beams are equal, which promotes a significantly higher water flow from rock to the inside of the waste compartments. In general, flow rates through other vault elements are nearly unaffected by concrete floor degradation, with the exception of bottom gravel.

Table 5-1. Summary of total flow ($m^3 \cdot year^{-1}$) through the 1BMA vault and waste domain for the concrete floor degradation case (Case 1) and the three shoreline positions. Increase in the waste flow with respect to the Base case is expressed in orders of magnitude.

Case 1 Degradation state	Vault total flow ($m^3 \cdot year^{-1}$)	Waste total flow ($m^3 \cdot year^{-1}$)	Waste flow increase	Waste/Vault ratio
	Shoreline position 1			
Base Case	4.67E–02	2.95E–06	1	0.0%
Moderate	4.67E–02	1.06E–05	4	0.0%
Severe	4.67E–02	4.36E–04	100	0.9%
Complete	4.67E–02	1.07E–02	1,000	22.9%
	Shoreline position 2			
Base Case	29.9	9.33E–04	1	0.0%
Moderate	29.9	2.78E–03	3	0.0%
Severe	29.9	1.37E–01	100	0.5%
Complete	29.9	3.64	1,000	12.2%
	Shoreline position 3			
Base Case	65.1	2.10E–03	1	0.0%
Moderate	65.1	6.50E–03	3	0.0%
Severe	65.1	3.18E–01	100	0.5%
Complete	65.1	8.15	1,000	12.5%

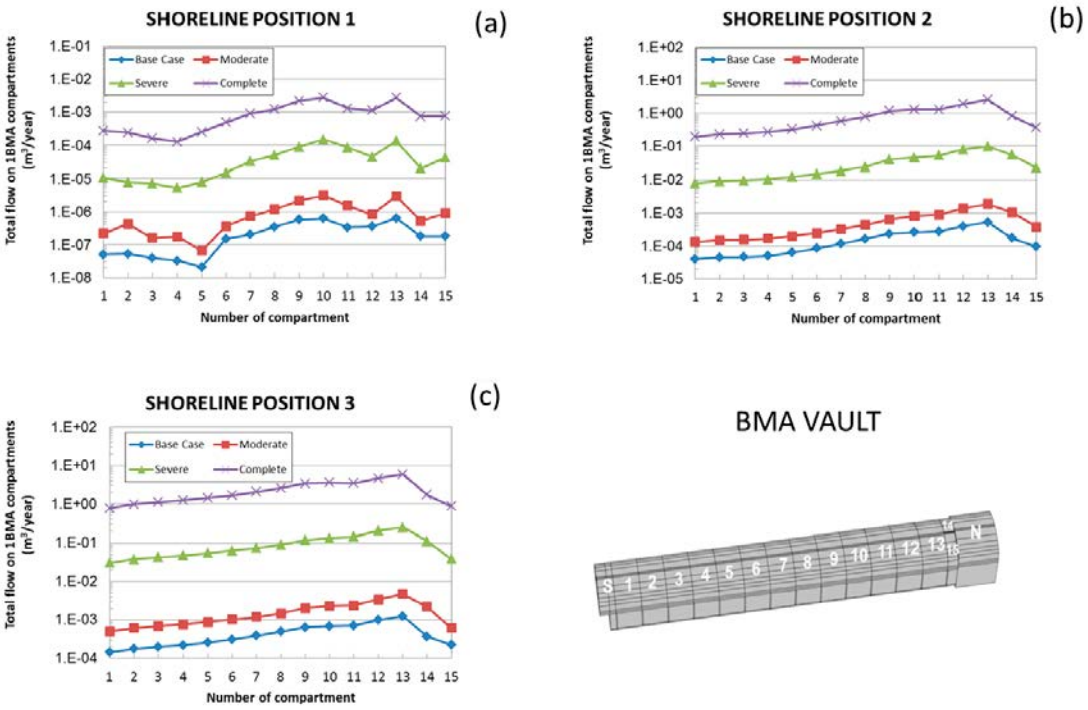

Figure 5-2. *Flow rates ($m^3 \cdot year^{-1}$) through the waste compartments of 1BMA submodel for floor degradation.*

5.1.2 Case 2: Degradation of floor and inner walls

Degradation of the concrete floor and inner walls should increase the connectivity between waste compartments, and thus also increase the flow rates with respect to the Base case and the case of floor degradation only (Case 1). This is reflected in Figure 5-3, which shows that flow rates for moderate degradation significantly depart from flow rates of the Base case. Also, degradation of inner walls lead to less of a difference in flow rates between severe and moderate degradation states for all shoreline positions. As in the previous case, all the flow rates profiles have a similar shape compared to the respective profile of the Base case.

The increase in the total flow through the waste is more than four orders of magnitude for the complete degradation state for all shoreline positions, compared to the Base case (Table 5-2).

The total flow through the waste obtained in Case 2 for complete degradation is about 4 times the total flow obtained in Case 1. The total flow through the vault shows only a small decrease compared to the Base case at shoreline position 1 and a slight increase at shoreline positions 2 and 3. A significant increase in the ratio of flow through the waste and flow through the vault is obtained for severe and complete degradation for all shoreline positions. Degradation of inner walls increases the hydraulic connectivity between compartments and with the rock.

The increase in flow through the waste is compensated with a partial reduction of flow through the top and west gravel (see Appendix C, Figure C-5 and Figure C-8). In particular, complete degradation also leads to a reduction in the flow through the bottom gravel (Figure C-6).

Conclusions: The degradation of the floor and inner concrete walls significantly increases the flow rates with respect to the Base case and the case of concrete floor degradation only (Case 1). The increase in the total flow through the waste compared to the Base case is more than four orders of magnitude for the complete degradation state for all shoreline positions. In addition, degradation of inner walls lead to a smaller difference in flow rates comparing the severe and moderate degradation states for all shoreline positions. In addition, increased flow rate through the waste is compensated by a reduction of flow through other vault elements.

Table 5-2. Summary of total flow ($m^3 \cdot year^{-1}$) through the 1BMA vault and waste domain for the concrete floor and inner walls degradation case (Case 2) and the three shoreline positions. Increase in the waste flow with respect to the Base case is expressed in orders of magnitude.

Case 2 Degradation state	Vault total flow ($m^3 \cdot year^{-1}$)	Waste total flow ($m^3 \cdot year^{-1}$)	Waste flow increase	Waste/Vault ratio
	Shoreline position 1			
Base case	4.67E–02	2.95E–06	1	0.0%
Moderate	4.65E–02	9.30E–05	10	0.2%
Severe	4.63E–02	5.46E–03	1,000	11.8%
Complete	4.63E–02	2.48E–02	1,000	53.5%
	Shoreline position 2			
Base case	29.9	9.33E–04	1	0.0%
Moderate	29.9	3.76E–02	10	0.1%
Severe	30.0	2.31	1,000	7.7%
Complete	30.0	12.27	10,000	40.9%
	Shoreline position 3			
Base case	65.1	2.10E–03	1	0.0%
Moderate	65.2	9.28E–02	10	0.1%
Severe	65.4	5.59	1,000	8.5%
Complete	65.5	27.43	10,000	41.9%

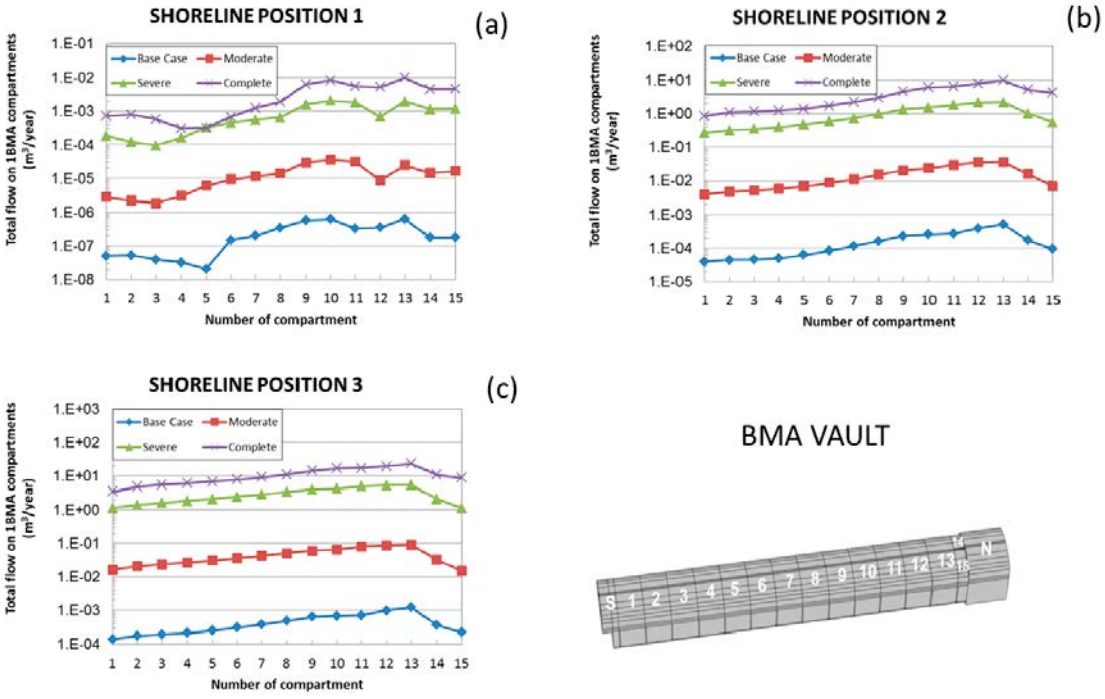

Figure 5-3. *Flow rates ($m^3 \cdot year^{-1}$) through the waste compartments of 1BMA submodel for degradation of floor and inner walls.*

5.1.3 Case 3: Degradation of one outer wall

The next case analyzes the degradation of the east outer wall of the waste compartments.

Figure 5-4 shows the flow rates through the waste compartments. Degradation causes an increase in the flow rates through the waste. Note that waste compartment n° 14 has only an outer west wall and is separated from compartment n° 15 only by a longitudinal inner concrete wall, which is not degraded in this case. Consequently, the flow rate in waste compartment n° 14 is almost unaffected by degradation of the outer east wall of compartment n° 15.

Table 5-3 shows that the effect on the total flow through the waste is an increase of about 4 times for moderate degradation, and an increase of about 1 and 3 orders of magnitude for severe and complete degradation, respectively. The ratio of waste flow to vault flow is appreciably lower compared to Cases 1 and 2.

Degradation of east outer wall does not cause changes in the flow rates through other vault elements (see Appendix C, Figure C-9 to Figure C-12), except a slight increase in the flow through east gravel at shoreline position 2 and complete degradation (Figure C-11).

Conclusions: Degradation of east outer wall causes an increase in the flow rates through the waste. This increase is smaller than observed for Cases 1 and 2. Degradation of east outer wall does not cause changes in the flow rates through other vault elements.

Table 5-3. Summary of total flow ($m^3 \cdot year^{-1}$) through the 1BMA vault and waste domain for the concrete degradation of the east outer walls (Case 3) and the three shoreline positions. Increase in the waste flow with respect to the Base case is expressed in orders of magnitude.

Case 3 Degradation state	Vault total flow ($m^3 \cdot year^{-1}$)	Waste total flow ($m^3 \cdot year^{-1}$)	Waste flow increase	Waste/Vault ratio
	Shoreline position 1			
Base case	4.67E–02	2.95E–06	1	0.0%
Moderate	4.67E–02	4.74E–06	2	0.0%
Severe	4.67E–02	1.64E–04	10	0.4%
Complete	4.67E–02	6.84E–03	1,000	14.7%
	Shoreline position 2			
Base case	29.9	9.33E–04	1	0.0%
Moderate	29.9	4.71E–03	5	0.0%
Severe	29.9	4.91E–02	10	0.2%
Complete	29.9	1.91	1,000	6.4%
	Shoreline position 3			
Base case	65.1	2.10E–03	1	0.0%
Moderate	65.1	8.52E–03	4	0.0%
Severe	65.100	6.49E–02	10	0.1%
Complete	65.1	3.39	1,000	5.2%

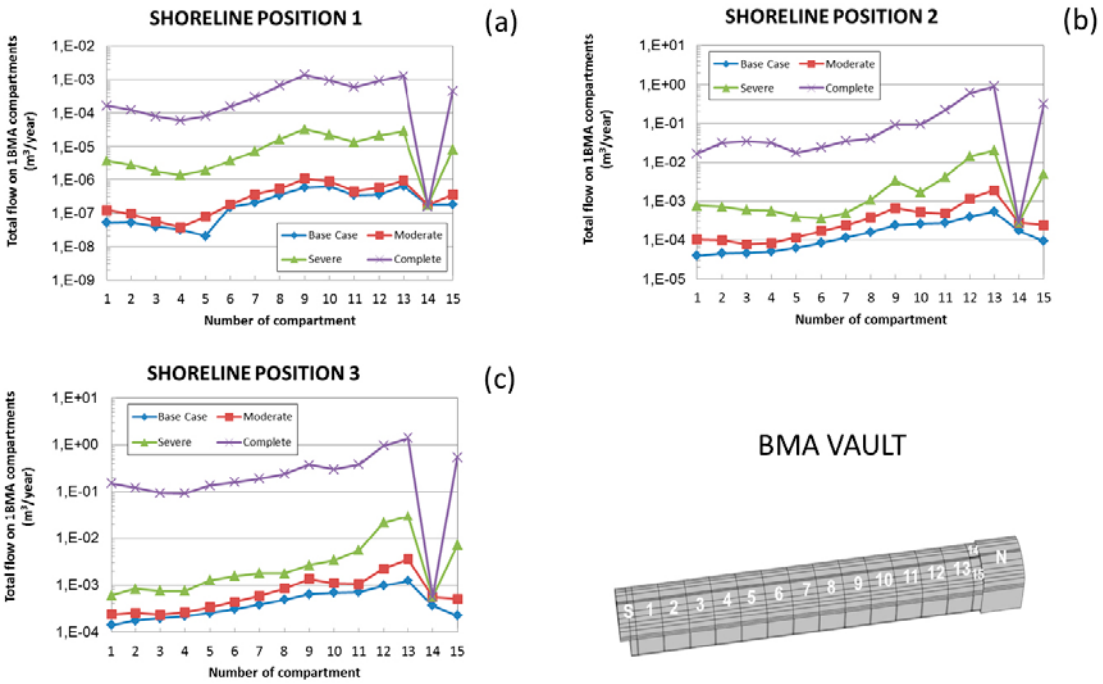

Figure 5-4. *Flow rates ($m^3 \cdot year^{-1}$) through the waste compartments of 1BMA submodel for degradation of east outer wall.*

5.1.4 Case 4: Degradation of outer walls

The present case considers degradation of both outer walls. Comparing Figure 5-5 and Figure 5-4 it is confirmed that degradation of both outer walls significantly modifies the flow through the waste domain. In particular, all degradation states lead to a significant departure from the Base case scenario for all shorelines positions. The ratio of waste flow to vault flow is appreciably larger than in Case 3 (Table 5-4). Recall that at shoreline positions 2 and 3 the groundwater flow is predominantly horizontal. It is worth mentioning that compared to the Base case scenario, a more abrupt decrease in the waste flow rate between compartments 13 and 14–15 is found for all degradation states. In part, this can be due to degradation of both outer walls promotes a higher flow outside the waste compartments around the deformation zone ZFMNNW1209 located around these compartments (see Figure 4-43).

A comparison of the total flow in the waste domain between Case 4 and Case 3 (see Table 5-4) indicates that moderate and severe degradation states lead to an increase of about 10 to 100 times the total flow compared to the Base case for shoreline positions 2 and 3. For shoreline position 1 the increase is 10 to 15 times the total flow in the Base case.

As shown in Figure C-15 and Figure C-16 (Appendix C) the flow through the east and west gravels also increases under complete degradation of both outer walls at shoreline positions 2 and 3. This is an expected result given the proximity of degraded outer walls to lateral gravels. As explained in Section 4.2.4, complete degradation of the west outer wall establishes a hydraulic connection between the rock (actually the backfill) and waste compartments, especially around the fracture zones, promoting higher water flow to the west gravel.

Conclusions: Degradation of both concrete outer walls leads to a significant increase in flow rates within the waste with respect to the Base case for all shoreline positions and degradation states. Flow through lateral gravels also increases under complete degradation of both outer walls at shoreline positions 2 and 3. Flow rates through other vault elements are not changed compared to the Base case.

Table 5-4. Summary of total flow ($m^3 \cdot year^{-1}$) through the 1BMA vault and waste domain for the concrete outer walls degradation case (Case 4) and the three shoreline positions. Increase in the waste flow with respect to the Base case is expressed in orders of magnitude.

Case 4 Degradation state	Vault total flow ($m^3 \cdot year^{-1}$)	Waste total flow ($m^3 \cdot year^{-1}$)	Waste flow increase	Waste/Vault ratio	Case4/Case3 waste total flow ratio
	Shoreline position 1				
Base case	4.67E–02	2.95E–06	1	0.0%	1.00
Moderate	4.67E–02	4.33E–05	10	0.1%	9.12
Severe	4.67E–02	2.55E–03	100	5.5%	15.6
Complete	4.67E–02	1.24E–02	1,000	26.5%	1.81
	Shoreline position 2				
Base case	29.9	9.33E–04	1	0.0%	1.00
Moderate	29.9	6.12E–02	10	0.2%	13.0
Severe	29.9	3.74	1,000	12.5%	76.2
Complete	29.9	10.8	10,000	36.1%	5.65
	Shoreline position 3				
Base case	65.1	2.10E–03	1	0.0%	1.00
Moderate	65.1	1.03E–01	10	0.2%	12.0
Severe	65.1	6.26	1,000	9.6%	96.5
Complete	65.2	18.8	1,000	28.9%	5.53

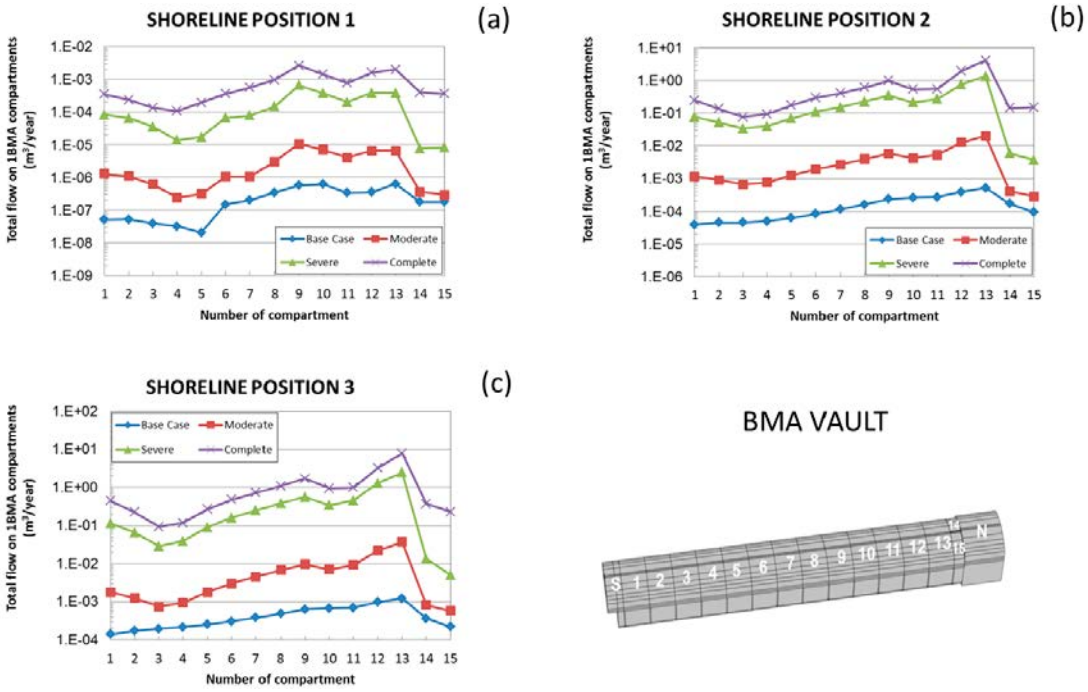

Figure 5-5. *Flow rates ($m^3 \cdot year^{-1}$) through the waste compartments of 1BMA submodel for degradation of outer walls.*

5.1.5 Case 5: Degradation of inner and outer walls

The present case studies the degradation of all the inner and outer concrete walls of the 1BMA. Evidently, this scenario enhances the hydraulic connectivity between waste compartments and between rock and vault around high permeability zones. Consequently, the flow through the waste is expected to increase when compared to previous cases (especially the horizontal flow component).

Flow rates within the waste are shown in Figure 5-6. As for Case 4, the degradation of inner and outer walls significantly increases the flow through the waste domain, compared to the Base case scenario at all shorelines positions. Note that the flow decrease from compartments 12 to 15 found in Case 4 (Figure 5-5) is substantially lower. This is a direct consequence of a higher connectivity between the waste compartments caused by degradation of inner walls. That is, degradation of inner walls of compartments 12, 13, 14 and 15 compensates the increase in connectivity between the vault and the deformation zone ZFMNNW1209 caused by degradation of outer walls around that zone. In fact, spatial variability on waste flow rates is similar to Case 2, which also considers degradation of inner walls. The fraction of the total tunnel flow corresponding to the waste domain is also similar to that obtained in Case 2 (see Table 5-2 and Table 5-5).

A comparison of the total flow in the waste domain between Case 5 and Case 4 (see Table 5-5) indicates that moderate, severe and complete degradation lead to an increase of 20 to 35%, 30 to 40% and 60 to 66% of the total flow, respectively, compared to the Base case.

On the other hand, moderate degradation of inner and outer walls of a 1BMA with high permeability beams induces a considerably higher flow through the waste domain, compared to the low permeability scenario (see Figure 4-25) for which the difference with the Base case is small.

At the vault level, the increase in the waste domain is compensated by a reduction in the flow through top, bottom and west gravel, especially for complete degradation (see Appendix C, Figure C-17, Figure C-18 and Figure C-20).

Conclusions: Flow rates through the waste compartments are significantly affected by all degradation states at all shoreline positions. The impact of degradation is also larger compared to the scenario of low permeability beams, for which the difference found with the Base case for moderate degradation is small. The increase in the flow through the waste domain is one order of magnitude for moderate degradation, three orders of magnitude for severe degradation and four orders of magnitude for complete degradation. The higher connectivity between the waste compartments caused by degradation of inner walls leads to a more smooth flow decrease from compartments 12 to 15 than in Case 4. This is because degradation of inner walls of compartments 12, 13, 14 and 15 compensates the increase in connectivity between the vault and the deformation zone ZFMNNW1209 caused by degradation of outer walls around that zone.

Table 5-5. Summary of total flow ($m^3 \cdot year^{-1}$) through the 1BMA vault and waste domain for the concrete inner and outer walls degradation case (Case 5) and the three shoreline positions. Increase in the waste flow with respect to the Base case is expressed in orders of magnitude.

Case 5 Degradation state	Vault total flow ($m^3 \cdot year^{-1}$)	Waste total flow ($m^3 \cdot year^{-1}$)	Waste flow increase	Waste/Vault ratio	Case5/Case4 waste total flow ratio
	Shoreline position 1				
Base case	4.67E–02	2.95E–06	1	0.0%	1.00
Moderate	4.65E–02	5.32E–05	10	0.1%	1.22
Severe	4.63E–02	3.30E–03	1,000	7.1%	1.30
Complete	4.62E–02	2.02E–02	1,000	43.6%	1.63
	Shoreline position 2				
Base case	29.9	9.33E–04	1	0.0%	1.00
Moderate	29.9	7.59E–02	100	0.3%	1.24
Severe	30.0	4.72	1,000	15.7%	1.26
Complete	30.0	16.0	10,000	53.3%	1.48
	Shoreline position 3				
Base case	65.1	2.10E–03	1	0.0%	1.00
Moderate	65.2	1.38E–01	10	0.2%	1.35
Severe	65.4	8.68	1,000	13.3%	1.39
Complete	65.5	31.2	10,000	47.7%	1.66

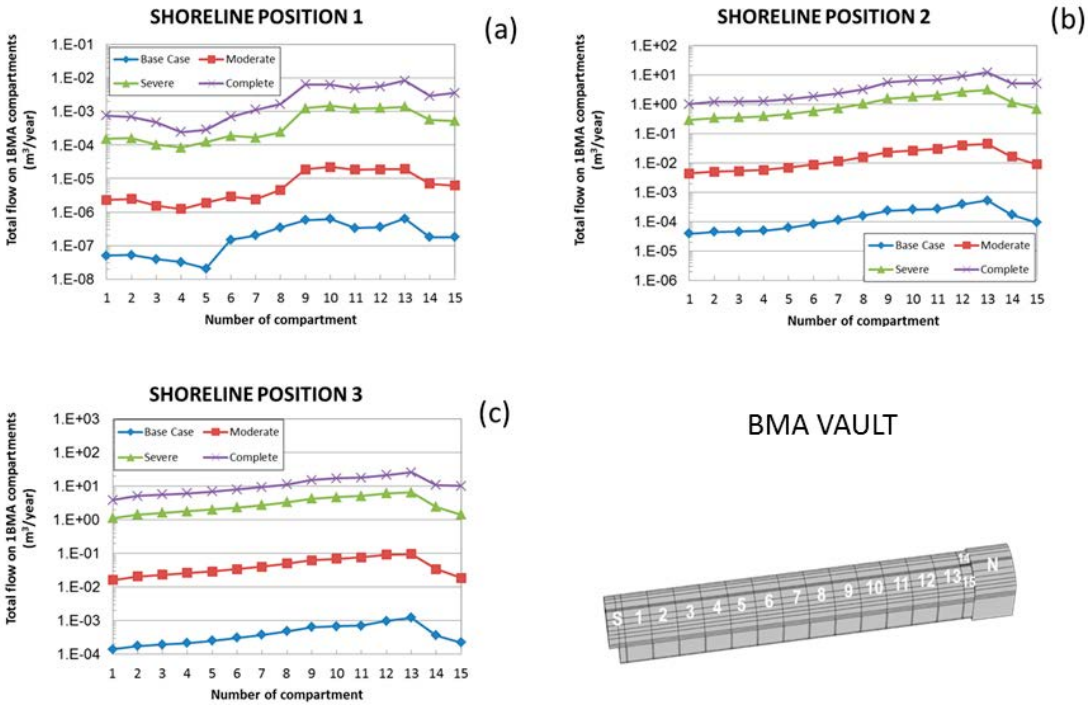

Figure 5-6. *Flow rates ($m^3 \cdot year^{-1}$) through the waste compartments of the 1BMA submodel for degradation of inner and outer concrete walls.*

5.1.6 Case 6: Degradation of outer walls, lids and floor

The last case of vault element degradation considers degradation of concrete floor, lids and outer walls. Flow rates through the waste compartments of the present case are depicted in Figure 5-7. The flow behavior displays some of the characteristics of degradation Cases 1 and 4 (see Figure 5-2 and Figure 5-5). Similar to Case 4 additional degradation of lids and floor significantly increase the flow through the waste domain, compared to the Base case for all shorelines positions. Again, the flow decrease from compartments 12 to 15 found in Case 4 (Figure 5-5) is smoother. This can be explained by an increase in hydraulic connectivity between waste compartments caused by degradation of lids of compartments 12, 13, 14 and 15. This compensates the increase in lateral water exchange through degraded outer walls of compartments in contact with the deformation zone ZFMNNW1209.

As occurred with a 1BMA vault with low permeability beams, considering concrete lids degradation in combination with concrete floor and outer walls degradation promotes higher flow rates for all degradation states and shoreline positions (Table 5-6), compared to floor degradation only or outer walls degradation only. The fraction of the total tunnel flow corresponding to the waste domain is significantly higher than in Cases 1 and 4.

In addition, concrete degradation increases the flow rates through the bottom gravel of the first 11 compartments at shoreline positions 2 and 3 (see Appendix C, Figure C-22). Flow rates through both lateral gravels (Figure C-23 and Figure C-24) decrease with degradation at shoreline position 1. Flow rates within west gravel increase some degree at shoreline positions 2 and 3.

Conclusions: Flow rates through the waste compartments are significantly affected by concrete degradation of lids, floor and outer walls. Considering lids degradation in combination with floor and outer walls degradation leads to higher flow rates for all degradation states and shoreline positions compared to the degradation of only the floor or only the outer walls. The decrease in waste flow from compartments 12 to 15 found in Case 4 is smoother. This is probably due to an increase in hydraulic connectivity between waste compartments caused by degradation of lids of compartments 12, 13, 14 and 15, which compensates the increase in lateral water exchange through degraded outer walls of compartments in contact with the deformation zone ZFMNNW1209. Flow rates through bottom and west gravel increases some degree respect to the Base case at shoreline positions 2 and 3.

Table 5-6. Summary of total flow ($m^3 \cdot year^{-1}$) through the 1BMA vault and waste domain for the concrete floor, lids, and outer walls degradation case (Case 6) and the three shoreline positions. Increase in the waste flow with respect to the Base case is expressed in orders of magnitude.

Case 6 Degradation state	Vault total flow ($m^3 \cdot year^{-1}$)	Waste total flow ($m^3 \cdot year^{-1}$)	Waste flow increase	Waste/Vault ratio	Case 6/Case 4 waste total flow ratio
	Shoreline position 1				
Base case	4.67E–02	2.95E–06	1	0.0%	1.00
Moderate	4.67E–02	3.42E–04	100	0.7%	7.91
Severe	4.67E–02	1.50E–02	1,000	32.0%	5.88
Complete	4.67E–02	3.34E–02	10,000	71.4%	2.70
	Shoreline position 2				
Base case	29.9	9.33E–04	1	0.0%	1.00
Moderate	29.9	1.03E–01	100	0.3%	1.68
Severe	29.9	5.17	1,000	17.3%	1.38
Complete	29.9	14.9	10,000	49.9%	1.38
	Shoreline position 3				
Base case	65.1	2.10E–03	1	0.0%	1.00
Moderate	65.1	2.29E–01	100	0.4%	2.24
Severe	65.1	11.1	1,000	17.1%	1.78
Complete	65.2	30.7	10,000	47.0%	1.63

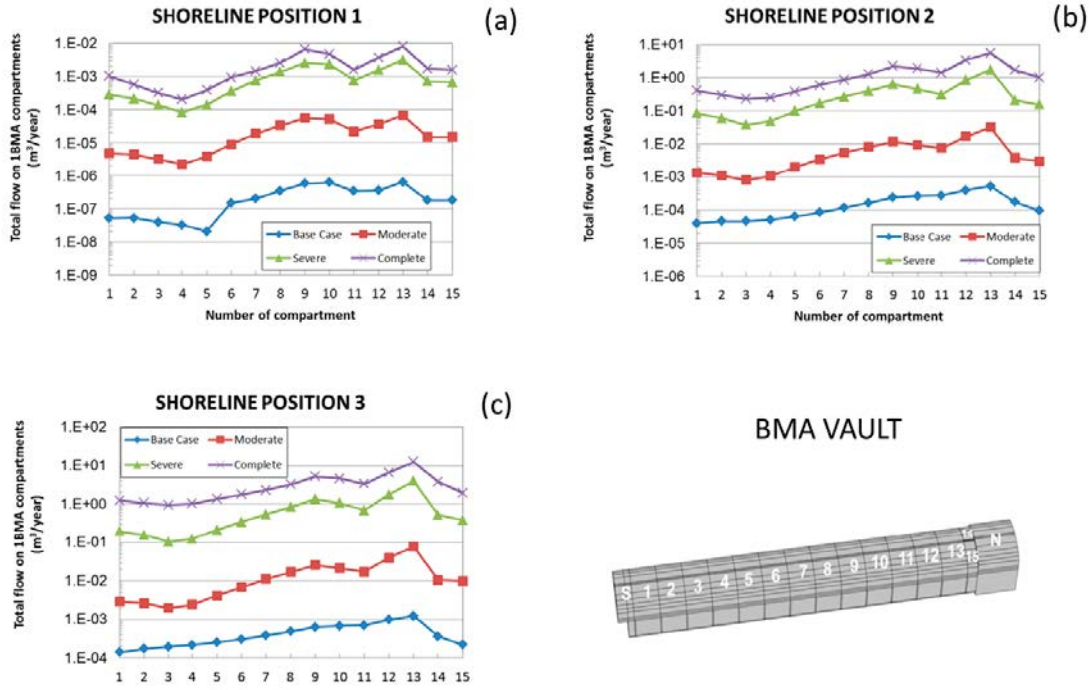

Figure 5-7. Flow rates ($m^3 \cdot year^{-1}$) through the waste compartments of the 1BMA submodel for degradation of outer walls, lids, and floor.

5.1.7 Summary of vault elements degradation scenarios

The results presented for the vault elements degradation cases in a scenario of high permeability beams are summarized in Table 5-7, Table 5-8 and Figure 5-8 to Figure 5-10. Differences included in Table 5-7 and Table 5-8 correspond to the relative difference between the total flow for a given degradation state with respect to the total flow of the Base case. The results indicate that concrete degradation has almost no impact on the total flow through the 1BMA vault. The relative difference is less than 1% for all degradation cases and all shoreline positions. The highest increments in the total tunnel flow are found in the cases considering degradation of inner walls (Cases 2 and 5).

In contrast, significant effects of concrete degradation are observed for the flow profiles in the waste compartments and the total flow through the waste domain for all the cases. Table 5-8 shows that the highest differences with respect to the Base case are found for shoreline position 2. Degradation of concrete elements of a 1BMA vault with high permeability beams also result in an internal redistribution of the flow. The model simulations show that in a vault with high permeability beams, the degradation of the floor, inner and outer walls (Cases 2, 5 and 6) has a major impact on total flow through the waste domain.

As occurs in a 1BMA vault with low permeability beams, degradation of east outer wall (Case 3) and both outer walls (Case 4) also causes a significant increase in the flow rates through the waste domain, but have a smaller effect compared to the other degradation cases.

Contrary to the Case 3, where other barriers are not affected, complete degradation of both outer walls (Case 4) increases the flow through the east and west gravels. This is because complete degradation of the west outer wall establishes a hydraulic connection between the backfill and waste compartments, especially around the fracture zones, promoting higher water flow to the west gravel. The degradation of inner walls and lids (Cases 5 and 6) increases the hydraulic connectivity between the waste compartments, leading to a more smooth flow decrease from compartments 12 to 15 than the decrease observed for degradation of outer walls (Case 4). The degradation of lids and/or inner walls of compartments 12, 13, 14 and 15 compensates the increase in lateral water exchange through degraded outer walls of compartments in contact with the deformation zone ZFMNNW1209.

Table 5-7. Summary of total flow rates ($m^3 \cdot year^{-1}$) through the 1BMA vault for different vault elements degradation cases. Differences with respect to the Base case (positive values indicate higher flow with respect to the Base case).

Case	ID	Shoreline position 1		Shoreline position 2		Shoreline position 3	
		Total flow rate ($m^3 \cdot year^{-1}$)	Difference	Total flow rate ($m^3 \cdot year^{-1}$)	Difference	Total flow rate ($m^3 \cdot year^{-1}$)	Difference
Case 1	1	4.67E–02	0.0%	29.9	0.0%	65.1	0.0%
	2	4.67E–02	0.0%	29.9	0.0%	65.1	0.0%
	3	4.67E–02	0.0%	29.9	0.0%	65.1	0.1%
Case 2	4	4.65E–02	0.4%	29.9	0.2%	65.2	0.18%
	5	4.63E–02	0.8%	30.0	0.5%	65.4	0.5%
	6	4.63E–02	0.8%	30.0	0.5%	65.5	0.6%
Case 3	7	4.67E–02	0.0%	29.9	0.0%	65.1	0.0%
	8	4.67E–02	0.0%	29.9	0.0%	65.1	0.0%
	9	4.67E–02	0.0%	29.9	0.0%	65.1	0.0%
Case 4	10	4.67E–02	0.0%	29.9	0.0%	65.1	0.0%
	11	4.67E–02	0.0%	29.9	0.0%	65.1	0.0%
	12	4.67E–02	0.0%	29.9	0.1%	65.2	0.1%
Case 5	13	4.65E–02	0.4%	29.9	0.2%	65.2	0.2%
	14	4.63E–02	0.8%	30.0	0.4%	65.4	0.5%
	15	4.63E–02	1.0%	30.0	0.5%	65.5	0.6%
Case 6	16	4.67E–02	0.0%	29.9	0.0%	65.1	0.0%
	17	4.67E–02	0.0%	29.9	0.0%	65.1	0.0%
	18	4.67E–02	0.0%	29.9	0.2%	65.2	0.2%

Table 5-8. Summary of total flow rates ($m^3 \cdot year^{-1}$) through waste domain of the 1BMA vault for different vault elements degradation cases. Differences are expressed in order of magnitude with respect to the Base case (positive values indicate higher flow with respect to the Base case).

	ID	Shoreline position 1		Shoreline position 2		Shoreline position 3	
		Total flow rate ($m^3 \cdot year^{-1}$)	Difference	Total flow rate ($m^3 \cdot year^{-1}$)	Difference	Total flow rate ($m^3 \cdot year^{-1}$)	Difference
	1	1.1E–05	2	2.8E–03	2	0.01	2
Case 1	2	4.4E–04	100	0.14	100	0.32	100
	3	1.1E–02	1,000	3.64	1,000	8.15	1,000
	4	9.3E–05	10	0.04	10	0.09	10
Case 2	5	5.5E–03	1,000	2.31	1,000	5.59	1,000
	6	2.5E–02	1,000	12.3	10,000	27.4	10,000
	7	4.7E–06	1	4.7E–03	4	0.01	3
Case 3	8	1.6E–04	10	0.05	10	0.06	10
	9	6.8E–03	1,000	1.91	1,000	3.39	1,000
	10	4.3E–05	10	0.06	10	0.10	10
Case 4	11	2.5E–03	100	3.74	1,000	6.26	1,000
	12	1.2E–02	1,000	10.8	10,000	18.8	1,000
	13	5.3E–05	10	0.08	10	0.14	10
Case 5	14	3.3E–03	1,000	4.72	1,000	8.68	1,000
	15	2.0E–02	1,000	16.0	10,000	31.2	10,000
	16	3.4E–04	100	0.10	100	0.23	100
Case 6	17	1.5E–02	1,000	5.17	1,000	11.1	1,000
	18	3.3E–02	10,000	14.9	10,000	30.7	10,000

In terms of the total flow rates and the differences with respect to the Base case (Table 5-8), degradation of inner and outer walls (Case 5) is the most unfavorable situation. Flow rates through the waste compartments are significantly affected by all degradation states. The impact of degradation is also larger compared to the scenario of low permeability beams, for which the difference found with the Base case for moderate degradation is small.

Degradation of lids, floor and outer walls (Case 6) is the second most unfavorable scenario. Lids degradation in combination with floor and outer walls degradation leads to higher flow rates for all degradation states and shoreline positions than considering the degradation of only floor or outer walls.

In general, flow rates through other vault elements are nearly unaffected by concrete degradation. Exceptions exist, where the waste flow increase is compensated by a reduction of flow through other elements.

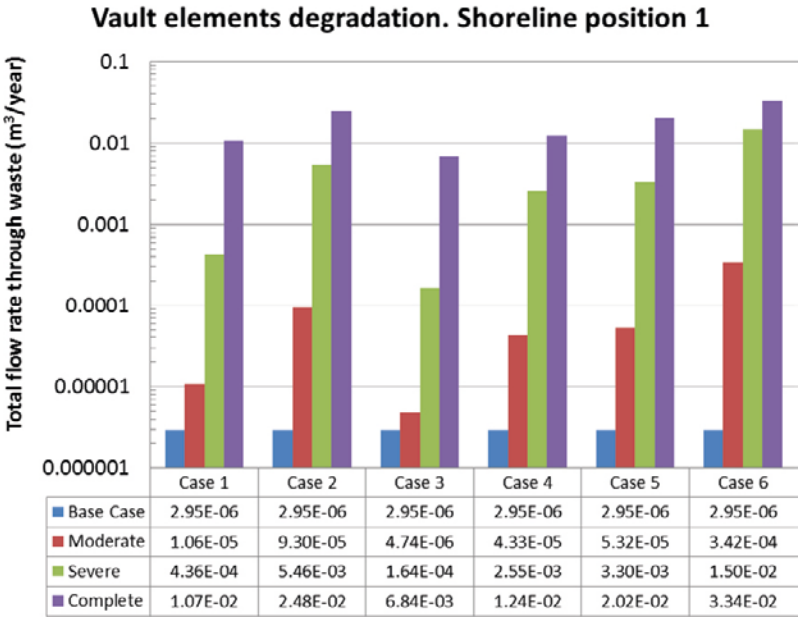

	Case 1	Case 2	Case 3	Case 4	Case 5	Case 6
Base Case	2.95E-06	2.95E-06	2.95E-06	2.95E-06	2.95E-06	2.95E-06
Moderate	1.06E-05	9.30E-05	4.74E-06	4.33E-05	5.32E-05	3.42E-04
Severe	4.36E-04	5.46E-03	1.64E-04	2.55E-03	3.30E-03	1.50E-02
Complete	1.07E-02	2.48E-02	6.84E-03	1.24E-02	2.02E-02	3.34E-02

Figure 5-8. *Total flow rates through the waste zone of 1BMA submodel for different scenarios of vault elements degradation and comparison with the Base case at shoreline position 1.*

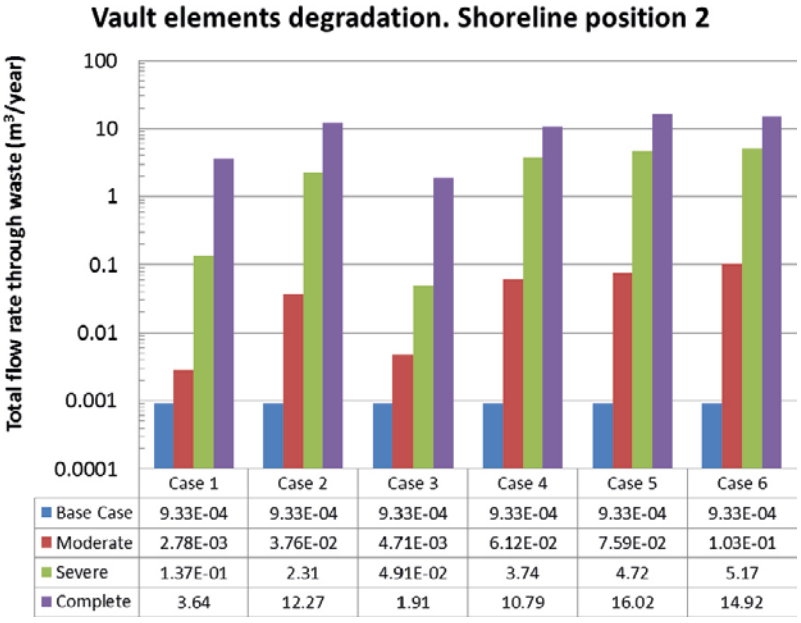

	Case 1	Case 2	Case 3	Case 4	Case 5	Case 6
Base Case	9.33E-04	9.33E-04	9.33E-04	9.33E-04	9.33E-04	9.33E-04
Moderate	2.78E-03	3.76E-02	4.71E-03	6.12E-02	7.59E-02	1.03E-01
Severe	1.37E-01	2.31	4.91E-02	3.74	4.72	5.17
Complete	3.64	12.27	1.91	10.79	16.02	14.92

Figure 5-9. *Total flow rates through the waste zone of 1BMA submodel for different scenarios of vault elements degradation and comparison with the Base case at shoreline position 3.*

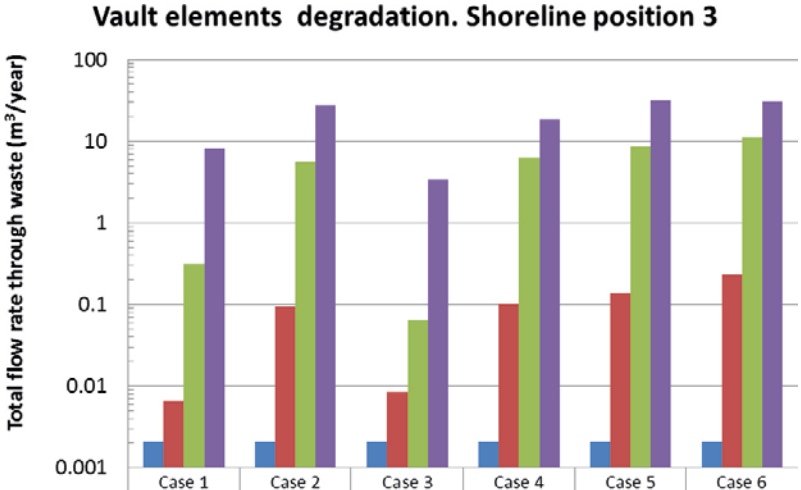

	Case 1	Case 2	Case 3	Case 4	Case 5	Case 6
Base Case	2.10E-03	2.10E-03	2.10E-03	2.10E-03	2.10E-03	2.10E-03
Moderate	6.50E-03	9.28E-02	8.52E-03	1.03E-01	1.38E-01	2.29E-01
Severe	3.18E-01	5.59	6.49E-02	6.26	8.68	11.12
Complete	8.15	27.43	3.39	18.80	31.20	30.68

Figure 5-10. *Total flow rates through the waste zone of 1BMA submodel for different scenarios of vault elements degradation and comparison with the Base case at shoreline position 3.*

5.2 Compartment degradation

The methodology described in Section 4 has been followed to study the degradation of compartments. The effect of the waste encapsulation degradation (floor, lid, and inner and outer concrete walls) has been studied for a moderate, severe and complete degradation state. The same four compartment degradation cases described in Section 4.2 have been repeated, under the assumption of high permeability beams.

The concrete hydraulic conductivity for each waste compartment for simulation Cases 1–3 can be found in Table 4-12 and in Table 5-10 for Case 4. The hydraulic conductivity of other vault materials is equal to the values presented in Table 4-3. An exception is the hydraulic conductivity assigned to the concrete beams, assumed to be equal to the backfill conductivity (10^{-3} m s^{-1}). 36 simulations of concrete degradation were performed. In addition, the Base case simulations with highly conductive beams (10^{-3} m s^{-1}) for the three shoreline positions were performed. In these base case simulations the total flow through the 1BMA waste compartments also displays spatial variability (Figure 5-1). The effect on the waste flow rates due to variability of the concrete hydraulic conductivity for the different waste compartments have been analyzed.

5.2.1 Case 1: Degradation in deformation zone ZFMNNW1209

This section explores the effect of a differential concrete degradation in the compartments 12 to 15. These compartments are associated with the vertical deformation zone ZFMNNW1209. Figure 5-11 shows the results of the total flow rate through the 1BMA waste compartments for the different concrete degradation states and the three shoreline positions. As can be observed, the total flow through compartments 12 to 15 increases as the concrete degrades for all shoreline positions. The waste flow increase is mainly due to a redistribution of water within the vault itself, since the decrease (shoreline position 1) and increase (shoreline positions 2 and 3) in the tunnel flow respect to the Base case are very small (Table 5-10).

The redistribution of flow results in a reduction of the flow through the top and west gravel sections corresponding to the degraded waste compartments, especially in severe degradation states (see Figure D-1 and Figure D-4 of Appendix D).

Conclusions: The concrete degradation of the compartments associated with the zone ZFMNNW1209 significantly increases the flow rate in the degraded waste compartments (more than four orders of magnitude in severe degradation state respect the Base case). The degradation have a minor effect in the tunnel flow.

Table 5-9. Hydraulic conductivity (m s^{-1}) in concrete of waste compartments assumed in compartment degradation proportional to the flow rate (Case 4).

	Shoreline position 1			Shoreline position 3			Shoreline position 3		
Compartment	Moderate	Severe	Complete	Moderate	Severe	Complete	Moderate	Severe	Complete
WC1	8.32E–10	1.07E–09	2.50E–08	3.97E–09	3.18E–07	3.17E–05	1.21E–08	1.14E–06	1.14E–04
WC2	8.32E–10	1.08E–09	2.59E–08	4.42E–09	3.63E–07	3.62E–05	1.49E–08	1.42E–06	1.42E–04
WC3	8.32E–10	9.82E–10	1.61E–08	4.47E–09	3.68E–07	3.67E–05	1.66E–08	1.59E–06	1.59E–04
WC4	8,31E–10	9.21E–10	9.91E–09	4.80E–09	4.01E–07	4.00E–05	1.83E–08	1.77E–06	1.76E–04
WC5	8.30E–10	8.30E–10	8.30E–10	5.80E–09	5.02E–07	5.01E–05	2.13E–08	2.06E–06	2.06E–04
WC6	8.40E–10	1.87E–09	1.04E–07	7.51E–09	6.74E–07	6.73E–05	2.56E–08	2.50E–06	2.50E–04
WC7	8.45E–10	2.29E–09	1.47E–07	9.94E–09	9.19E–07	9.19E–05	3.16E–08	3.10E–06	3.10E–04
WC8	8.56E–10	3.44E–09	2.62E–07	1.36E–08	1.29E–06	1.29E–04	4.00E–08	3.95E–06	3.95E–04
WC9	8.74E–10	5.28E–09	4.46E–07	1.96E–08	1.89E–06	1.89E–04	5.24E–08	5.20E–06	5.20E–04
WC10	8.78E–10	5.65E–09	4.83E–07	2.16E–08	2.09E–06	2.09E–04	5.58E–08	5.55E–06	5.55E–04
WC11	8.55E–10	3.37E–09	2.55E–07	2.26E–08	2.20E–06	2.20E–04	5.76E–08	5.72E–06	5.72E–04
WC12	8.56E–10	3.49E–09	2.67E–07	3.23E–08	3.17E–06	3.17E–04	7.91E–08	7.89E–06	7.89E–04
WC13	8.79E–10	5.79E–09	4.97E–07	4.27E–08	4.22E–06	4.22E–04	1.00E–07	1.00E–05	1.00E–03
WC14	8.42E–10	2.09E–09	1.27E–07	1.46E–08	1.39E–06	1.39E–04	3.01E–08	2.96E–06	2.96E–04
WC15	8.42E–10	2.09E–09	1.27E–07	8.26E–09	7.50E–07	7.49E–05	1.88E–08	1.81E–06	1.81E–04

Table 5-10. Total flow ($m^3 \cdot year^{-1}$) through the 1BMA vault and waste domain for the differential degradation of compartments 12–15 (Case 1) and the three shoreline positions. Increase in the waste flow with respect to the Base case is expressed in orders of magnitude.

Case 1 Degradation state	Vault total flow ($m^3 \cdot year^{-1}$)	Waste total flow ($m^3 \cdot year^{-1}$)	Waste flow increase	Waste/Vault ratio
	Shoreline position 1			
Base case	4.67E–02	2.95E–06	1	0.0%
Moderate	4.65E–02	1.44E–04	10%	0.3%
Severe	4.63E–02	6.36E–03	1,000%	13.7%
Complete	4.63E–02	1.59E–02	1,000%	34.4%
	Shoreline position 2			
Base case	29.9	9.33E–04	1	0.0%
Moderate	29.9	6.99E–02	100	0.2%
Severe	30.0	3.73	1,000	12.4%
Complete	30.0	14.3	10,000	47.5%
	Shoreline position 3			
Base case	65.1	2.10E–03	1	0.0%
Moderate	65.2	1.56E–01	100	0.2%
Severe	65.4	8.18	1,000	12.5%
Complete	65.5	31.0	10,000	47.4%

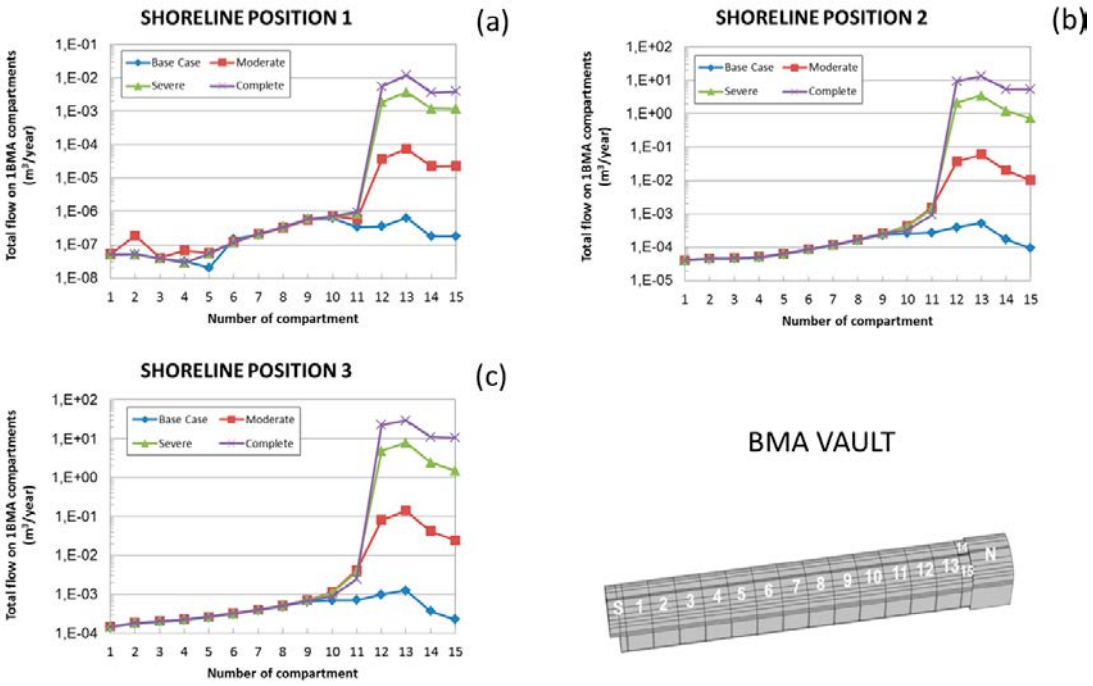

Figure 5-11. *Flow rates ($m^3 \cdot year^{-1}$) through the 1BMA waste compartments for Case 1 of the compartments degradation analysis.*

5.2.2 Case 2: Degradation of low flow compartments

The waste flow profiles in the case of high permeability beams (Figure 5-1) show an increase of waste flow from south to north at shoreline positions 2 and 3. In contrast, at shoreline position 1, the waste flow rate decreases between compartments 1 and 5. Nevertheless, at all shoreline positions the lowest waste flow compartments are located at the South end of the 1BMA vault. Compartments 3 and 4 have been again chosen to analyze the effect of concrete degradation in low flow compartments. Even though these compartments are not the compartments with the lowest waste flow for all shoreline positions, they are among the five lowest flow compartments. The total waste and tunnel flow rates calculated for this case are summarized in Table 5-11. It is worth noticing that the tunnel flow remains unaltered for all the degradation states. In turn, the increase of total waste flow is about 2 and 3 orders of magnitude for severe and complete degradation, respectively, at all shoreline positions. The spatial distribution of the waste flow (Figure 5-12) evidences an increase in the waste flow rates in the degraded compartments 3 and 4 for all shoreline positions. At shoreline position 1, the increase of flow affects the two neighboring compartments (1 and 5). At shoreline positions 2 and 3, the increase in flow rates affects the two upstream compartments (1 and 2). Comparing these results with those of Figure 4-45, it is observed that the high permeability beams avoid the flow redistribution and the shadow effect observed in the case of low permeability beams. Because degradation affects a lower number of compartments, the fraction of the total flow that enters to the waste domain is appreciably lower than in Case 1.

The flow increase in the degraded compartments is also compensated by changes in the surrounding backfill zones (east and west gravel areas, see Figure D-7 and Figure D-8 of Appendix D).

Conclusions: The concrete degradation of the low flow waste compartments has no effect on the total tunnel flow. Again, the main effect of degradation with high permeability beams is basically restricted to the degraded waste compartments and, to a minor extent, to the neighbor upstream compartments. Moderate concrete degradation lead to an total waste flow increase in the range of one order of magnitude above the flow of Base case, whereas severe and complete degradation increase the total waste flow in about 3 orders magnitude above the Base case.

Table 5-11. Total flow ($m^3 \cdot year^{-1}$) through the 1BMA vault and waste domain for the degradation of low flow compartments (Case 2) and the three shoreline positions. Increase in the waste flow with respect to the Base case is expressed in orders of magnitude.

Case 2 Degradation state	Vault total flow ($m^3 \cdot year^{-1}$)	Waste total flow ($m^3 \cdot year^{-1}$)	Waste flow increase	Waste/Vault ratio
	Shoreline position 1			
Base case	4.67E–02	2.95E–06	1	0.0%
Moderate	4.67E–02	8.57E–06	3	0.0%
Severe	4.67E–02	3.07E–04	100	0.7%
Complete	4.67E–02	9.47E–04	100	2.0%
	Shoreline position 2			
Base case	29.9	9.33E–04	1	0.0%
Moderate	29.9	4.73E–03	5	0.0%
Severe	29.9	0.23	100	0.8%
Complete	29.9	1.13	1,000	3.8%
	Shoreline position 3			
Base case	65.1	2.10E–03	1	0.0%
Moderate	65.1	1.89E–02	10	0.0%
Severe	65.1	1.12	100	1.7%
Complete	65.1	5.62	1,000	8.6%

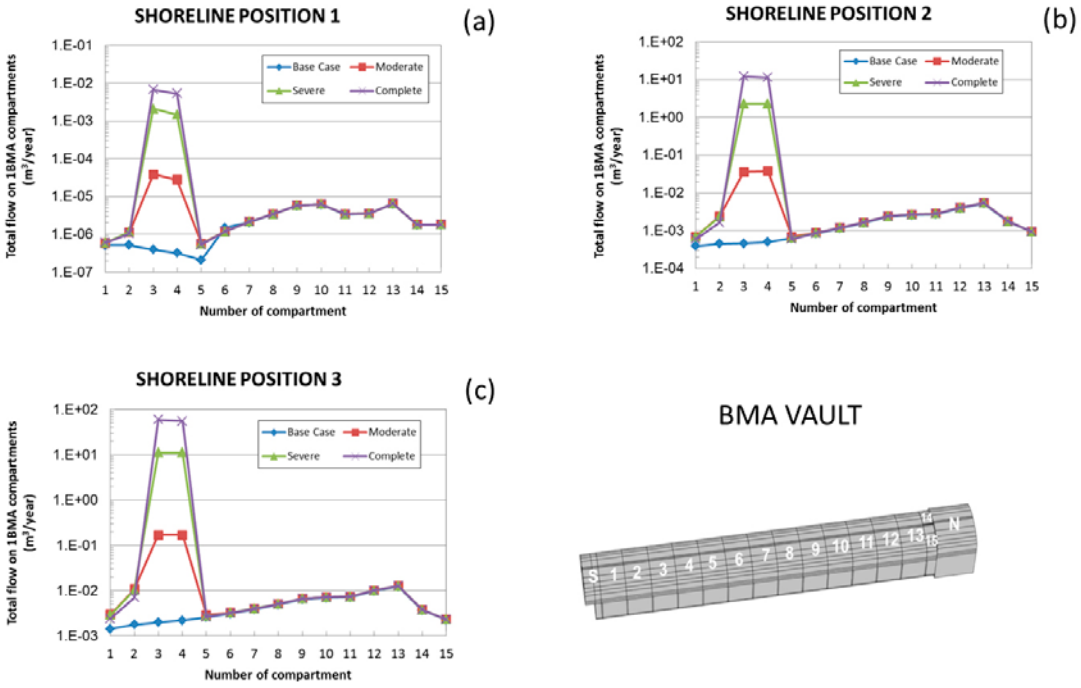

Figure 5-12. *Flow rates ($m^3 \cdot year^{-1}$) through the waste compartments of the 1BMA vault for the degradation of the low flow compartments.*

5.2.3 Case 3: Simultaneous degradation of all compartments affected by fracture zones

Case 3 considers the degradation of compartments 9, 10, 12, 13, 14 and 15, which are affected by the 2 minor fractures and the deformation zone ZFMNNW1209. In fact, comparing Figure 5-11 and Figure 5-13 it is seen that the same effects described in Case 1 (degradation of deformation zone ZFMNNW1209) are also observed in this case. Flow rates through waste compartments 9 and 10 also increase with degradation, as expected. Like in previous cases, degradation does not play a role on the total tunnel flow (see Table 5-12). A major effect is observed on the flow redistribution within the vault. For the complete degradation case, the ratio of total flow through the waste with respect to the total tunnel flow increases from less than 1% to 62% at shoreline position 1, and to about 70% at shoreline positions 2 and 3.

The distribution of flow along the waste compartments (Figure 5-13) shows an increase in flow in compartments 12 to 15, which is similar to the calculated for Case 1. The compartments 9 and 10, in turn, respond to the concrete degradation with a flow increase of the same order of magnitude as the compartments located in the deformation zone ZFMNNW1209. At shoreline positions 2 and 3, flow rates in compartments 7 and 8 also experience a slight increase above the Base case flow rates. A flow decrease is observed in compartment 8 for the severe degradation at shoreline position 1. Compartment 11, located in between the degraded compartments experiences a constant increase in flow at all shoreline positions, that is, does not depend on the concrete degradation state. Nonetheless, the flow redistribution and shadow effect are significantly minimized compared to the scenario of high permeability beams (Section 4).

The flow redistribution affects also the backfill domains (Appendix D). Flow across these zones decreases (especially for the complete degradation state) at the top and west gravel domains at shoreline positions 2 and 3 (see Figure D-9 and Figure D-12), and at the east gravel at shoreline position 1 (see Figure D-11).

Conclusions: Degradation of the concrete located in compartments affected by fracture zones practically does not impact the total tunnel flow. Degradation has a major effect on water redistribution within the vault. The waste/tunnel total flow ratio increases up to 70% for the completely degraded concrete case. The concrete degradation of all the compartments associated with fracture zones yields a flow increase in the degraded waste compartments that affects the neighboring compartments.

Table 5-12. Total flow ($m^3 \cdot year^{-1}$) through the 1BMA vault and waste domain for the degradation of compartments 9, 10, 12–15 (Case 3) and the three shoreline positions. Increase in the waste flow with respect to the Base case is expressed in orders of magnitude.

Case 3 Degradation state	Vault total flow ($m^3 \cdot year^{-1}$)	Waste total flow ($m^3 \cdot year^{-1}$)	Waste flow increase	Waste/Vault ratio	Waste flow Case 3/ Case 1
	Shoreline position 1				
Base case	4.67E–02	2.95E–06	1	0.0%	1.00
Moderate	4.65E–02	2.53E–04	10	0.5%	1.76
Severe	4.63E–02	1.17E–02	1,000	25.3%	1.84
Complete	4.63E–02	2.87E–02	10,000	61.9%	1.81
	Shoreline position 2				
Base case	29.9	9.33E–04	1	0.0%	1.00
Moderate	29.9	9.08E–02	100	0.3%	1.30
Severe	30.0	4.96	1,000	16.5%	1.33
Complete	30.0	20.3	10,000	67.4%	1.42
	Shoreline position 3				
Base case	65.1	2.10E–03	1	0.0%	1.00
Moderate	65.2	2.06E–01	100	0.3%	1.32
Severe	65.4	11.2	1,000	17.1%	1.37
Complete	65.5	47.1	10,000	71.9%	1.52

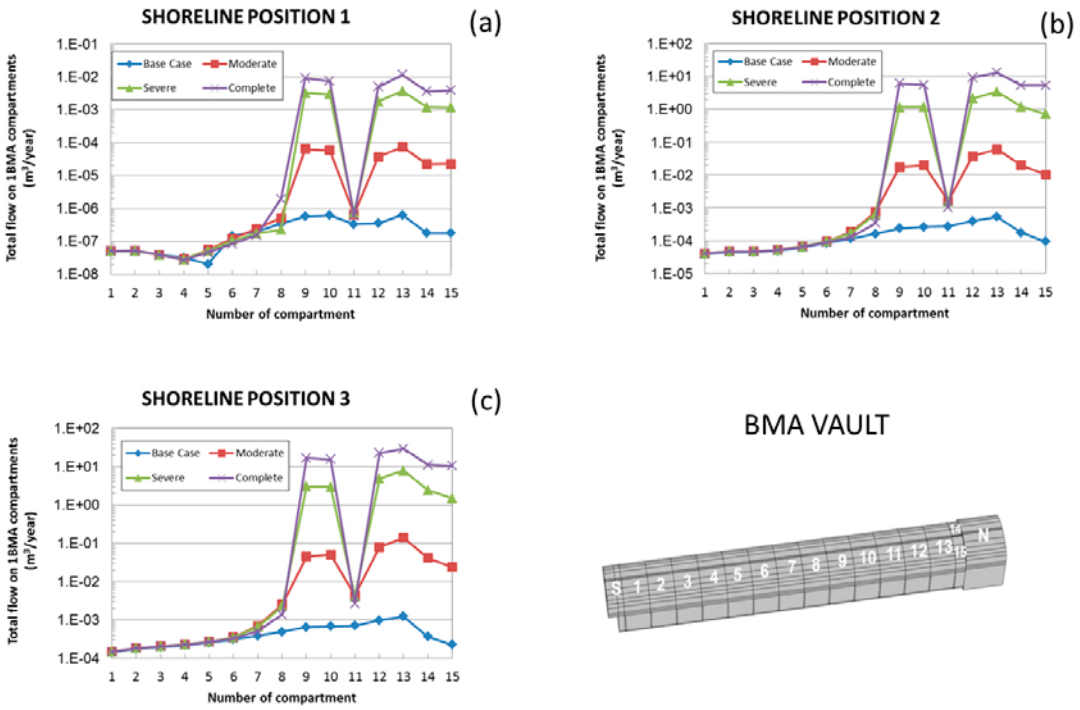

Figure 5-13. *Flow rates ($m^3 \cdot year^{-1}$) through the waste compartments of 1BMA submodel for the three shoreline positions for the simultaneous degradation of all the compartments affected by fracture zones: 9, 10, 12, 13, 14, and 15.*

5.2.4 Case 4: Compartment degradation proportional to the flow rate

This case analyzes the effect of a concrete degradation proportional to the total flow per waste compartment given by the Base case. Thus, the permeability of the concrete encapsulation of each waste compartment is set proportional to the waste flow calculated for the Base case shown in Figure 5-2. Similarly to the scenario of low permeability beams, for each degradation state, a hydraulic conductivity of $8.3 \cdot 10^{-10}$ m·s^{-1} is assigned to the compartment with the lowest total flow rate. The hydraulic conductivity of the compartment with maximum flow is set to the conductivity of the corresponding degradation state ($1.0 \cdot 10^{-7}$ m·s^{-1} in the moderate case; $1.0 \cdot 10^{-5}$ m·s^{-1} in the severe case; $1.0 \cdot 10^{-3}$ m·s^{-1} in the complete degradation case). The linear relationships between the concrete hydraulic conductivity and the waste flow for the three cases is summarized in Table 5-13 and shown graphically in Figure 5-14 (plotted in log-log scale). All cases start with a hydraulic conductivity of $8.3 \cdot 10^{-10}$ m·s^{-1} for the lowest hydraulic conductivity compartment. The three degradation cases result in very different slopes (Table 5-13). The resulting hydraulic conductivity for each compartment is presented in Figure 5-15 for the three different degradation states and the three shoreline positions. Hydraulic conductivity profiles reflect the flow profiles shown in Figure 5-1. The Base case flow profiles with high permeability beams show an almost monotonically increase of flow from south to north at shoreline positions 2 and 3. A decrease in the waste flow rate profile at compartment 5 is found at shoreline position 1. Therefore, the maximum hydraulic conductivity values for complete, severe, and moderate degradation states are found for compartment 13, while the minimum hydraulic conductivity values are found for compartment 1 at shoreline positions 2 and 3, and compartment 5 at shoreline position 1 (convex flow profile).

Table 5-13. Slope (m) and the y-intercept (A) that define the linear relationship between the concrete hydraulic conductivity per compartment (in m·s^{-1}) and the waste flux (in $m^3 \cdot m^{-2} \cdot s^{-1}$).

	m	A
Moderate	1.65E–12	8.28E–10
Severe	1.66E–10	6.64E–10
Complete	1.66E–08	–1.58E–08

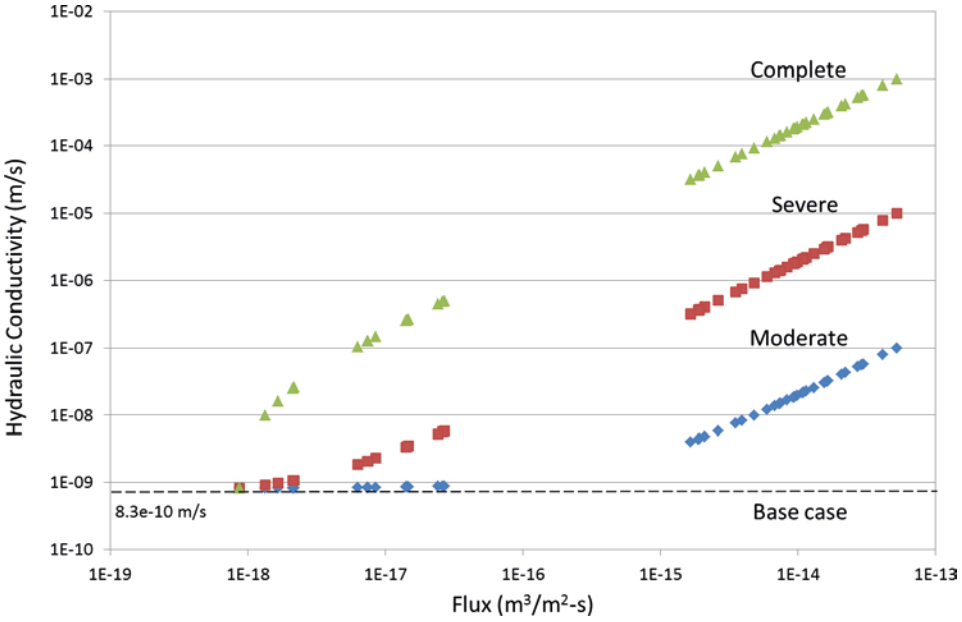

Figure 5-14. *Relationship between concrete hydraulic conductivity ($m \cdot s^{-1}$) and waste fluxes ($m^3 \cdot m^{-2} \cdot s^{-1}$).*

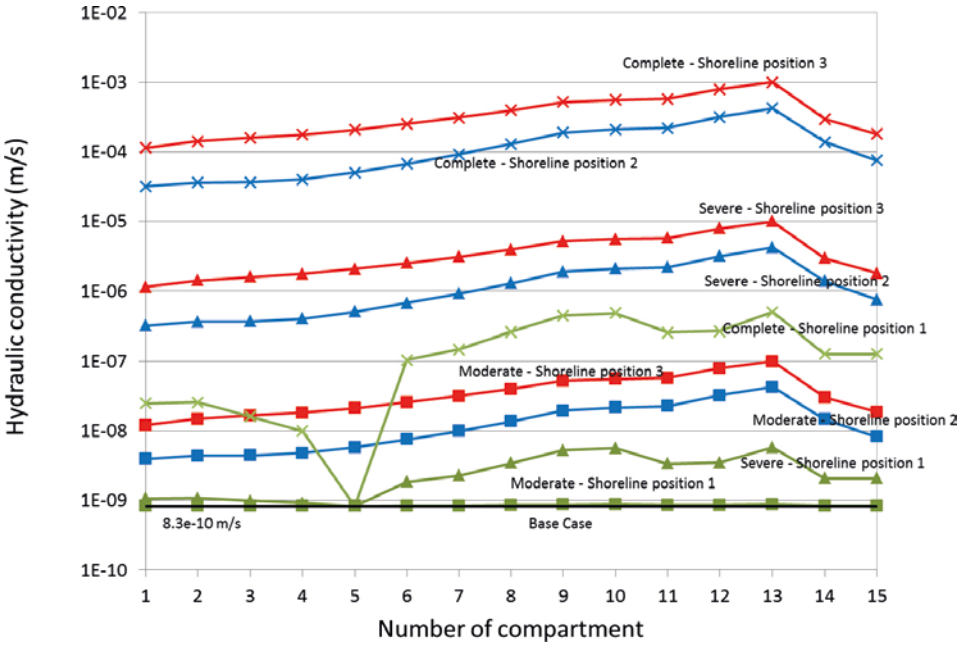

Figure 5-15. *Hydraulic conductivity ($m \cdot s^{-1}$) for each waste compartment for the three concrete degradation states and the three shoreline positions: the variation in the different compartments depends on the concrete degradation state.*

The results show that the tunnel flow variations are lower than 1%. There is an important increase in the waste flow with respect to the Base case for the extreme degradation state, especially for shoreline positions 2 and 3 (Table 5-14). For the severe and complete degradation cases, at shoreline position 1, there is an increase of more than one order of magnitude with respect to the intact case. For shoreline positions 2 and 3 the waste flow increases three and four orders of magnitude respect to the Base case, respectively. The worst scenario is found at shoreline position 3 and complete degradation, for which the waste flow accounts for approximately 56% of the total tunnel flow, respectively.

Table 5-14. Total flow ($m^3 \cdot year^{-1}$) through the 1BMA vault and waste domain for the degradation of compartments proportional to the total waste flow (Case 4) and the three shoreline positions. Increase in the waste flow with respect to the Base case is expressed in orders of magnitude.

Case 4 Degradation state	Vault total flow ($m^3 \cdot year^{-1}$)	Waste total flow ($m^3 \cdot year^{-1}$)	Waste flow increase	Waste/Vault ratio
	Shoreline position 1			
Base case	4.67E–02	2.95E–06	1	0.0%
Moderate	4.67E–02	3.11E–06	1	0.0%
Severe	4.67E–02	1.50E–05	5	0.0%
Complete	4.65E–02	1.14E–03	100	2.5%
	Shoreline position 2			
Base case	29.9	9.33E–04	1	0.0%
Moderate	29.9	3.03E–02	100	0.1%
Severe	30.0	2.22	1,000	7.4%
Complete	30.0	15.8	10,000	52.4%
	Shoreline position 3			
Base case	65.1	2.10E–03	1	0.0%
Moderate	65.1	1.68E–01	10	0.3%
Severe	65.4	9.17	1,000	14.0%
Complete	65.5	36.8	10,000	56.1%

Figure 5-16 shows the spatial distribution of the total flow through the waste compartments. The results for the degraded states at shoreline position 1 present a heterogeneous distribution of waste flow that reflect the intact case profile. The compartments 1 to 5 present the lowest flow for all the degradation stages, whereas compartments 9,10 and 13, which are affected by deformation zones, present peaks of high flow. The results for shoreline positions 2 and 3 present a common pattern with a profile that follows the hydraulic conductivity profile (Figure 5-15). The increase of flow is monotonic from south to north with the highest flow located in compartment 13. The flow redistribution affects also the gravel compartments (Appendix D). In general, the flow through the top, east, and west gravel areas is reduced in the complete concrete degradation cases.

Conclusions: The concrete degradation proportional to the waste flow does not result in a significant increase of tunnel flow. The waste flow increases orders of magnitude compared to the intact case. At shoreline position 1, only the complete concrete degradation yields a waste flow increase of one order of magnitude. However, at shoreline positions 2 and 3, the moderate, severe and complete degradation stages lead to a waste flow increase of one, three and four orders of magnitude, respectively. The worst case scenario occurs for the completely degraded case and the shoreline position 2 and 3 (waste flow is 53–56% of the tunnel flow).

5.2.5 Summary of compartments degradation scenarios

The results presented for the compartments degradation cases and the three shoreline positions are summarized in Table 5-15 and Table 5-16, and graphically in Figure 5-17, Figure 5-18, Figure 5-19, and Figure B-17. to Figure D-19 of Appendix D. Differences included in Table 5-15 and Table 5-16 correspond to the relative difference between the total flow for a given degradation state with respect to the total flow of the Base case. The results indicate that compartment concrete degradation has a very low impact in the total flow through the 1BMA vault.

In general, the effect of the compartment degradation scenarios is a redistribution of the flow within the vault. The waste flow increases locally in the degraded waste compartments and affects slightly to the adjacent compartments. The waste flow increase in the neighbor compartments is independent on the degradation stage. The total flow through the gravel area also decreases to compensate the increase in the degraded compartments.

The total flow through the waste domain is shown in Figure 5-17, Figure 5-18 and Figure 5-19, for shoreline positions 1, 2, and 3, respectively. For all shoreline positions the worst case scenario corresponds to the complete concrete degradation state of all compartments affected by fractures. Conversely, the degradation of low flow compartments (Case 2) presents the lowest impact. This result can be explained by the lower number of compartments degraded in this case (2).

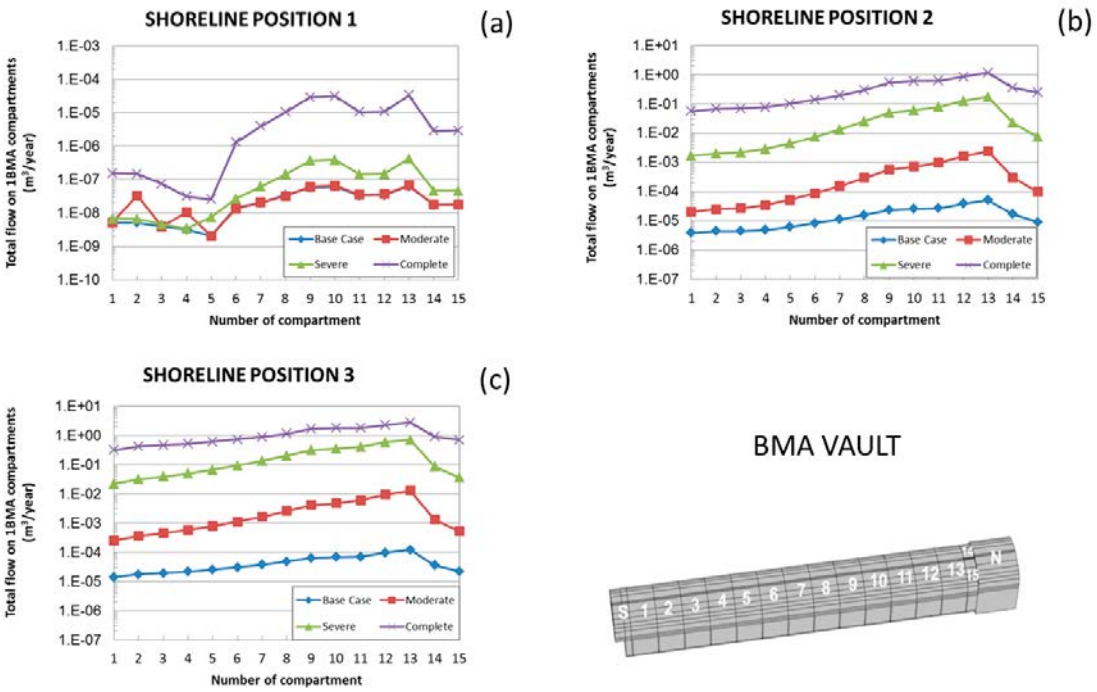

Figure 5-16. *Flow rates ($m^3 \cdot year^{-1}$) through the waste compartments of 1BMA submodel for degradation proportional to the Base case waste flow (Case 4) and the three shoreline positions.*

Table 5-15. Total tunnel flow rates ($m^3 \cdot year^{-1}$) calculated for different compartments degradation cases and the three shoreline positions.

	ID	Shoreline position 1		Shoreline position 2		Shoreline position 3	
		Total flow rate ($m^3 \cdot year^{-1}$)	Difference	Total flow rate ($m^3 \cdot year^{-1}$)	Difference	Total flow rate ($m^3 \cdot year^{-1}$)	Difference
Case 1	1	4.65E–02	0.4%	29.9	0.2%	65.2	0.2%
	2	4.63E–02	0.8%	30.0	0.5%	65.4	0.5%
	3	4.63E–02	0.8%	30.0	0.5%	65.5	0.6%
Case 2	4	4.67E–02	0.0%	29.9	0.0%	65.1	0.0%
	5	4.67E–02	0.0%	29.9	0.0%	65.1	0.0%
	6	4.67E–02	0.0%	29.9	0.0%	65.1	0.0%
Case 3	7	4.65E–02	0.4%	29.9	0.2%	65.2	0.2%
	8	4.63E–02	0.8%	30.0	0.5%	65.4	0.5%
	9	4.63E–02	0.8%	30.0	0.5%	65.5	0.6%
Case 4	10	4.67E–02	0.0%	29.9	0.0%	65.1	0.0%
	11	4.67E–02	0.0%	30.0	0.4%	65.4	0.5%
	12	4.65E–02	0.4%	30.0	0.6%	65.5	0.6%

Table 5-16. Total waste flow rates ($m^3 \cdot year^{-1}$) calculated for different compartments degradation cases and the three shoreline positions. Differences are expressed in orders of magnitude with respect to the Base case (positive values indicate higher flow with respect to the Base case).

	ID	Shoreline position 1		Shoreline position 2		Shoreline position 3	
		Total flow rate ($m^3 \cdot year^{-1}$)	Difference	Total flow rate ($m^3 \cdot year^{-1}$)	Difference	Total flow rate ($m^3 \cdot year^{-1}$)	Difference
Case 1	1	1.4E–04	10	0.07	10	0.16	10
	2	6.4E–03	1,000	3.73	1,000	8.18	1,000
	3	1.6E–02	1,000	14.3	10,000	31.0	10,000
Case 2	4	8.6E–06	2	4.7E–03	4	0.02	8
	5	3.1E–04	100	0.23	100	1.12	100
	6	9.5E–04	100	1.13	1,000	5.62	1,000
Case 3	7	2.5E–04	10	0.09	100	0.21	100
	8	1.2E–02	1,000	4.96	1,000	11.2	1,000
	9	2.9E–02	10,000	20.3	10,000	47.1	10,000
Case 4	10	3.1E–06	1	0.03	10	0.17	10
	11	1.5E–05	4	2.22	1,000	9.17	1,000
	12	1.1E–03	100	15.8	10,000	36.8	10,000

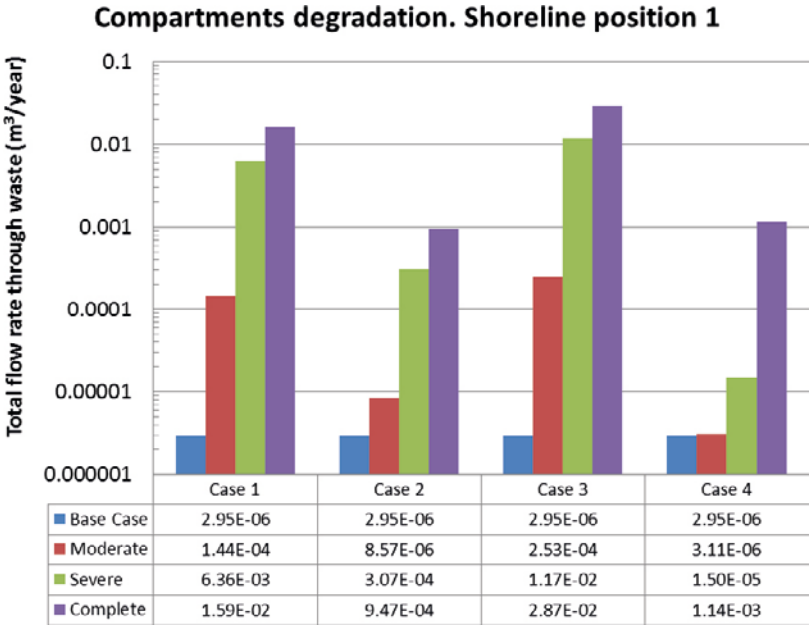

Figure 5-17. *Total flow rates ($m^3 \cdot year^{-1}$) through the waste domain of 1BMA submodel for different cases of compartments degradation and comparison with the Base case for shoreline position 1.*

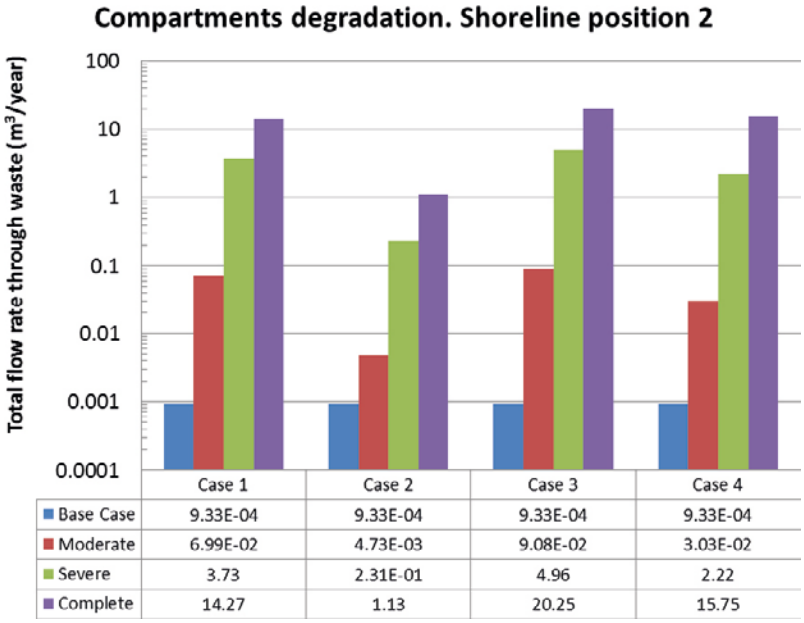

	Case 1	Case 2	Case 3	Case 4
Base Case	9.33E-04	9.33E-04	9.33E-04	9.33E-04
Moderate	6.99E-02	4.73E-03	9.08E-02	3.03E-02
Severe	3.73	2.31E-01	4.96	2.22
Complete	14.27	1.13	20.25	15.75

Figure 5-18. *Total flow rates ($m^3 \cdot year^{-1}$) through the waste domain of 1BMA submodel for different cases of compartments degradation and comparison with the Base case for shoreline position 2.*

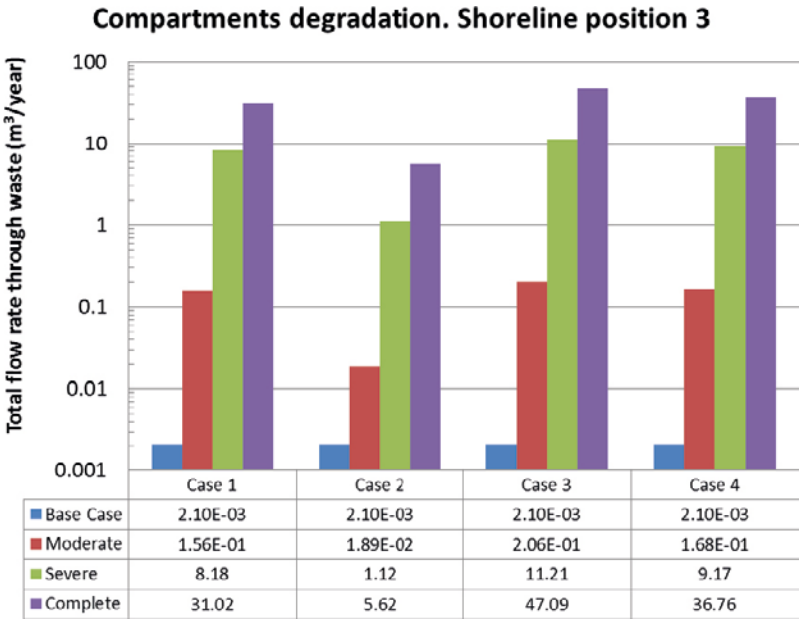

	Case 1	Case 2	Case 3	Case 4
Base Case	2.10E-03	2.10E-03	2.10E-03	2.10E-03
Moderate	1.56E-01	1.89E-02	2.06E-01	1.68E-01
Severe	8.18	1.12	11.21	9.17
Complete	31.02	5.62	47.09	36.76

Figure 5-19. *Total flow rates ($m^3 \cdot year^{-1}$) through the waste domain of 1BMA submodel for different cases of compartments degradation and comparison with the Base case for shoreline position 3.*

6 Non-reactive solute transport in the Silo near-field

6.1 Model description

6.1.1 Model Domain and discretization

The model domain of the Silo (Figure 6-1), delimited by the coordinates in Table 6-1, has been set up based on the following criteria:

- The domain must be large enough to represent the transport of radionuclides potentially diffusing from the Silo.
- It must contain the Silo plugs while minimizing the intersection with access tunnels.
- It must not interfere with the domain of the rest of the vault submodels.
- It must be contained in the SFR 1 repository-scale model domain defined in Abarca et al. (2013).

The domain has been truncated with a vertical plane defined by points 2 and 6 to adapt it to the SFR 1 repository-scale model. The total volume of the model domain is $2.318 \cdot 10^6$ m^3 and the surface of the outer box is $1.053 \cdot 10^5$ m^2. The finite element mesh consists of 1,779,468 tetrahedral quadratic elements (Figure 6-1).

Table 6-1. Coordinates of the vertices at Figure 6-1.

Point ID	Absolute coordinates (x, y, z) in meters
1	(6,457.50, 10,149.62, –165.03)
2	(6,587.84, 10,149.62, –165.03)
3	(6,457.50, 10,149.62, –45.03)
4	(6,457.50, 10,279.62, –45.03)
5	(6,617.50, 10,279.62, –45.03)
6	(6,617.50, 10,246.51, –45.03)

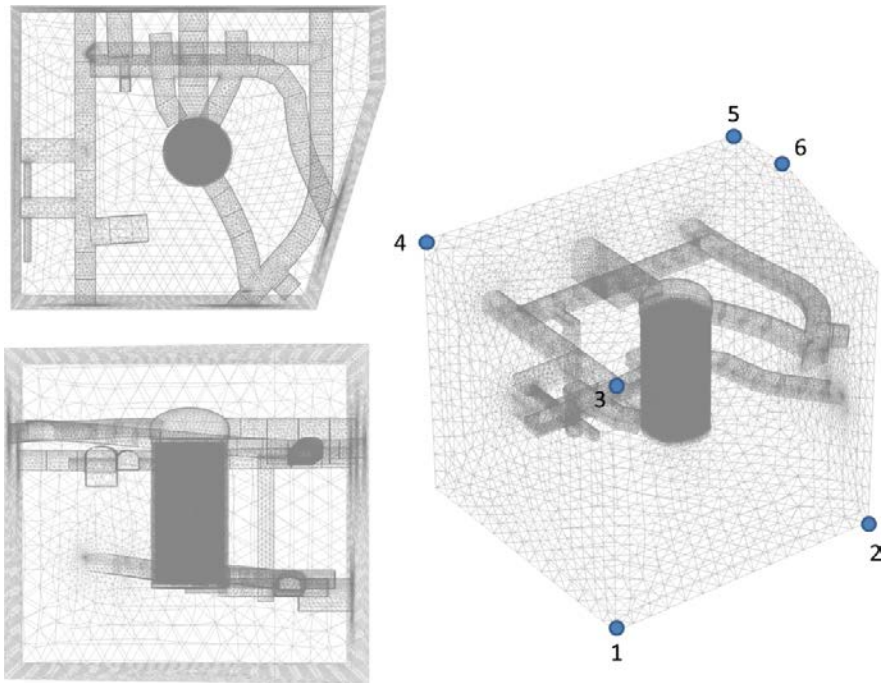

Figure 6-1. *Silo model domain and finite element mesh. The numbered points correspond to the vertices which coordinates are described in Table 6-1.*

6.1.2 Flow submodel

- **Boundary conditions**

Flow simulations for the three shoreline positions under study have been performed to obtain the velocity fields for the solute transport calculations. Prescribed driving pressures have been fixed on the boundaries of the selected box domain using the driving pressures obtained from SFR 1 repository-scale model. Values have been interpolated from nodes to boundary faces by linear interpolation.

- **Hydraulic parameters**

The properties of the Silo materials are those defined for the Base case in Abarca et al. (2013) and are summarized in Table 6-2.

6.1.3 Steady-state non-reactive solute transport model

The non-reactive solute transport steady-state model includes the surrounding rock and the repository domains shown in Figure 6-2. The Silo structure is excluded from the model domain. Instead, a fixed tracer concentration in the Silo-rock interface has been considered (i.e. tracers are released from the Silo-rock interface area). This assumes that (1) the transport of radionuclides within the Silo is much faster than in the bedrock, and (2) there is an inexhaustible source of radionuclides within the Silo.

- **Transport equations**

The conservation of solute mass is described by:

$$\frac{\partial (\phi c)}{\partial t} = -\nabla \cdot (\boldsymbol{q}c - \boldsymbol{D}_c \nabla c) \qquad (6\text{-}1)$$

where ϕ is the porosity of the rock ($m^3 \cdot m^{-3}$), $\boldsymbol{q}$ is the Darcy flux ($m^3 \cdot m^{-2} \cdot s^{-1}$), $\boldsymbol{D}$ is the effective diffusion tensor ($m^2 \cdot s^{-1}$), and $\boldsymbol{c}$ is the solute concentration ($kg \cdot m^{-3}$).

Under steady-state conditions the equation reduces to the divergence free expression:

$$\nabla \cdot (\boldsymbol{q}c - \boldsymbol{D}e \nabla c) = 0 \qquad (6\text{-}2)$$

With finite elements, several stability problems can arise with this type of hyperbolic equation, especially when the Peclet number restriction is not fulfilled. In order to avoid these numerical instabilities, consistent stabilization techniques provided with the 'Transport of Diluted Species Interface' of COMSOL Multiphysics has been used. More information about these techniques can be found in COMSOL (2012a).

Table 6-2. Hydraulic conductivity of Silo materials.

Repository components	Materials		K (m/s)
Access tunnels	Backfill		1.00E–03
Silo	Top layer (90% sand, 10% bentonite)		1.00E–09
	Bottom layer (90% sand, 10% bentonite)		1.00E–09
	Waste		8.30E–07
	Silo concrete lid with gas evacuation pipes	K_x=K_y	8.30E–10
		K_z	3.00E–07
	Silo Bentonite Walls		1.54E–12.0·z(m) + 2.11E–10
Plugs	Structural plug		1.00E–06
	Sealed hydraulic bentonite section		1.00E–12

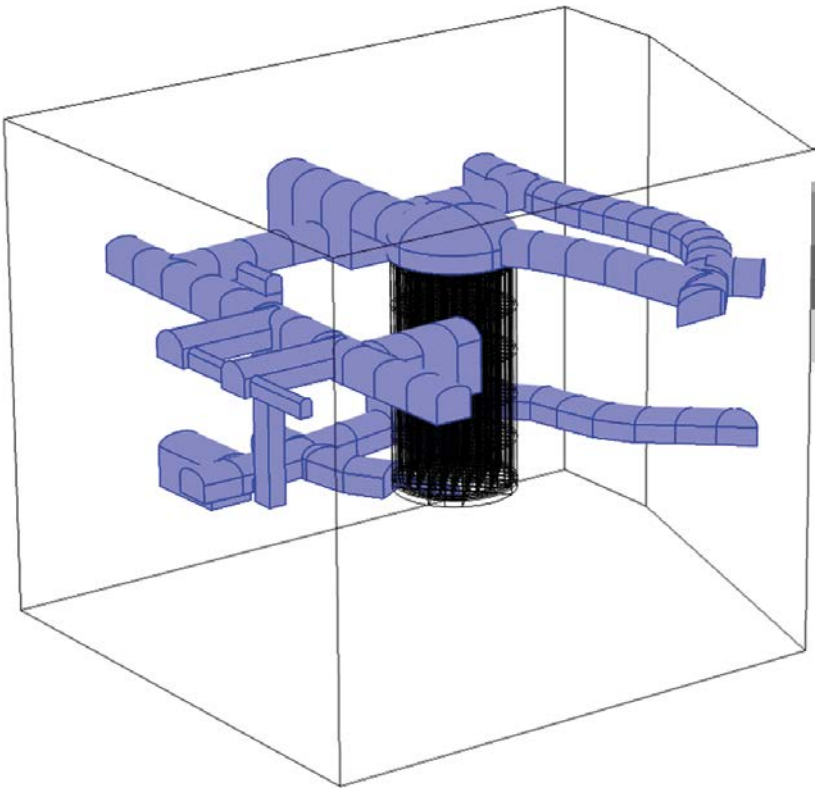

Figure 6-2. *Repository domains used in the non-reactive solute problem . Note that the Silo is not included.*

Since steady-state simulations do not include information on the temporal evolution of the system, particle tracking simulations using the 'Particle Tracing Module' of COMSOL (COMSOL 2012b) have also been performed to gain insight in the residence-time of particles leaving the Silo walls. These simulations have only considered advection as transport mechanism and are only representative of advective-dominated problems. In the latter case, the position of a particle, which may be associated with the transport of solute species, can be tracked over time with the following expression

$$\frac{\partial \boldsymbol{x}_p}{\partial t} = \frac{\boldsymbol{q}}{\phi} \tag{6-3}$$

where $\boldsymbol{x}_p$ (m) represents the position of the particle.

- **Boundary conditions**

A prescribed concentration $c_{prescribed} = 1$ has been adopted along the Silo-rock interface area. In turn, an open boundary condition was specified in the outer boundaries of the rock. In this way, the incoming water enters the domain with $c_{inflow} = 0$ while it leaves the domain with a concentration that depends on the flow and the prescribed concentration boundary condition.

- **Transport Parameters**

The parameters used in the transport simulations are reproduced in Table 6-3 and were extracted from SKB (2001).

Table 6-3. Effective diffusivity and porosity of the Silo materials.

Material	D_e ($m^2 \cdot s^{-1}$)	ϕ ($m^3 \cdot m^{-3}$)
rock	1.00E–13	0.005
concrete	1.00E–11	0.15
bentonite	1.00E–10	0.61
backfill	6.00E–10	0.30

6.2 Simulation cases: rock description

Three different conductivity fields of the rock have been simulated for the three shoreline positions. The first rock realization used corresponds to the hydraulic conductivity field of the Base case (Base_Case1_DFN_R85 in Odén et al. 2014). In addition to the Base case, two additional realizations of the rock conductivity have been selected based on previous results of the regional DarcyTools model. They are considered as representative of two cases that lead to a higher and a lower average tunnel flow compared to the Base case. They will be referred to as High and Low flow realizations, respectively (see Table 6-4 for correspondence with respective DarcyTools simulations).

6.3 Transport indicators

Two different indicators of the potential radionuclide migration have been analyzed: the water outflow rate, denoted as Q_{out} ($m^3 \cdot s^{-1}$), and the equivalent flow rate, denoted as Q_{eq} ($m^3 \cdot s^{-1}$).

The water outflow rate Q_{out} ($m^3 \cdot s^{-1}$) is calculated from the results of a steady-state solute transport calculation. It indicates the water outflow rate containing solute concentration. It can be obtained by solving a problem where a prescribed concentration $c_{prescribed}$ is set in the source boundaries (Silo-rock interface). Q_{out} ($m^3 \cdot s^{-1}$) can then be expressed by:

$$Q_{out} = \frac{\dot{m}_{out}}{c_{prescribed}} \tag{6-4}$$

where the mass rate $\dot{m}_{out}$ is the mass that leaves the domain per unit time ($kg \cdot s^{-1}$). Using the divergence theorem, $\dot{m}_{out}$ can be calculated by integrating the outflow mass fluxes over the box domain:

$$\dot{m}_{out} = \int_{A_{box}} (\boldsymbol{q}c - \boldsymbol{D}_c \nabla c) \cdot \boldsymbol{n} \cdot dS \tag{6-5}$$

where A_{box} is the surface of the outer box ($1.053 \cdot 10^5$ m^2), and $\boldsymbol{n}$ is the normal vector. At steady-state, this mass flux should be independent of the chosen closed surface containing the Silo.

The second indicator, the equivalent flow rate Q_{eq} ($m^3 \cdot s^{-1}$), has been proposed in previous studies (Neretnieks, 1980, Neretnieks et al. 1987) as the flow magnitude of water in the rock near the Silo that becomes contaminated by out-diffusing radionuclides. It assumes that the rock can be described as a porous medium.

The equivalent flow rate of radionuclides from the Silo to the groundwater can be calculated according to Bird et al. (1960) as:

$$Q_{eq} = A_w \phi_{rock} \left(\frac{4D_w}{\pi t_{res}} \right)^{0.5} \tag{6-6}$$

where A_w (m^2) is the surface area between the part of the Silo containing the waste and the rock, ϕ_{rock} is the rock porosity, D_w ($m^2 \cdot s^{-1}$) is the molecular diffusivity of the nuclides in water, and t_{res} (s) is the residence time of the water in contact with the Silo, which can be calculated as $t_{res} = L\phi_{rock}/u_0$, where u_0 ($m \cdot s^{-1}$) is the flux of the approaching non-contaminated water, and L (m) is the pathway length of the flow near the Silo (Figure 6-3).

Table 6-4. Nomenclature of the three equiprobable realizations of the rock conductivity field in the Silo submodel and the regional-scale model (Odén et al. 2014).

This model	Case number in regional-scale model	Regional-scale model name
Base case	Case 1	Base_Case1_DFN_R85
High Flow case	Case 11	nc_DEP_R07_DFN_R85
Low Flow case	Case 15	nc_NoD_R01_DFN_R18

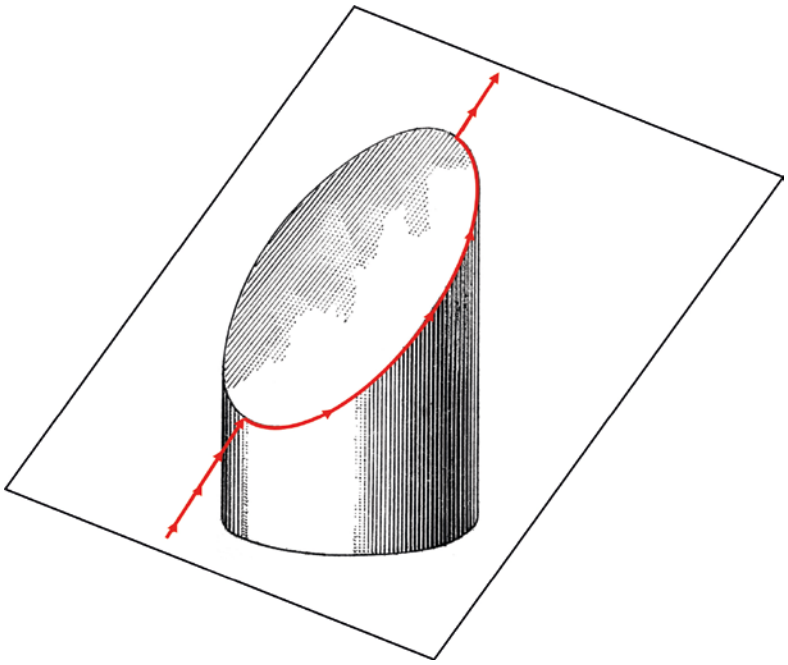

Figure 6-3. *Intersection of the Silo with an averaged flow field in an oblique plane. Water will ideally follow a semi-elliptical pathway (in red).*

In this work, u_0 is calculated as the magnitude of the Darcy flux field, i.e. q ($m^3 \cdot m^{-2} \cdot s^{-1}$). An average value of q is calculated over a cylindrical surface coaxial with the Silo, but with a radius 5 m larger than that of the Silo. This reason to evaluate the flux on such a surface is due to the need to evaluate realistic fluxes in the rock domain in the vicinity of the Silo, and not at the interface, where the flux is modified by the presence of the barriers.

To estimate Q_{eq} using Equation 6-6 the following data has been used: A_w equal to the area of the cylinder of the bentonite walls and including the top and bottom surfaces of the lid and floor, respectively (6,476 m^2), a rock porosity of 0.005 (SKB 2001), and a molecular diffusivity of the nuclides in water of $2 \cdot 10^{-9}$ $m^2 \cdot s^{-1}$.

To estimate the length of the pathway L, it is considered that an averaged groundwater flow field with magnitude q intersects the Silo at an angle, as shown in the figure below. In this case, water will ideally flow following a semi-elliptical pathway. The length of this pathway depends on the angle between the averaged flow field and a horizontal plane (θ) which can be approximated from the averaged velocity field. The half-perimeter ($p_{½}$) of an ellipse is approximated by

$$p_{½} = \pi \, (3(r_m + r_M) - \sqrt{(3r_m + r_M)(r_m + 3r_M)}) \qquad (6\text{-}7)$$

where r_m (m) and r_M (m) are the minor and major axes divided by 2, respectively. Assuming that r_m equals the radius of the Silo, r_M can be calculated as $r_m = r_{silo} / cos(\theta)$.

6.4 Results

The groundwater flow rates of the Silo submodel are compared with the flow rates computed with the SFR 1 repository-scale model for the three rock realizations and the three shoreline positions.

6.4.1 Flow results

A comparison of the fluxes obtained with the Silo submodel and the SFR 1 repository-scale model is shown for the three different rock cases in Figure 6-4, Figure 3-3 and Figure 6-6 and also in Table 6-5, Table 6-6, and Table 6-7.

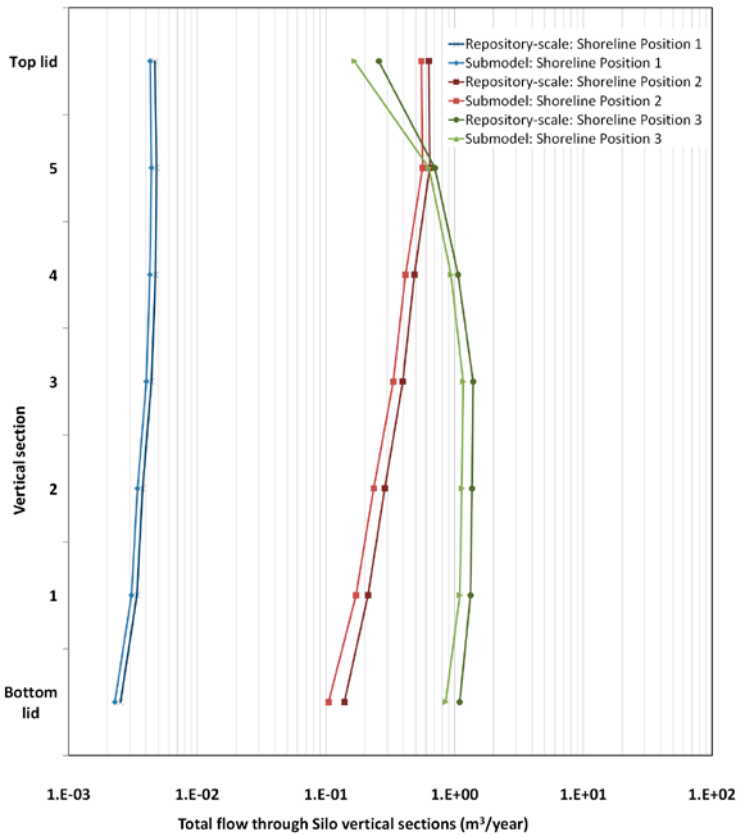

Figure 6-4. *Total flow in Silo vertical sections for the Base case for different shoreline positions for the SFR 1 repository-scale model and the Silo submodel.*

Table 6-5. Total flow ($m^3 \cdot year^{-1}$) obtained in Silo vertical sections for the Base case and the three shoreline positions in the SFR 1 repository-scale model and relative differences calculated with respect to the Silo submodel.

Section	Shoreline position 1		Shoreline position 2		Shoreline position 3	
	Total flux ($m^3 \cdot year^{-1}$)	Difference	Total flux ($m^3 \cdot year^{-1}$)	Difference	Total flux ($m^3 \cdot year^{-1}$)	Difference
Bottom lid	2.29E–03	–10%	1.05E–01	–25%	8.52E–01	–22%
1	3.08E–03	–9%	1.71E–01	–19%	1.10E+00	–17%
2	3.44E–03	–9%	2.35E–01	–18%	1.14E+00	–17%
3	4.02E–03	–9%	3.34E–01	–16%	1.17E+00	–16%
4	4.28E–03	–10%	4.15E–01	–15%	9.37E–01	–12%
5	4.41E–03	–9%	5.64E–01	–12%	6.33E–01	–10%
Top lid	4.31E–03	–8%	5.52E–01	–12%	1.66E–01	–35%
Total	2.58E–02	–9%	2.37E+00	–15%	5.99E+00	–17%

Similar total flux patterns can be observed for the three different rock realizations in Figure 6-4, Figure 6-5 and Figure 6-6. Relative differences between repository-scale model and Silo submodel for the Silo section range between 0% and 54%. They appear to be relatively small for shoreline position 1, although they increase for the other two shoreline positions.

6.4.2 Solute transport results

- **2D and 1D cuts**

One vertical and one horizontal cross planes and a 1D line (Figure 6-7) are used to analyze the solute concentration under steady-state conditions for the different rock realizations and the three shoreline positions.

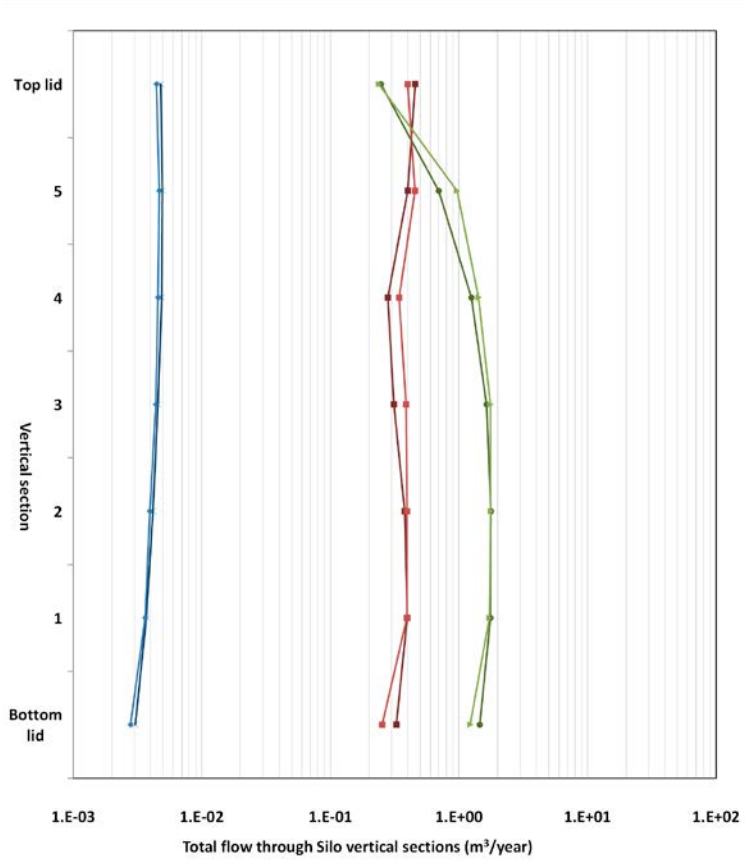

Figure 6-5. *Total flow in Silo vertical sections for the High Flow case for different shoreline positions for the SFR 1 repository-scale model and the Silo submodel.*

Table 6-6. Total flow obtained in Silo vertical sections for High Flow case for different shoreline positions in the SFR 1 repository-scale model and relative differences calculated with respect to the Silo submodel.

Section	Shoreline position 1		Shoreline position 2		Shoreline position 3	
	Total flux ($m^3 \cdot year^{-1}$)	Difference	Total flux ($m^3 \cdot year^{-1}$)	Difference	Total flux ($m^3 \cdot year^{-1}$)	Difference
Bottom lid	2.79E–03	–8%	2.53E–01	–23%	1.22E+00	–16%
1	3.63E–03	–2%	3.94E–01	–1%	1.73E+00	–2%
2	3.95E–03	–5%	3.94E–01	4%	1.77E+00	0%
3	4.40E–03	–4%	3.88E–01	24%	1.76E+00	7%
4	4.57E–03	–6%	3.43E–01	22%	1.42E+00	14%
5	4.68E–03	–5%	4.56E–01	14%	9.69E–01	39%
Top lid	4.45E–03	–7%	4.00E–01	–13%	2.39E–01	–4%
Total	2.85E–02	–6%	2.63E+00	3%	9.10E+00	3%

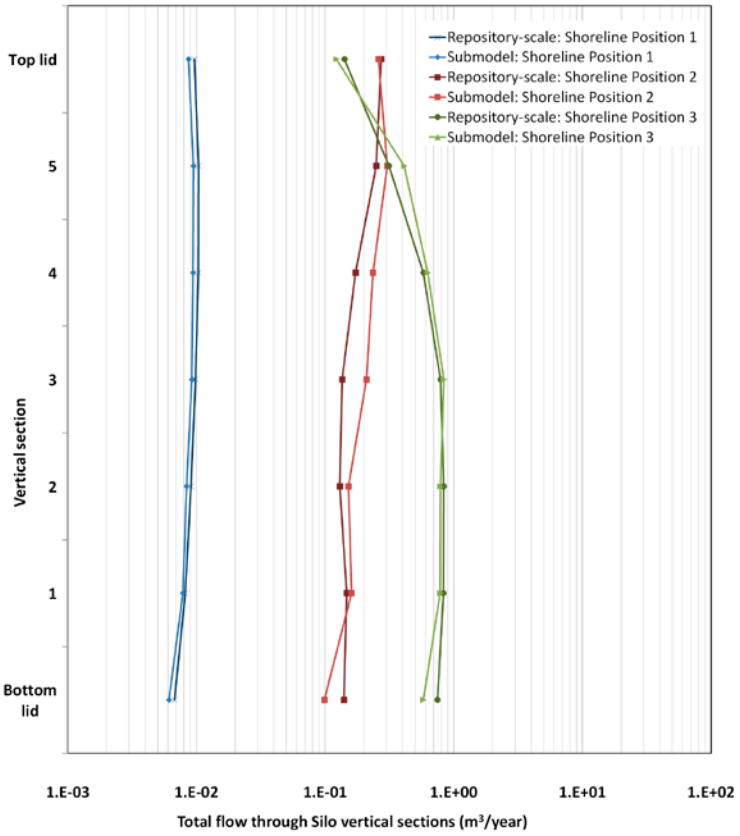

Figure 6-6. *Total flow in Silo vertical sections for the Low Flow case for different shoreline positions for the SFR 1 repository-scale model and the Silo submodel.*

Table 6-7. Total flow obtained in Silo vertical sections for the Low Flow case for different shoreline positions in the SFR 1 repository-scale model and relative differences calculated with respect to the Silo submodel.

Section	Shoreline position 1		Shoreline position 2		Shoreline position 3	
	Total flux ($m^3 \cdot year^{-1}$)	Difference	Total flux ($m^3 \cdot year^{-1}$)	Difference	Total flux ($m^3 \cdot year^{-1}$)	Difference
Bottom lid	6.12E–03	–9%	9.87E–02	–30%	5.80E–01	–22%
1	7.85E–03	–4%	1.61E–01	9%	7.85E–01	–6%
2	8.38E–03	–8%	1.52E–01	17%	7.89E–01	–6%
3	9.21E–03	–6%	2.10E–01	54%	8.37E–01	6%
4	9.42E–03	–9%	2.36E–01	37%	6.28E–01	8%
5	9.48E–03	–9%	3.04E–01	22%	4.12E–01	31%
Top lid	8.69E–03	–10%	2.60E–01	–5%	1.22E–01	–13%
Total	5.92E–02	–8%	1.42E+00	14%	4.15E+00	–2%

Figure 6-8 shows the concentration distribution in a vertical and a horizontal plane (defined in Figure 6-7) for the Base case for the three shoreline positions. Note that, for shoreline position 1, flux has a main upward vertical component and the velocities are two orders of magnitude lower than for the other shoreline positions. The transport is diffusion dominated and the solute plume has a larger spread. On the other hand, the solute transport is advection-dominated for shorelines positions 2 and 3. In these cases, the plume is narrower around the Silo as compared with shoreline position 1, but extends upwards and downwards conditioned by the most permeable fracture zones.

Figure 6-9 and Figure 6-10 show the concentration distribution for the High Flow case and Low Flow case, respectively. As can be observed, the solute plumes for the High Flow case and the Base case are similar. However, for the Low flow case, due to the lower conductivity of the rock around the Silo, the extent of the solute plume is confined to the vicinity of the Silo even when the advective transport contribution increases (shoreline positions 2 and 3).

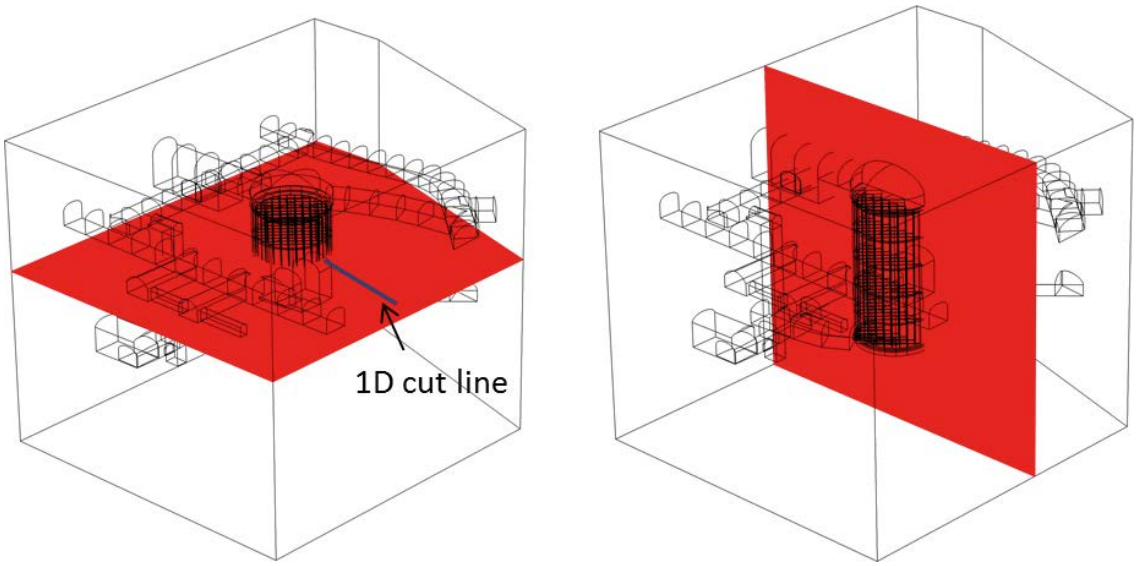

Figure 6-7. *Vertical xz (y= 6,552.6 m) and horizontal xy (z = –96 m) planes and 1D line used for the results comparison.*

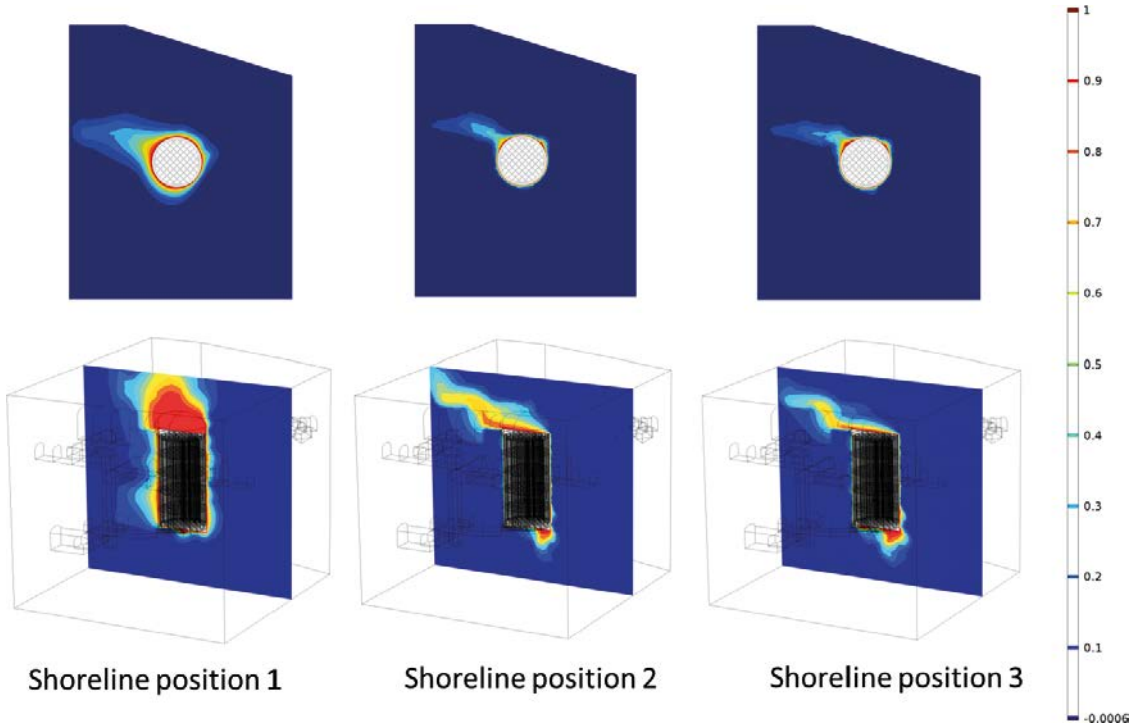

Figure 6-8. *Normalized 2D concentration profiles (–) for different shoreline positions for the Base case.*

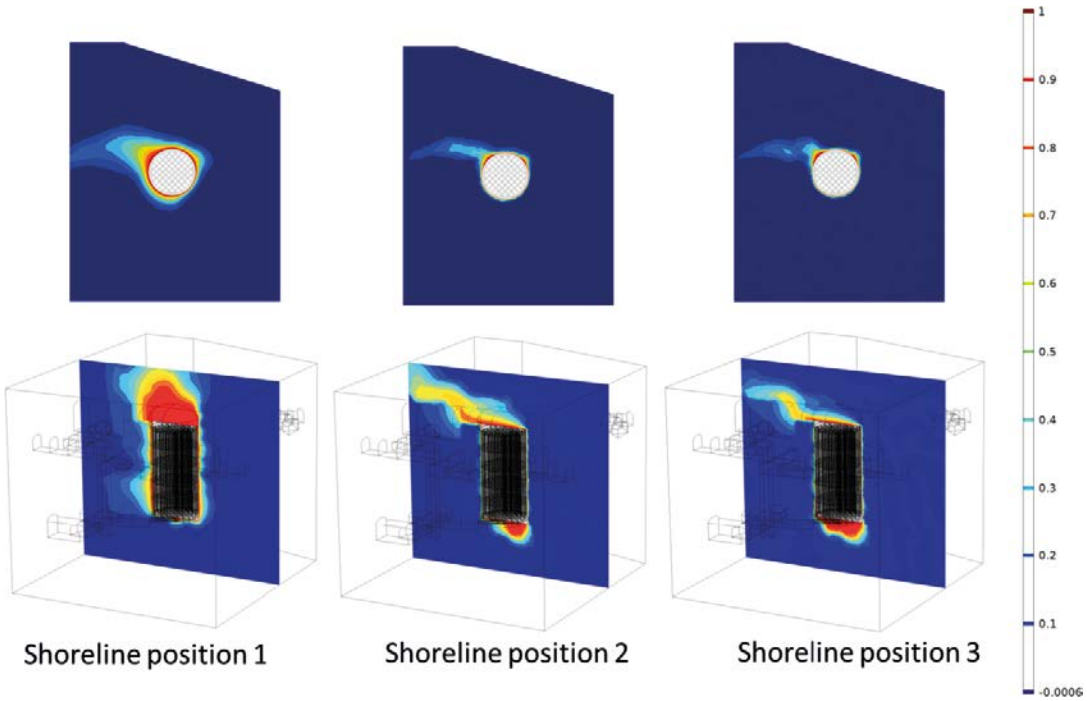

Figure 6-9. *Normalized 2D concentration profiles (–) for different shoreline positions for the High Flow case.*

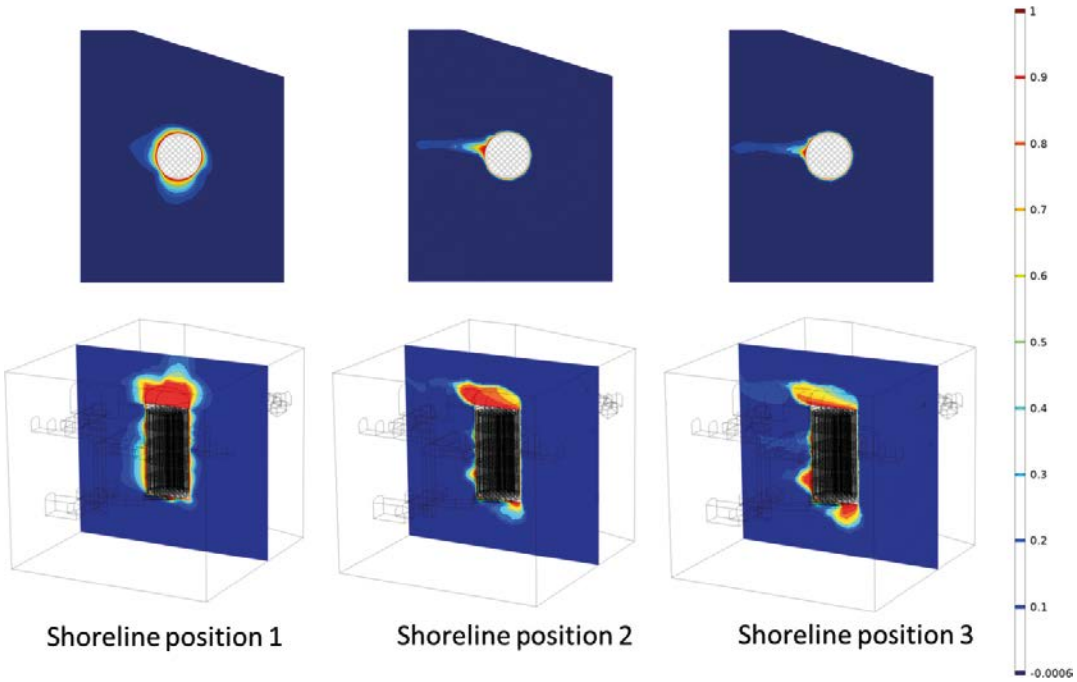

Figure 6-10. *Normalized 2D concentration profiles (–) for different shoreline positions for the Low Flow case.*

The results does not provide information of the time required to reach steady-state conditions. As discussed in the next paragraphs, a diffusive-dominated steady-state situation (shoreline position 1) will be reached more slowly than an advective-dominated scenario (shoreline position 2 and 3) due to the different characteristic times of these processes. Furthermore, the extension of the plume does not give an idea of the mass rate released by the Silo: despite it is larger for shoreline position 1, this is the configuration with less releasing capacity.

The different regimes (diffusive and advective) for the different shoreline positions can be also observed in Figure 6-11, Figure 6-12 and Figure 6-13, where concentrations are drawn along the 1D line shown in Figure 6-7. Again, the concentration profiles for shoreline position 1 evidence a diffusive behavior while the concentration profiles for shoreline positions 2 and 3 show sharp fronts due to the control of advection.

- **Q_{eq} and Q_{out}**

The values obtained for Q_{eq} and Q_{out} over different rock realizations and boundary conditions are shown in Table 6-8.

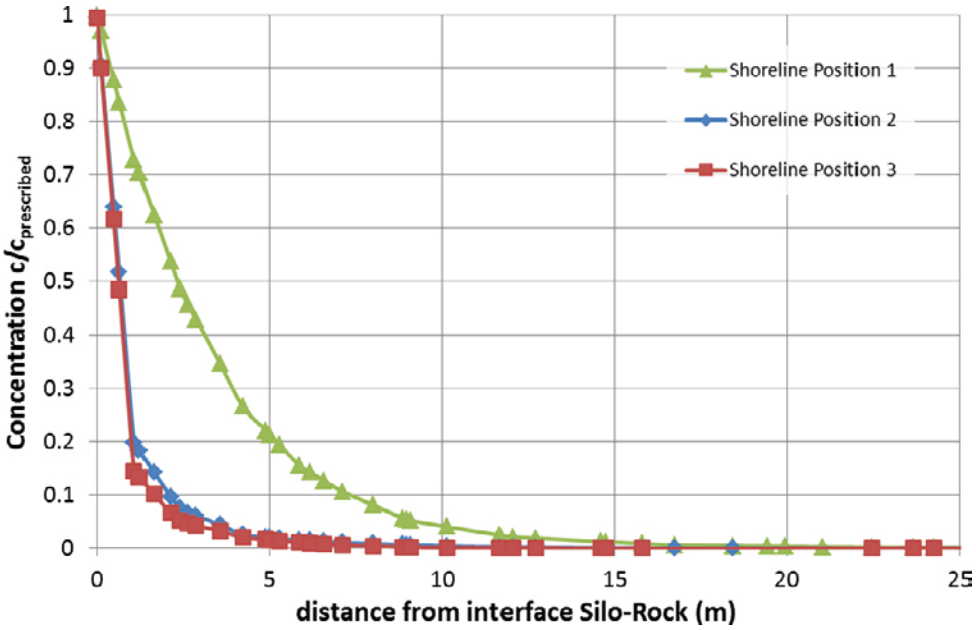

Figure 6-11. *Concentration profiles for each shoreline position for the Base case along the 1D line showed in Figure 6-7.*

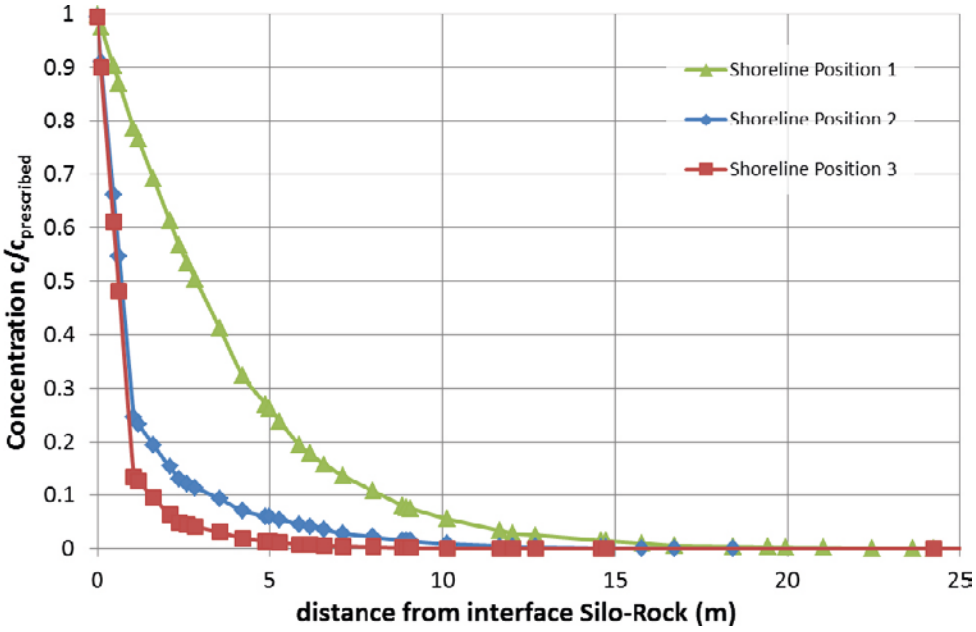

Figure 6-12. *Concentration profiles for each shoreline position for the High Flow case along the 1D line showed in Figure 6-7.*

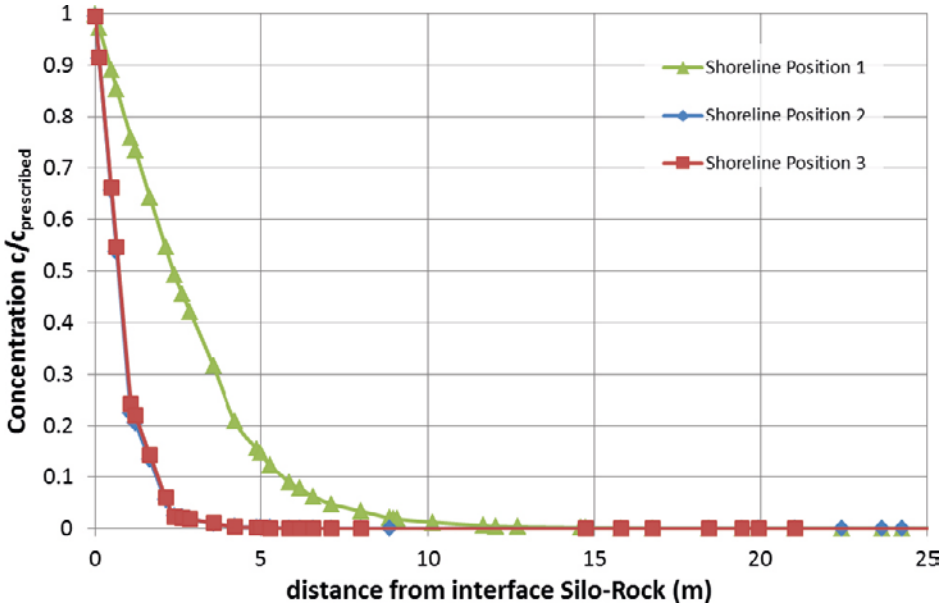

Figure 6-13. *Concentration profiles for each shoreline position for the Low Flow case along the 1D line showed in Figure 6-7.*

Table 6-8. Calculated Q_{eq} and Q_{out} ($m^3 \cdot year^{-1}$).

Simulation Case	Shoreline position	Q_{eq} ($m^3 \cdot year^{-1}$)	Q_{out} ($m^3 \cdot year^{-1}$)
Base case	1	3.16E–02	2.37E–02
	2	7.17E–01	4.95E+00
	3	1.11E+00	7.95E+00
High Flow case	1	3.60E–02	2.39E–02
	2	8.39E–01	5.01E+00
	3	1.33E+00	8.66E+00
Low Flow case	1	4.32E–02	3.50E–02
	2	5.79E–01	2.23E+00
	3	8.72E–01	3.77E+00

The calculated Q_{eq} values for shoreline position 1 are of the same order as the Q_{eq} values in Lindgren et al. (2001), which range from 0.043 to 0.059 $m^3 \cdot year^{-1}$. The Q_{eq} values in Lindgren et al. (2001) present little variation between shorelines positions, correlating with relatively small changes in local hydrology presented by Holmén and Stigsson (2001). In the present analysis, groundwater velocity for shoreline position 1 is two orders of magnitude smaller than for shoreline positions 2 and 3. In these cases, the Q_{out} values calculated in this work exceed the values in Lindgren et al. (2001) by more than one order of magnitude.

Q_{eq} values for the Silo evaluated from the the repository-scale SRF model of Abarca et al. (2013) are presented in Appendix E. The differences in Q_{eq} values compared to the vault-scale model presented in Table 6-8 are mainly due to the different rock porosity values considered in the different cases. In the present study, a rock porosity value of 0.005 was considered, in agreement with the value used in SKB (2001). For the estimations made using the repository-scale model (Appendix E) a porosity value was calculated as an average in the Silo vicinity, based on the regional hydrogeology model of Odén et al. (2014). Porosity values of $2.29 \cdot 10^{-5}$, $2.30 \cdot 10^{-5}$, $1.21 \cdot 10^{-5}$ were found for the Base case, the High flow case, and the Low flow case, respectively. That porosity difference results in the consequent reduction in the estimated Q_{eq} as it scales with the square root of the porosity.

Although variables Q_{eq} and Q_{out} are calculated using different types of information, both result are in the same order of magnitude for shoreline position 1. This result is to be expected since the analytical solution to obtain Q_{eq} is based on assumptions that are met at the shoreline position 1: vertical flow direction and a diffusion-dominated system. The larger values obtained for Q_{out} could be due to the fact that Q_{out} has been estimated taking into account the mass flux through the vertical walls and the top and bottom surfaces of the Silo, whereas Q_{eq} only considers the vertical walls of the Silo for its estimation.

Q_{eq} and Q_{out} differ by up to an order of magnitude for shoreline positions 2 and 3. In these cases, the flow field does not meet the assumptions for which the Q_{eq} concept is defined. Therefore, in these cases Q_{out} seems to be a more realistic variable to estimate a mass flow of solute released from the Silo.

When comparing the values obtained for the different rock conductivity fields, higher Q_{out} is obtained for shoreline positions 2 and 3, especially for the Base case and High Flow case rocks, as compared with shoreline position 1 (which is two orders of magnitude lower).

- **Particle tracking and travel time**

Solute concentrations resulting from steady-state conditions lack information about residence times and radionuclide velocity. Therefore, particle tracking simulations following Equation 6-3 have been performed to increase the understanding of these aspects. The particles are transported exclusively by advection so that no diffusion is considered in these cases.

Almost 10,000 particles uniformly distributed along the Silo-rock interface (except for the top of the Silo, where particles were distributed over the interface between the concrete lids on top of the shafts and the backfilled domain) are released under the influence of the velocity field generated by the respective flow simulation cases. A simulation time of 1000 years has been considered. The results obtained consist of maps of particles and their footprints, which are colored according to the particle time-of-flight. Figure 6-14, Figure 6-15 and Figure 6-16 show the comparison between the steady-state transport simulations, illustrated as 3D concentration isosurfaces, and the particles footprints for the three rock conductivity fields (Base case, High Flow case and Low Flow case). As expected, for the advective-dominated cases (i.e. shoreline positions 2 and 3) there is a clear correlation between the isosurfaces and the corresponding particle footprints. For the shoreline position 1 (diffusion dominated) the particle tracking simulation shows that a particle leaving the Silo will be almost in the same location after 1000 years. In this case, advection plays no role in radionuclide release, which is a diffusion-driven process.

The time that a particle takes to leave the modeled domain can give an idea of the residence time scales for each shoreline position. A good indicator could be the fraction of the released particles that leave the domain as a function of time. Figure 6-17, Figure 6-18 and Figure 6-19 show the temporal evolution of this fraction (expressed in percentage).

In fractured media, solutes tend to travel following major fractures. In this context, a useful indicator of the fastest travel times is the time needed for the 5% of the fastest particles to leave the model domain (Table 6-9). Small times are probably related with high velocities along fractures that connect the Silo with the boundaries.

Shoreline position 3 is the configuration presenting the shortest times, whereas no particles leave the domain for the shoreline position 1. Under the same boundary conditions the influence of the different rock realizations appear to be ordered by their velocity classification, being the High Flow case the one with shortest times and the Low Flow case the one with longest times.

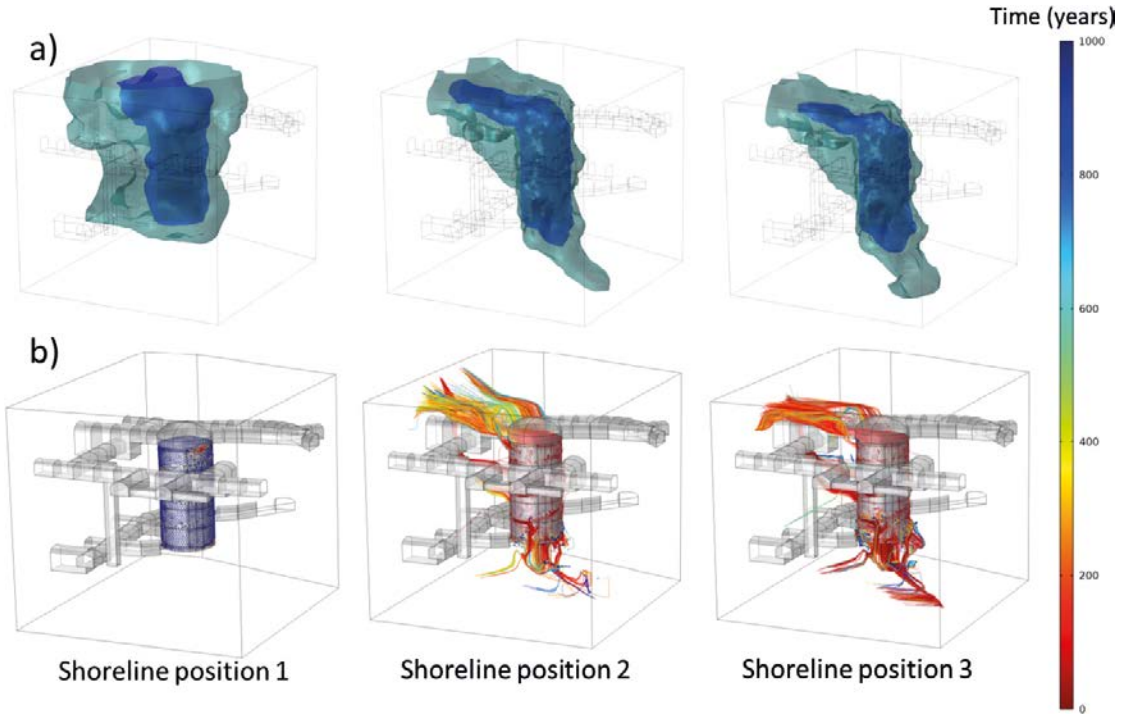

Figure 6-14. *Results of the steady-state conservative tracer simulations corresponding to the Base case: a) iso-concentration maps for c=0.02 (light blue) and c=0.5 (dark blue) and b) footprints of the particles released from the Silo walls and colored by time-of-flight in years (right scale).*

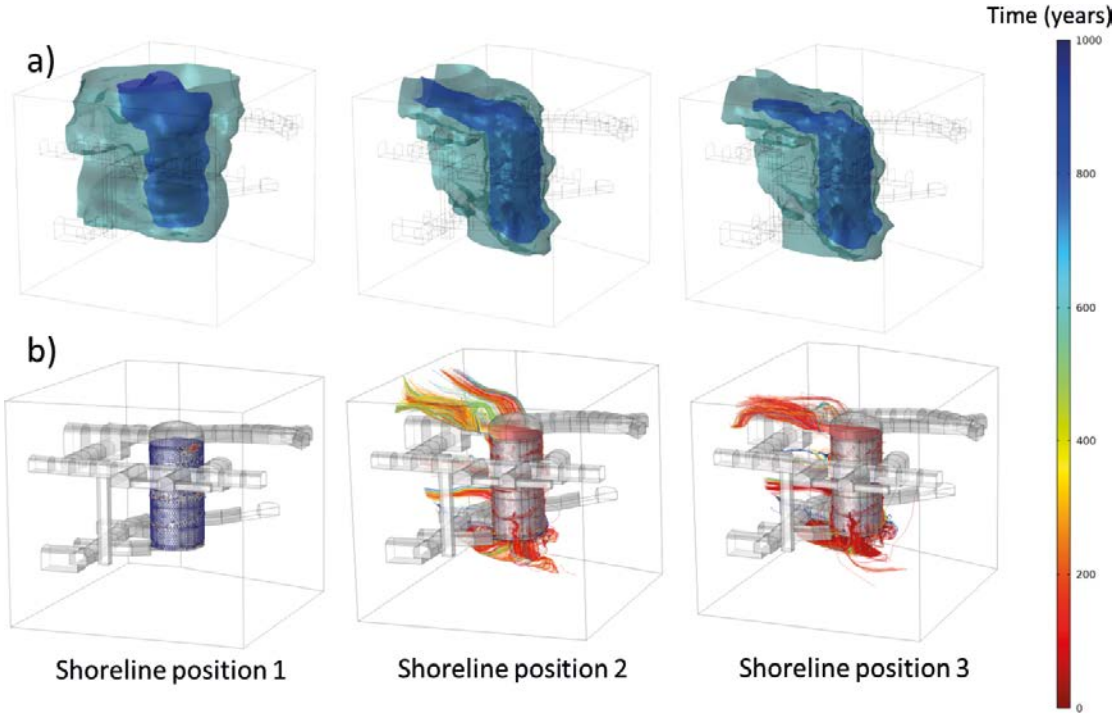

Figure 6-15. *Results of the steady-state conservative tracer simulations corresponding to the High Flow case: a) iso-concentration maps for c=0.02 (light blue) and c=0.5 (dark blue) and b) footprints of the particles released from the Silo walls and colored by time-of-flight in years (right scale).*

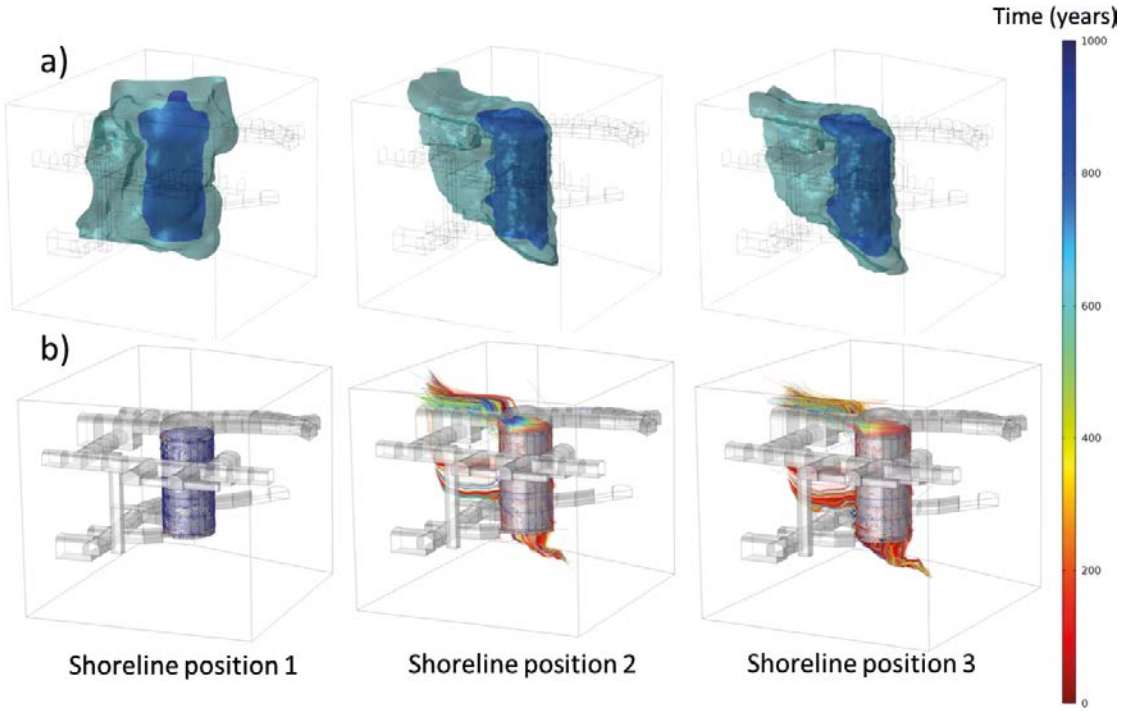

Figure 6-16. *Results of the steady-state conservative tracer simulations corresponding to the Low Flow case: a) iso-concentration maps for c=0.02 (light blue) and c=0.5 (dark blue) and b) footprints of the particles released from the Silo walls and colored by time-of-flight in years (right scale).*

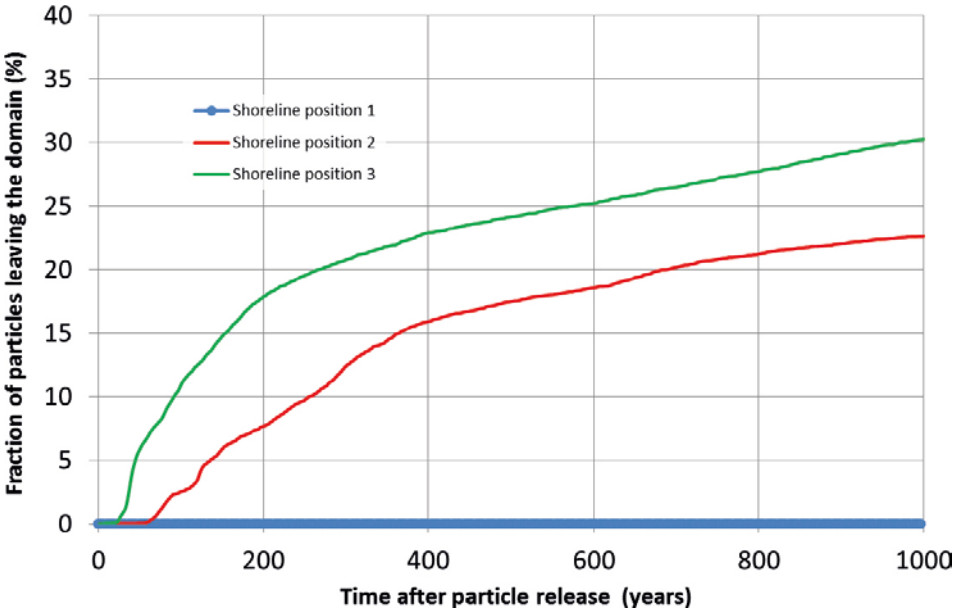

Figure 6-17. *Fraction (%) of particles released from the Silo-rock interface that leave the model domain for the Base case.*

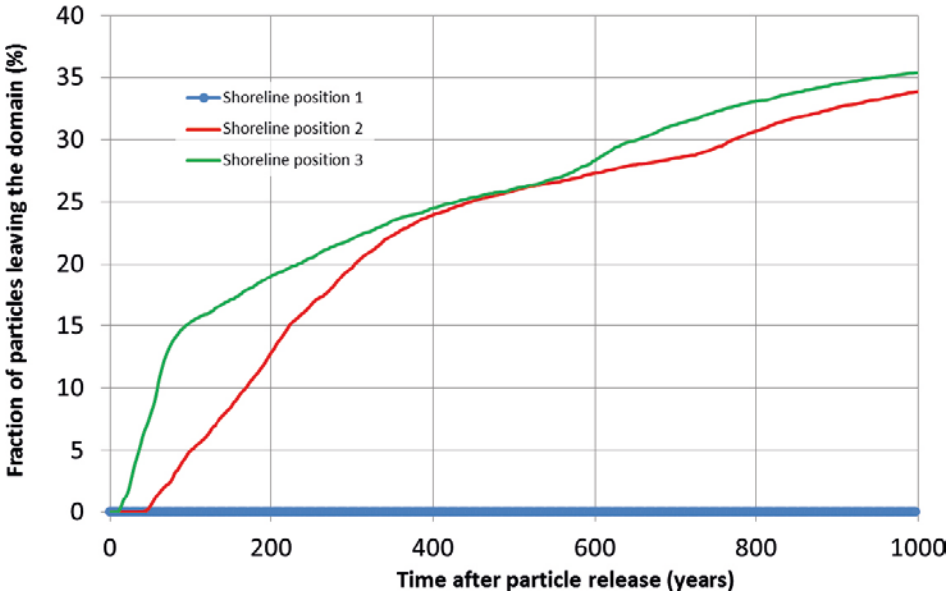

Figure 6-18. *Fraction (%) of particles released from the Silo-rock interface leaving the model domain for the High Flow case.*

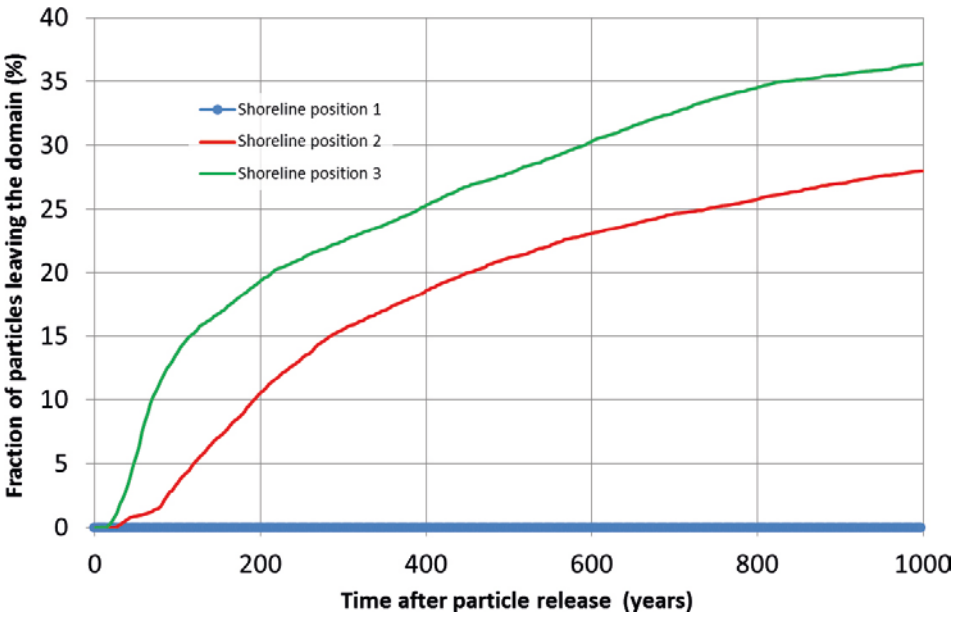

Figure 6-19. *Fraction (%) of particles released from the Silo-rock interface that leave the model domain for the Low flow case.*

Table 6-9. Time that 5% of the released particles take to leave the model domain.

Simulation	Shoreline position	Travel time (years)
Base case	1	Not reached
	2	136.8
	3	45.0
High Flow case	1	Not reached
	2	100.1
	3	36.7
Low Flow case	1	Not reached
	2	120.1
	3	46.7

7 Discussion and conclusions

Eleven separate vault-scale submodels have been extracted from the geometry of the SFR 1 and SFR 3 repository-scale models. The submodels are implemented in separate COMSOL files and run for the Base case (shoreline positions 1, 2, and 3). As a verification of their correct implementation, the results of the vault-scale submodels have been post-processed and compared with the repository-scale model results in terms of the flow rates within the vault. Overall, the differences with the repository-scale models are less than 10% in the SFR 1 submodels (with the exception of the Silo, with differences up to 26% in some cases) and less than 5% in the SFR 3 submodels (with the exception of the 2BMA, with differences up to 24% in some cases), which is thought to be satisfactory.

A mesh sensitivity analysis was carried out using the 1BMA model. The convergence of the solution with increasing refinement is analyzed with the ratio Q_{waste}/Q_{vault}, where Q_{waste} and Q_{vault} are the total flow rates through the waste and vault, respectively. The results of the ratio Q_{waste}/Q_{vault} for the different meshes show no significant influence of the mesh refinement on the solution. The relative error, calculated as the difference between the solutions obtained with successive finer meshes, is lower than 2%.

Thereafter, the 1BMA submodel has been utilized to study the effects of concrete degradation on the flow rates in the different vault elements. Due to the uncertainty in the effective conductivity of the concrete 1BMA beams/drainage system, we considered two hydraulic scenarios: (i) a case with a low effective conductivity of the beams/drains system equal to the structural concrete conductivity; (ii) a case of high conductivity beams. For both scenarios, two types of concrete degradation of the 1BMA vault have been studied. First, a homogeneous degradation of different elements of the vault (e.g. concrete floor, concrete walls, etc) has been considered. Thereafter, alternative situations where only some of the waste compartments of the vault are degraded due to preferential flow paths from the SFR 1 repository-scale model have been analyzed.

For the case of low conductivity beams, the results of the vault element concrete degradation indicate that concrete degradation has a moderate impact in the total flow in the 1BMA vault. The highest increments in the total tunnel flow occur in the cases considering the concrete floor degradation. In contrast, significant effects of concrete degradation are predicted on the flow profiles in the waste compartments and the total flow through the waste domain. The largest differences with respect to the Base case are found for shoreline position 2. The results have shown that the degradation of concrete vault elements induces an internal redistribution of the flow. Degradation of parts of the waste compartments drives the flow through zones of the waste compartment neighbouring the degraded elements, reducing the flow through intact waste compartment elements.

According to the model, the degradation of the inner and outer concrete walls of the waste compartments has the highest impact on total flow through the waste domain. Degradation of lids, floor, and outer walls is the second most unfavorable situation, especially for the complete degradation state. A redistribution of flow rates with respect to the Base case is again observed near the deformation zone ZFMNNW1209. The degradation of one outer concrete wall and both outer concrete walls, although inducing a significant increase in flow rates through the waste domain, have a minor impact compared to the other degradation cases.

The compartment concrete degradation has a moderate impact on the total flow through the 1BMA vault. Shoreline position 1 is the most sensitive to the increase of tunnel flow with a maximum increase of 12%. The two cases in which both fracture areas are degraded yield the highest tunnel flows. In general, the effect of the compartment degradation scenarios is a redistribution of the flow within the vault. The waste flow increases locally in the degraded waste compartments. This increase in flow is compensated by a reduction in the waste flow in the adjacent intact compartments. The flow reduction is enhanced in the compartment located between degraded zones in the case of the concrete degradation of all the compartments associated with fracture zones. The total flow through the gravel area also decreases to compensate the increase in the degraded compartments.

For the case of high conductivity beams, concrete degradationhas little effect on the total tunnel flow. It does however significantly affect the flow through the waste domain and, consequently, on the flow redistribution within the 1BMA vault. The degradation of elements in contact with

the backfill plays an important role in the redistribution of flow within the vault. Hydraulic conductivity contrast between degraded elements and backfill is significantly reduced by concrete degradation, which enhances the water exchange between the waste and the fractures. The model simulations show that in a vault with high conductivity beams, the degradation of the floor, inner and outer walls has a major impact on the total flow through the waste domain. Degradation of the inner and outer walls is the most unfavorable situation. Differences in the total flow rates with respect to the Base case are higher and the flow rates through the waste compartments are significantly affected by all degradation states. The impact of degradation is also larger compared to the scenario of low conductivity beams, for which the difference found with the Base case for moderate degradation is small. Degradation of lids, floor and outer walls is the second most unfavorable scenario. For all the degradation states and shoreline positions, the lids degradation in combination with floor and outer walls degradation leads to higher flow rates than when considering the degradation of only floor or outer walls. In general, the flow rates through other vault elements are almost unaffected by concrete degradation, with some few exceptions where the waste flow increase is compensated by a reduction of flow through other elements.

The compartment concrete degradation also results in a redistribution of the flow within the vault where the waste flow increases locally in the degraded waste compartments and slightly affects the adjacent compartments. The local increase is of up to four orders of magnitude for the complete degradation cases in shoreline positions 2 and 3. The total flow through the gravel area also decreases to compensate the increase in the degraded compartments. The effect of the compartment degradation on the tunnel flow is negligible. For all shoreline positions the worst case scenario corresponds to the complete concrete degradation state of all compartments affected by fractures whereas the degradation of low flow compartments (Case 2) presents the lowest impact since the number of degraded compartments is the lowest.

The Silo submodel has been used to setup a local mass transport model under steady-state conditions in order to evaluate an effective flow rate transporting solutes originating from the repository. For the shoreline position 1, the groundwater flow field has a main upward vertical component and the velocities are two orders of magnitude lower than for the other shoreline positions. The transport of mass from the Silo is diffusion-dominated and the solute plume is relatively widespread. On the other hand, the solute transport is advection-dominated for shorelines positions 2 and 3. In these cases, the plume is narrower around the Silo compared to shoreline position 1, but extends upwards and downwards conditioned by the most permeable fracture zones. Solute concentrations resulting from steady-state conditions lack information about residence times and mass velocities. Therefore, particle tracking simulations have been performed to increase the understanding of those additional aspects. These particles are transported exclusively by advection. A simulation time of 1000 years has been considered. The results obtained consist of maps of particles and their footprints, which are colored according to the particle time-of-flight. As expected, for the advective-dominated cases (i.e. shoreline positions 2 and 3) there is a clear correlation between the isosurfaces and the corresponding particle footprints. For shoreline position 1 (diffusion dominated) the particle tracking simulation shows that a particle leaving the Silo will be almost in the same location after 1000 years. In this case, advection plays no role in release of mass. To have an estimate of the mass release rate, two different indicators have been analyzed: the water outflow rate, denoted as Q_{out}, and the equivalent flow rate, Q_{eq}. Although variables Q_{eq} and Q_{out} are calculated using different types of information, both result in values of the same order of magnitude for shoreline position 1. This result is to be expected since the analytical solution to obtain Q_{eq} is based on assumptions that are met in this case: vertical flow direction and a diffusion-dominated system. The larger values obtained for Q_{out} could be due to the fact that Q_{out} has been estimated taking into account the mass flux through the vertical walls and the top and bottom surfaces of the Silo, whereas Q_{eq} only considers the vertical walls of the Silo for its estimation. On the other hand, Q_{eq} and Q_{out} differ by several orders of magnitude for shoreline positions 2 and 3. In these cases, the flow field does not meet the assumptions for which the Q_{eq} concept is defined. Therefore, in these cases Q_{out} may be considered a more realistic variable to estimate the mass flow of solute released from the Silo.

References

SKB's (Svensk Kärnbränslehantering AB) publications can be found at www.skb.se/publications.

Abarca E, Idiart A, de Vries L M, Silva O, Molinero J, von Schenck H, 2013. Flow modelling on the repository scale for the safety assessment SR-PSU. SKB TR-13-08, Svensk Kärnbränslehantering AB.

Bird R B, Stewart W E, Lightfoot E N, 1960. Transport phenomena. New York: Wiley.

COMSOL, 2012a. COMSOL Multiphysics Reference Guide. Version 4.3a. Burlington, MA: COMSOL Inc.

COMSOL, 2012b. COMSOL Particle Tracing Module. User's guide. Version 4.3a. Burlington, MA: COMSOL Inc.

Curtis P, Markström I, Petersson, J, Triumf C-A, Isaksson H, Mattsson H, 2011. Site investigation SFR. Bedrock geology. SKB R-10-49, Svensk Kärnbränslehantering AB.

Holmén J G, Stigsson M, 2001. Modelling of future hydrogeological conditions at SFR. SKB R-01-02, Svensk Kärnbränslehantering AB.

Lindgren M, Pettersson M, Karlsson S, Moreno L, 2001. Project SAFE. Radionuclide release and dose from the SFR repository. SKB R-01-18, Svensk Kärnbränslehantering AB.

Neretnieks I, 1980. Diffusion in the rock matrix: an important factor in radionuclide migration. Journal of Geophysical Research: Solid Earth 85, 4379–4397.

Neretnieks I, Arve S, Moreno L, Rasmuson A, Zhu M, 1987. Degradation of concrete and transport of radionuclides from SFR – repository for low and intermediate level nuclear waste. SKB SFR 87-11, Svensk Kärnbränslehantering AB.

Odén M, Follin S, Öhman J, Vidstrand P, 2014. SR-PSU Bedrock hydrogeology. Groundwater flow modelling methodology, setup and results. SKB R-13-25, Svensk Kärnbränslehantering AB.

SKB, 2001. Project SAFE. Compilation of data for radionuclide transport analysis. SKB R-01-14, Svensk Kärnbränslehantering AB.

SKB, 2013. Site description of the SFR area at Forsmark at completion of the site investigation phase. SDM-PSU Forsmark. SKB TR-11-04, Svensk Kärnbränslehantering AB.

Appendix A

Vault elements degradation of 1BMA vault with low conductivity beams

Case 1. Floor degradation

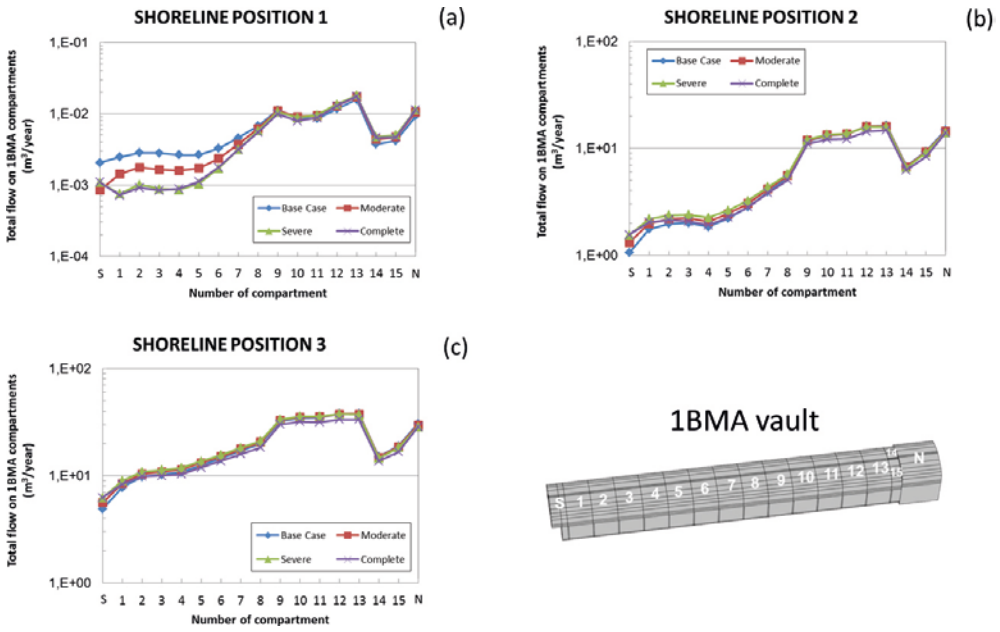

Figure A-1. Flow rates through the top gravel of 1BMA submodel for floor degradation.

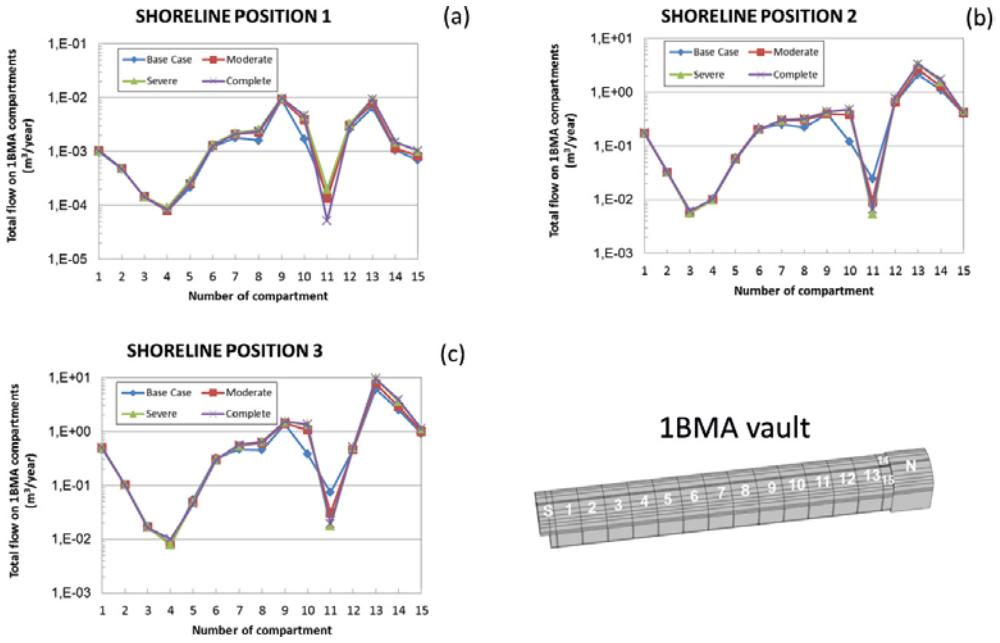

Figure A-2. Flow rates through the bottom gravel of 1BMA submodel for floor degradation.

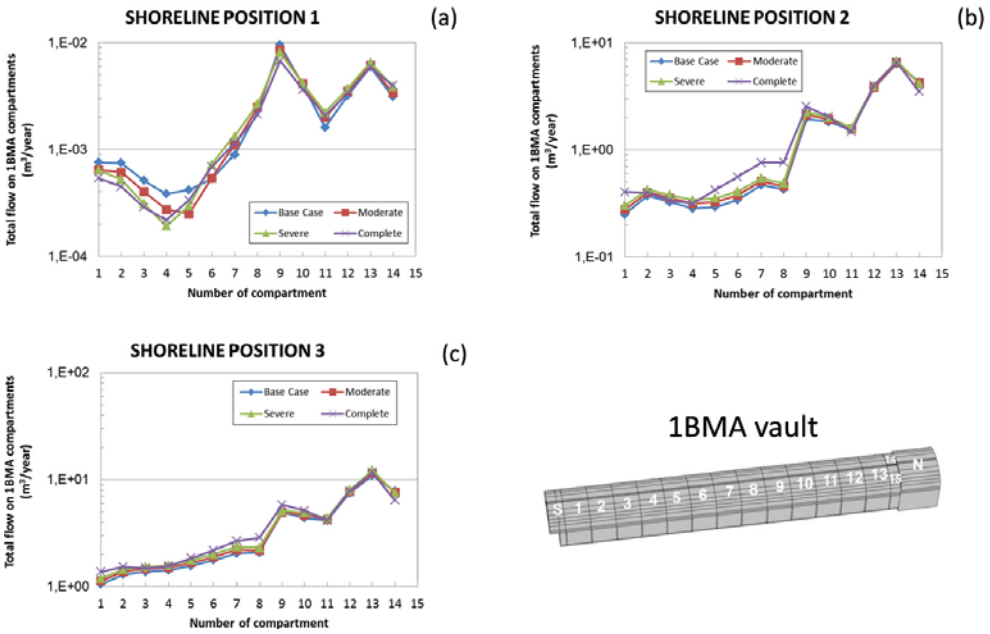

Figure A-3. *Flow rates through the east gravel of 1BMA submodel for floor degradation.*

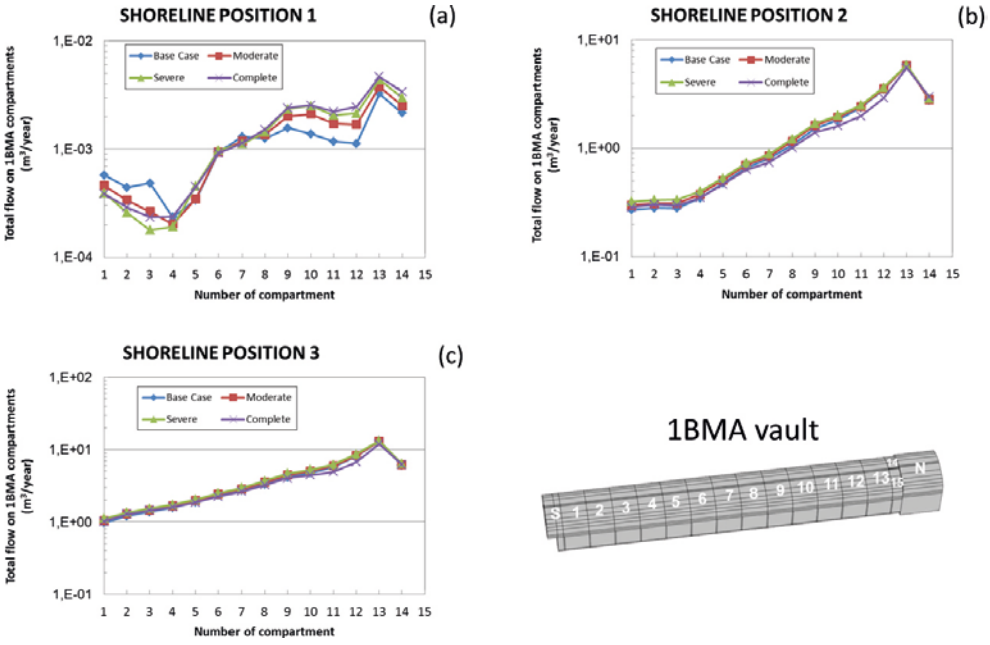

Figure A-4. *Flow rates through the west gravel of 1BMA submodel for floor degradation.*

Case 2. Degradation of floor and inner walls

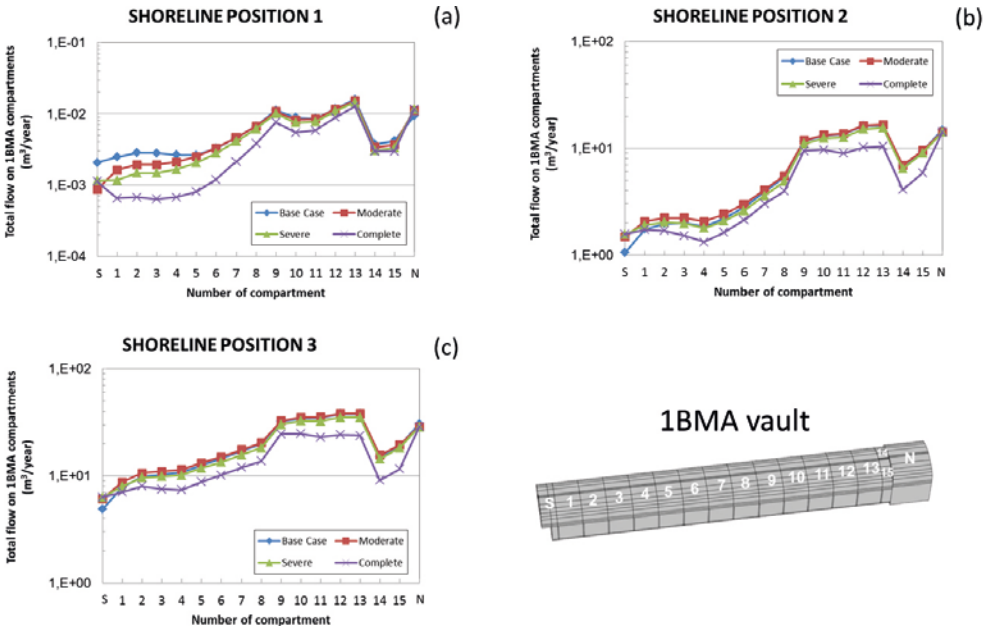

Figure A-5. *Flow rates through the top gravel of 1BMA submodel for floor and inner walls degradation.*

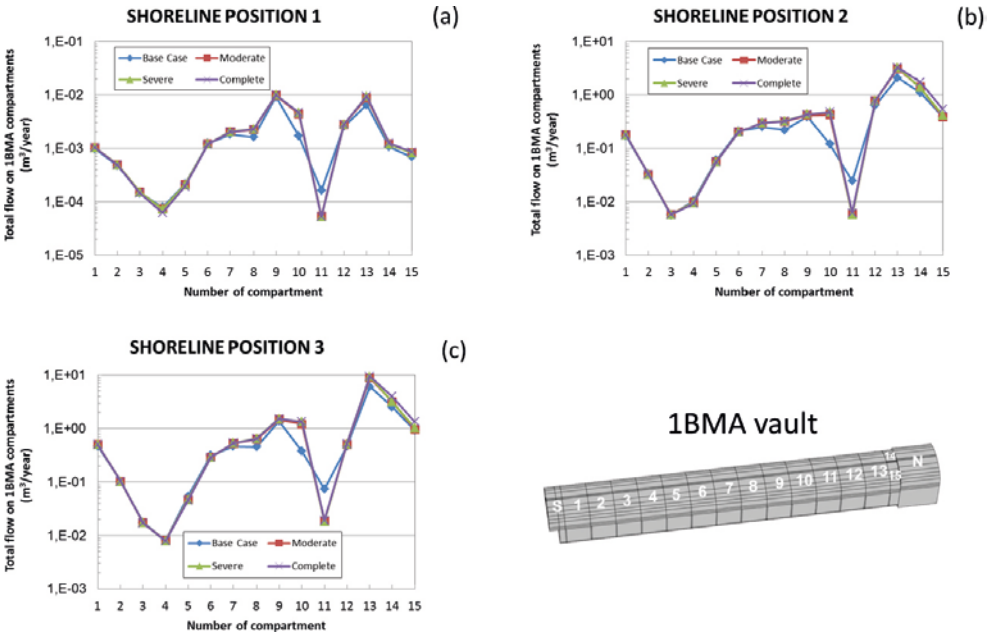

Figure A-6. *Flow rates through the bottom gravel of 1BMA submodel for floor and inner walls degradation.*

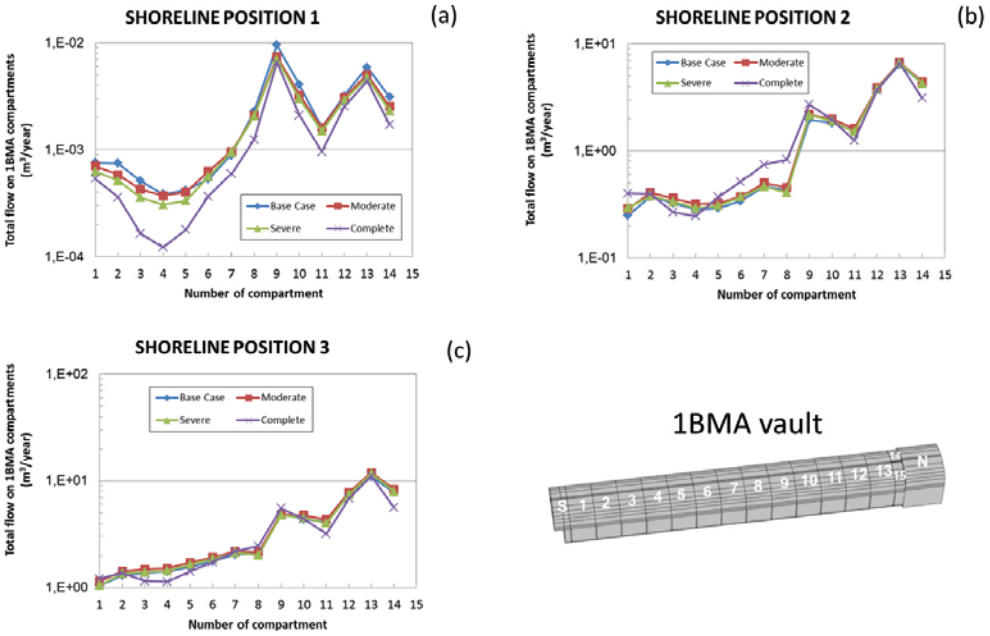

Figure A-7. *Flow rates through the east gravel of 1BMA submodel for floor and inner walls degradation.*

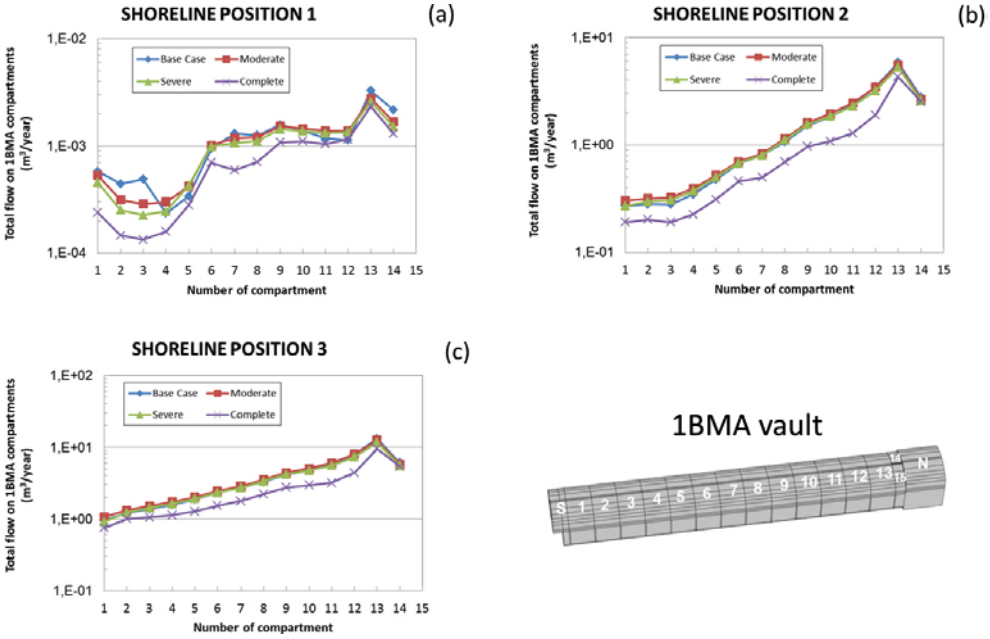

Figure A-8. *Flow rates through the west gravel of 1BMA submodel for floor and inner walls degradation.*

Case 3. Degradation of one outer wall

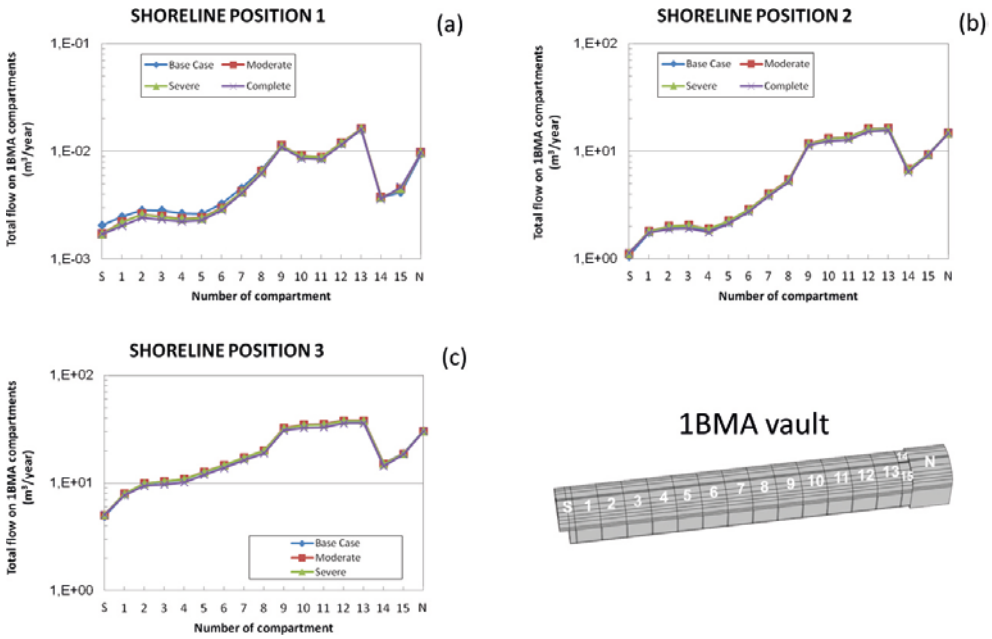

Figure A-9. *Flow rates through the top gravel of 1BMA submodel for degradation of one outer wall.*

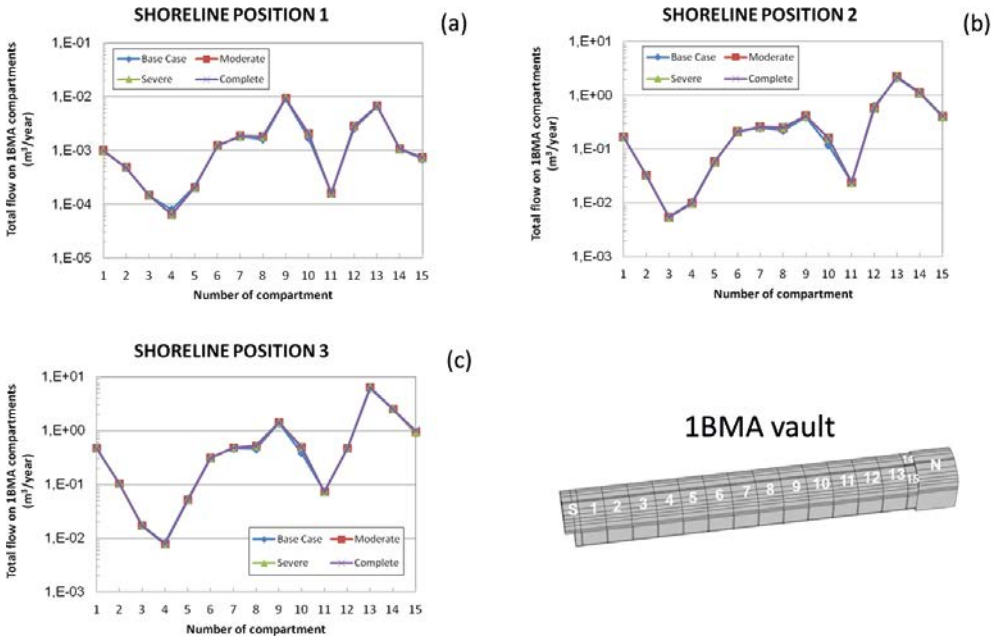

Figure A-10. *Flow rates through the bottom gravel of 1BMA submodel for degradation of one outer wall.*

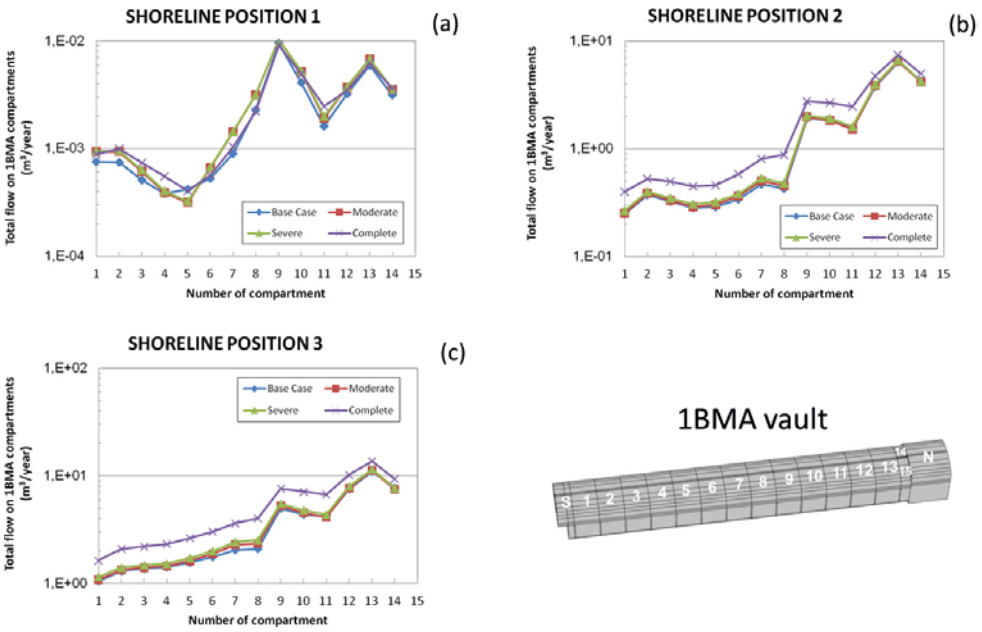

Figure A-11. *Flow rates through the east gravel of 1BMA submodel for degradation of one outer wall.*

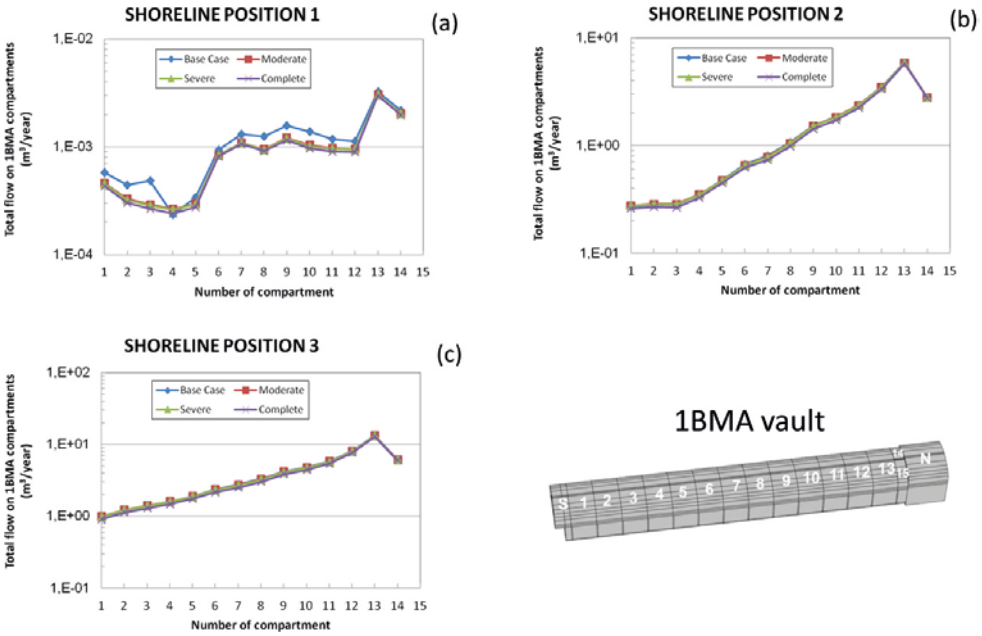

Figure A-12. *Flow rates through the west gravel of 1BMA submodel for degradation of one outer wall.*

Case 4. Degradation of both outer walls

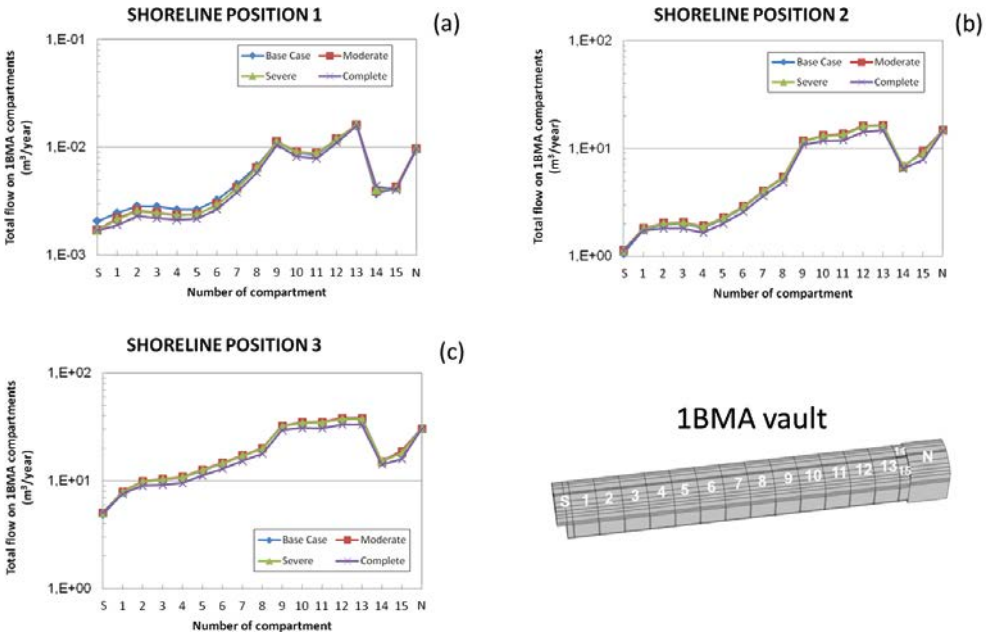

Figure A-13. *Flow rates through the top gravel of 1BMA submodel for degradation of both outer walls.*

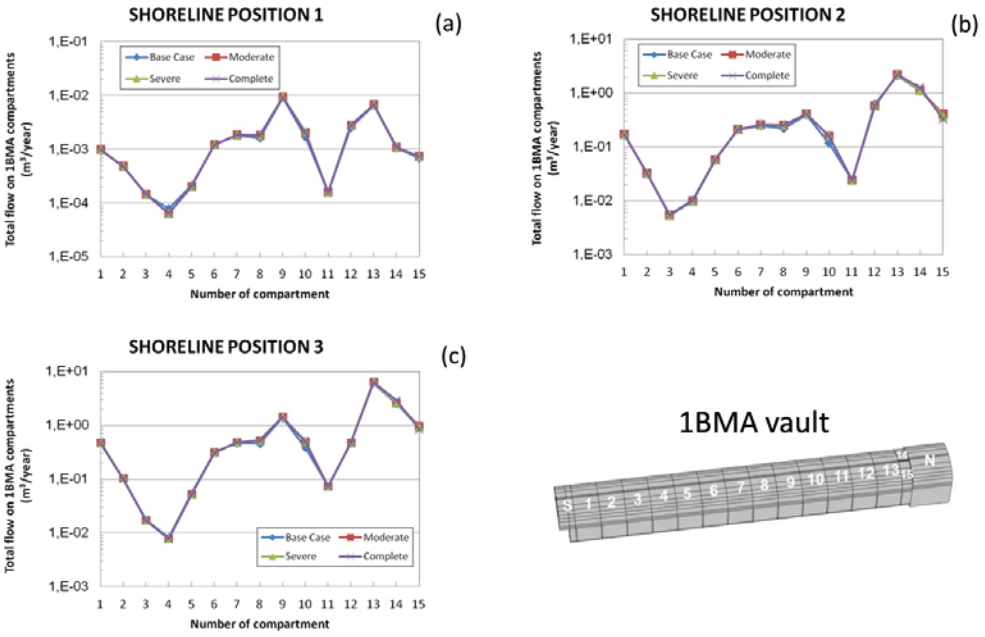

Figure A-14. *Flow rates through the bottom gravel of 1BMA submodel for degradation of both outer walls.*

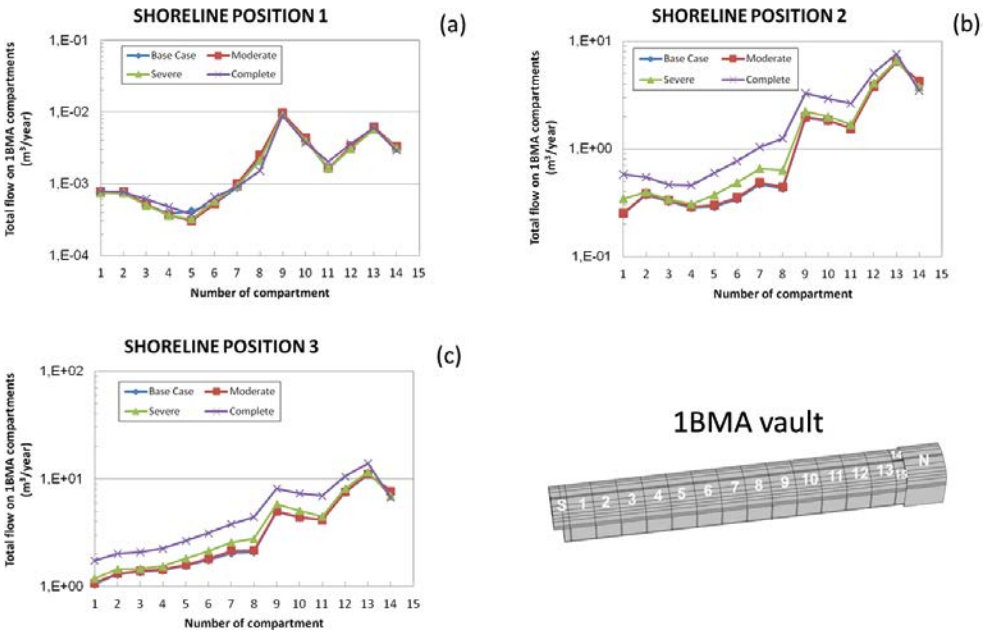

Figure A-15. *Flow rates through the east gravel of 1BMA submodel for degradation of both outer walls.*

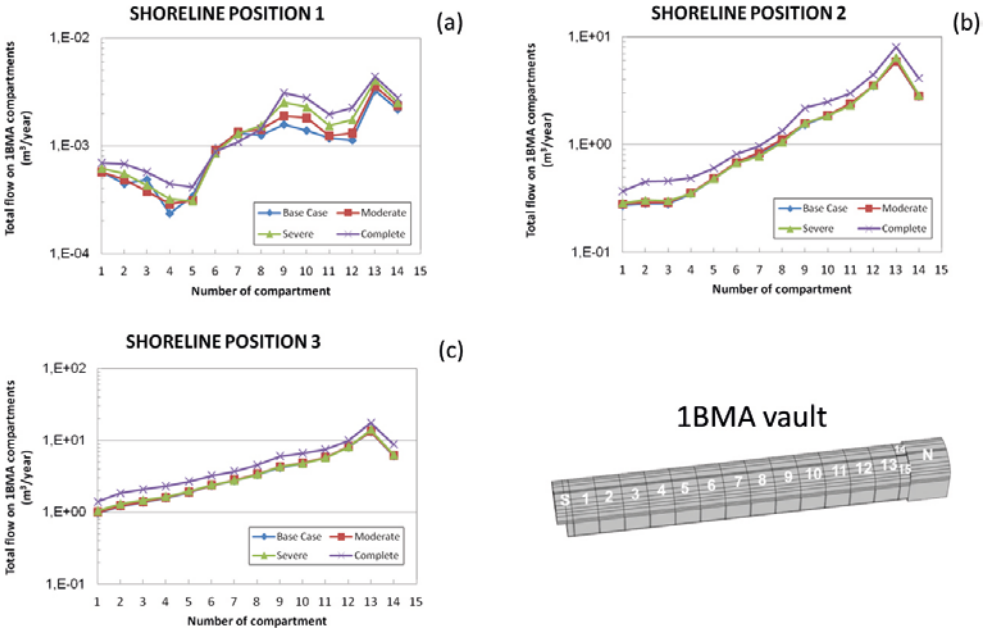

Figure A-16. *Flow rates through the west gravel of 1BMA submodel for degradation of both outer walls.*

Case 5. Degradation of inner and outer walls

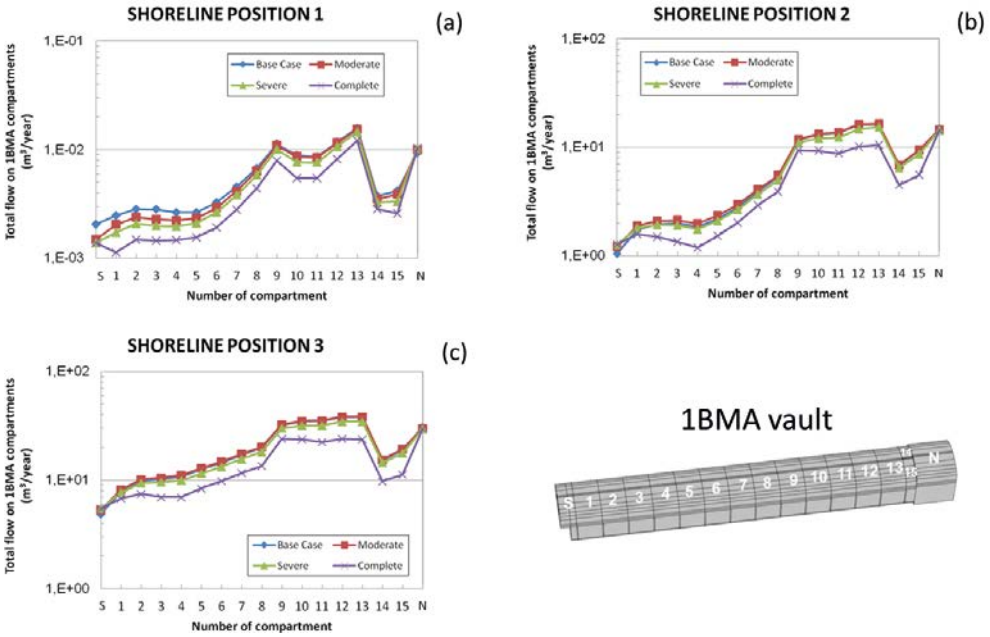

Figure A-17. *Flow rates through the top gravel of 1BMA submodel for degradation of inner and outer walls.*

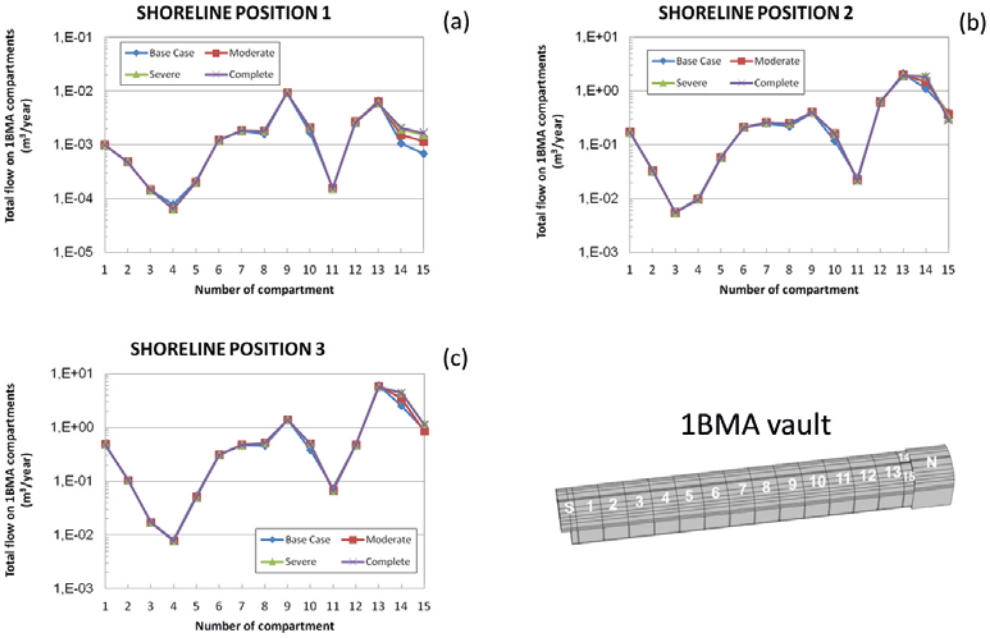

Figure A-18. *Flow rates through the bottom gravel of 1BMA submodel for degradation of inner and outer walls.*

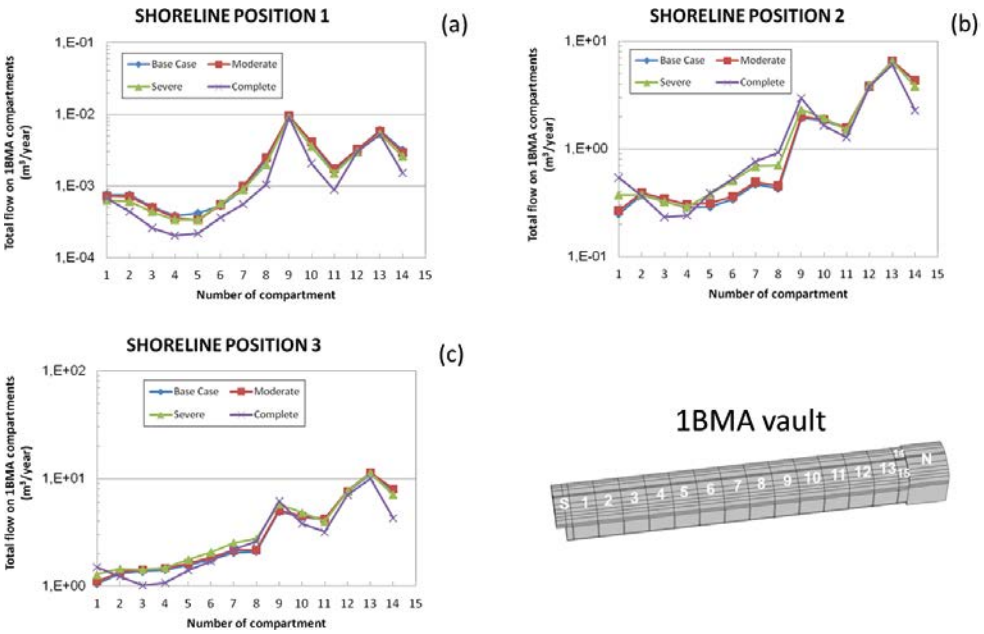

Figure A-19. *Flow rates through the east gravel of 1BMA submodel for degradation of inner and outer walls.*

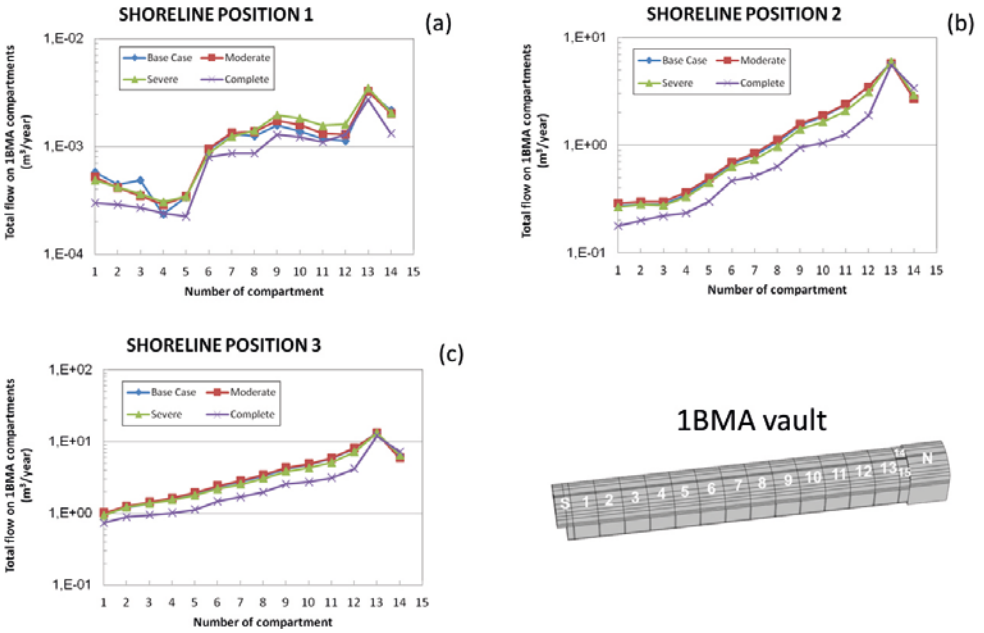

Figure A-20. *Flow rates through the west gravel of 1BMA submodel for degradation of inner and outer walls.*

Case 6. Degradation of outer walls, lids and floor

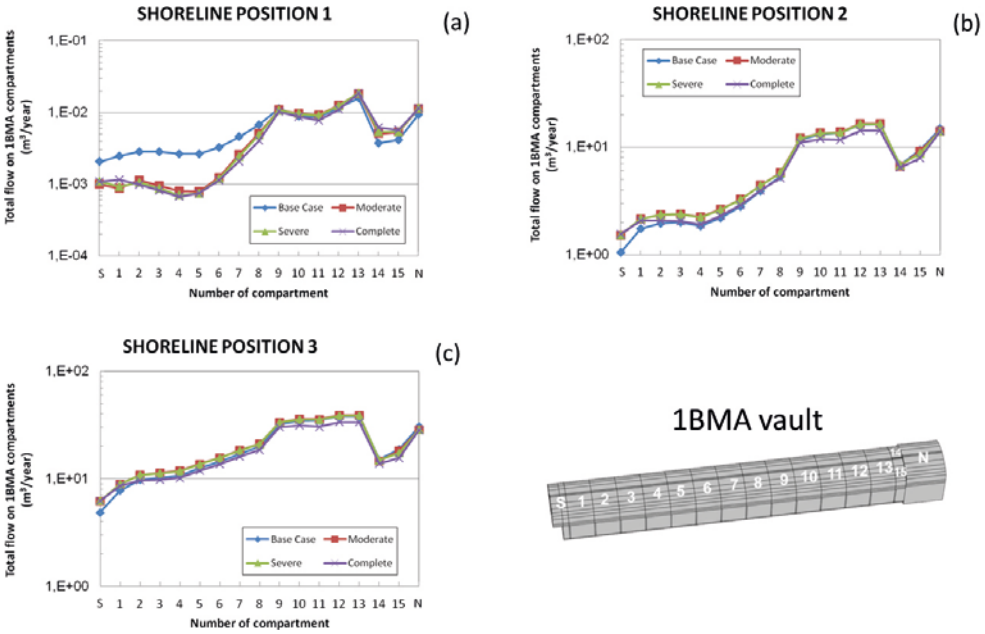

Figure A-21. *Flow rates through the top gravel of 1BMA submodel for degradation of outer walls, lids and floor.*

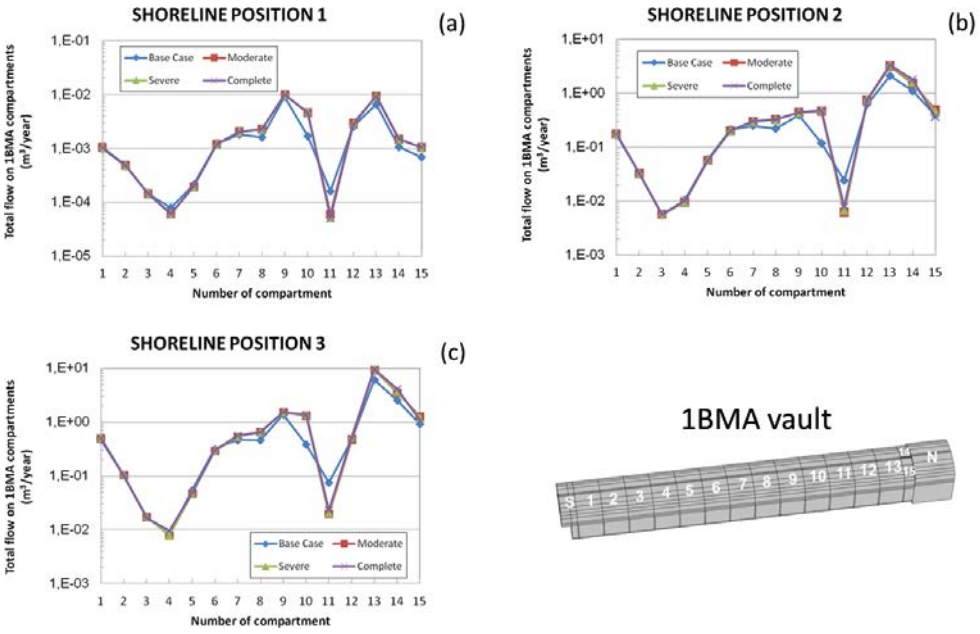

Figure A-22. *Flow rates through the bottom gravel of 1BMA submodel for degradation of outer walls, lids and floor.*

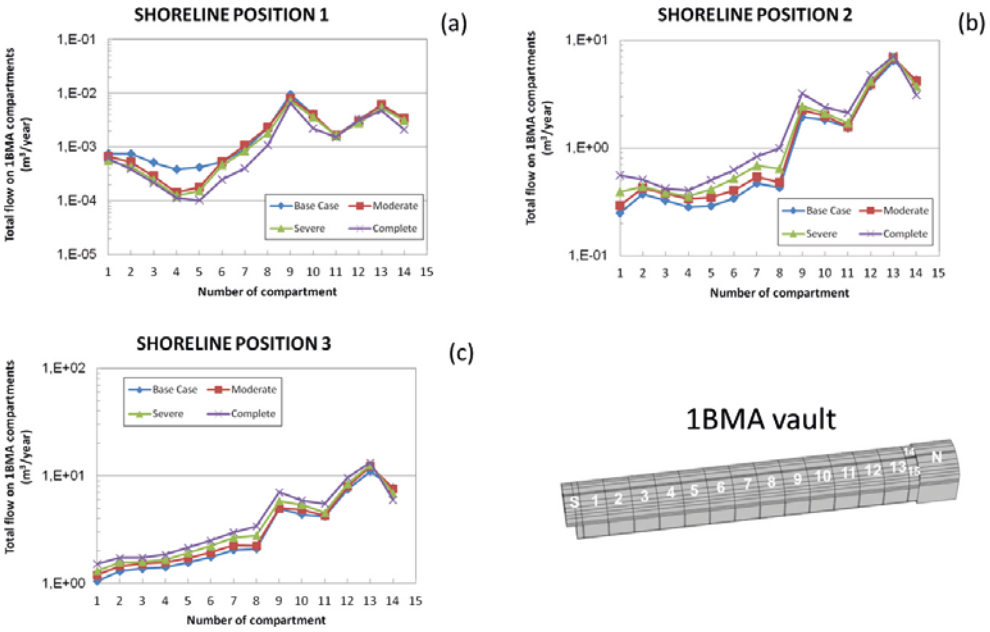

Figure A-23. *Flow rates through the east gravel of 1BMA submodel for degradation of outer walls, lids and floor.*

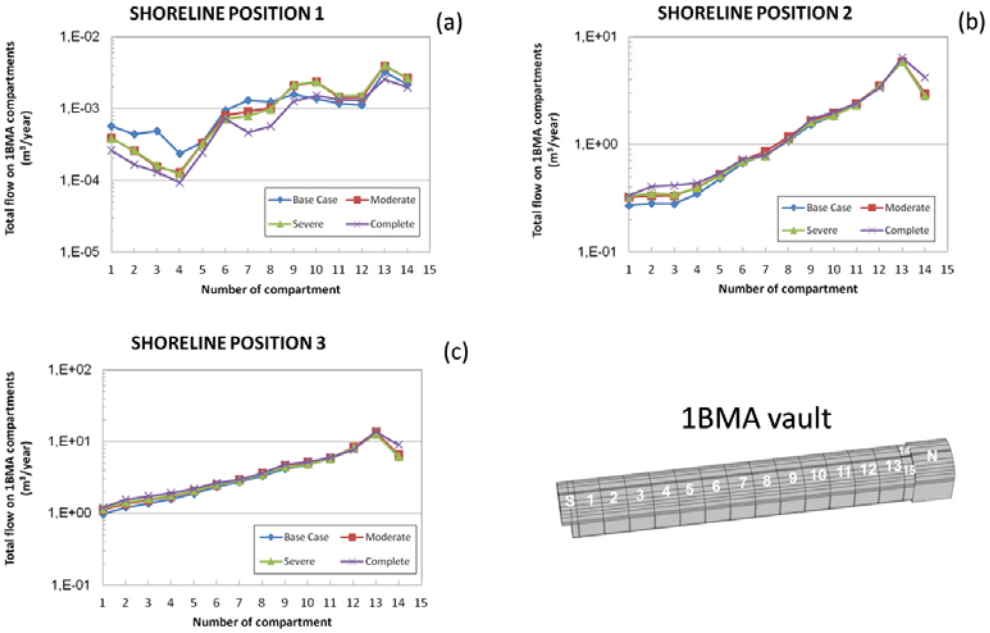

Figure A-24. *Flow rates through the west gravel of 1BMA submodel for degradation of outer walls, lids and floor.*

Total flow rates through the 1BMA vault for vault element degradation

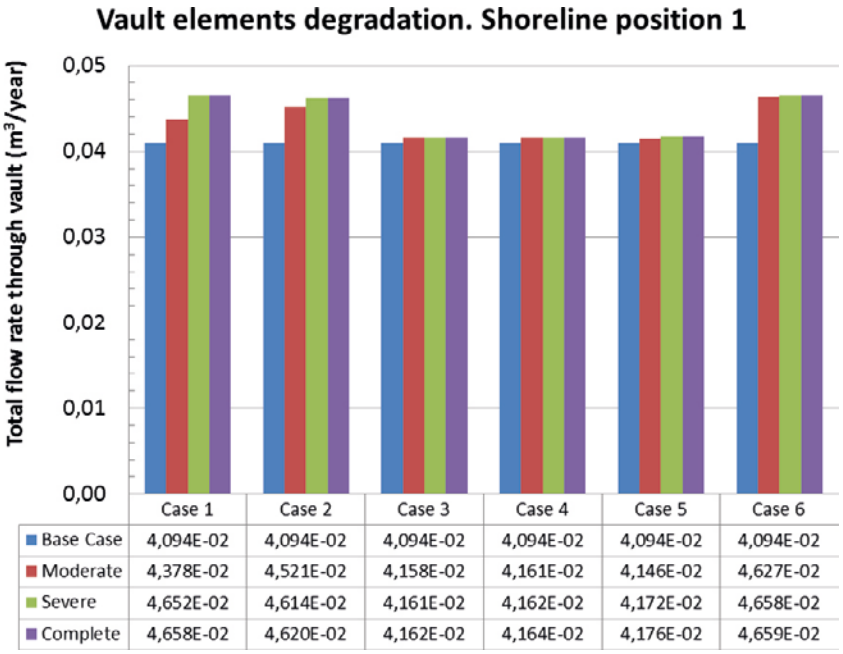

	Case 1	Case 2	Case 3	Case 4	Case 5	Case 6
Base Case	4,094E-02	4,094E-02	4,094E-02	4,094E-02	4,094E-02	4,094E-02
Moderate	4,378E-02	4,521E-02	4,158E-02	4,161E-02	4,146E-02	4,627E-02
Severe	4,652E-02	4,614E-02	4,161E-02	4,162E-02	4,172E-02	4,658E-02
Complete	4,658E-02	4,620E-02	4,162E-02	4,164E-02	4,176E-02	4,659E-02

Figure A-25. *Total flow rates through the 1BMA vault for different scenarios of vault elements degradation and comparison with the Base case at shoreline position 1.*

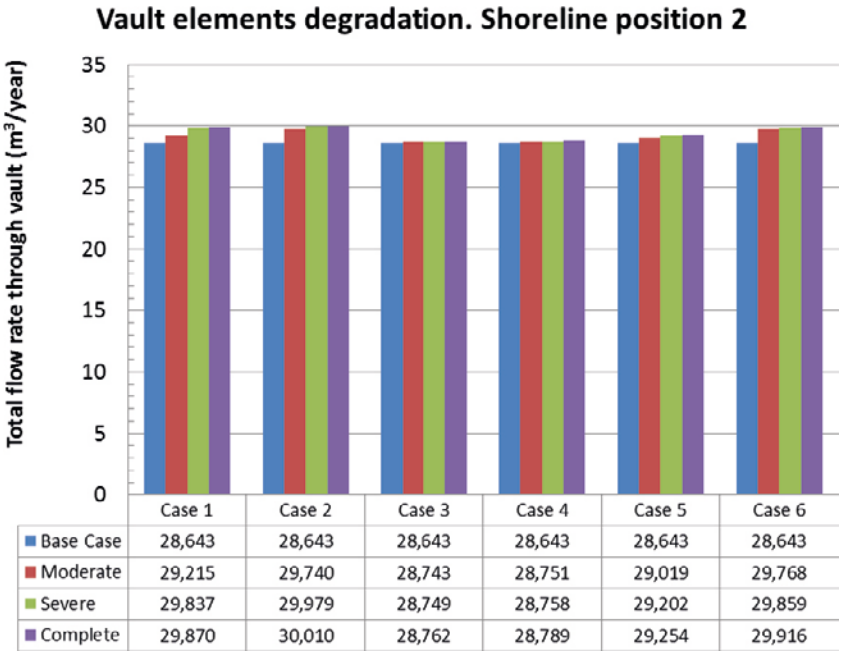

	Case 1	Case 2	Case 3	Case 4	Case 5	Case 6
Base Case	28,643	28,643	28,643	28,643	28,643	28,643
Moderate	29,215	29,740	28,743	28,751	29,019	29,768
Severe	29,837	29,979	28,749	28,758	29,202	29,859
Complete	29,870	30,010	28,762	28,789	29,254	29,916

Figure A-26. *Total flow rates through the 1BMA vault for different scenarios of vault elements degradation and comparison with the Base case at shoreline position 2.*

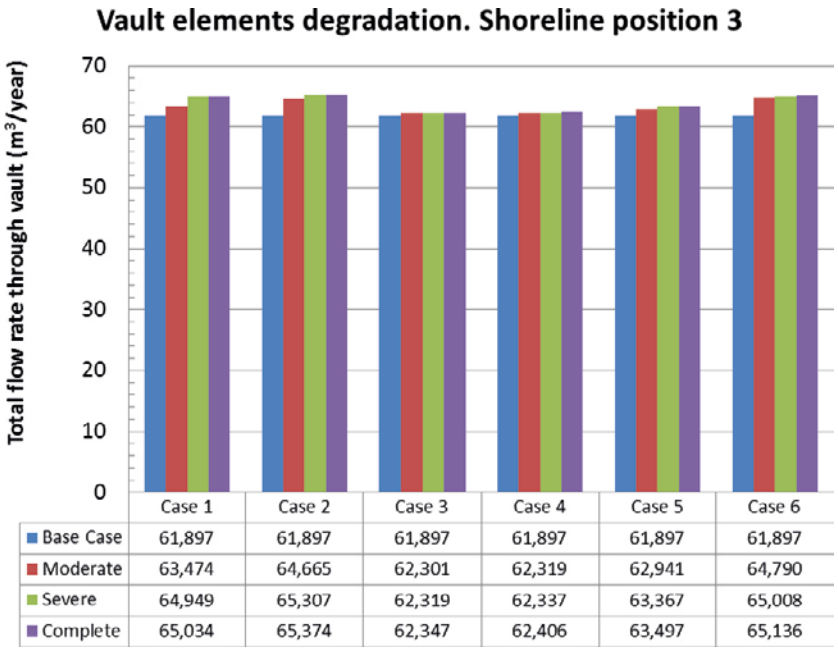

	Case 1	Case 2	Case 3	Case 4	Case 5	Case 6
Base Case	61,897	61,897	61,897	61,897	61,897	61,897
Moderate	63,474	64,665	62,301	62,319	62,941	64,790
Severe	64,949	65,307	62,319	62,337	63,367	65,008
Complete	65,034	65,374	62,347	62,406	63,497	65,136

Figure A-27. *Total flow rates through the 1BMA vault for different scenarios of vault elements degradation and comparison with the Base case at shoreline position 3.*

Appendix B

Compartment degradation of 1BMA vault with low conductivity beams

Case 1. Degradation of deformation zone ZFMNNW1209

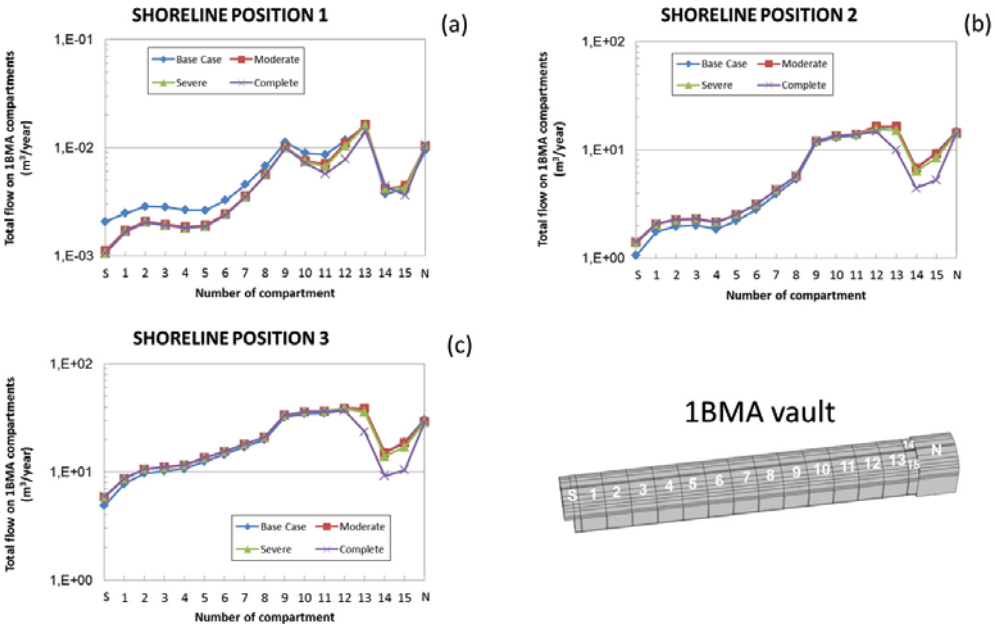

Figure B-1. *Flow rates through the top gravel of 1BMA submodel for degradation of deformation zone ZFMNNW1209.*

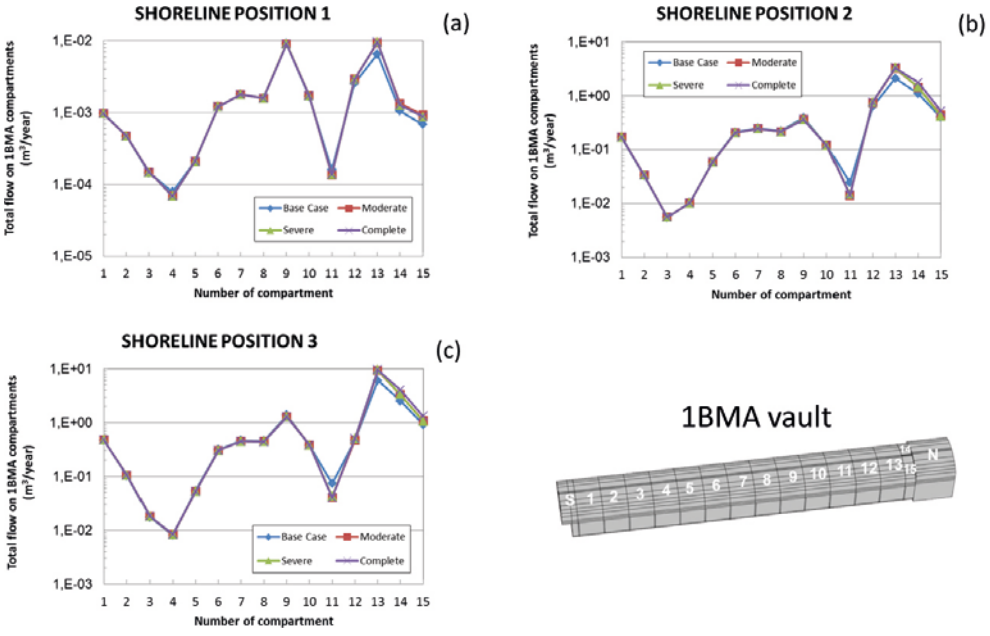

Figure B-2. *Flow rates through the bottom gravel of 1BMA submodel for degradation of deformation zone ZFMNNW1209.*

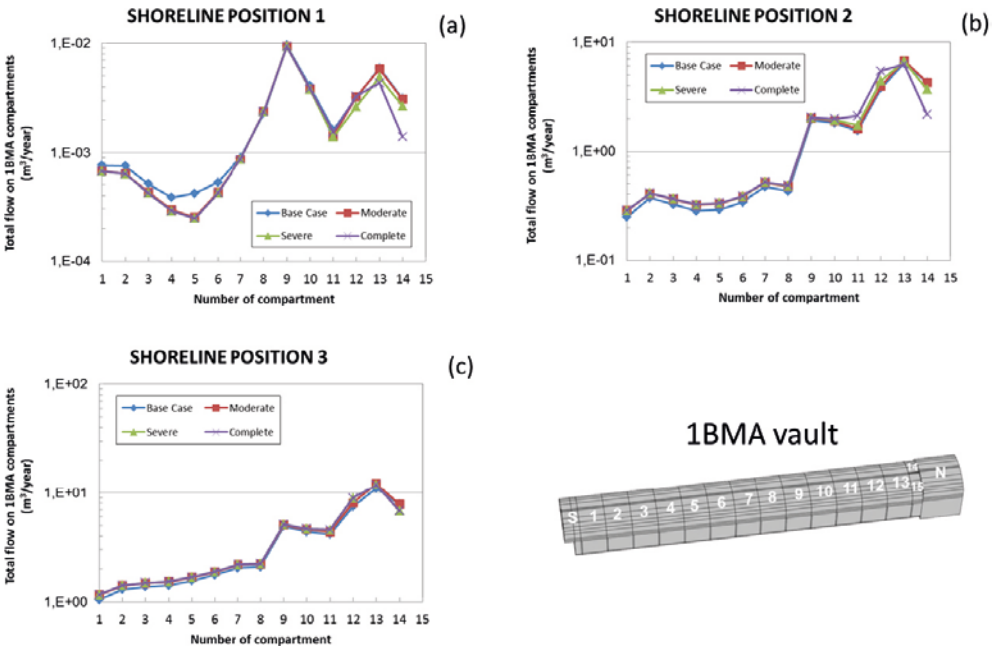

Figure B-3. *Flow rates through the east gravel of 1BMA submodel for degradation of deformation zone ZFMNNW1209.*

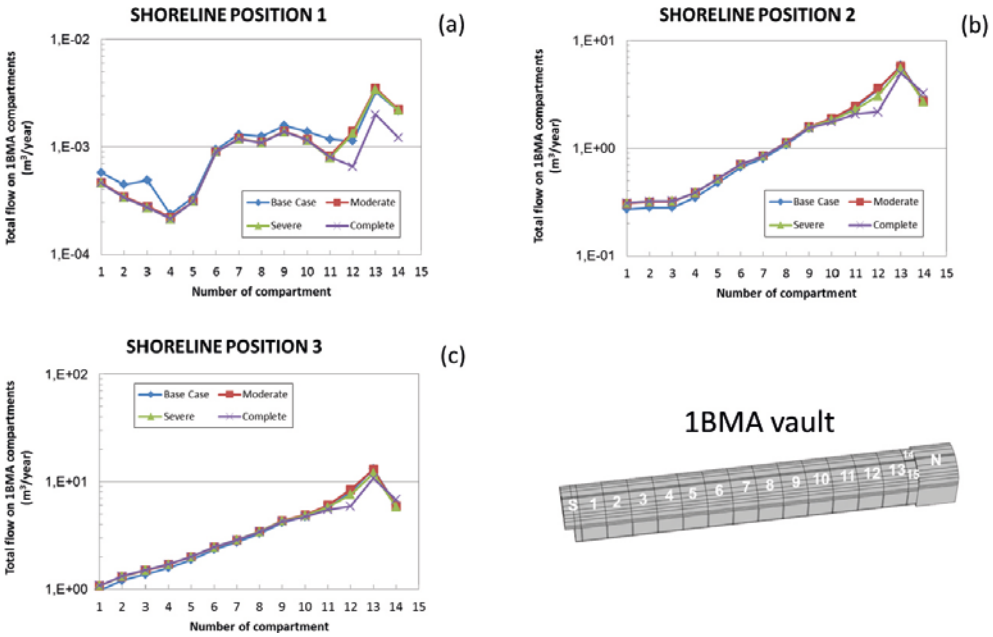

Figure B-4. *Flow rates through the west gravel of 1BMA submodel for degradation of deformation zone ZFMNNW1209.*

Case 2. Degradation of low flow compartments

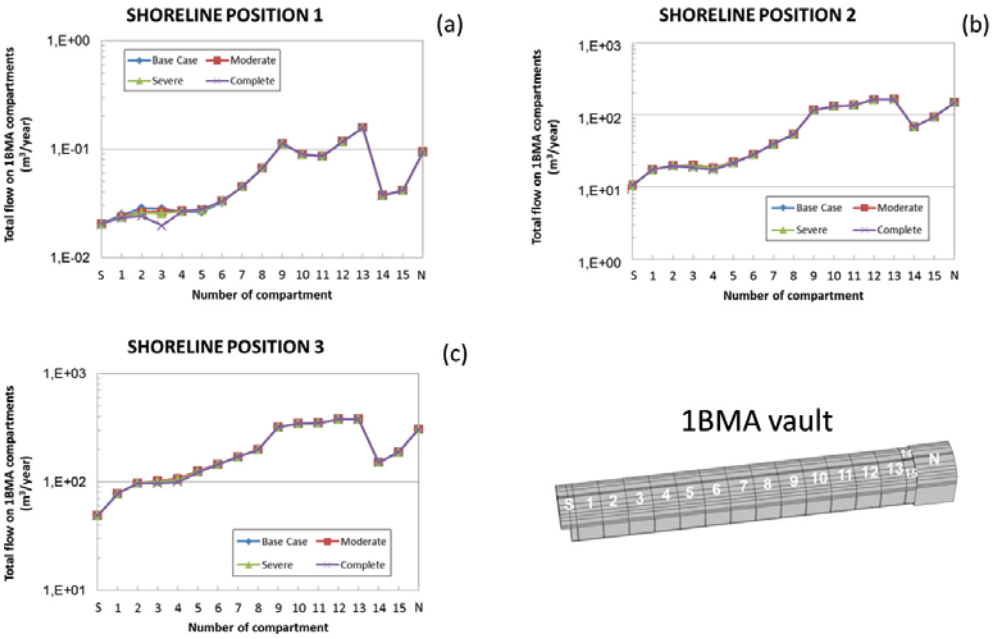

Figure B-5. *Flow rates through the top gravel of 1BMA submodel for degradation of low flow compartments.*

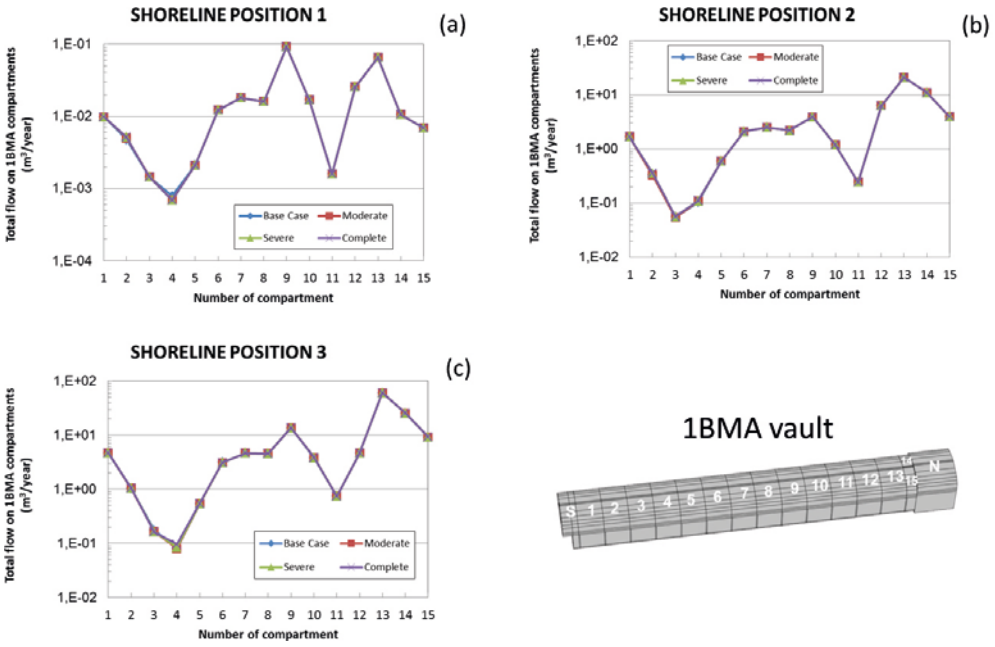

Figure B-6. *Flow rates through the bottom gravel of 1BMA submodel for degradation of low flow compartments.*

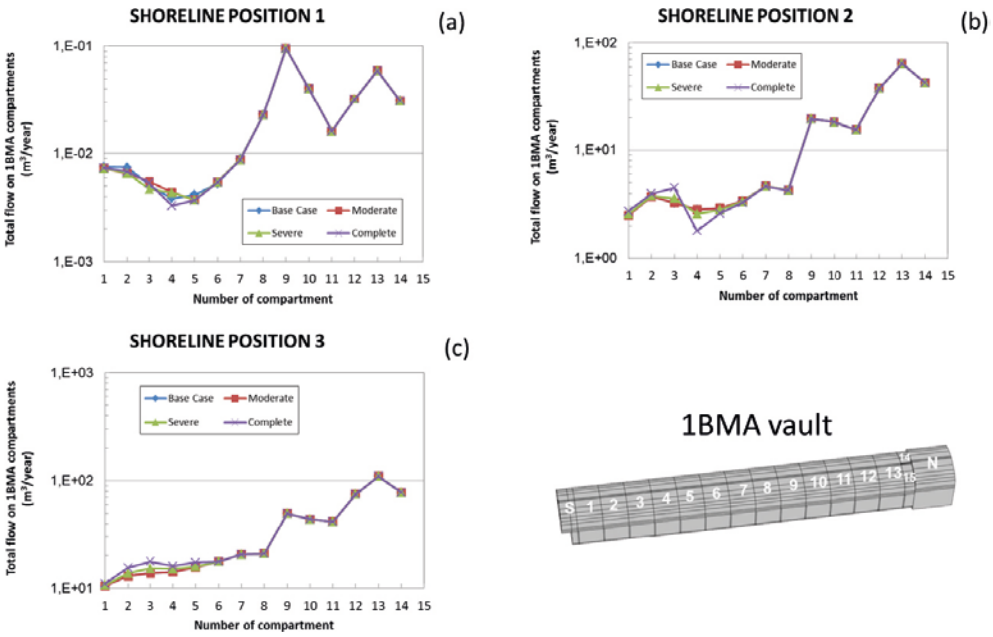

Figure B-7. *Flow rates through the east gravel of 1BMA submodel for degradation of low flow compartments.*

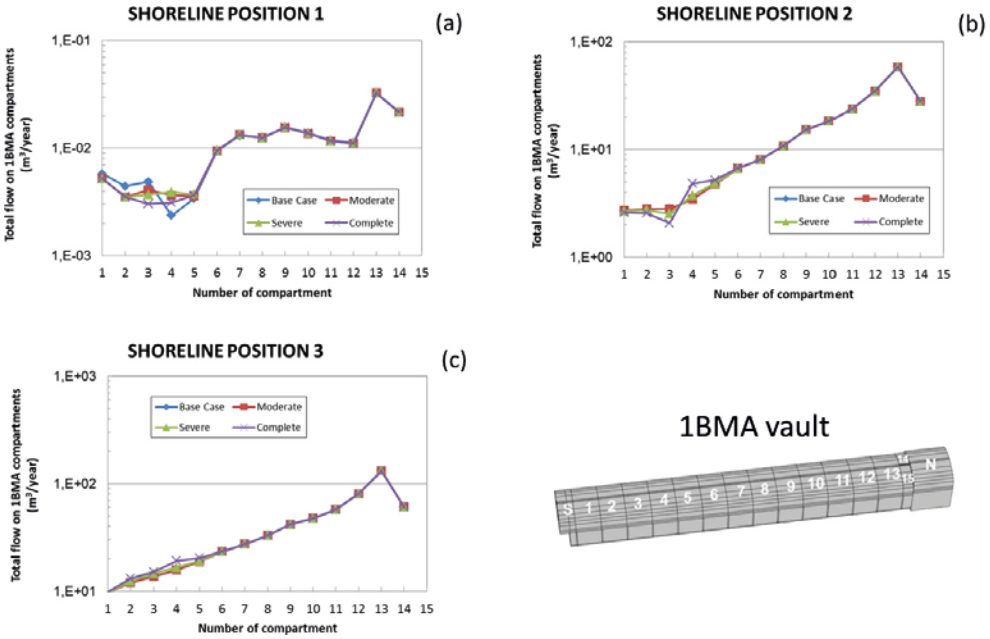

Figure B-8. *Flow rates through the west gravel of 1BMA submodel for degradation of low flow compartments.*

Case 3. Simultaneous degradation of all the compartments affected by fracture zones

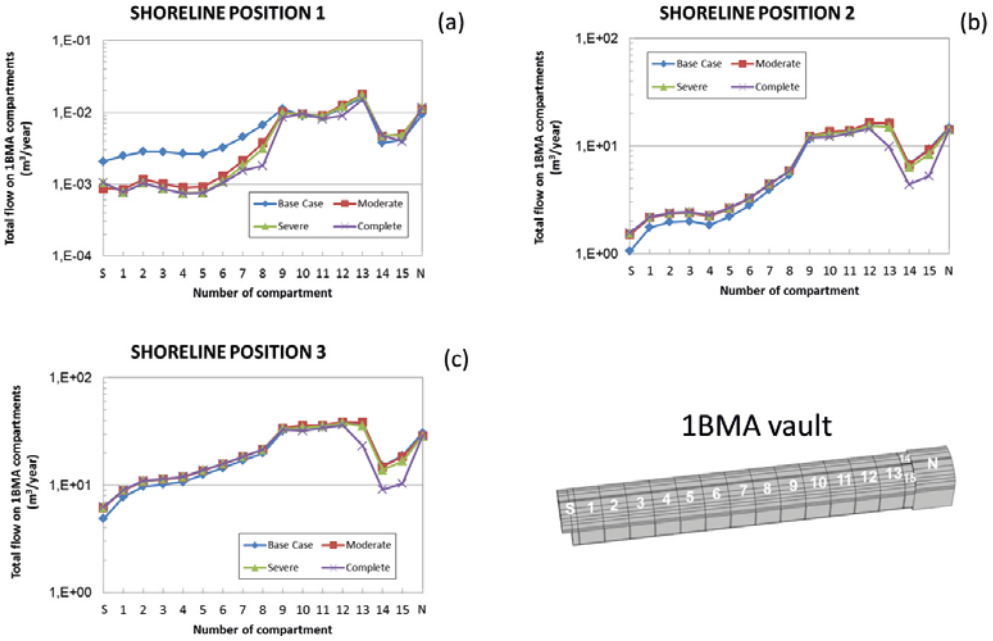

Figure B-9. *Flow rates through the top gravel of 1BMA submodel for simultaneous degradation of all the compartments affected by fracture zones.*

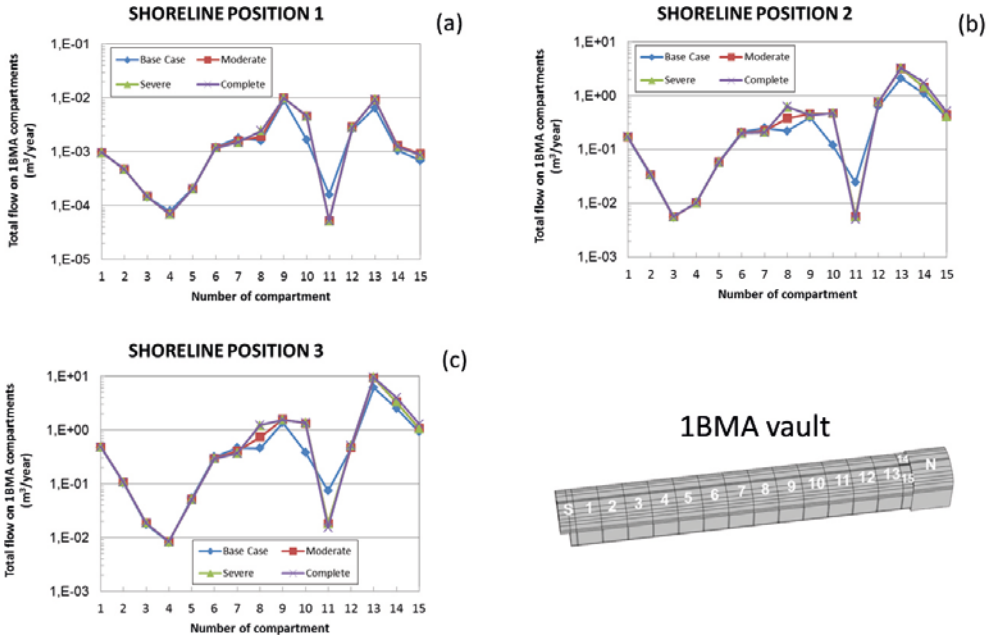

Figure B-10. *Flow rates through the bottom gravel of 1BMA submodel for simultaneous degradation of all the compartments affected by fracture zones.*

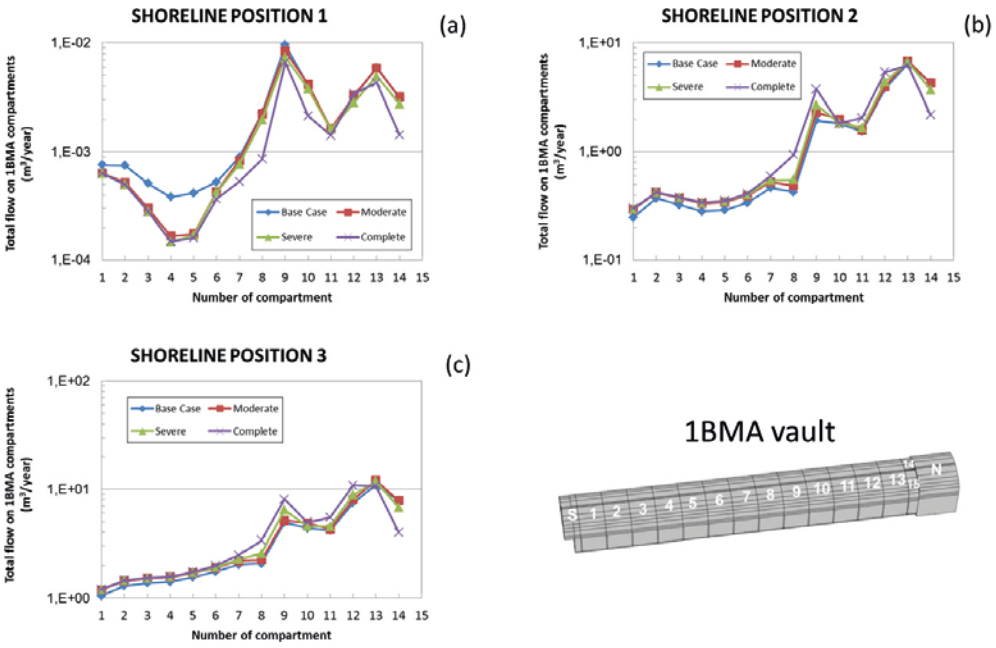

Figure B-11. *Flow rates through the east gravel of 1BMA submodel for simultaneous degradation of all the compartments affected by fracture zones.*

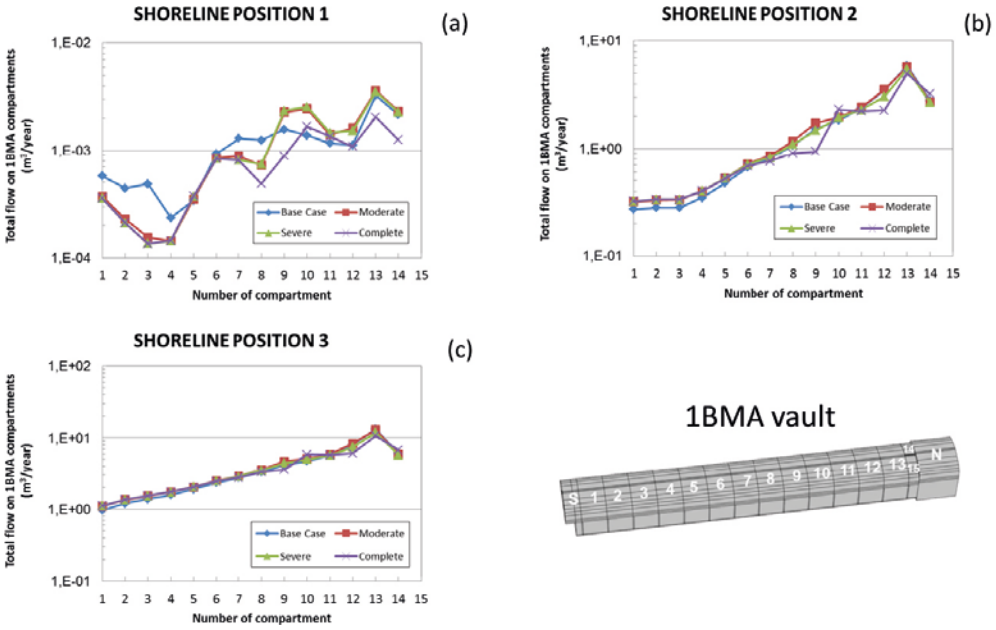

Figure B-12. *Flow rates through the west gravel of 1BMA submodel for simultaneous degradation of all the compartments affected by fracture zones.*

Case 4. Compartment degradation proportional to the flow rate

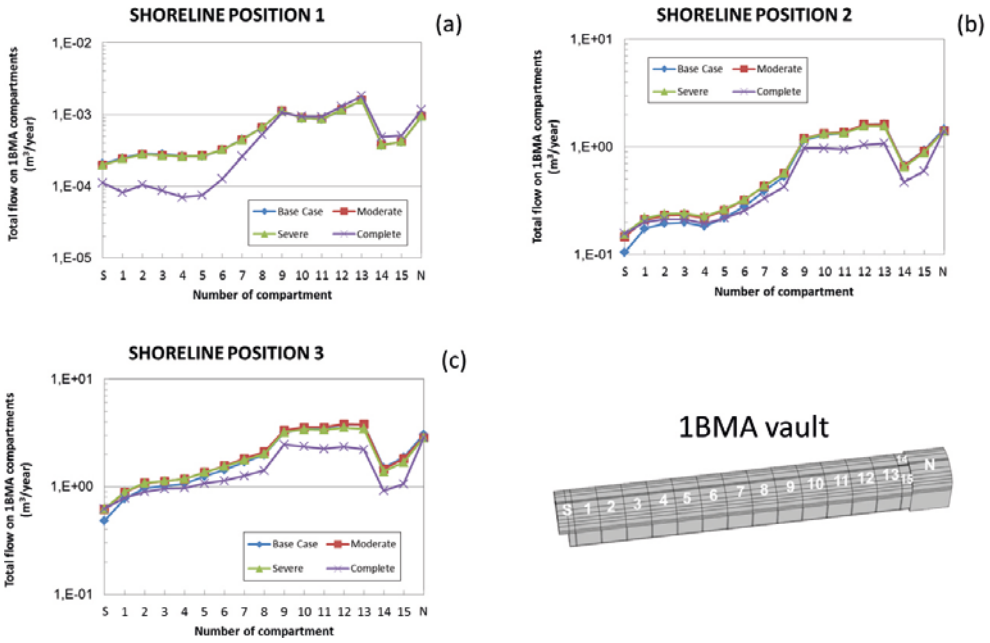

Figure B-13. *Flow rates through the top gravel of 1BMA submodel for degradation proportional to the Base case waste flow.*

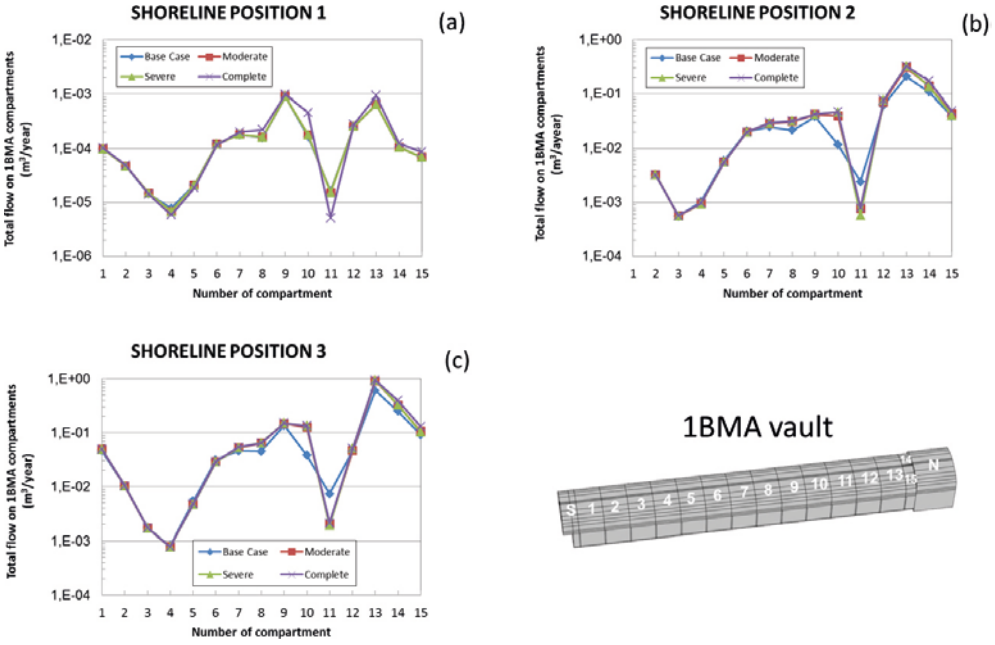

Figure B-14. *Flow rates through the bottom gravel of 1BMA submodel for degradation proportional to the Base case waste flow.*

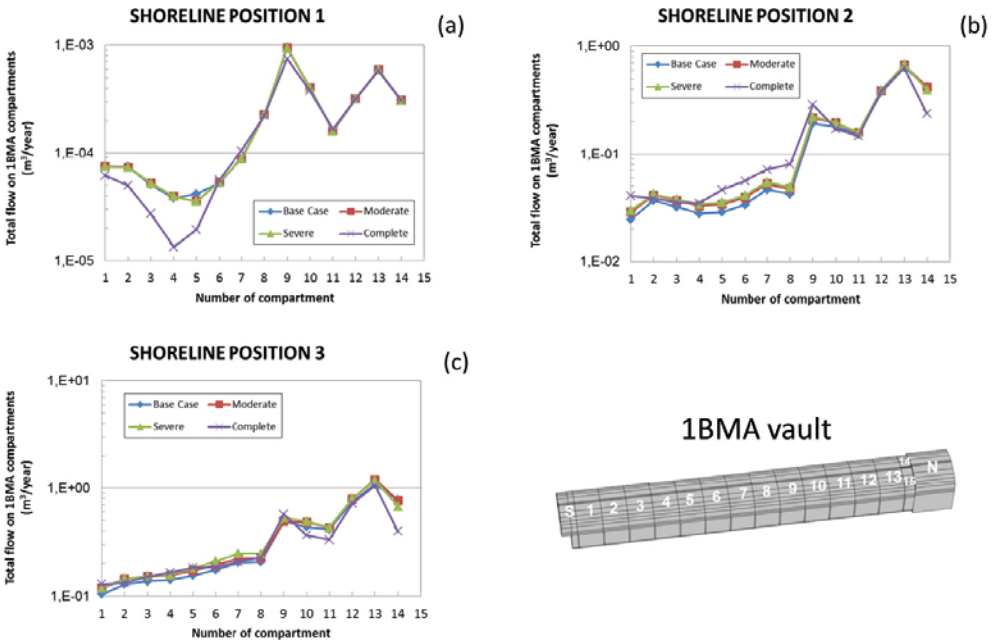

Figure B-15. *Flow rates through the east gravel of 1BMA submodel for degradation proportional to the Base case waste flow.*

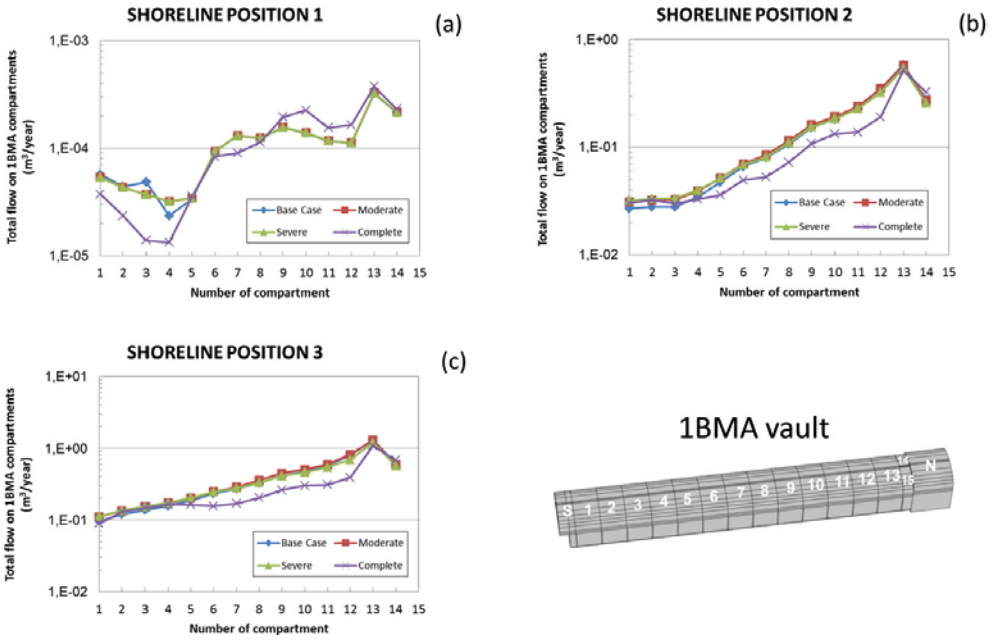

Figure B-16. *Flow rates through the west gravel of 1BMA submodel for degradation proportional to the Base case waste flow.*

Total flow rates through the 1BMA vault for compartment degradation

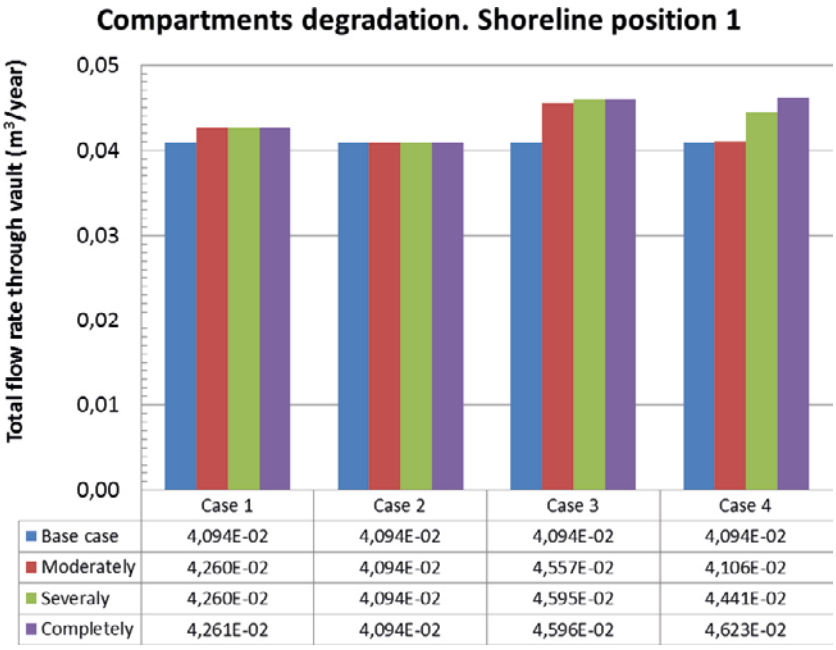

	Case 1	Case 2	Case 3	Case 4
Base case	4,094E-02	4,094E-02	4,094E-02	4,094E-02
Moderately	4,260E-02	4,094E-02	4,557E-02	4,106E-02
Severaly	4,260E-02	4,094E-02	4,595E-02	4,441E-02
Completely	4,261E-02	4,094E-02	4,596E-02	4,623E-02

Figure B-17. *Total flow rates through the 1BMA vault for different scenarios of compartments degradation and comparison with the Base case at shoreline position 1.*

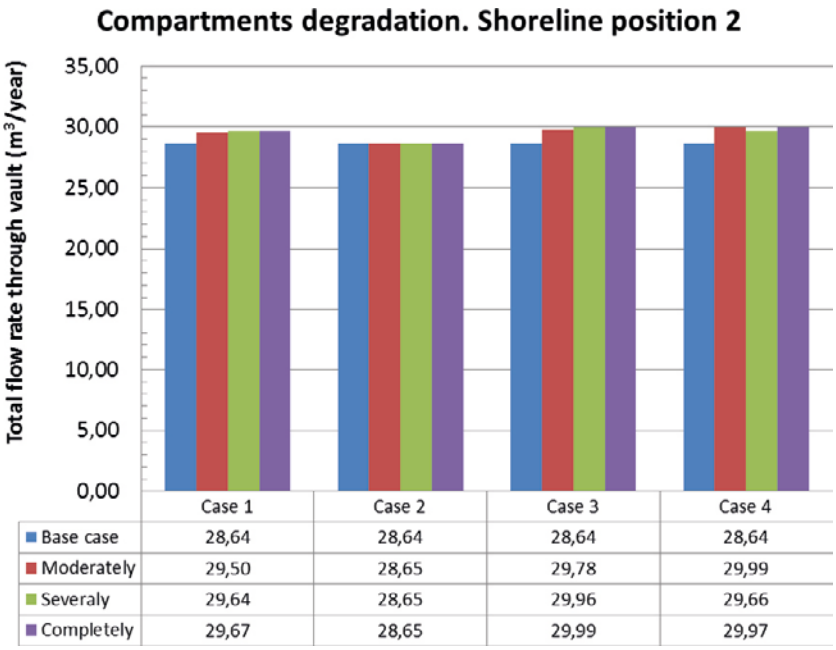

	Case 1	Case 2	Case 3	Case 4
Base case	28,64	28,64	28,64	28,64
Moderately	29,50	28,65	29,78	29,99
Severaly	29,64	28,65	29,96	29,66
Completely	29,67	28,65	29,99	29,97

Figure B-18. *Total flow rates through the 1BMA vault for different scenarios of compartments degradation and comparison with the Base case at shoreline position 2.*

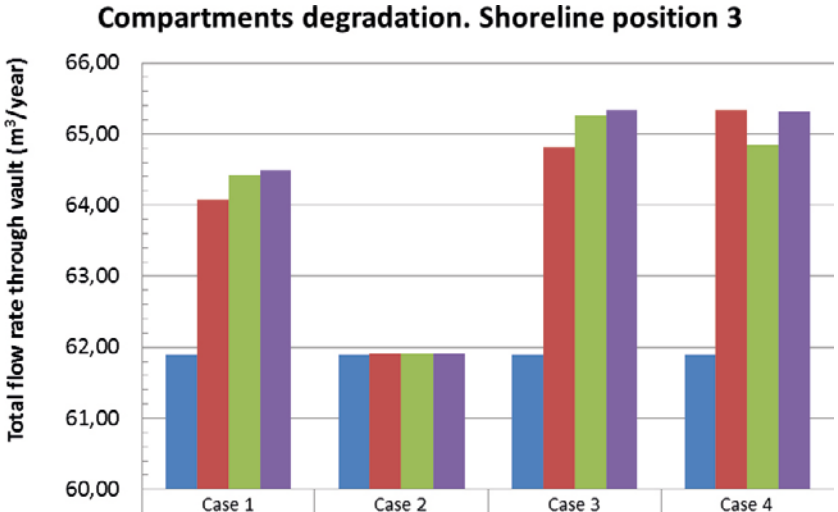

	Case 1	Case 2	Case 3	Case 4
Base case	61,90	61,90	61,90	61,90
Moderately	64,08	61,90	64,82	65,34
Severaly	64,43	61,91	65,26	64,85
Completely	64,50	61,91	65,34	65,31

Figure B-19. *Total flow rates through the 1BMA vault for different scenarios of compartments degradation and comparison with the Base case at shoreline position 3.*

Vault element degradation of 1BMA vault with high conductivity beams

Case 1. Floor degradation

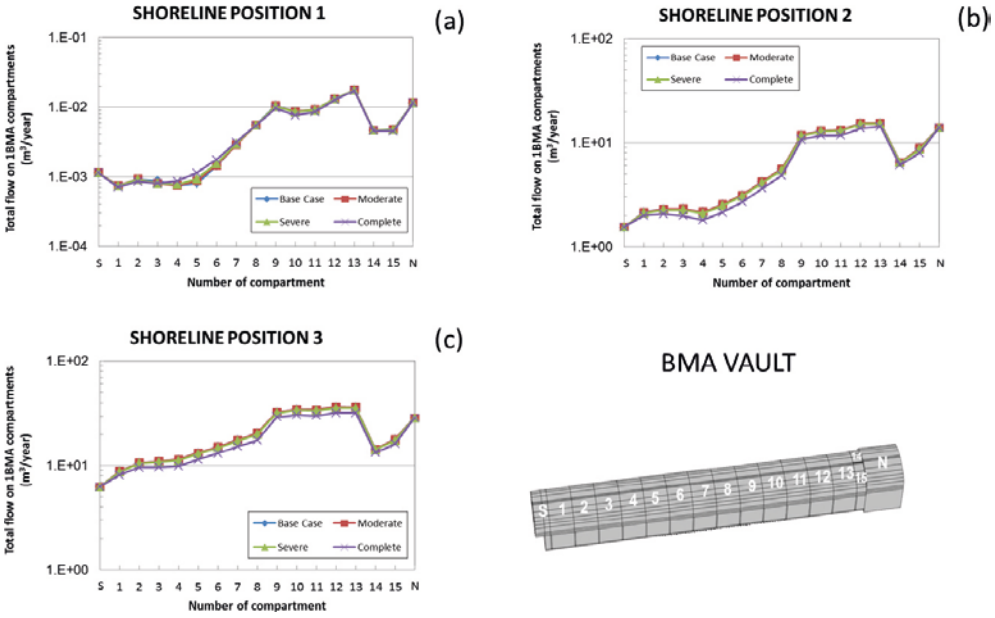

Figure C-1. *Flow rates through the top gravel of 1BMA submodel for floor degradation.*

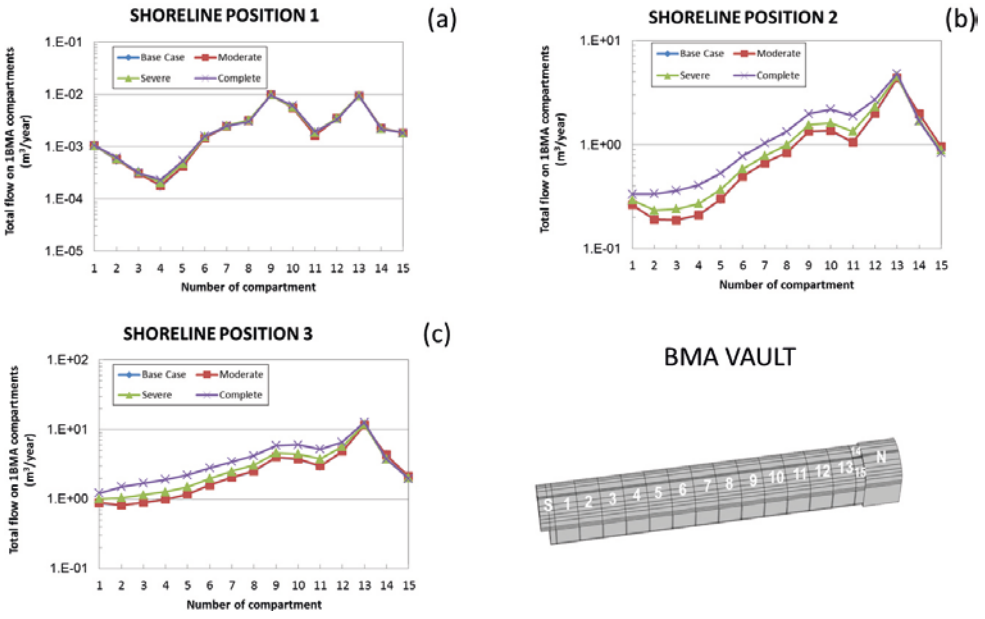

Figure C-2. *Flow rates through the bottom gravel of 1BMA submodel for floor degradation.*

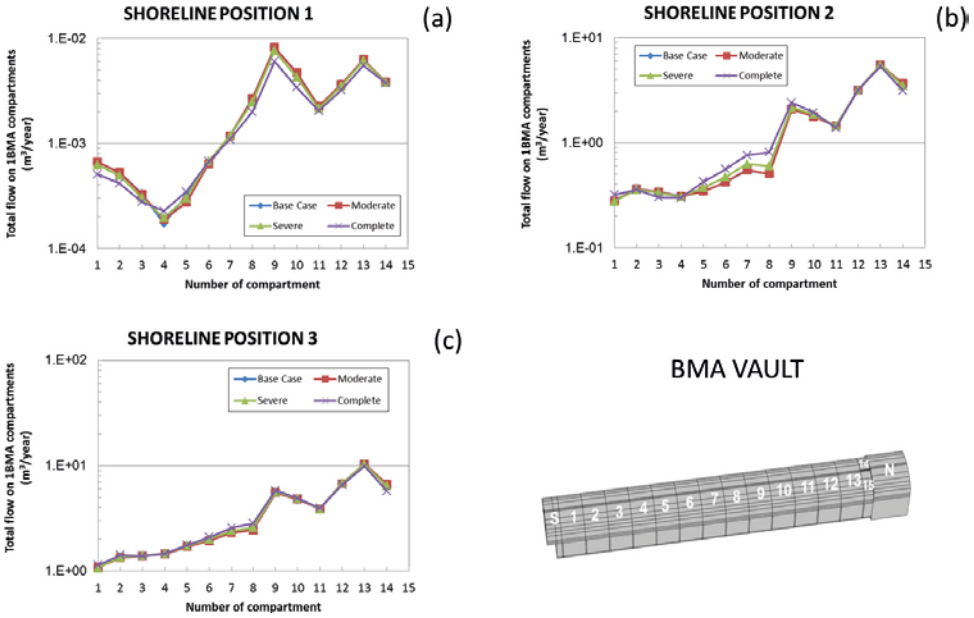

Figure C-3. *Flow rates through the east gravel of 1BMA submodel for floor degradation.*

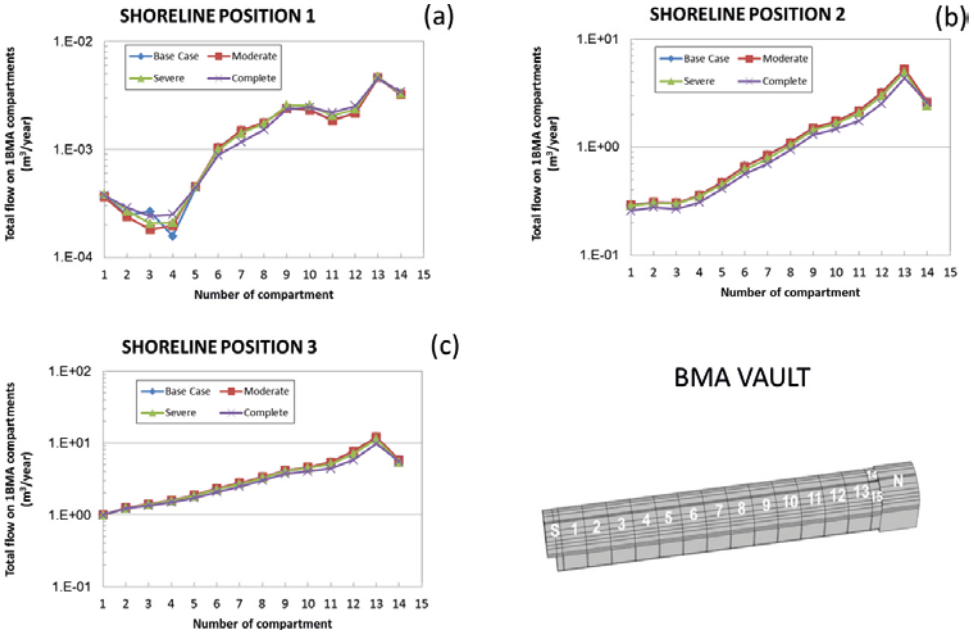

Figure C-4. *Flow rates through the west gravel of 1BMA submodel for floor degradation.*

Case 2. Degradation of floor and inner walls

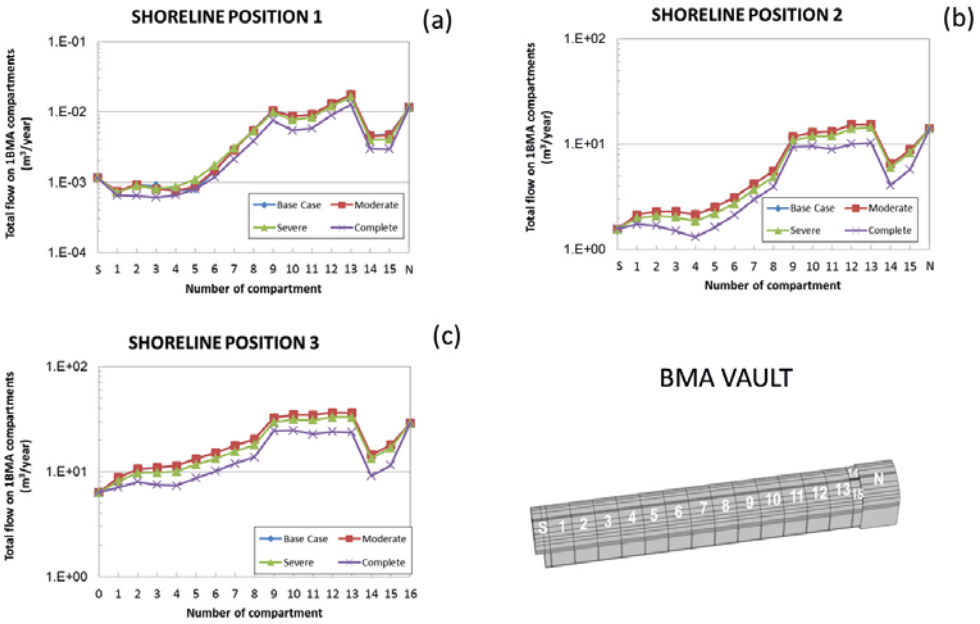

Figure C-5. *Flow rates through the top gravel of 1BMA submodel for floor and inner walls degradation.*

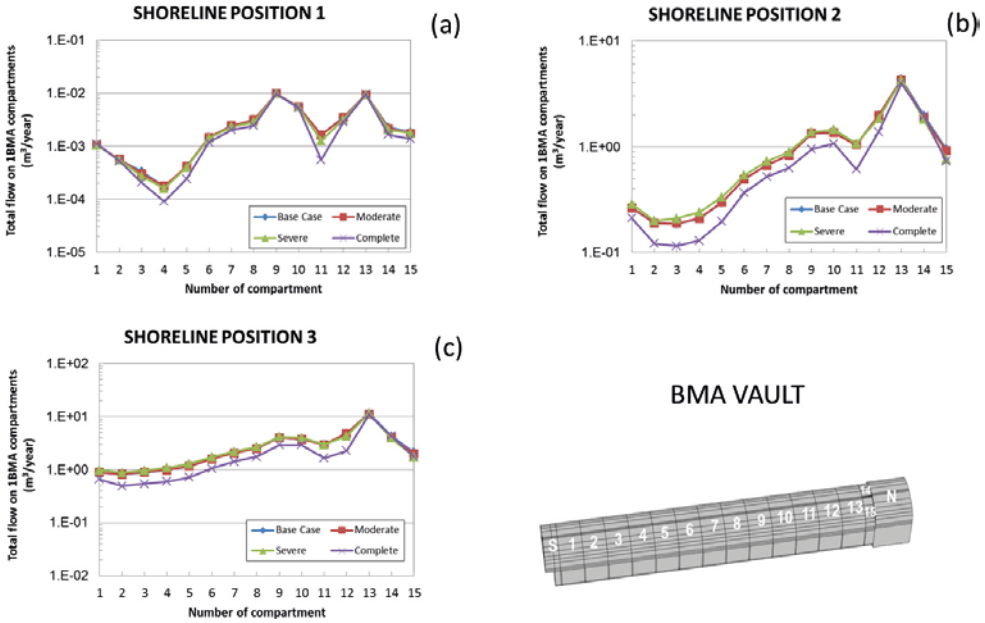

Figure C-6. *Flow rates through the bottom gravel of 1BMA submodel for floor and inner walls degradation.*

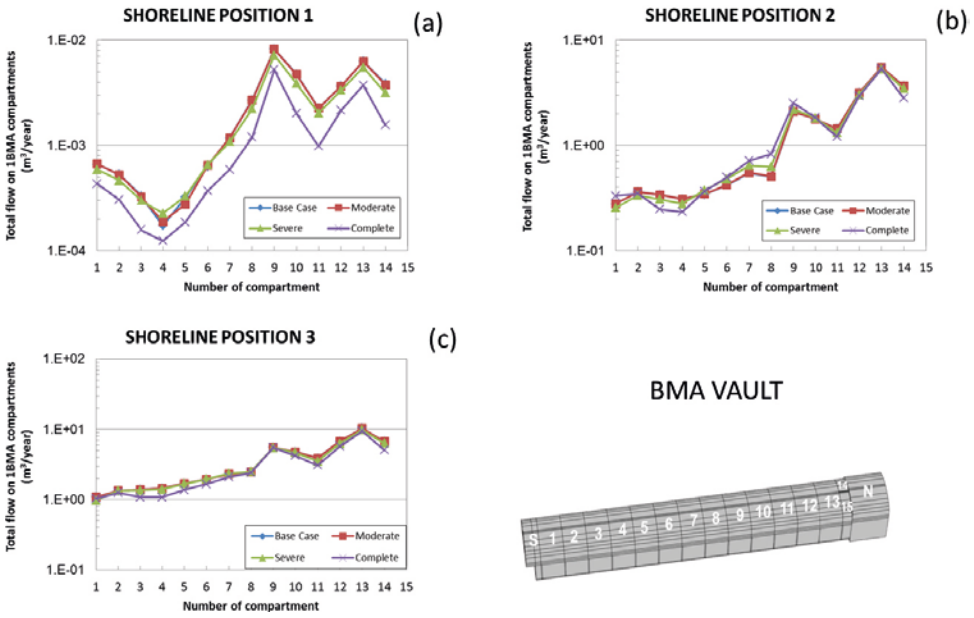

Figure C-7. *Flow rates through the east gravel of 1BMA submodel for floor and inner walls degradation.*

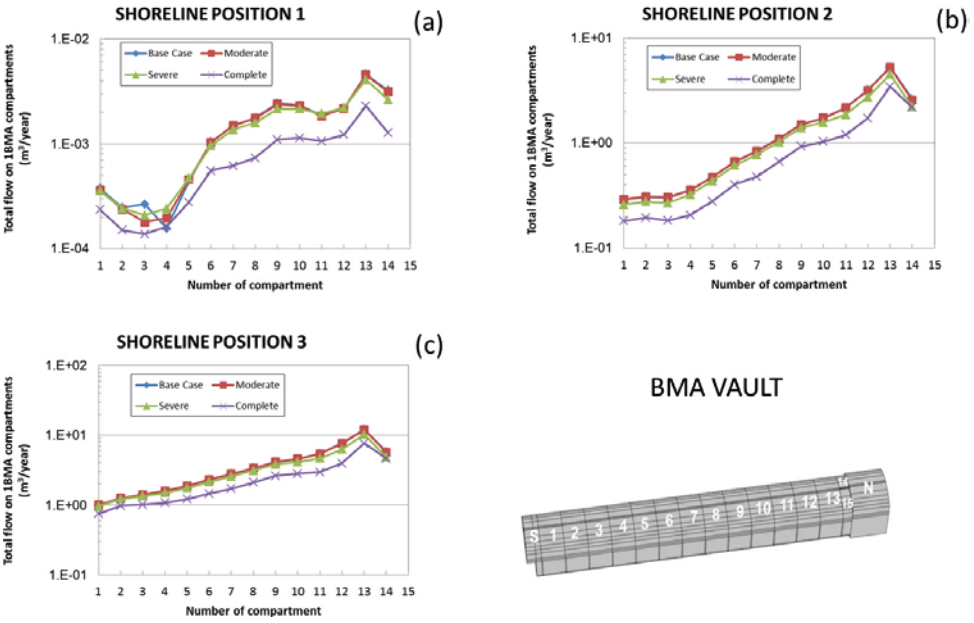

Figure C-8. *Flow rates through the west gravel of 1BMA submodel for floor and inner walls degradation.*

Case 3. Degradation of one outer wall

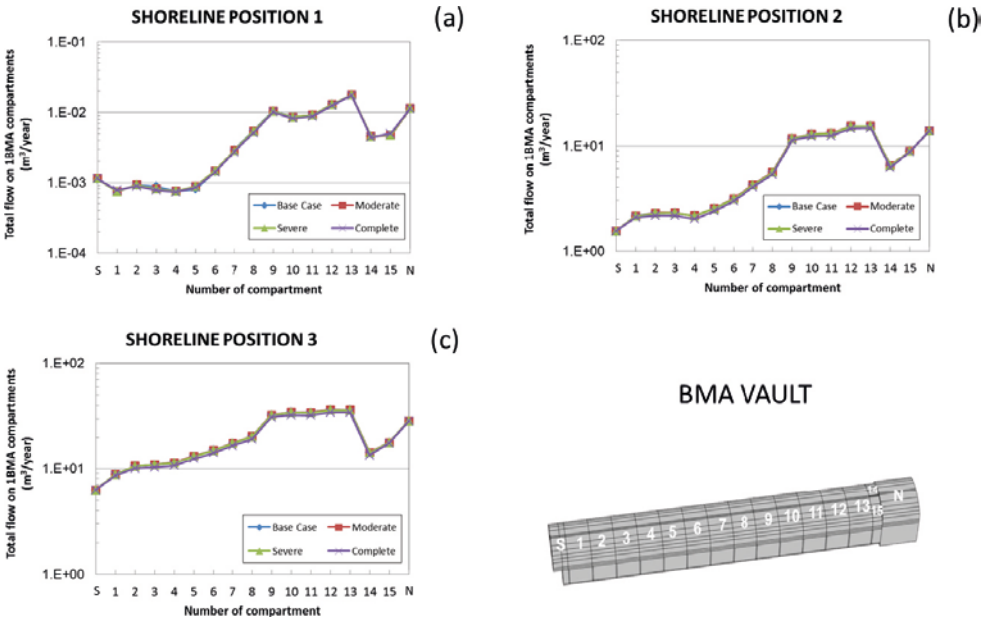

Figure C-9. *Flow rates through the top gravel of 1BMA submodel for degradation of one outer wall.*

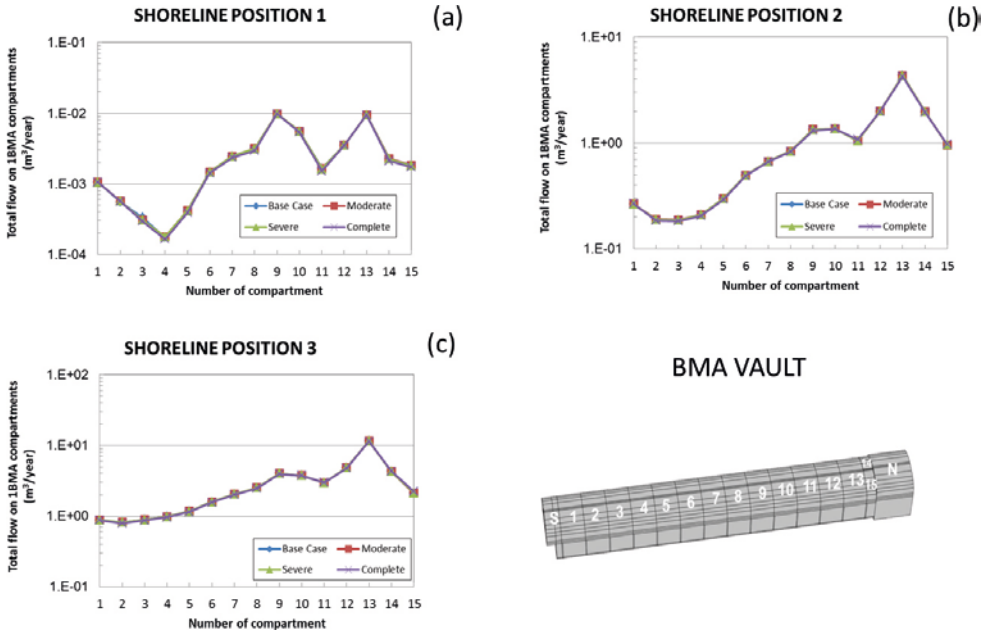

Figure C-10. *Flow rates through the bottom gravel of 1BMA submodel for degradation of one outer wall.*

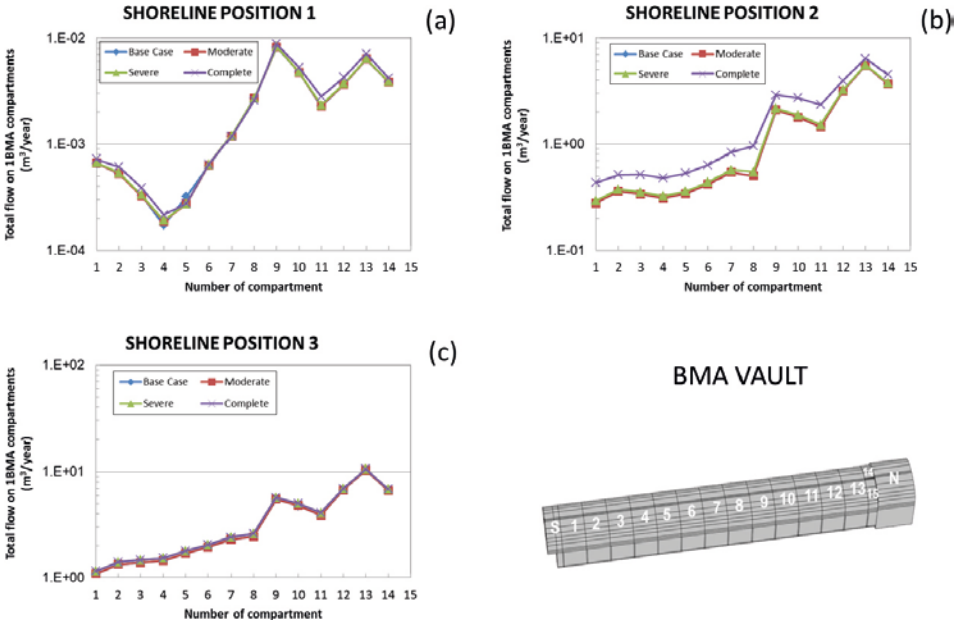

Figure C-11. *Flow rates through the east gravel of 1BMA submodel for degradation of one outer wall.*

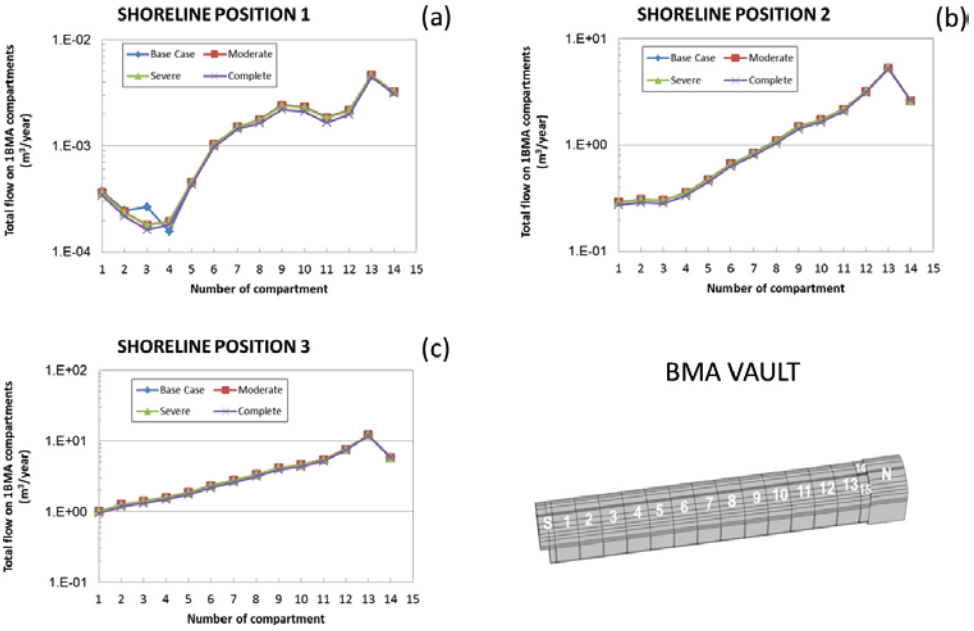

Figure C-12. *Flow rates through the west gravel of 1BMA submodel for degradation of one outer wall.*

Case 4. Degradation of both outer walls

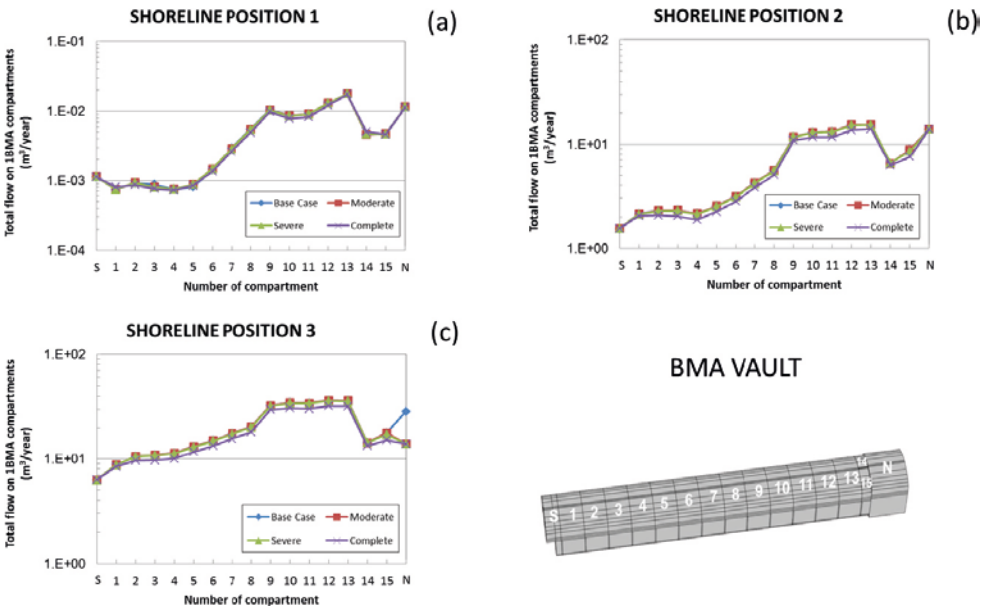

Figure C-13. *Flow rates through the top gravel of 1BMA submodel for degradation of both outer walls.*

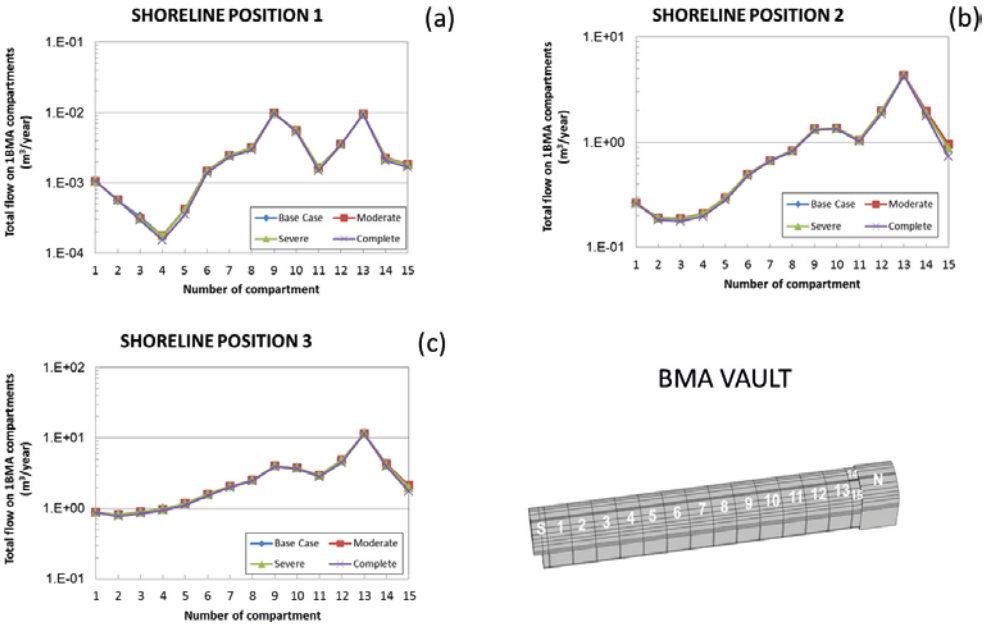

Figure C-14. *Flow rates through the bottom gravel of 1BMA submodel for degradation of both outer walls.*

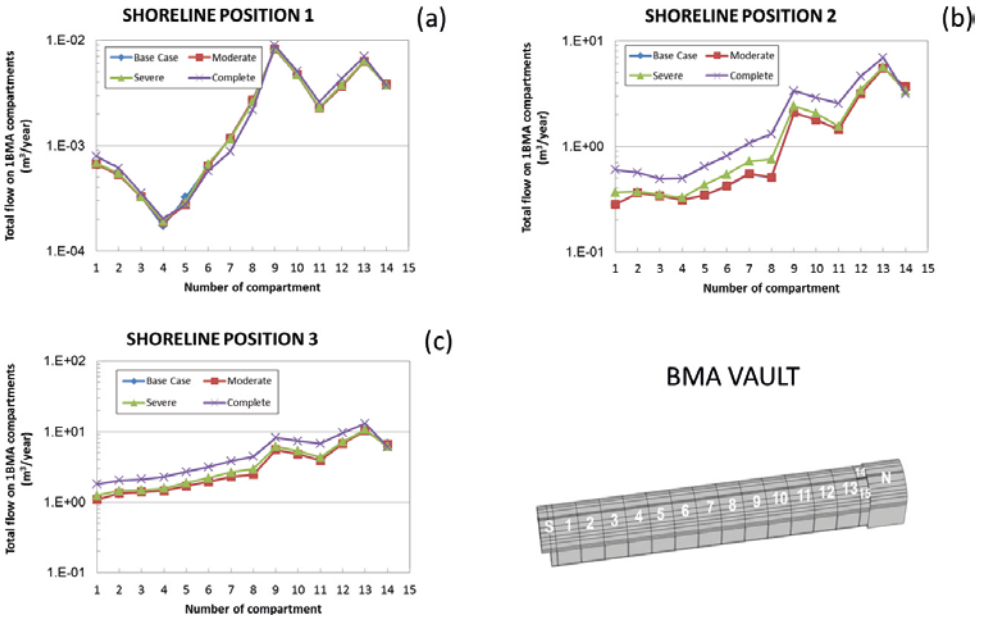

Figure C-15. *Flow rates through the east gravel of 1BMA submodel for degradation of both outer walls.*

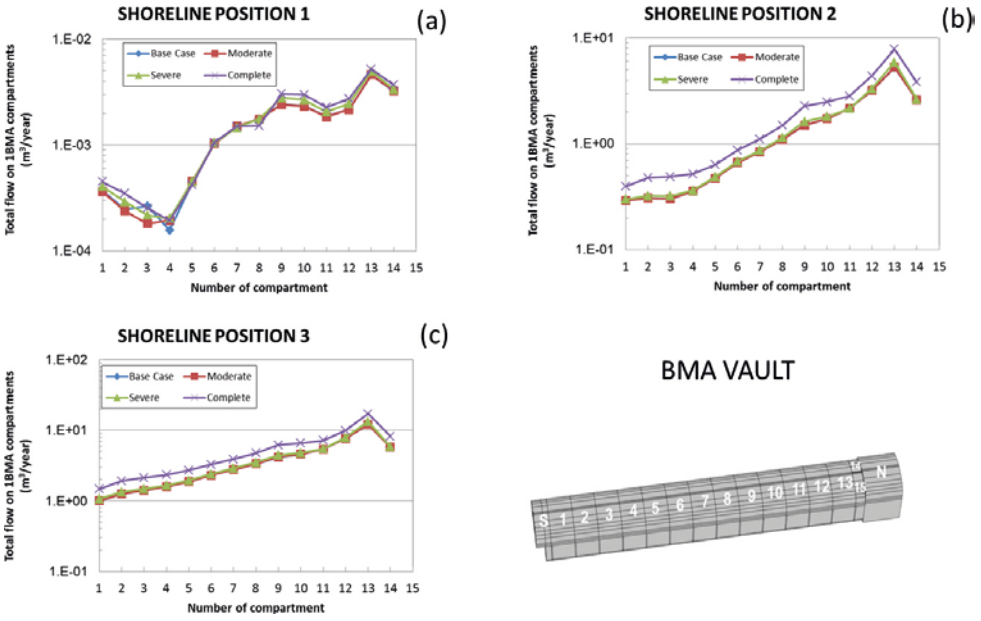

Figure C-16. *Flow rates through the west gravel of 1BMA submodel for degradation of both outer walls.*

Case 5. Degradation of inner and outer walls

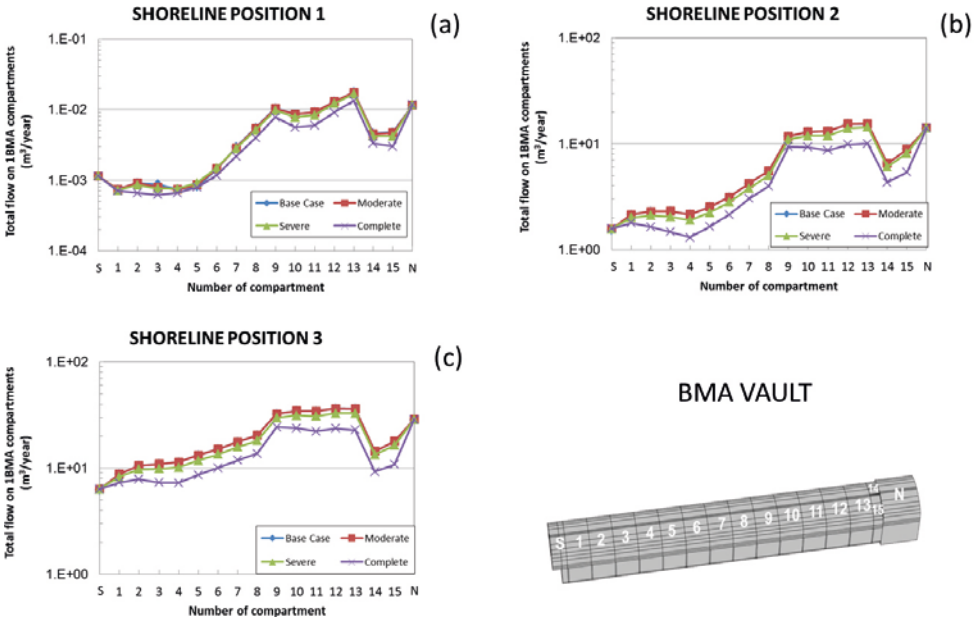

Figure C-17. *Flow rates through the top gravel of 1BMA submodel for degradation of inner and outer walls.*

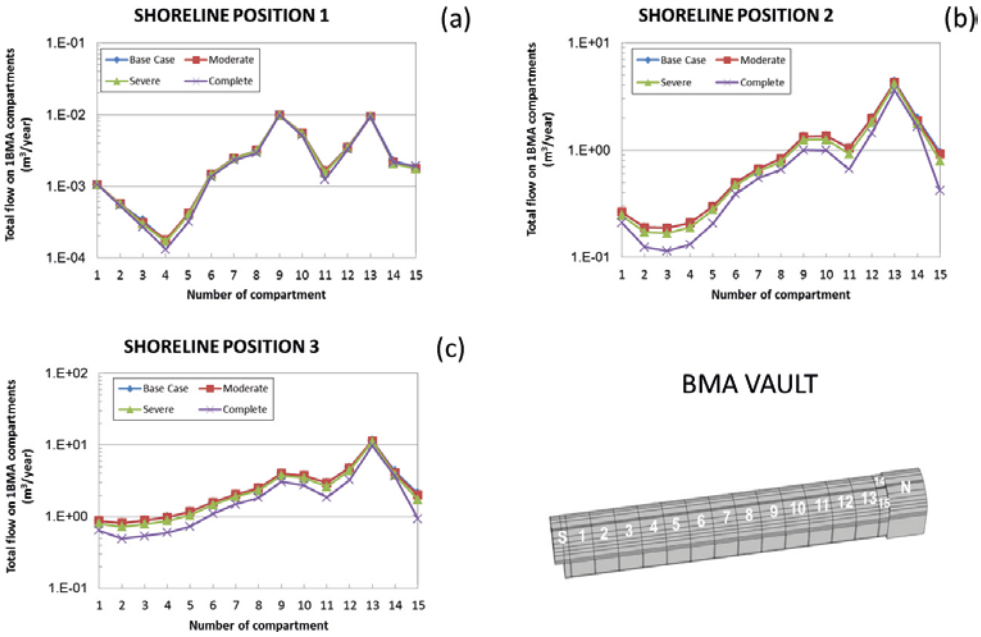

Figure C-18. *Flow rates through the bottom gravel of 1BMA submodel for degradation of inner and outer walls.*

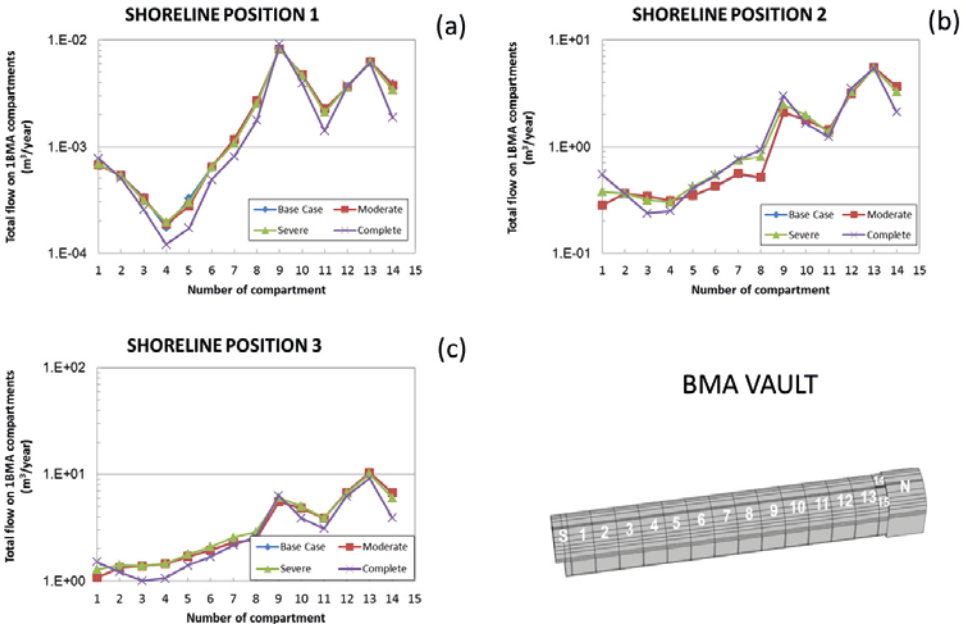

Figure C-19. *Flow rates through the east gravel of 1BMA submodel for degradation of inner and outer walls.*

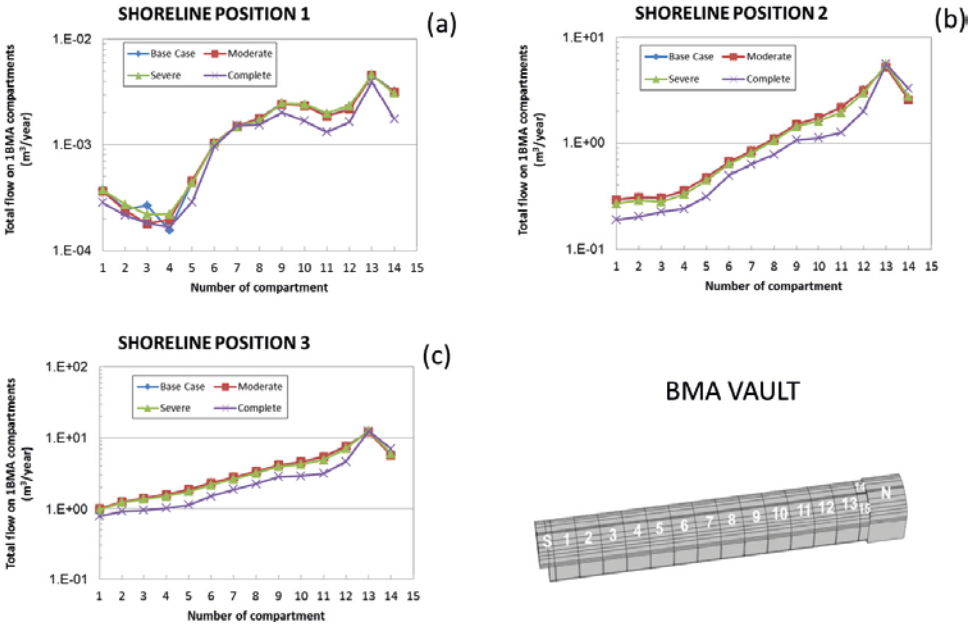

Figure C-20. *Flow rates through the west gravel of 1BMA submodel for degradation of inner and outer walls.*

Case 6. Degradation of outer walls, lids and floor

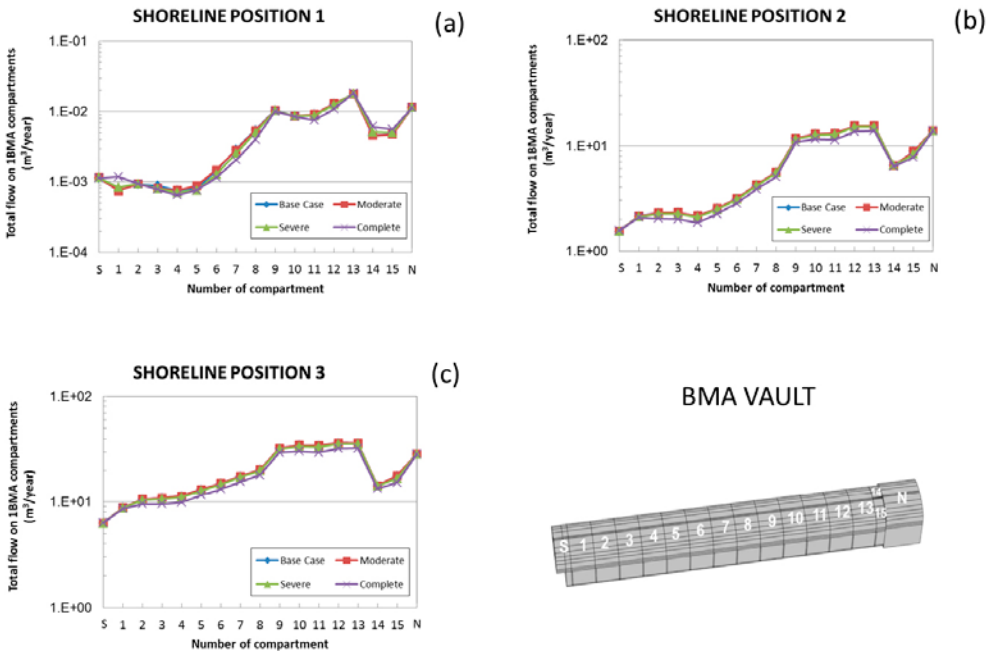

Figure C-21. *Flow rates through the top gravel of 1BMA submodel for degradation of outer walls, lids and floor.*

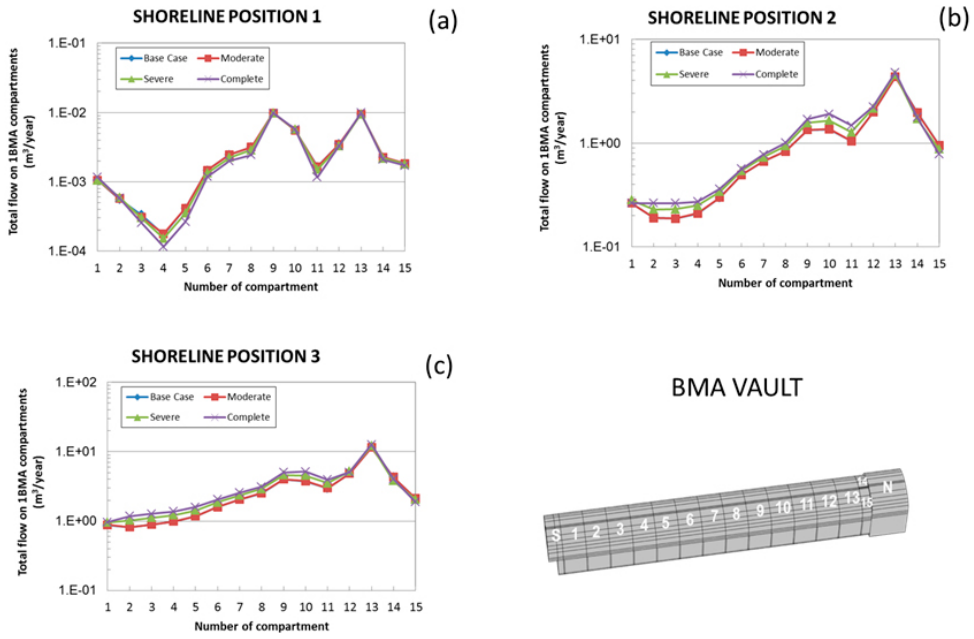

Figure C-22. *Flow rates through the bottom gravel of 1BMA submodel for degradation of outer walls, lids and floor.*

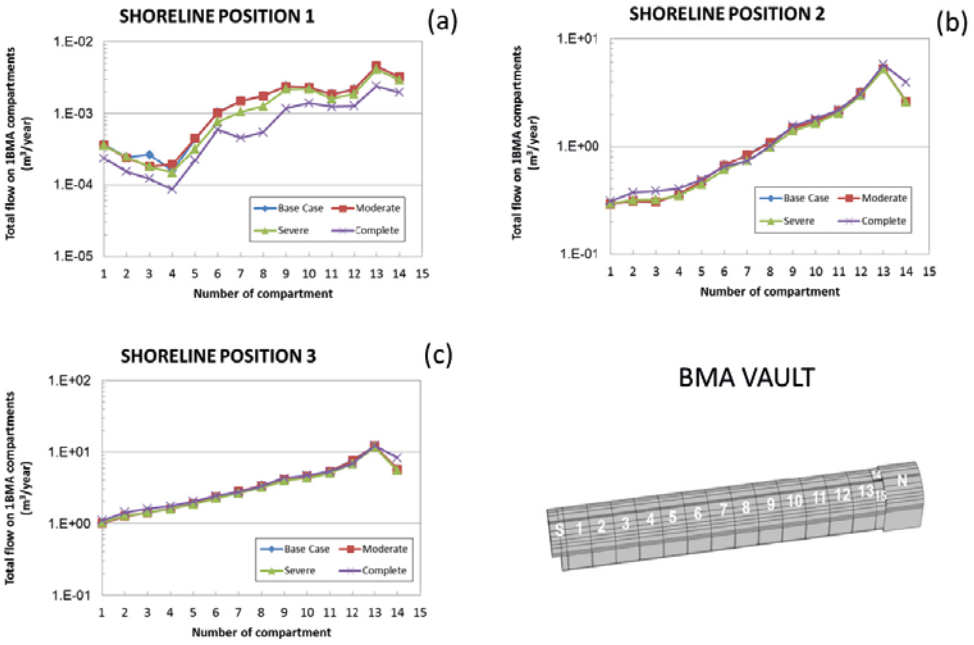

Figure C-23. *Flow rates through the east gravel of 1BMA submodel for degradation of outer walls, lids and floor.*

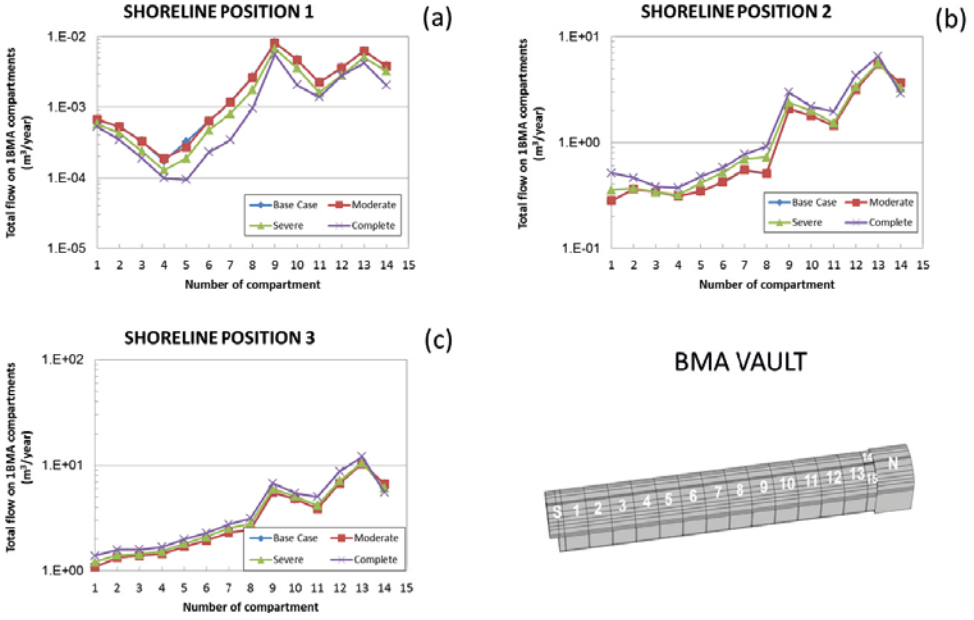

Figure C-24. *Flow rates through the west gravel of 1BMA submodel for degradation of outer walls, lids and floor.*

Appendix D

Compartment degradation of 1BMA vault with high conductivity beams

Case 1. Degradation of deformation zone ZFMNNW1209

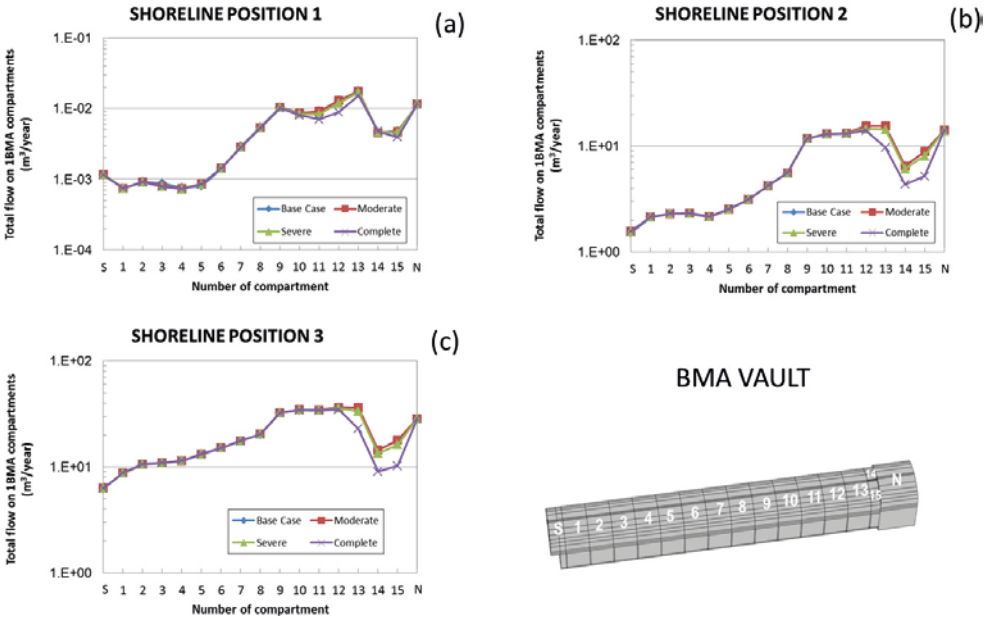

Figure D-1. *Flow rates through the top gravel of 1BMA submodel for degradation of deformation zone ZFMNNW1209.*

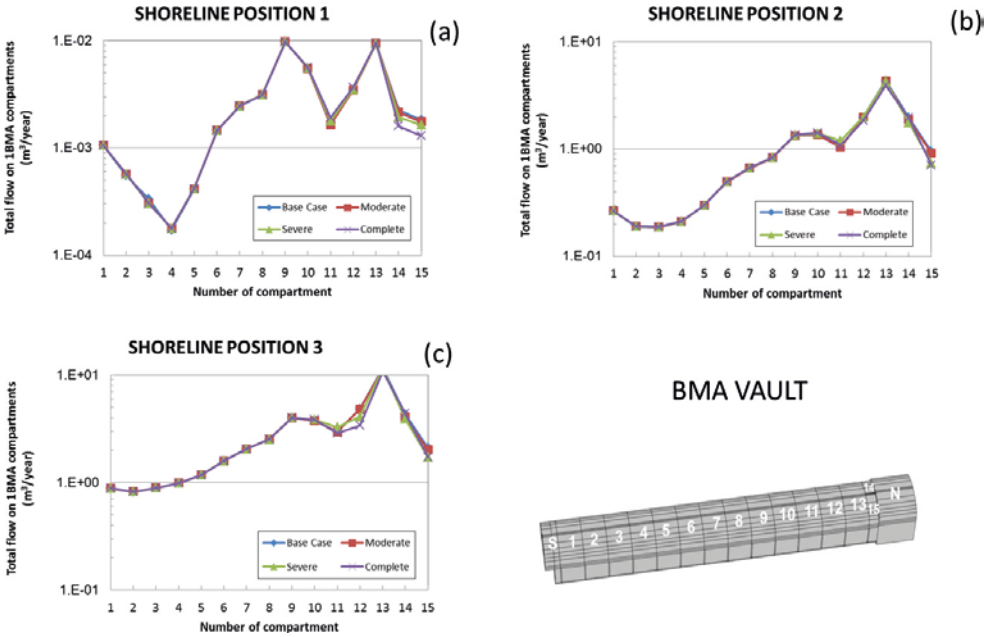

Figure D-2. *Flow rates through the bottom gravel of 1BMA submodel for degradation of deformation zone ZFMNNW1209.*

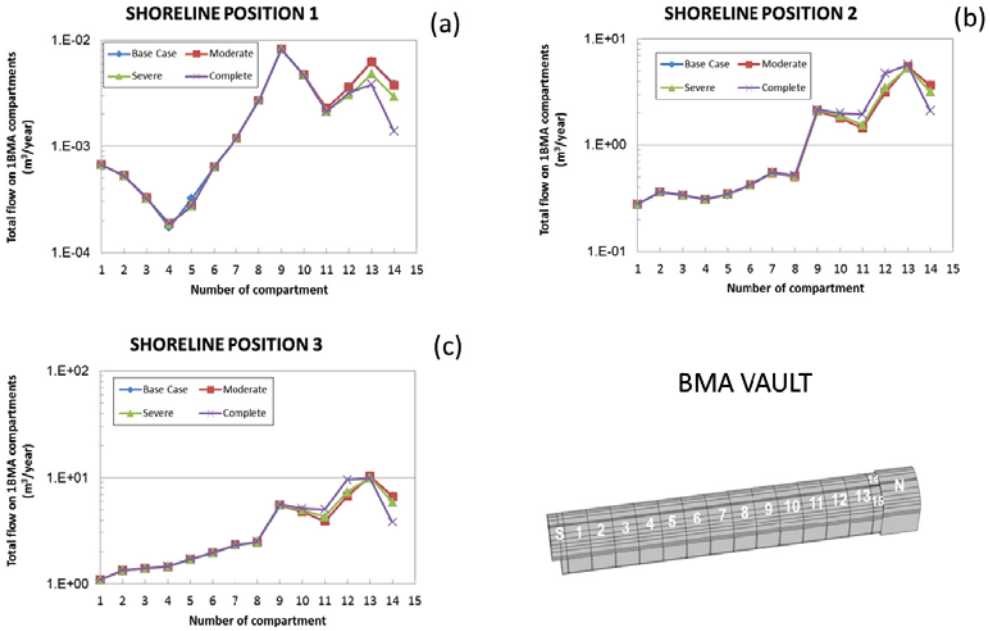

Figure D-3. *Flow rates through the east gravel of 1BMA submodel for degradation of deformation zone ZFMNNW1209.*

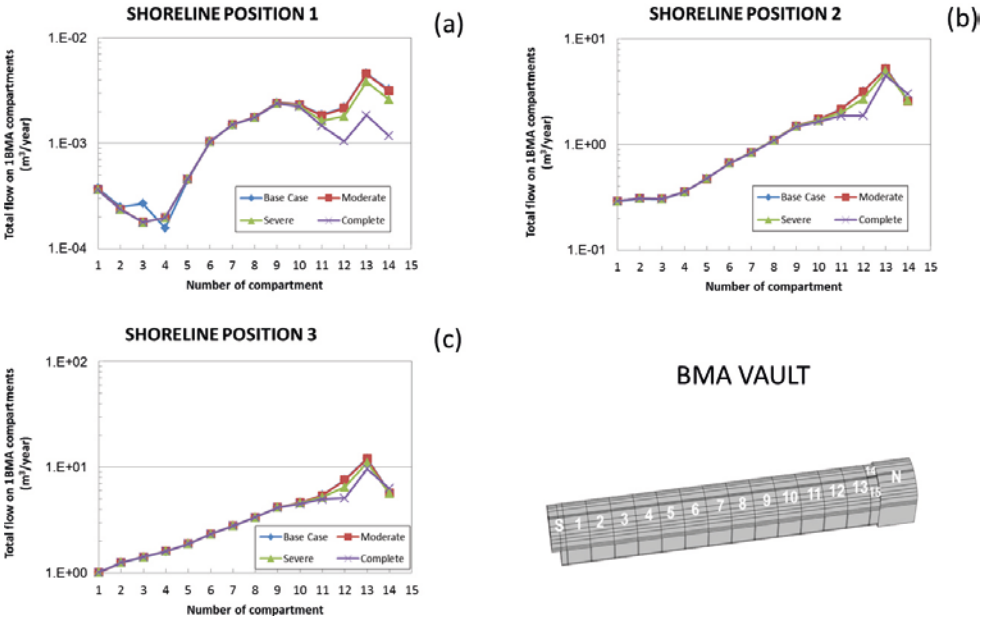

Figure D-4. *Flow rates through the west gravel of 1BMA submodel for degradation of deformation zone ZFMNNW1209.*

Case 2. Degradation of low flow compartments

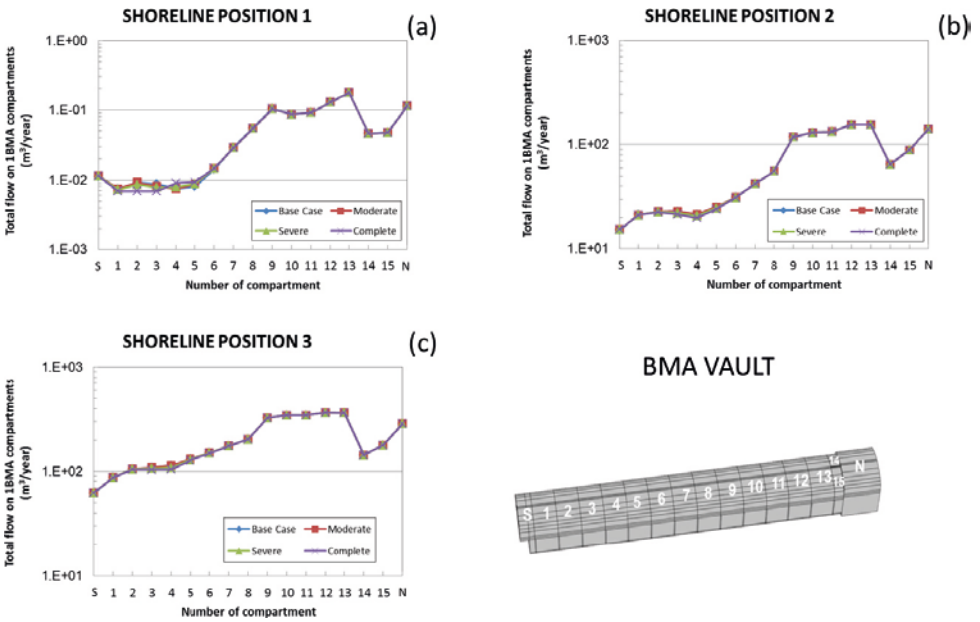

Figure D-5. *Flow rates through the top gravel of 1BMA submodel for degradation of low flow compartments.*

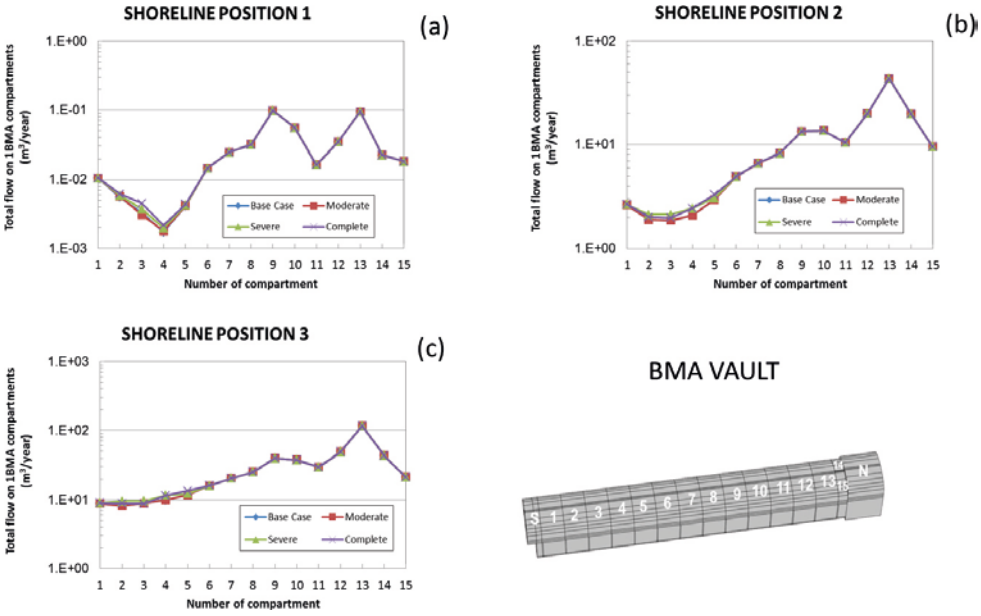

Figure D-6. *Flow rates through the bottom gravel of 1BMA submodel for degradation of low flow compartments.*

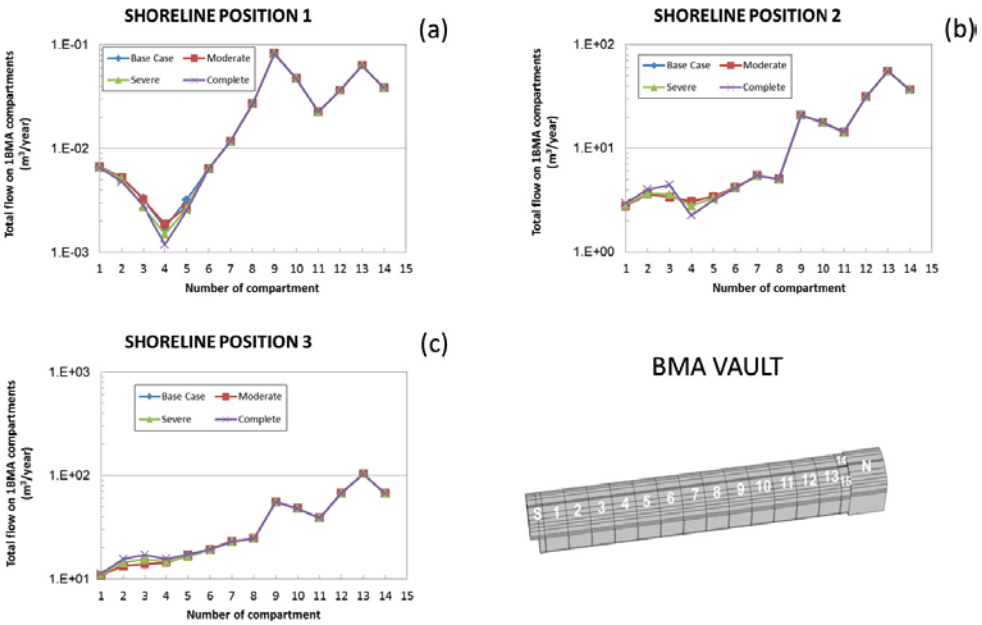

Figure D-7. *Flow rates through the east gravel of 1BMA submodel for degradation of low flow compartments.*

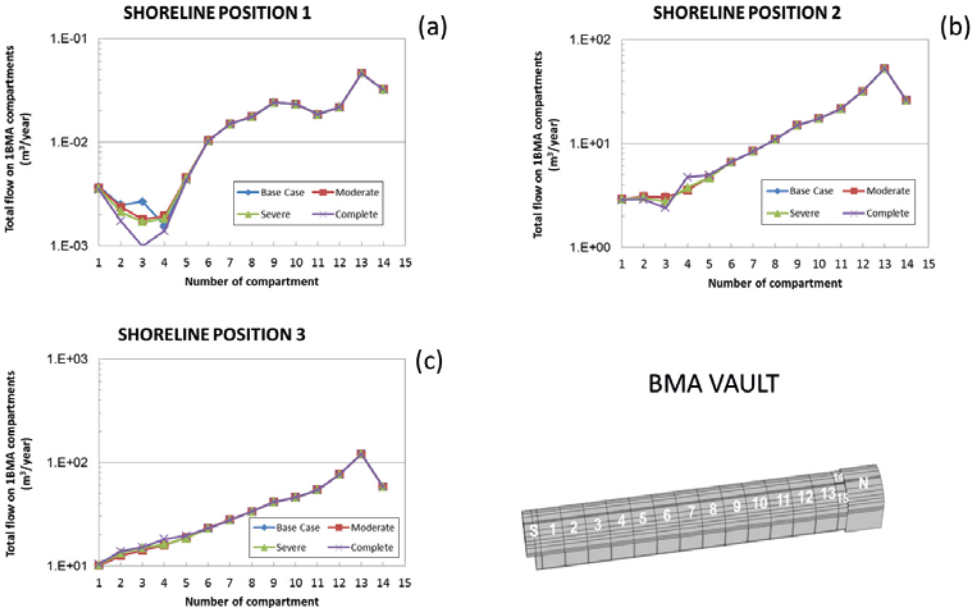

Figure D-8. *Flow rates through the west gravel of 1BMA submodel for degradation of low flow compartments.*

Case 3. Simultaneous degradation of all the compartments affected by fracture zones

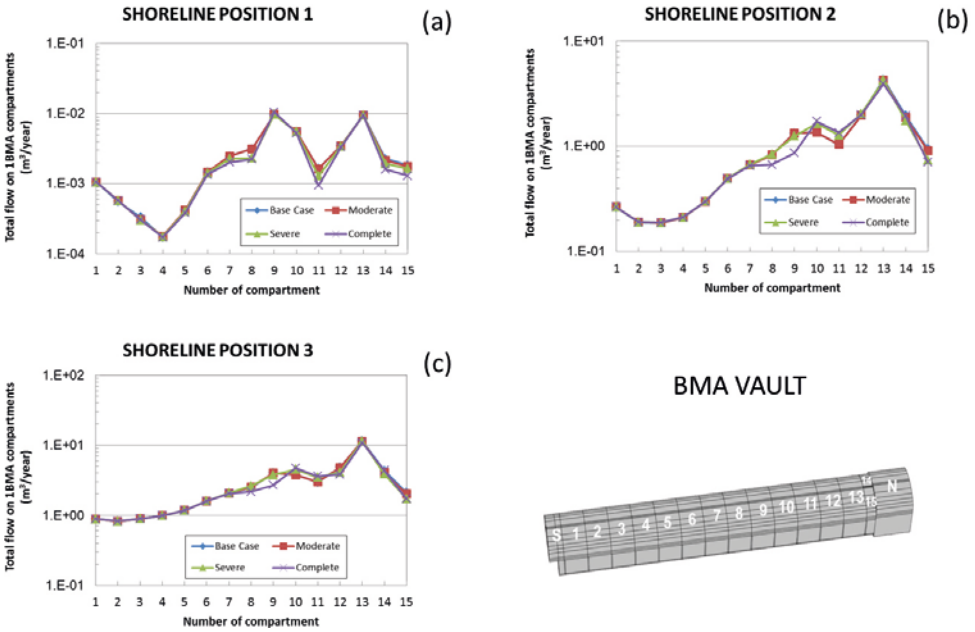

Figure D-9. *Flow rates through the top gravel of 1BMA submodel for simultaneous degradation of all the compartments affected by fracture zones.*

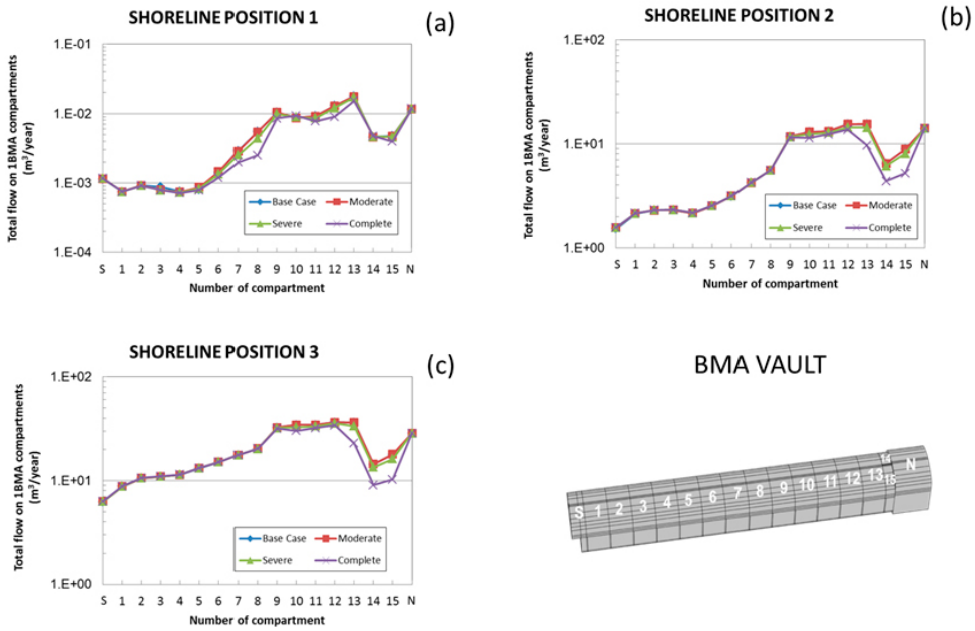

Figure D-10. *Flow rates through the bottom gravel of 1BMA submodel for simultaneous degradation of all the compartments affected by fracture zones.*

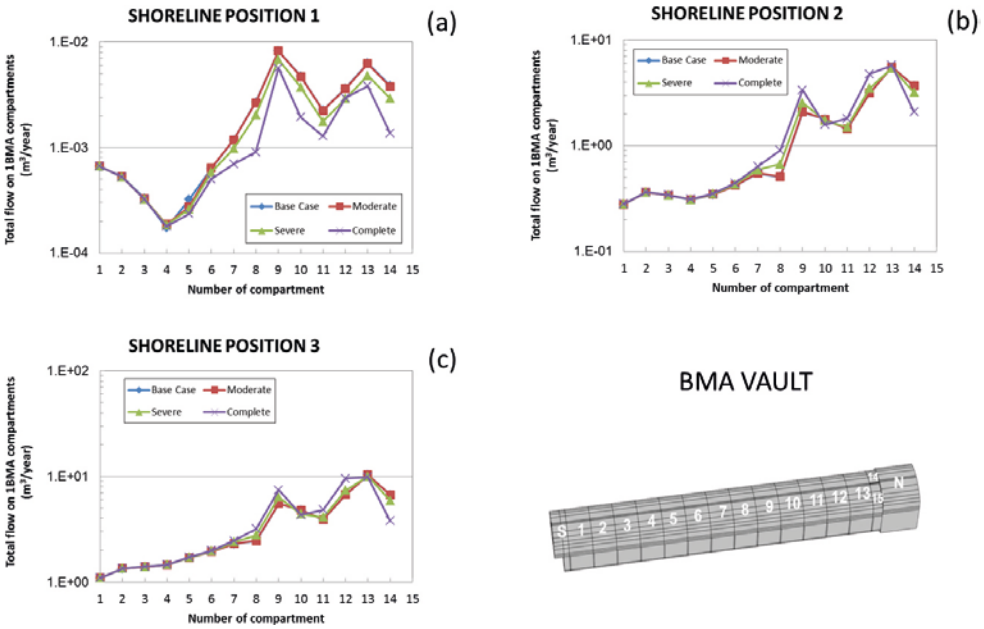

Figure D-11. *Flow rates through the east gravel of 1BMA submodel for simultaneous degradation of all the compartments affected by fracture zones.*

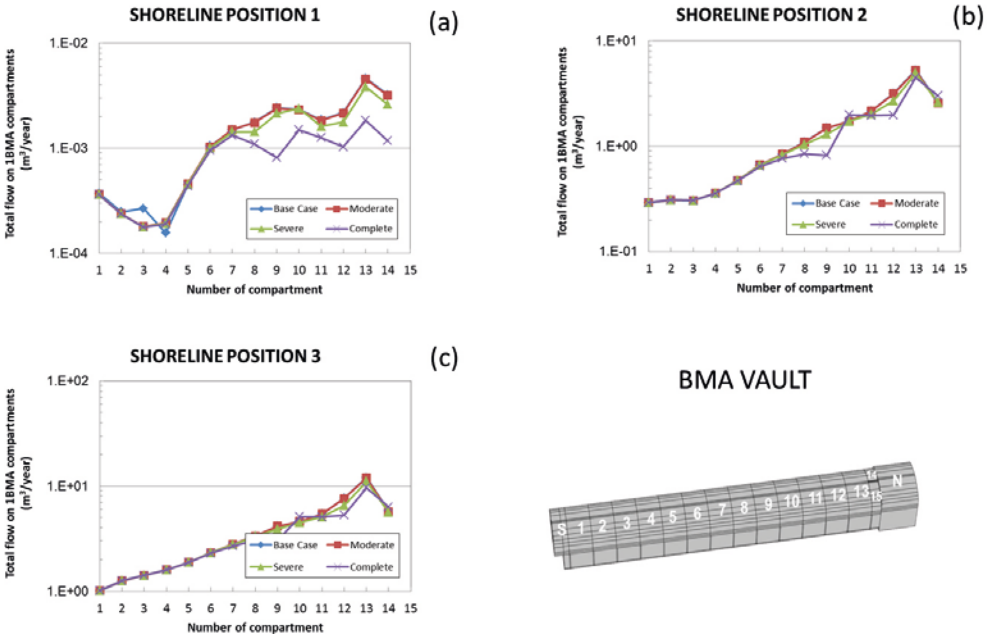

Figure D-12. *Flow rates through the west gravel of 1BMA submodel for simultaneous degradation of all the compartments affected by fracture zones.*

Case 4. Compartment degradation proportional to the flow rate

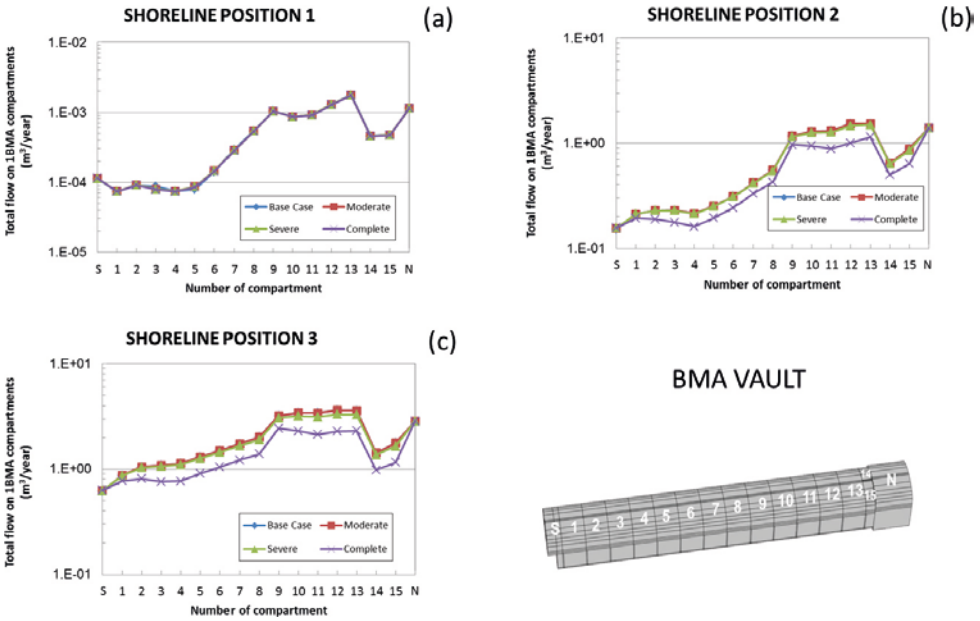

Figure D-13. *Flow rates through the top gravel of 1BMA submodel for degradation proportional to the Base case waste flow.*

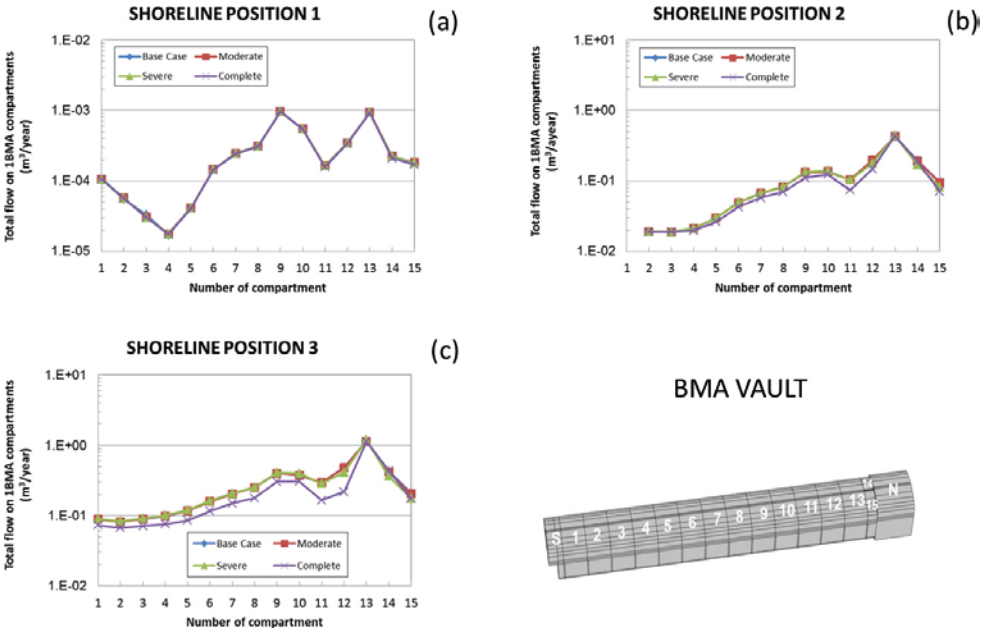

Figure D-14. *Flow rates through the bottom gravel of 1BMA submodel for degradation proportional to the Base case waste flow.*

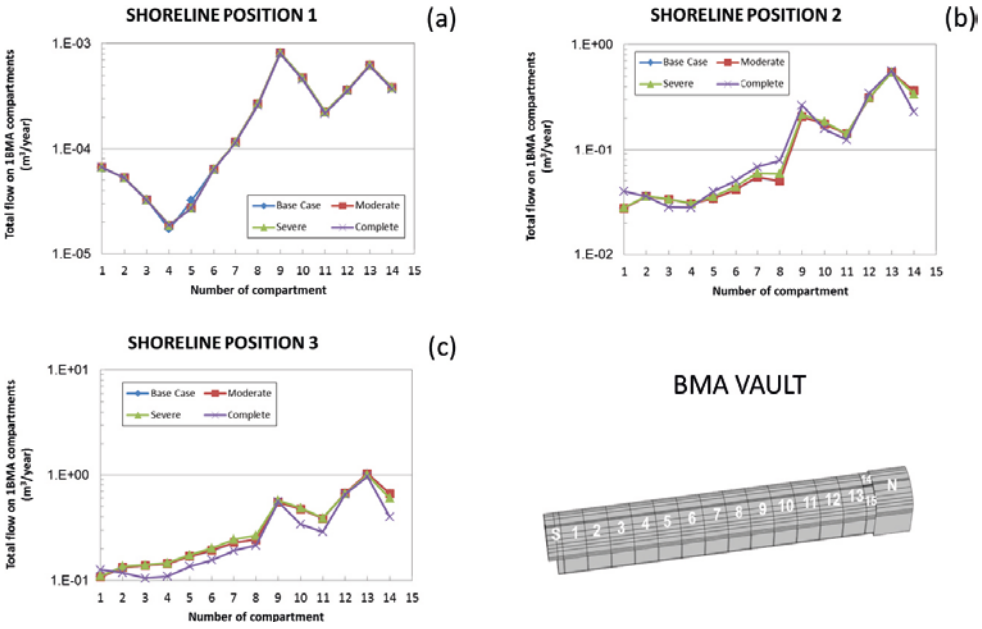

Figure D-15. *Flow rates through the east gravel of 1BMA submodel for degradation proportional to the Base case waste flow.*

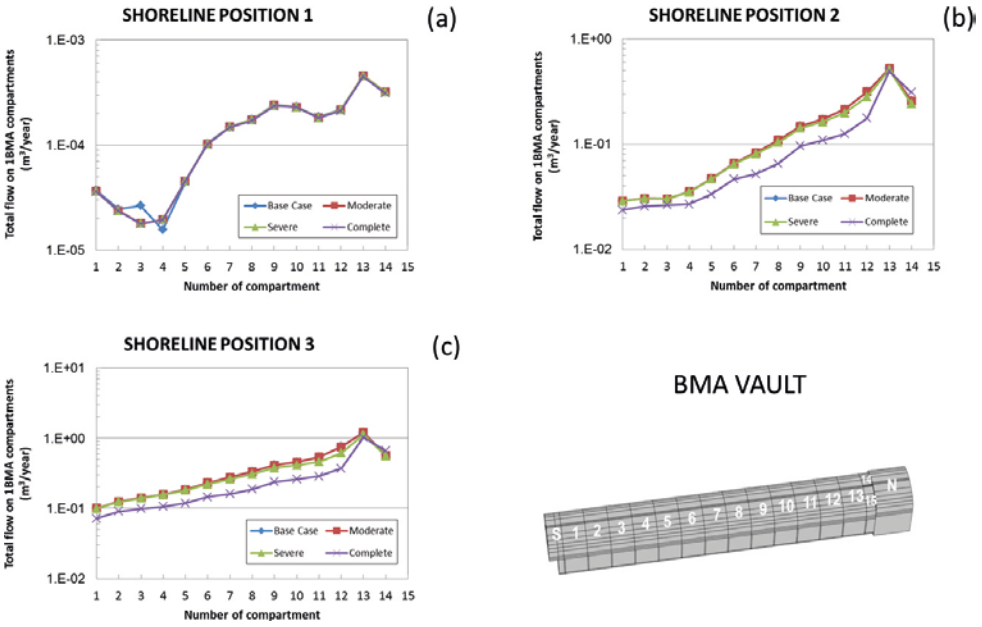

Figure D-16. *Flow rates through the west gravel of 1BMA submodel for degradation proportional to the Base case waste flow.*

Total flow rates through the 1BMA vault for compartments degradation

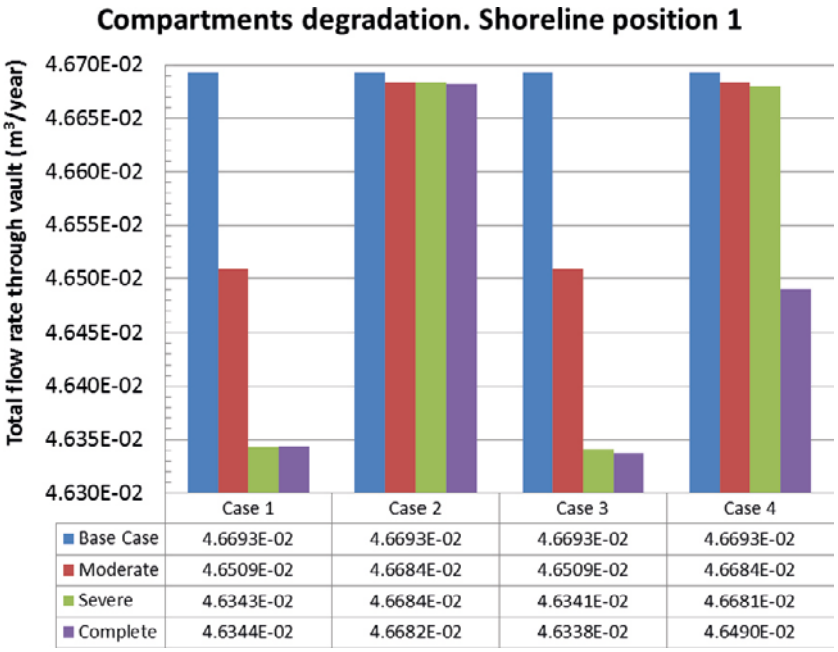

	Case 1	Case 2	Case 3	Case 4
Base Case	4.6693E-02	4.6693E-02	4.6693E-02	4.6693E-02
Moderate	4.6509E-02	4.6684E-02	4.6509E-02	4.6684E-02
Severe	4.6343E-02	4.6684E-02	4.6341E-02	4.6681E-02
Complete	4.6344E-02	4.6682E-02	4.6338E-02	4.6490E-02

Figure D-17. *Total flow rates through the 1BMA vault for different scenarios of compartments degradation and comparison with the Base case at shoreline position 1.*

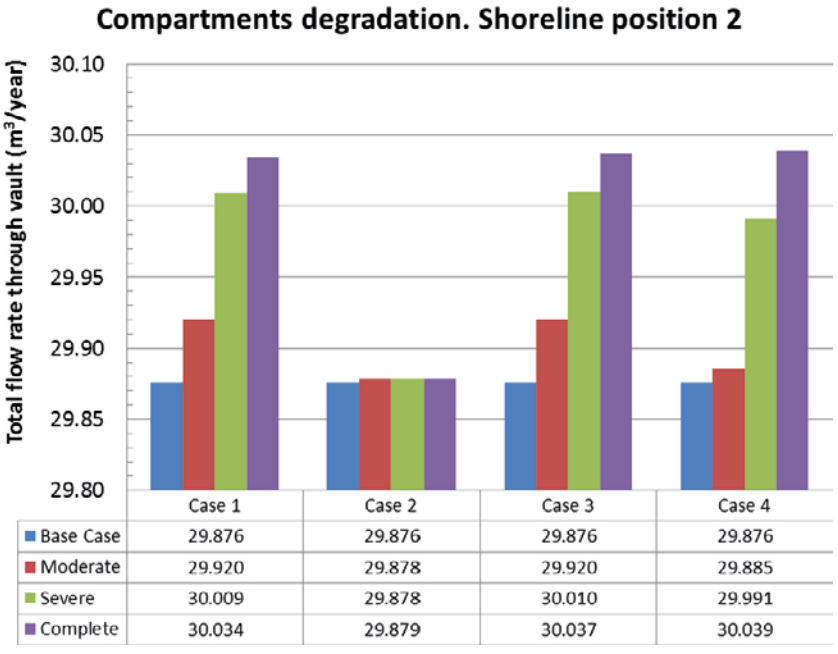

	Case 1	Case 2	Case 3	Case 4
Base Case	29.876	29.876	29.876	29.876
Moderate	29.920	29.878	29.920	29.885
Severe	30.009	29.878	30.010	29.991
Complete	30.034	29.879	30.037	30.039

Figure D-18. *Total flow rates through the 1BMA vault for different scenarios of compartments degradation and comparison with the Base case at shoreline position 2.*

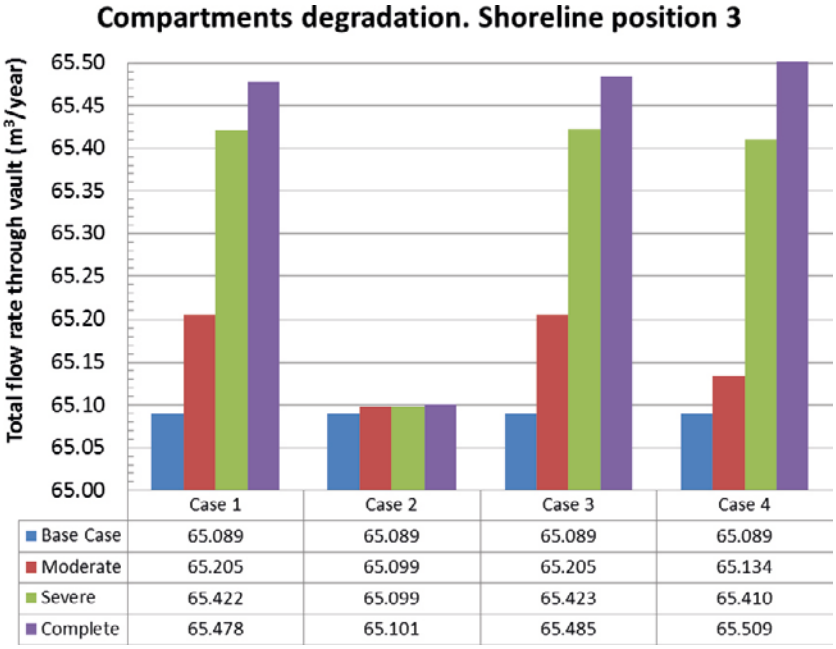

	Case 1	Case 2	Case 3	Case 4
Base Case	65.089	65.089	65.089	65.089
Moderate	65.205	65.099	65.205	65.134
Severe	65.422	65.099	65.423	65.410
Complete	65.478	65.101	65.485	65.509

Figure D-19. *Total flow rates through the 1BMA vault for different scenarios of compartments degradation and comparison with the Base case at shoreline position 3.*

Appendix E

Silo Q_{eq} for repository-scale model

For each of the scenarios described in Abarca et al. (2013) the equivalent flow rate Q_{eq}, as defined by Neretnieks (1980), has been estimated. This flow rate corresponds to the water flowing through the rock near the Silo and that becomes contaminated by out-diffusion of radionuclides. For this estimation the following data has been assumed: a surface area A_w between the rock and the backfill of 5,000 m^2, a diffusivity of the nuclides in the water $D_w = 2 \cdot 10^{-9}$ m^2/s, and a pathlength L of 50 m, in agreement to the data assumed for the simulations of radionuclide transport in ECOLEGO. The equivalent flow rate of radionuclides from the backfill to the groundwater was calculated according to Bird et al. (1960)

$$Q_{eq} = A_w \phi_{rock} \left(\frac{4 D_w}{\pi \cdot t_{res}} \right)^{0.5}$$

where ϕ_{rock} is the flow porosity and t_{res} is the residence time of the water in contact with the backfill, which can be calculated as $t_{res} = L \cdot \phi_{rock} / u_0$, where u_0 is the flux of the approaching non-contaminated water. In this work, u_0 coincides with the vertical component of the velocity field, i.e. v_z.

The porosity was estimated by surface averaging the porosity fields as extracted from the DarcyTools model (COMSOL flow simulations do not use porosity as an input parameter) for the Base case, High Flow case and Low Flow case. In this averaging step the porosity values of the tunnels located on top and bottom of the Silo have been neglected, since they do not contribute to the radionuclides transport to the water flowing around the Silo. The average porosity calculated in this way is $2.3 \cdot 10^{-5}$ for both the Base case and the High Flow case and $1.2 \cdot 10^{-5}$ for the Low Flow case. The average values of velocity components and its magnitude are shown in Table E-1 for all cases. The corresponding flow rates of radionuclides Q_{eq} are shown in Table E-2 and Table E-3. It is noted that the values obtained for the shoreline position 3 from the COMSOL simulations are comparable to the value of 63.6 l/year obtained by Neretnieks at al. (1987) from scoping calculations.

The flow of radionuclides escaping from the Silo is directly affected by the evolution of the groundwater flow which in turn is influenced by the conductivity field. The different conductivity rock scenarios considered in the study show a slightly oscillatory behavior of the contaminated flow. Note that for shoreline position 1, the upward vertical flow is higher both for the highest and lowest conductivity rock descriptions, for which the vertical component of the flow is higher (lower resident times). For shoreline position 2 the vertical component of the flow obtained with highest and lowest conductivity rock descriptions is lower than in other cases (higher resident times), leading to a lower flow of radionuclides from the Silo. Finally, for shoreline position 3 a higher flow of radionuclides from the Silo results from the highest conductivity rock description.

It can be observed that the contamination of the passing water by out-diffusion of radionuclides from the Silo is significantly higher than the rest of cases in the no barriers case, while the degradation of the concrete does not lead to any significant changes. For shoreline position 3 the contaminated flow is four times higher than the flow of nuclides obtained in other cases. As expected, a higher conductivity of the rock leads to an increase of Q_{eq}. However, the flows obtained fall within the range of the values corresponding to the Base case.

If the High Flow and Low Flow cases are considered as bounds for the uncertainty in the rock hydraulic properties, it may be concluded that the variations in the Q_{eq} due to changes in the repository hydraulic properties are relatively small, except for the freezing case.

Table E-1. Average values of velocity components and its magnitude for the three shoreline positions and several scenarios.

Simulation	Shoreline position 1				Shoreline position 2				Shoreline position 3			
	v, m/s	v_x, m/s	v_y, m/s	v_z, m/s	v, m/s	v_x, m/s	v_y, m/s	v_z, m/s	v, m/s	v_x, m/s	v_y, m/s	v_z, m/s
Base case	1.54E–13	2.98E–14	9.10E–14	6.51E–14	7.83E–11	2.24E–11	4.25E–11	4.38E–12	1.83E–10	3.74E–11	1.01E–10	–8.19E–12
Alternative Closure	9.64E–14	2.34E–14	4.39E–14	4.96E–14	4.66E–11	1.27E–11	1.41E–11	1.48E–11	1.08E–10	1.74E–11	3.31E–11	–1.09E–11
Moderately degraded	1.54E–13	2.86E–14	8.89E–14	6.44E–14	7.82E–11	2.25E–11	4.25E–11	4.33E–12	1.83E–10	3.79E–11	1.01E–10	–8.17E–12
Severely degraded	1.54E–13	2.84E–14	8.90E–14	6.47E–14	7.82E–11	2.25E–11	4.25E–11	4.41E–12	1.83E–10	3.78E–11	1.01E–10	–8.00E–12
Completely degraded	1.54E–13	2.84E–14	8.90E–14	6.47E–14	7.82E–11	2.25E–11	4.25E–11	4.41E–12	1.83E–10	3.78E–11	1.01E–10	–8.00E–12
Moderately degraded plugs									1.88E–10	3.81E–11	1.03E–10	–8.44E–12
Severely degraded plugs									6.81E–10	–1.02E–10	5.34E–10	–1.28E–11
Fully degraded plugs									5.83E–09	–1.47E–09	5.27E–09	1.00E–11
Abandoned repository	2.16E–12	–5.48E–13	1.95E–12	6.62E–14	–	–	–	–	5.89E–09	–1.49E–09	5.33E–09	1.63E–11
High conductivity	1.71E–13	5.20E–14	9.42E–14	7.70E–14	9.28E–11	3.47E–11	5.23E–11	3.45E–11	2.24E–10	7.31E–11	1.32E–10	–8.50E–12
Low conductivity	2.79E–13	2.42E–14	6.36E–14	2.10E–13	4.46E–11	8.78E–12	2.50E–11	8.84E–13	1.01E–10	1.11E–11	5.77E–11	–1.20E–11
No barriers	–	–	–	–	–	–	–	–	1.13E–08	–1.25E–09	6.09E–09	–1.23E–10
Ice lens	1.54E–13	2.98E–14	9.10E–14	6.51E–14	7.83E–11	2.24E–11	4.25E–11	4.38E–12	1.83E–10	3.74E–11	1.01E–10	–8.19E–12

Table E-2. Estimation of the flow rate of radionuclides from the Silo for the three shoreline positions and several scenarios.

Simulation	Shoreline position 1			Shoreline position 2			Shoreline position 3		
	u_0/ϕ_{rock}, m^3/m^2-s	t_{res}, year	Q_{eq}, l/year	u_0/ϕ_{rock}, m^3/m^2-s	t_{res}, year	Q_{eq}, l/year	u_0/ϕ_{rock}, m^3/m^2-s	t_{res}, year	Q_{eq}, l/year
Base case	2.85E–09	556.60	1.37	1.91E–07	8.28	11.26	3.58E–07	4.43	15.40
Alternative Closure	2.17E–09	731.33	1.20	6.49E–07	2.44	20.72	4.75E–07	3.34	17.74
Moderately degraded	2.82E–09	562.93	1.37	1.89E–07	8.37	11.20	3.57E–07	4.44	15.38
Severely degraded	2.83E–09	560.73	1.37	1.93E–07	8.22	11.30	3.50E–07	4.53	15.22
Completely degraded	2.83E–09	560.74	1.37	1.93E–07	8.23	11.30	3.50E–07	4.53	15.22
Moderately degraded plugs							3.69E–07	4.30	15.63
Severely degraded plugs							5.59E–07	2.83	19.24
Fully degraded plugs							4.39E–07	3.61	17.05
Abandoned repository	2.89E–09	547.89	1.38				7.11E–07	2.23	21.69
High conductivity	3.34E–09	474.03	1.50	1.50E–06	1.06	31.71	3.69E–07	4.29	15.74
Low conductivity	1.74E–08	91.11	1.79	7.33E–08	21.62	3.68	9.95E–07	1.59	13.54
No barriers							5.39E–06	0.29	59.72
Ice lens	2.85E–09	556.60	1.37	1.91E–07	8.28	11.26	3.58E–07	4.43	15.40

Table E-3. Estimation of the flow rate of radionuclides from the Silo for the three shoreline positions and several scenarios.

Simulation	Shoreline position 1			Shoreline position 2			Shoreline position 3		
	u_0/ϕ_{rock}, m^3/m^2-s	t_{res}, year	Q_{eq}, m^3/year	u_0/ϕ_{rock}, m^3/m^2-s	t_{res}, year	Q_{eq}, m^3/year	u_0/ϕ_{rock}, m^3/m^2-s	t_{res}, year	Q_{eq}, m^3/year
Base case	2.85E–09	556.60	1.373E–03	1.91E–07	8.28	1.126E–02	3.58E–07	4.43	1.540E–02
Alternative Closure	2.17E–09	731.33	1.198E–03	6.49E–07	2.44	2.072E–02	4.75E–07	3.34	1.774E–02
Moderately degraded	2.82E–09	562.93	1.366E–03	1.89E–07	8.37	1.120E–02	3.57E–07	4.44	1.538E–02
Severely degraded	2.83E–09	560.73	1.368E–03	1.93E–07	8.22	1.130E–02	3.50E–07	4.53	1.522E–02
Completely degraded	2.83E–09	560.74	1.368E–03	1.93E–07	8.23	1.130E–02	3.50E–07	4.53	1.522E–02
Moderately degraded plugs							3.69E–07	4.30	1.563E–02
Severely degraded plugs							5.59E–07	2.83	1.924E–02
Fully degraded plugs							4.39E–07	3.61	1.705E–02
Abandoned repository	2.89E–09	547.89	1.384E–03				7.11E–07	2.23	2.169E–02
High conductivity	3.34E–09	474.03	1.498E–03	1.50E–06	1.06	3.171E–02	3.69E–07	4.29	1.574E–02
Low conductivity	1.74E–08	91.11	1.791E–03	7.33E–08	21.62	3.676E–03	9.95E–07	1.59	1.354E–02
No barriers							5.39E–06	0.29	5.972E–02
Ice lens	2.85E–09	556.60	1.373E–03	1.91E–07	8.28	1.126E–02	3.58E–07	4.43	1.540E–02